EFFECT OF TYPES OF INTERNAL MIXER ON FILLER DISPERSION AND PROCESSING CHARACTERISTICS OF SILICA FILLED EPOXIDIZED NATURAL RUBBER TYRE TREAD COMPOUNDS

Ahmad Kifli Che Aziz, Teku Zakwan Zaeimoedin & Mazlina Mustafa Kamal
Malaysian Rubber Board, RRIM Research Station, 47000 Sungai Buloh, Selangor.

Abstract

Preparing a filled rubber compound is a complicated process that depends on a considerable number of variables, as reflected by the complexity of industrial mixing time. The interactions between rubber and filler particles are obviously initiated in the early stage of mixing. Indeed, for rubber filler interactions to take place, one must have first a good wetting of particles by the polymer chains, a physical process that obviously concomitant with the dispersion and distribution of the filler aggregates. In this work, a silica filled epoxidised natural rubber for passenger car and truck tyre tread compounds by using two different kinds of internal mixer namely, *Banbury*® BR 1600 (tangential rotor) and *Intermix*® K1 Mk4 (intermeshing rotor)were prepared. The effects on dispersion and processing characteristics were measured by *disperGrader*^{TM}, rheometer and Rubber Process Analyzer. Experimental result showed that greater filler dispersion was observed with compounds prepared in K1 Mk4 mixer as compared to BR 1600 mixer. As therefore, lower viscosity value, shear viscosity and elastic torque was obtained as an indication of weak filler-filler interaction and filler agglomeration. However, a greater reversion was obtained with passenger tyre tread compounds as indicated by rheometer curves measured at 172°C. Further improvement in physical properties of the compounds mixed in BR 1600 as compared to compound mixed in K1 Mk4 mixer was observed, though the compounds exhibited an initial torque rise at the very beginning of the vulcanisation and also shorter scorch time, $t_{S2,}$

Keywords**:** *ENR, filler dispersion, physical properties, rheological properties, silica*

Introduction

Green tyre compound has the advantages of having low rolling resistance, improved wet grip and enhanced handling [1]. It is reported that a 3% decrease in rolling resistance is equivalent to 1% saving in fuel, and thus giving green tyre the economic benefit and consumer satisfaction. These green tyre properties can be achieved by utilizing silica as the main filler in the tyre tread compound. Michelin has introduced the first durable silica-filled tyre, also known as green tyres [2]. However, previous studies have found that silica have poor interaction and dispersion in non-polar tyre rubbers compared to carbon black [3]. Generally, silica particles possess very strong particle–particle interactions. Silica is much more difficult to disperse than carbon black of equivalent particle size or BET surface area [4]. Coupling agent is widely used to improve interaction between silica and rubber. Several studies reported the possibility of rubber compound filled with silica without the use of coupling agents such as silane. On the other hand, epoxidised natural rubber (ENR), the modified form of natural rubber give better compatibility to silica, and higher reinforcement for silica compound compared to natural rubber (NR). The epoxy group of ENR can react with the silanol group of silica, where the use of coupling agents such as silane [5, 6] can be eliminated or greatly reduced. Eco-friendly tire has been developed by using at least 97% by weight of tire based on non-petroleum raw materials including natural rubber or modified natural rubber and silica in the compound recipe [7]. An experimental study of mixing silica, carbon black, and talc into styrene butadiene rubber (SBR) in an internal mixer with intermeshing and tangential double-flighted rotors has been carried out by Chanvoot et al [4]. This work will investigate the behaviour and properties of silica filled ENR compounds for tyre tread prepared in BR 1600 and K1 Mk4 internal mixers.

BR 1600 is a *Banbury*® type mixer builds up with tangential rotor where the rotor like rolls of mill, can rotate independently and therefore, at different speed [8]. The mixing principle relies tapering nip between the rotor and the chamber wall of mixer to give mix dispersion [9]. K1 Mk4 is a *Intermix*® type mixer build up with intermeshing rotor where the rotor like gear wheels of same diameter, and must rotate at same speed. The mixing principle relies tapering nip between two rotors blade of mixer to give mix dispersion. Figure 1 shows the geometry of intermeshing and tangential rotors of internal mixer.

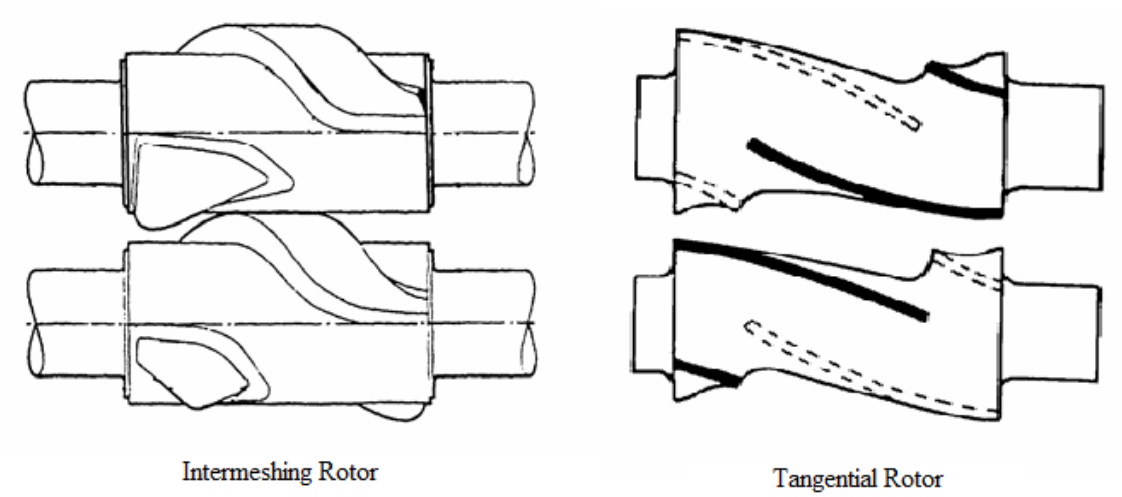

Figure 1: Geometry of intermeshing and tangential rotors [10]

Materials and Method

The effects of types of internal mixers were investigated in this study. Formulations and materials used are given in Table 1**.** In this work, two types of tyre tread compounds were prepared, passenger car (PCR) tyre treads and truck tyre treads and, two types of internal mixers were used, namely internal mixer BR 1600 (tangential rotors) and K1 Mk4 (intermeshing rotors) for comparison purposes.

Table 1: Formulations for tyre tread compounds

Ingredients	PCR tread	Truck tread
ENR 25[a]	100	100
Silica[b]	75	55
Black N234	5	5
Naphthenic oil	20	5
Zinc oxide	3	3
Stearic acid	3	3
Antioxidant[c]	2	2
Calcium stearate	2	2
Sulphur	1.8	1.3
Accelerator[d]	2.4	1.5

a. *Ekoprena*™ 25 from Malaysian Rubber Board
b. *Zeosil*® *1165MP* from Rhodia
c. *Santoflex*® *6PPD* from Solutia
d. N-Tert-Butyl-2-Benzothiazole Sulfenamide (TBBS)

Mixing

Mixing was carried out in 3 stages, Table 2, while the sequence of mixing is shown in Table 3. In this work, silica filler and oil were pre-blended prior mixing. The silica from was kept in air-conditioned room to avoid moisture absorption. The fill factor and rotor speed of BR 1600 were set at 0.7 and 110 rpm respectively while fill factor and rotor speed of K1 Mk4 were set at 0.7 and 90 rpm respectively. All of masterbatches were sheeted out on warm two-roll mills with minimal passes.

Table 2: Summary of mixing steps

Mixing step	Equipment
1st stage mixing	Internal mixer
2nd stage mixing(Re-milling step)	Internal mixer
Final stage mixing (finalizing)	Two roll mill

Table 3: Mixing cycle of the mixing process

Internal Mixer	BR 1600	K1 Mk4
Mixing cycle 1st stage		
0	Rubber	Rubber
1/2 mins	Powder	Powder
1 1/2 mins	1/2Fillers + 1/2 oil	1/2Fillers + 1/2 oil
2 1/2 mins	1/2Fillers + 1/2 oil	1/2Fillers+ 1/2 oil
3 1/2 mins	Sweep	Sweep
(*Dump**) mins	Dump at 165°C or 7 mins	Dump at 165°C or 7 mins
Mixing cycle 2nd stage	BR 1600	K1 Mk4
0	Masterbatch	Masterbatch
1/2 mins	Zinc oxide	Zinc oxide
3 mins	Dump	Dump

* Mixing time depending on the time to reach dump temperature

Mooney Viscosity Determination by using Mooney Viscometer

Mooney viscosity measurements were carried out using the MV2000 Viscometer (large rotor) at 100°C based on ISO 289-1. The sample weights were in the range of 25-30 g. The testing was conducted on masterbatch and final compound.

Tan Delta and Elastic Torque Determination by using Rubber Process Analyzer

The processability test was performed by using Rubber Process Analyzer (RPA) from Alpha Technologies Ltd. The RPA subtest adopted was as follows: frequency was set between 6 to 1500 cycles per minute (c.p.m), while strain and temperature were fixed at 1° (or 14%) and 100°C respectively. For the RPA test, about 10 g of rubber sample per test was used. Processability of rubber was based on Tangent delta value measurement as given by the following equation:

$$\text{Tan delta} = \frac{G''}{G'} \quad (1)$$

where; G"- Viscous (or loss) modulus
G' - Elastic (or storage) modulus

Viscosity Determination by using Capillary Rheometer

The viscosity test was conducted by using *Gottfert Rheograph 75* Capillary rheometer. In this study, the test temperature was set at 100°C; similar to the temperature setting for the *Mooney* viscometer and RPA measurement. The apparent shear rate, was set between 10 to 2000 sec^{-1} while die ratio were fixed at 20/1 and 10/1. The die size of 1 mm diameter, 20 mm and 10 mm length were used to conduct this test. Each rubber sample (in sheet form) was cut into strips of approximately 6 mm × 6 mm × 50 mm in size. The sample was then inserted into the barrel, compressed and packed before the testing was started.

The actual viscosity of rubber, ETA is given by the following equation:

$$\text{Viscosity, } \eta = \frac{\tau}{\dot{\gamma}} \qquad (2)$$

where; τ is the true shear stress (in unit Pascal) and $\dot{\gamma}$ is the corrected shear rate (In unit 1/sec). For a non-Newtonian material such as rubber, the true shear stress is obtained by using the Bagley correction and meanwhile, the shear rate is corrected by using the Rabinowitch equation.

Cure Characteristic

The cure characteristics were performed on 5 g of compound at 150°C for truck tread and 172°C for passenger car tread in 30 min with oscillation amplitude of 0.5° using a *Monsanto MDR 2000P* based on ISO 6502 standard.

Filler Dispersion

Filler dispersion study was conducted by using *DisperGrader™* based on ISO 11345 on cured compounds. Sample preparation involved cutting of hardness test piece sample to generate a 'fresh face' for analysis and observed using *DisperGrader™* optical light microscope.

Physical Properties

The physical properties test was conducted according to standard methods as tabulated in Table 4.

Table 4: Physical properties test

Physical Properties Test	Standard Method
Tensile Strength	MS ISO 37:1998
Hardness (IRHD)	MS ISO 48:2002
Abrasion Resistant Index	ISO 4649:2002

Results and Discussion

Processing Characteristics

Mooney Viscosity Determination by using Mooney Viscometer

The Mooney viscosity of masterbatches and compounds of ENR filled silica for both passenger and truck tyre treads is shown in Table 5. It was found that, lower masterbatches and compounds viscosity produced from the K1 Mk4 mixer as compared to BR 1600 mixer regardless of type of tread. It is almost similar trend as experimental study on SBR mixes in intermeshing and tangential rotors [4]. This indicates greater chains breakdown of rubber molecules occur in K1 Mk4 mixer as compared to the other one. The presence of tapering nip between the rotor and the chamber wall of the mixer eventually promotes greater shear and friction.

Table 5: Mooney viscosity of masterbatches and compounds of ENR/silica

Mooney viscosity	PCR Tread		Truck Tread	
	BR1600	K1 Mk4	BR1600	K1 Mk4
Masterbatch	67.2	63.4	114.3	101.6
Compound	54.3	50.1	77.6	63.2

Tan Delta and Elastic Torque Determination by using Rubber Process Analyzer

The processing characteristics of silica filled ENR masterbatch/compound can also be assessed from the results of Tan delta and elastic torque property measured by Rubber Process Analyzer (RPA). In term of processability behaviour, tangent delta represented a ratio between viscous modulus (loss modulus) and elastic modulus (storage modulus). High tangent delta is indication of good permanent deformation and die swell properties during fabrication. The higher the tan delta values the better the processability of the rubber and vice versa. The elastic torque is the rotational force needed to deform the rubber shape. Usually high values in elastic torque indicate poor processability of rubber and high energy is needed in its processing due to its high elastic property. Figure 2 and 3, shows that higher tan delta value for both masterbatches, passenger and truck tyre tread mixed in K1 Mk4 mixer as compared to BR 1600 mixer. Indeed, the mixed possess lower elastic torque value for both passenger and truck tyre formulation Figure 4 and 5. This may due to the greater chain breakdown of rubber polymer in K1 Mk4 mixer compared to BR 1600 mixer which resultant in less elasticity and more viscous.

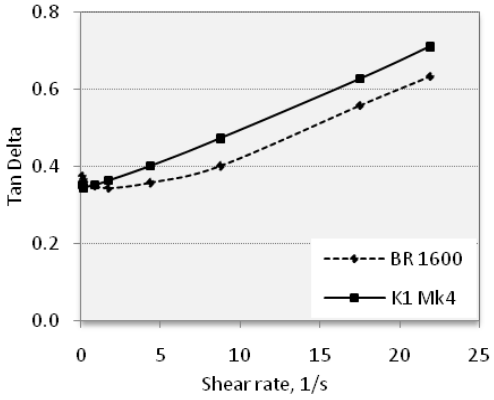

Figure 2: Tan delta, δ of passenger tyre tread

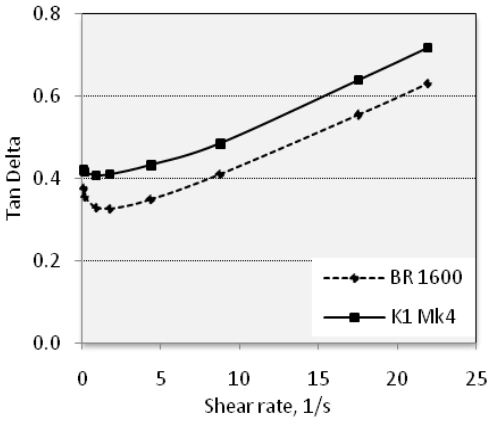

Figure 3: Tan delta, δ of truck tyre tread

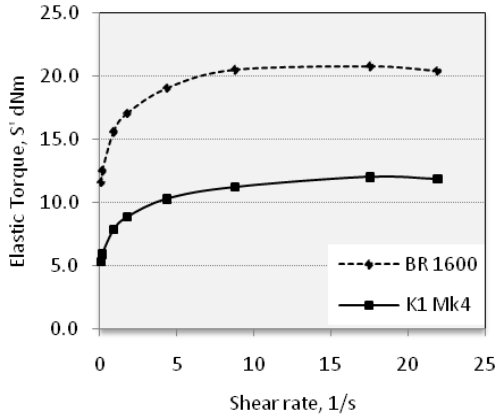

Figure 4: Elastic torque, S' of passenger tyre tread

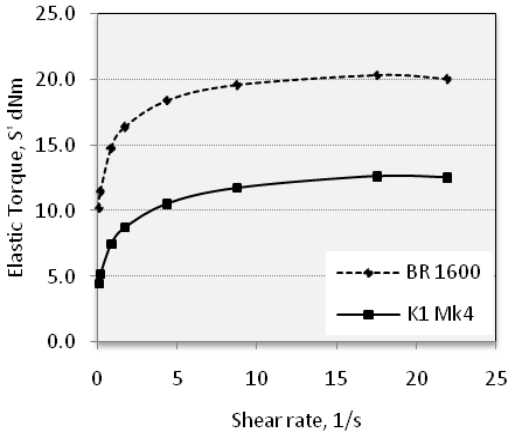

Figure 5: Elastic torque, S' of truck tyre tread

Viscosity Determination by using Capillary Rheometer

Viscosity is a measure of the resistance of a fluid (polymer) which is being deformed by shear stress. Based on the viscosity curves results of ENR filled silica compounds as shown in Figure 6 and 7, shows that the masterbatches mixed in K1 Mk4 mixer possess lower viscosity for the entire shear rates as compared to masterbatches mixed in BR 1600 mixer for both tyre tread mixes. This indicates that ENR-silica mixed in K1 Mk4 mixer gives better processability and flow behaviour properties which in agreement with results obtained in Mooney viscometer and RPA previously.

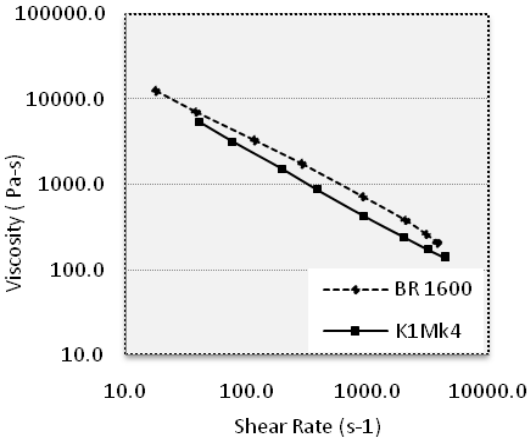

Figure 6: Viscosity curve of PCR tyre tread

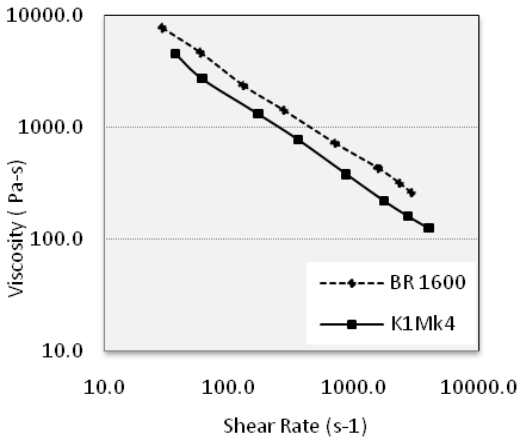

Figure 7: Viscosity curve of truck tyre tread

Cure characteristics

Figure 9 and Figure 10 presents the cure curves of silica filled ENR tyre tread compounds prepared with different type of internal mixers. Both PCR and truck compounds showed specific cure curves and characteristics. The BR 1600 mixed showed clear two steps of cure curves or initial torque rise for both types of PCR and Truck treads compounds in contrast to BR 1600 mixed. The two steps cure curves is associated with agglomeration or flocculation of fillers in the compounds. The filler dispersion is related with different rotors design for both types of internal mixers. Greater shear and friction of intermeshing rotors of K1 Mk4 internal mixer gives better fillers dispersion and distribution resultant in low tendency of fillers agglomeration and flocculation.

Table 6 presents the cure characteristics of the compounds. Both compounds produced by K1 Mk4 mixer exhibited low value of Δ torque, M_H - M_L, which could correlate to low crosslink density which resultant in low stiffness. On the other hand, it was found that shorter scorch time for compounds mixed in BR1600 mixer as compared to K1 Mk4 mixer. In addition, the optimum cure time,t_{95} of the compounds were remaining similar. The short scorch time is probably associated with fillers agglomeration or flocculation behaviour as indicated by the initial torque rise in the cure curves. However, due to high temperature curing, significant reversion behaviour was observed in PCR treads compounds as seen in Figure 8.

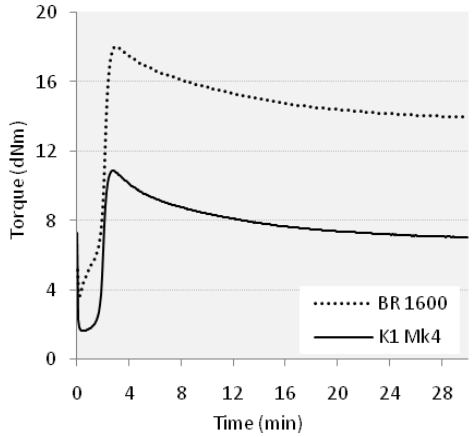

Figure 8: Cure curve of PCR tread at 172°C

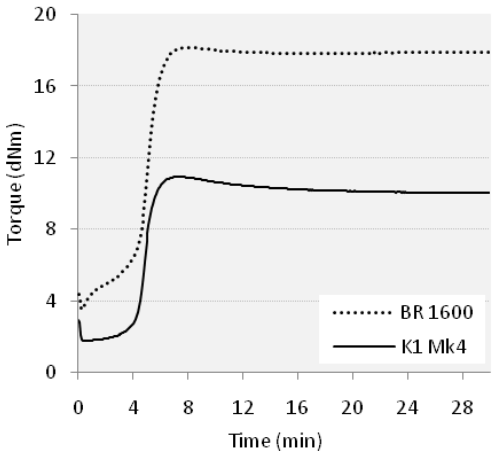

Figure 9: Cure curve of Truck tread at 150°C

Table 6: Cure characteristics of compounds

Properties	PCR Tread		Truck Tread	
	BR1600	K1 Mk4	BR1600	K1 Mk4
Min. torque (M_L), dNm	3.5	1.7	1.2	1.8
Max. torque (M_H), dNm	18.6	10.4	17.6	11.1
Δ torque (M_H - M_L), dNm	15.2	8.6	16.4	9.3
Rheometer Scorch (t_{S2}), min	0.8	1.2	0.1	8.5
Optimum Cure Time (t_{95}), min	1.9	1.7	10.6	10.3

Filler Dispersion

Figure 9 shows fewer white area and larger agglomerate of filler sizes of the vulcanizate prepared in BR 1600 mixer as compared toK1 Mk4 mixer resultant in, lower filler dispersion Table 7. In contrast, high shear and friction of intermeshing rotor in K1 Mk4 mixer, enhances filler distribution and dispersion by breaking down the filler particles and rubber chains which later reduce the compounds viscosity and increase the mobility. The efficiency of intermeshing rotors is also better compared to tangential rotors due to the enforced formation of thin layers of material between rotors [11]. On the other hand, higher filler dispersion was observed with truck tyre compound due to lower filler loading.

Table 7: Filler dispersion of vulcanizates

Parameter	PCR Tread		Truck Tread	
	BR 1600	K1 Mk4	BR 1600	K1 Mk4
Avg. Ag. Size, micron	17.4	14.1	17.6	12.8
White Area, %	19.2	9.0	19.2	6.0
Dispersion, %	50.1	86.2	48.2	93.5

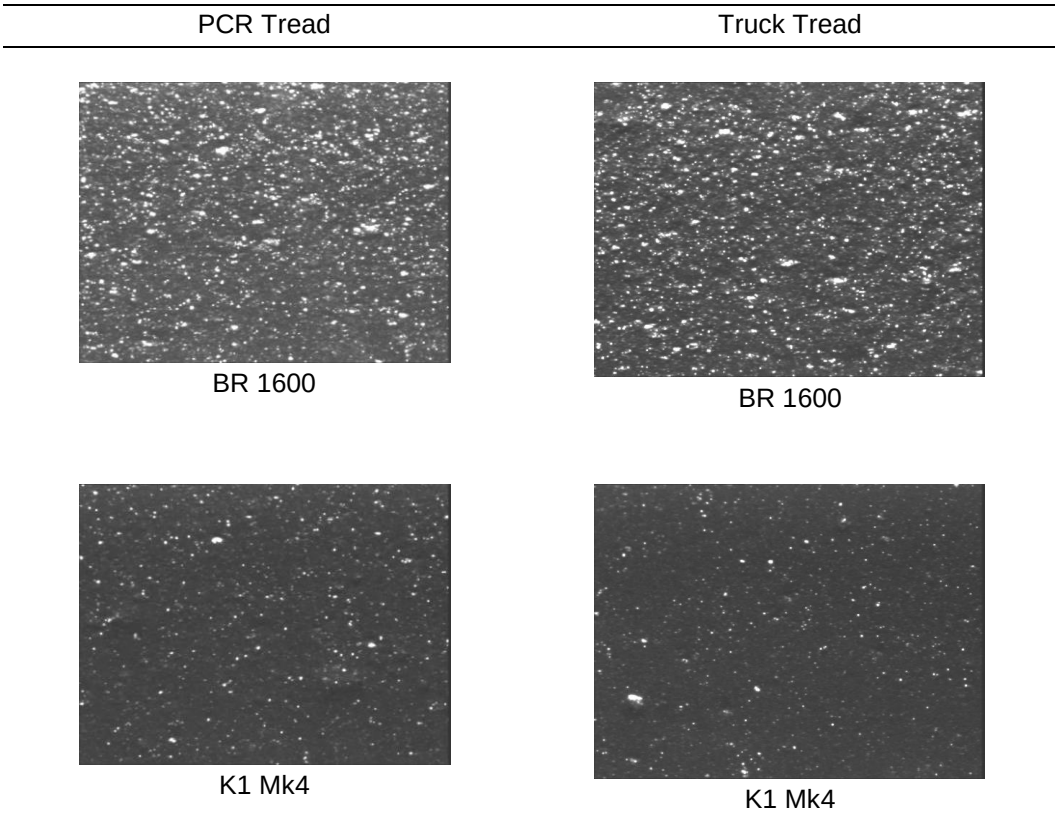

Figure 10: Filler dispersion image of vulcanizates

Physical Properties

Table 8 presents the physical properties of the vulcanizates. It was found that the vulcanizates prepared in BR 1600 mixer possess better tensile strength, elongation at break, modulus, hardness and abrasion resistant index compared to the vulcanizates prepared in K1 Mk4 mixer for both types of tyre treads. High Δ torque value of cured compounds prepared in BR 1600 mixer indicates of high crosslink density and stiffness. The lesser rubber chains breakdown occurred during mixing may offer minimum effects on vulcanizates physical properties.

Table 8: Physical properties of vulcanizates

Properties	PCR Tread		Truck Tread	
	BR 1600	K1 Mk4	BR 1600	K1 Mk4
Tensile Strength, MPa	17.2	15.1	22.5	20.5
Elongation at Break, %	379	377	437	403
M100, MPa	2.8	1.9	2.7	2.1
M300, MPa	12.6	10.8	13.1	13.4
Hardness, IRHD	69	58	71	62
Abrasion Resistance Index, %	77	55	105	86

Conclusion

In general filler dispersion, processing characteristics and physical properties of rubber compounds are influenced by the type of internal mixer or rotor used. The intermeshing rotors of K1 Mk4 internal mixer offer better fillers dispersion and processing characteristics than the tangential rotors of BR 1600 internal mixer. However, the physical properties of treads vulcanizates prepared in K1 Mk4 internal mixer were adversely affected due to excessive rubber molecular chain as compared to BR 1600 internal mixer.

Acknowledgements

Support and assistance rendered by Malaysian Rubber Board management, officers and staffs especially Mr. Mohd Ilias Ibrahim, Mr. N. Arumugam and Mr. Iskandar Shahrir is gratefully acknowledged.

References

[1] Ita P.A. 2005. Filler Requirements In the Tire Industry: Carbon Black & Precipitated Silica .*Tire Technology Expo & Conference 2005,* Koln Messe, Cologne, Germany.

[2] John D. 1995.Where the Silica Meets the Road, *Discover.* retrieved from http://discovermagazine.com/1995/apr/wherethesilicame497

[3] Billerica, J., Wang M. 2008. *Raw Materials and Applications*.*KGK January/February 2008*, 33-42

[4] Chanvoot, K. & James L.W. 2000. *Journal of Applied Polymer Science*, 78: 1551–1554

[5] Cataldo, F. 2002. *Macromolecular Materials and Engineering*, 287: *348-352.*

[6] George, K.M., Varkey, J.K., George, B., Joseph, S., Thomas, K.T. and Mathew, N.M. 2006. Physical and Dynamic Mechanical Properties of Silica Filled Nitrile Rubber Modified with Epoxidized Natural Rubber. *Elastomere und Kunststoffe, KGK Oktober 2006*. 544-549.

[7] Naohiko, K., Kazuo, H. and Takuya, H. 2007. Eco Tire. *U.S. Patent* No. 7275572

[8] Annicelli, R.A. 2001. *Rubber Technology: Compounding and Testing for Performance*. Munich: Hanser Verlag. 506-507.

[9] Carreau, P.J., DeKee, D.C.R. and Chabra, R.P. 1997. *Rheology of Polymeric Systems: Principles and Applications*. New York: Hanser. 61-71.

[10] Robert Dickstein. 2003. *Technical Rubber Course, Mixing Technology Machinery,*retrieved fromhttp://www.chicagorubbergroup.org/Farrel_Mixing_Presentation_051110.pdf

[11] Wilma Karola Dierkes. 2005. *Interaction Between The Chemistry of The Silica-Silane Reaction and The Physics of Mixing, Economic Mixing of Silica-Rubber Compounds*, Ph.D Thesis, Netherlands: University of Twente. 24-26.

THE DEGRADATION OF LINEAR LOW DENSITY POLYETHYLENE/SOYA POWDER BLENDS IN NATURAL COMPOST MEDIUM

S.T. Sam*[1,2], H. Ismail[3], Z. Ahmad[3]

[1]School of Bioprocess Engineering, Kompleks Pusat Pengajian Jejawi 3, Universiti Malaysia Perlis

[2]Center of Excellence Geopolymer & Green Technology (CEGeoGTech), Kompleks Pusat Pengajian Jejawi 2, Universiti Malaysia Perlis, 02600 Arau, Perlis, Malaysia

[3]School of Materials and Mineral Resources Engineering, 14300 Nibong Tebal, Pulau Pinang, Malaysia

Abstract

In this study, linear low density polyethylene (LLDPE) was blended with soya powder in a *Haake* internal mixer by melt mixing. The processing temperature was 150°C and the rotor speed was 50 rpm. The soya powder content was varied from 5 to 40% (w/w). Epoxidised natural rubber (ENR 50) was used as a compatibiliser to improve the compatibility of LLDPE and soya powder. Environmental degradation was evaluated by composting the blends sample into the natural soil. The exposure period was 1 year and the meteorology data was collected. After composting, LLDPE/soya powder blends were subjected to tensile test, weight loss and morphological tests. As expected, the tensile strength and elongation at break (Eb) of all blends ratios dropped after composting. The retention of the tensile strength and Eb decreased with increasing soya powder content after exposed to the natural compost medium. At the same soya powder content, ENR 50 compatibilised blends showed higher degradability compared to the control. The morphology of the composted surface was observed under scanning electron microscope (SEM). The pores and colonization of fungus can be observed on the composted samples. The weight loss of the compatibilised blends was higher than the control after being exposed to the soil.

Keywords: *Epoxidised natural rubber, natural compost medium, soya powder.*

Introduction

The limitation of the biopolymers was due to the high cost of biopolymer production as compared to petroleum based thermoplastic. The common thermoplastic such as polypropylene (PP), polyethylene (PE) and polystyrene (PS) have been widely used in various packaging purposes due to the cost. However, these polymers are highly resistance to UV, thermal, hydro- and bio-degradation. The properties of these polymers create environmental problems once they are disposed in the landfill.

The incorporation of starches into the non-degradable polymer is the cheapest alternative to produce degradable polymer. The incorporation of corn starch, sago starch, tapioca starch and rice starch into petroleum based polymer have been developed by various researchers [1-4]. Nevertheless, the soya protein based natural polymer is still rare to be incorporated in non-degradable polymer. Pavlath et al. [5] claimed that the protein based polymer is easier to be degraded than carbohydrate based polymer. Therefore, the use of the soya powder which is rich in protein is potential to accelerate the degradation of soya powder.

The compatibility of the hydrophilic protein based polymer with hydrophobic polymer is a challenge in polymer blends. Based on our previous investigation, the incorporation of polyethylene grafted maleic anhydride (PE-g-MA) [6] and epoxidised natural rubber with 50 mol% epoxidation (ENR 50) [7] had successfully compatibilised the linear low density polyethylene (LLDPE)/soya powder blends. In comparison, ENR 50 gave better compatibilisation effect compared to PE-g-MA. Thus, ENR 50 had been chosen as a compatibiliser in this study. It is interesting to compare the ENR 50 compatibilised blends with

the uncompatibilised blends in natural compost medium. In this study, the degradation of the blends after buried into natural compost medium was investigated through tensile test, observation of surface morphology and change in the weight of the samples.

Materials and Method

Materials and Sample Preparation

Linear low density polyethylene (LLDPE) was obtained from Polyethylene Malaysia Sdn. Bhd. It is available in pellet form with melting point of 122°C. Soya powder with a melt flow index of 1.0 g (10 min)$^{-1}$ was purchased from Hasrat Bestari (M) Sdn Bhd. The moisture content was 3.12% before drying and the average granular size was 12 μm. The protein content was 44.2%. ENR 50 was supplied by Rubber Research Institute of Malaysia (RRIM). Haake internal mixer was used to mix the materials. Prior to mixing, soya powder was dried in a vacuum oven at 70°C for 24 h. The LLDPE/soya powder blends were mixed at a temperature of 150°C with a rotor speed of 50 rpm. The blended samples were compressed in a compression moulding machine (Kao Tieh GoTech) at 150°C, at a pressure of 10 MPa for 10 min. Table 1 lists the blends with the various ratios of soya powder/LLDPE used in this study. ENR 50 was added into the blends based on 50% (w/w) of the soya powder content.

Table 1: Formulation of LLDPE/soya powder blends

Materials	Formulation % (w/w)
LLDPE/5 soya powder	95% LLDPE + 5% soya powder
LLDPE/10 soya powder	90% LLDPE + 10% soya powder
LLDPE/15 soya powder	85% LLDPE + 15% soya powder
LLDPE/20 soya powder	80% LLDPE + 20% soya powder
LLDPE/30 soya powder	70% LLDPE + 30% soya powder
LLDPE/40 soya powder	60% LLDPE + 40% soya powder

ENR 50 was added based on 50% (w/w) of soya powder

Natural Composting

The degradability of the LLDPE/soya powder blends was measured through natural composting. The test was carried out at Universiti Sains Malaysia, (latitude 5°8' N, longitude 100º29' E) from May 2008 to April 2009. Meteorology data such as average temperature, rainfall and relative humidity were recorded from the nearest meteorology station in Butterworth (latitude 5°28'N, longitude 100°23'E). The test was carried out based on the modified method from Kim et al. [8]. Samples were prepared, buried and dug-out in between 3 to 6 months and then later, the period was extended to 12 months. The samples were washed with distilled water and dried in an air drying oven at 70°C for 24 h before subjected to further testing.

Tensile Properties

Tensile specimens were cut from each sheet according to the dimension stated in ASTM D638. Tensile tests were performed using an *Instron* Universal Testing Machine at a crosshead speed of 50 mm·min^{-1}. Five measurements were obtained and the average was calculated. The retention of the tensile properties was calculated using the following equation:

$$\left(retention\,(\%) = \frac{Value\ \ after\ \ Degradation}{Value\ before\ Degradation} \right) \quad (1)$$

Surface Morphology

The composted surfaces of the samples were examined using scanning electron microscopy (SEM). After removing the samples from the soil, the surfaces were sputtered with gold prior to the SEM analyses. The model of the SEM is *VPFESEM SUPRA 35VP* with 10 kV of constant voltage.

Weight Loss

The composted samples were rinsed with distilled water and dried to a constant temperature at 70°C. The percentage of the weight loss percentage was calculated based on following equation:

$$\left(\% \, Weight \;\; Loss = \frac{(W_i - W_f)}{W_i} \times 100 \right) \qquad (2)$$

Results and Discussion

Figure 1 shows the trend of the tensile strength for ENR compatibilised blends after 1 year buried in natural soil. As expected, the tensile strength dropped over 1 year composting period. The degradation of the samples in the soil was mainly dependent on microorganism consumption and moisture interaction. Table 2 summarizes the retention of tensile properties for uncompatibilised and ENR 50 compatibilised blends after natural composting for 1 year. It was clearly showed that ENR 50 compatibilised blends exhibited slightly lower tensile strength retention compared to the uncompatibilised blends. The LLDPE/soya powder blends was easily oxidized with the presence of ENR 50. The oxidation might occur when the small quantity of oxygen penetrate into the soil. Therefore, the ENR compatibilised blends showed higher degradability than uncompatibilised blends. From the investigation of Sharma et al. [9], the incorporation of styrene butadiene rubber (SBR) and ENR 50 into sago starch/linear density polyethylene (LDPE) blends had successfully increased their degradation through thermo-oxidative test. The reason was due to the unsaturated double bond in these elastomers were easy to be degraded.

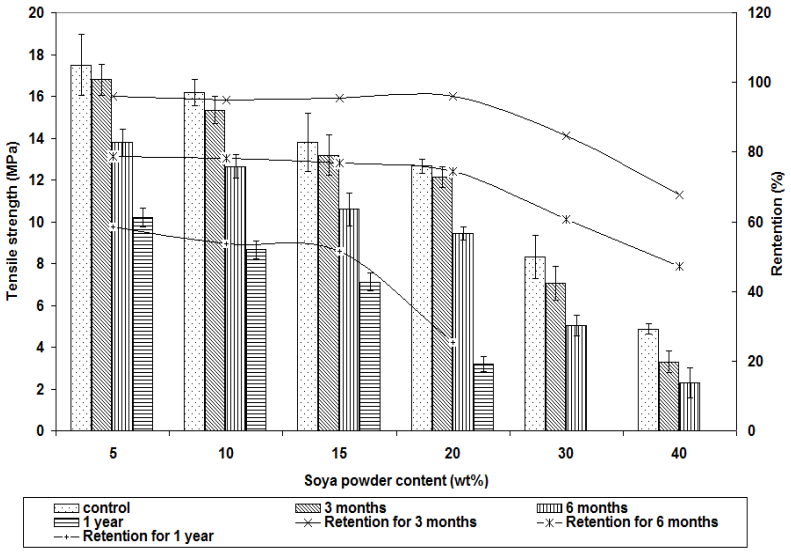

Figure 1: Tensile strength and the retention after different period of natural composting

Table 2: Retention of tensile properties for LLDPE/soya powder blends after 1 year composting

Sample	Retention of Uncompatibilised Blends (%)			Retention Compatibilised Blends (%)		
	Tensile strength	Elongation at break	Young's Modulus	Tensile strength	Elongation at break	Young's Modulus
LLDPE/ 5 soya powder	69.8	80.3	164.3	58.3	78.2	121.7
LLDPE/ 20 soya powder	27.2	43.5	200.9	25.2	32.5	153.4
LLDPE/ 40 soya powder	Fragmented	Fragmented	Fragmented	Fragmented	Fragmented	Fragmented

Figure 2 demonstrates the changes of Eb for ENR 50 compatibilised blends as a function of composting time. The Eb of ENR 50 shows the same trend as tensile strength. The Eb reduced as the increase of soya powder content in ENR 50 compatibilised blends indicating the occurrence of degradation. The compatibilised blends also showed lower Eb retention compared to uncompatibilised blends (see Table 2). This again indicates higher degradability of compatibilised blends in biotic environment. SEM micrographs for composted surface after natural composting (Figure3 (a)-(c) and Figure 4 (a)-(c)) indicate the degradation of the ENR 50 compatibilised blends. The formation of pores during degradation might due to the consumption of soya powder by microbe in the soil. The formation of pores for 6 months composting (Figure 3 (a)-(c)) was not obvious as the sample with 1 year composting time (Figure 4 (a)-(c)). The effect of microorganism colonization was apparently found in Figure 4(c). The fungi had been penetrated into the samples and consumed the soya powder. These pores became the weak point of the degraded sample, consequently reduced their tensile strength and Eb.

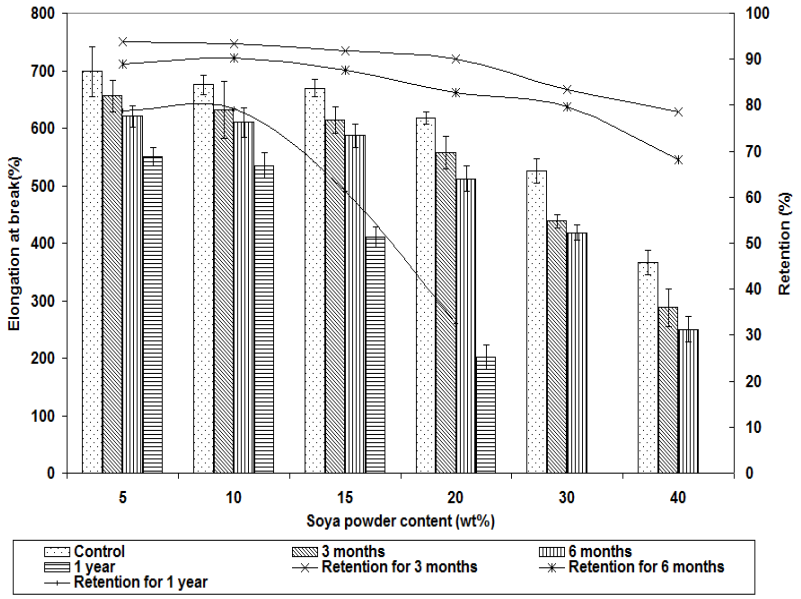

Figure 2: Elongation at break and the retention after different period of natural composting

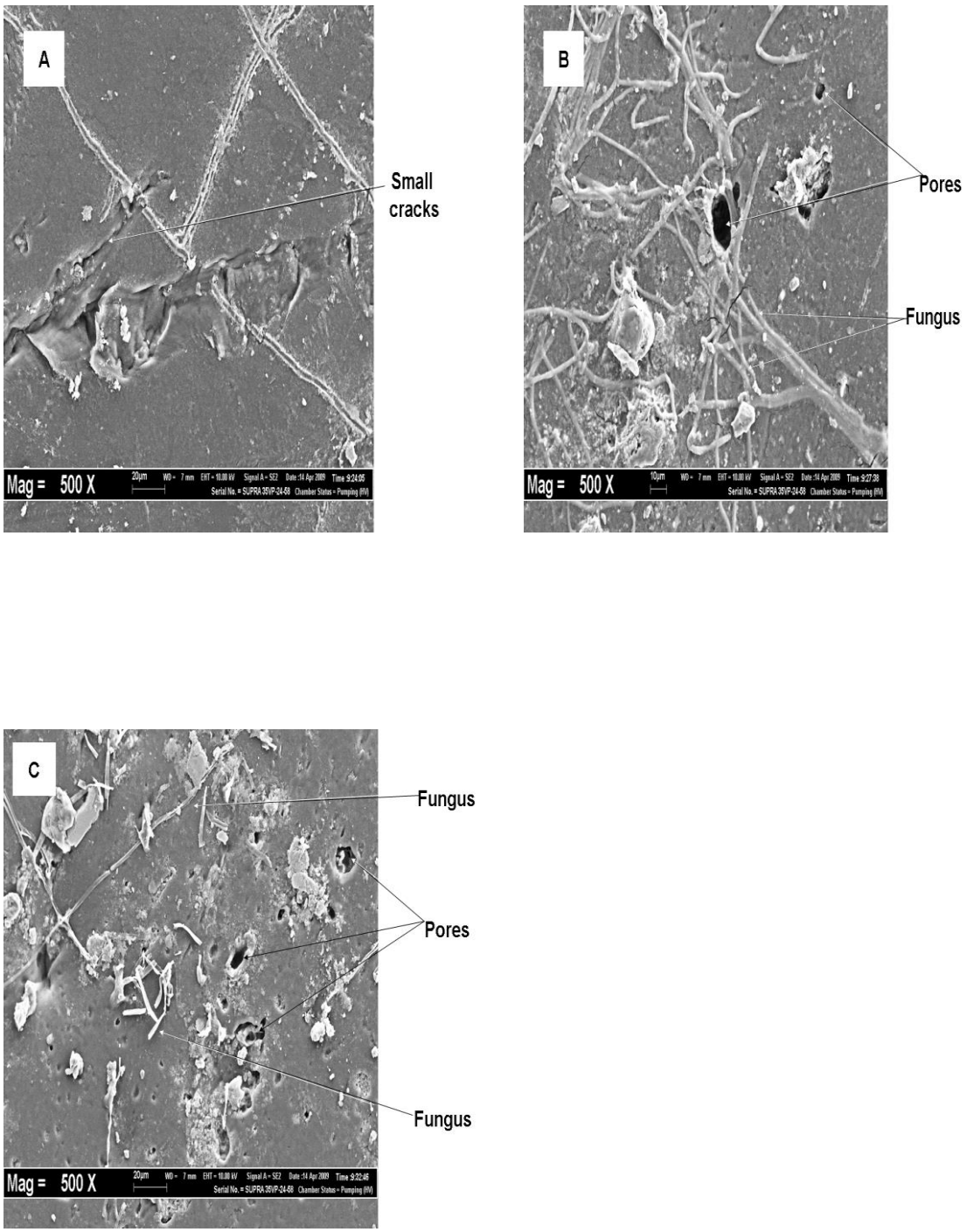

Figure 3: SEM micrographs of composted blends after 6 months composting with a)5% (w/w) b) 20% (w/w) and c) 30% (w/w) soya powder

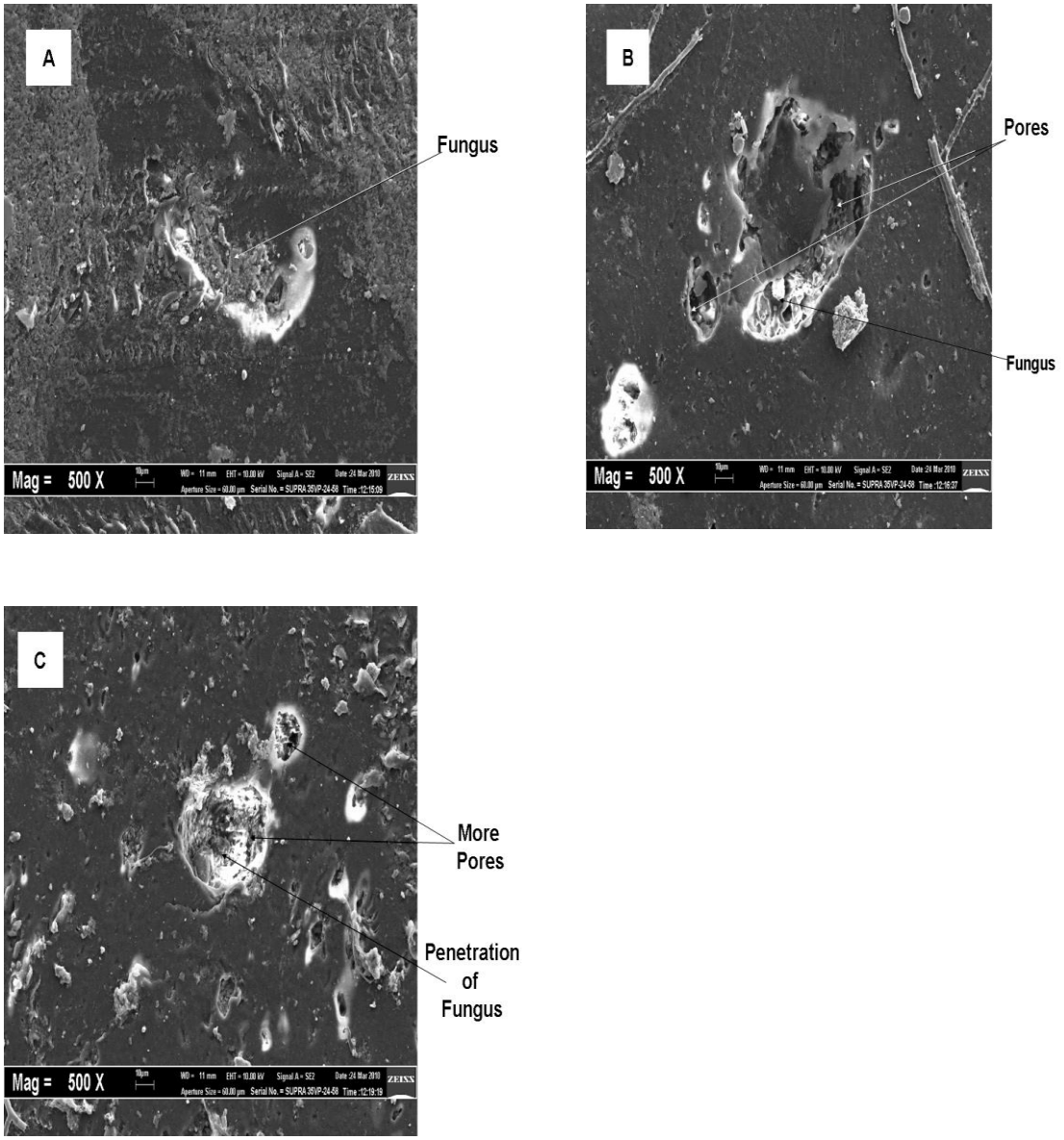

Figure 4: SEM micrographs of composted blends after 1 year composting with a) 5% (w/w) b) 20% (w/w) and c) 30% (w/w) soya powder

The Young's modulus of the compatibilised blends after natural composting is shown in Figure 5. The Young's modulus increased with increasing composting period. This was due to the embrittlement effect as a result of formation of radical crosslinking during degradation. Nevertheless, the Young's modulus retention for compatibilised blends was lower than uncompatibilised blends (see Table 2). This can due to the presence of elastomer i.e ENR 50 in the blends that resulted in higher elasticity compared to uncompatibilised blends.

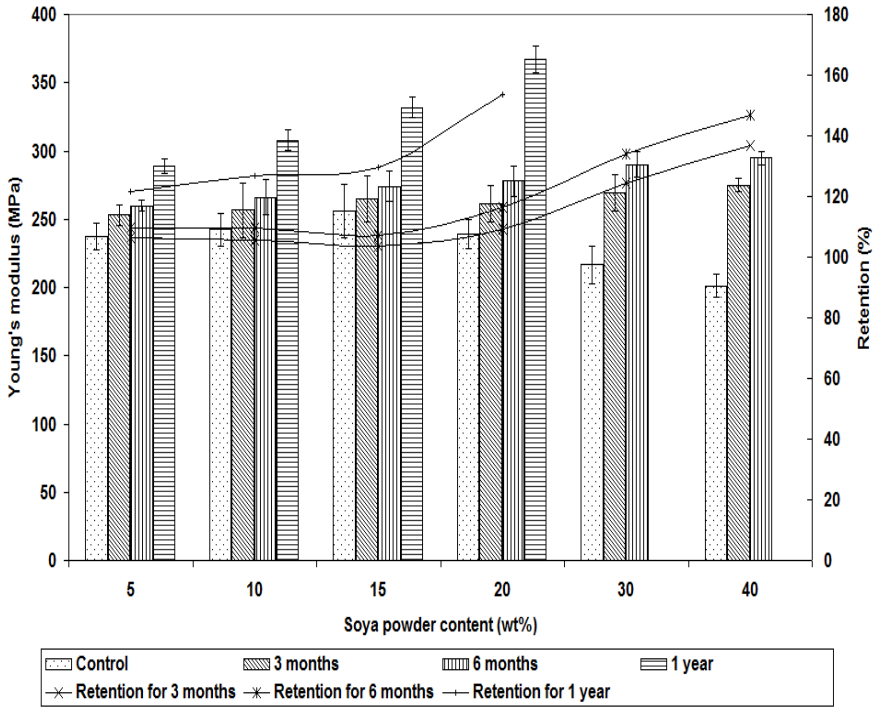

Figure 5: Young's modulus and the retention after different period of natural composting

Weight Loss

Based on Guohua et al. [10], natural composting is a bio-geophysical investigation that can provide a realistic environment to the samples as the soil humidity, temperature, and microorganism types are depending upon the season. The variation in weight of the samples as a function composting time is shown in Table 3. The weight change for neat LLDPE was insignificant even after 1 year of natural composting. The slight decrement might be due to the leaching of processing aid (≈ 0.7% of the matrix) of LLDPE. The weight loss of the blends increased with increasing soya powder in the blends. The trend is in agreement with the tensile test that the degradation increased with soya powder content. Microorganism such as fungi played an important role in degrading the blends by consuming the soya powder. Besides that, the blends with higher soya powder content were also found to be easily interacting with the moisture in the soil, consequently leached out from the blends. In comparison, it can be observed that the weight loss of the ENR 50 compatibilised blends was slightly higher than uncompatibilised blends. The polar group of ENR might attract the moisture from the compost medium and enhance the soya powder-water interaction in the compost medium. Therefore, the soya powder can be easily leached out from the blends. This indicates that ENR 50 can accelerate the degradation of LLDPE/soya powder blends in compost condition.

Table 3: Comparison of weight loss for uncompatibilised and ENR 50 compatibilised blends after 1 year composting

Sample	Uncompatibilised Blends		Compatibilised Blends	
	6 months	1 Year	6 months	1 Year
LLDPE	0.2	0.2	-	-
LLDPE/ 5 soya powder	0.6	0.8	0.7	1.0
LLDPE/ 10 soya powder	0.9	1.1	1.0	1.1
LLDPE/ 20 soya powder	1.8	2.1	1.9	2.4
LLDPE/ 40 soya powder	5.0	7.4	5.8	7.8

Conclusion

The LLDPE/soya powder blends can be degraded in natural compost medium. The incorporation of soya powder into LLDPE had accelerated the degradation of the blends after composting. The retention of the tensile strength and Eb reduced as the soya powder content increased upon composting. In comparison, the ENR 50 compatibilised blends has higher degradation rate compared to the uncompatibilised blends. The lower tensile strength, Eb and weight loss of compatibilised blends upon composting indicate that ENR 50 can fasten the degradation process.

References

[1] Yin, Q., Dong, A., Wang, J. And Yin, Y. 2008. *Polymer Composites.* 29(7):745-749.

[2] Abdul Majid, R., Ismail, H. and Mat Taib, R. 2009. *Polymer - Plastics Technology and Engineering.* 48(9): 919-924.

[3] Hamza, Z.P., Anna Dilfi, K.F., Kurian, T. and Bhat, S.G. 2009. *International Journal of Polymeric Materials.* 58(5): 257-266.

[4] Wahab, M.A. & Mottaleb, M.A. 2001. *Korea Polymer Journal.* 9(6): 297-302.

[5] Pavlath, A.E. & Robertson, G.H. 1999. *Critical Reviews in Analytical Chemistry.* 29(3): 231-241.

[6] Sam, S.T., Ismail, H. and Ahmad, Z. 2009. *Journal of Vinyl and Additive Technology,* 15(4): 252-259.

[7] Sam, S.T., Ismail, H. And Ahmad, Z. 2010. *Journal of Vinyl and Additive Technology.* 16(4): 238-245.

[8] Kim, H.-S, Kim, H.-J, Lee, J.W. and Choi, I.-G. 2006. *Polymer Degradation and Stability*. 91(5): 1117-1127

[9] Sharma, N., Chang, L.P., Chu, Y.L., Ismail, H., Ishiaku, U.S. and Mohd Ishak, Z.A. 2001. *Polymer Degradation and Stability.* 71(3): 381-393.

[10] Guohua, Z., Ya, L., Cuilan, F., Min, Z., Caiqiong, Z. and Zongdao, C. 2006. *Polymer Degradation and Stability.* 91(4): 703-711

PREPARATION AND CHARACTERISATION OF EPOXIDIZED NATURAL RUBBER/PALM STEARIN ALKYD BLENDS

Khong Yoke Kum & Gan Seng Neon
Chemistry Department, University of Malaya, 50603 Kuala Lumpur.

Abstract

A self-crosslinkable blend was obtained via blending of epoxidized natural rubber with 50% mol of epoxidation (ENR 50) and alkyd containing high carboxylic acid (-COOH) side chains at ambient temperature. In the present work, a series of alkyds with different -COOH contents were synthesised from palm stearin and the blend reactions of these alkyds with ENR 50 were analysed by FTIR. The decrease in the epoxide content after 4 h of blending suggests the consumption of the epoxide groups of ENR 50 via ring-opening reaction by the -COOH groups of alkyds. The extent of crosslink in the blends was reflected from the percentage of swelling in toluene, and from the glass transition temperature, T_g of the blends. The crosslink density in the blend was found to be proportional to the amount of -COOH groups of the alkyd prior to blending.

Keywords: *Alkyd, crosslink, epoxidized natural rubber, FTIR, glass transition temperature self-crosslinkable blend, swelling.*

Introduction

Alkyd resins are oil-modified polyesters which are widely used in the paint and surface coating industries. They are prepared through polycondensation of polyacids with polyhydric alcohols, and fatty acid is present as a major part of its composition [3]. The common raw materials used in preparation of alkyds are phthalic anhydride (PA), glycerol and fatty acids [2]. Although fatty acids are commonly used in alkyd formulations, some formulators chose to use whole oil instead as such approach is more economical. The types and compositions of oil used in the preparation of alkyd resin may influence the alkyd properties, such as its viscosity and adhesion.

Malaysia is the second largest producer of palm oil in the world after Indonesia, exporting a total of 23.06 million tonnes of palm oil products in the year 2010 [1]. Palm oil exists as semi solid at room temperature and can be fractionated into liquid (palm olein) and solid (palm stearin) fractions. Whilst palm olein receives higher demand as cooking oil, palm stearin is the less valuable component and is always traded at a lower price. It is used as hard fats in the production of baking goods and as a vegetable alternative to tallow in oleochemical industry [6]. Due to the lower cost, we have chosen palm stearin in the preparation of alkyds in this work.

Epoxidized natural rubber (ENR) is a chemically modified natural rubber where parts of the isoprene units are converted to oxirane rings. The increased level of epoxide groups in ENR caused it to be more polar, thus enhance its resistance towards oils and permeability to gas. In addition, ENR possesses better mechanical properties such as good abrasion resistance, higher wet grip and good damping properties compared to natural rubber [5]. ENR contains both unsaturated sites and epoxide groups, which provide sites for reactions with a large number of chemicals and functional groups. Several studies have shown that ENR formed self-vulcanisable blends with chlorosulfonated polyethylene, Hypalon [8]; poly(vinyl chloride), PVC [10]; zinc-sulfonated EPDM [7] and dodecanedioic acid [9].

In this work, 3 alkyds with different amount of -COOH contents were synthesized from palm stearin, glycerol and PA. These alkyds were then blended with ENR 50 at ambient temperature and the reaction between the blend components was investigated. Percentage of

swelling in toluene and DSC analysis were conducted to investigate the extent of crosslink in each blend.

Materials and Method

Materials

Refined, bleached and deodorised (R.B.D.) palm stearin and glycerol with 99.5% purity were kind gifts from Emery Oleochemicals Malaysia Sdn. Bhd., while ENR 50 was kind gift from Rubber Research Institute Malaysia (RRIM). PA was purchased from DC Chemical Korea Corporate Limited. All other reagent grade chemicals were used as received.

Alkyds syntheses

Alkyd P0 was synthesised in two stages which begins with alcoholysis of palm stearin with glycerol at temperature 210-220°C for 2 h with constant stirring at 220 rpm. This was then followed by esterification reaction where PA was added and temperature was raised to 220-230°C. The acid value of the reaction mixture was checked periodically. The reaction was preceded until the acid value reach ≤ 15 mg KOH/g resin. Alkyd P1 and Alkyd P2 were obtained by further reacting parts of the synthesised Alkyd P0 with PA. 4.23×10^{-4} mol of PA/g of Alkyd P0 was used in the synthesis of Alkyd P1 while 7.78×10^{-4} mol of PA/g of Alkyd P0 was used in the synthesis Alkyd P2.

FTIR analysis of alkyd

Thin film of alkyd was casted on potassium bromide (KBr) cell and the infrared spectra of the alkyd was recorded using *Perkin Elmer*, Spectrum 400 FTIR spectrometer with 16 scans from 400 to 4000 cm^{-1} at a resolution of 4 cm^{-1}.

Preparation of ENR 50/Alkyd blends

Mixing was performed at ambient temperature (28-30ºC). 23 g of 10% (w/w) ENR 50 solution (in toluene) were mixed with 3.8 g of 60% (w/w) alkyd solution (in toluene) in a covered sample bottle. The blend mixture was stirred for 4 h before being withdrawn and air-dried at room temperature for 24 h in fume hood. The sample was afterwards dried in a vacuum oven at 30°C. The compositions of the ENR 50/Alkyd blends are shown in Table 1.

Table 1: Amount of functional groups in the initial ENR 50/Alkyd blends

ENR 50/Alkyd blend	Weight of ENR 50/g	Weight of Alkyd /g	Amount of Functional groups /104 mol		Ratio of -COOH to epoxide
			Epoxide	-COOH[a]	
ENR50/AlkP0	2.30	2.30	151	5.0	0.03
ENR50/AlkP1	2.31	2.31	152	12.0	0.08
ENR50/AlkP2	2.30	2.30	151	18.2	0.12

[a]Amount of -COOH = (Final Acid value of alkyd)/ 56100 × weight of alkyd

Charaterisation of ENR 50/Alkyd blends

FTIR analysis

A thin layer of the viscous solution of ENR 50/Alkyd blends (in toluene) was spread onto a KBr cell immediately after the specified reaction time. The solvent was removed by blowing with hot air and the FTIR spectrum was recorded on a *Perkin Elmer* Spectrum 400 FTIR spectrometer, with 16 scans from 4000 cm^{-1} to 400 cm^{-1} and resolution of 4 cm^{-1}.

Swelling percentage in toluene

Known weight of dried blend sample was immersed in toluene for 48 h at room temperature. The weight of the gel (swollen blend sample) after the immersion was recorded as W_s. The gel was then dried in vacuum oven at 60°C until a constant dried gel weight, W_d was obtained. The swelling % was calculated using Equation 1.

$$\text{Swelling}\,\% = \frac{W_s - W_d}{W_d} \times 100 \quad (1)$$

DSC analysis

Mettler Toledo Differential Scanning Calorimeter (Model No: DSC 822e) equipped with sub-ambient cooling accessory and nitrogen flow gas was used to determine the T_g of the samples. 5-10 mg of the sample was encapsulated in an aluminium sample pan and was scanned from -60ºC to 60ºC at a heating rate of 20ºC·min^{-1}.

Results and Discussion

Preparation and characterisation of alkyds

Figure 1 outlines the plausible reaction scheme for the synthesis of PA-modified alkyd. The first step involved the preparation of Alkyd P0, which begins with alcoholysis of triglycerides (from palm stearin) with glycerol into monoglyceride precursors, followed by esterification with PA. Later, parts of the Alkyd P0 were reacted with calculated amount of PA in order to form PA-modified alkyds, Alkyd P1 and Alkyd P2. It is noteworthy that during incorporation of PA into Alkyd P0, there is no water collected. Such occurrence suggests that the added PA could have reacted with the free hydroxyl (-OH) groups of Alkyd P0 by opening its anhydride ring to form monoester thus increased the amount of free -COOH groups in the alkyd chains.

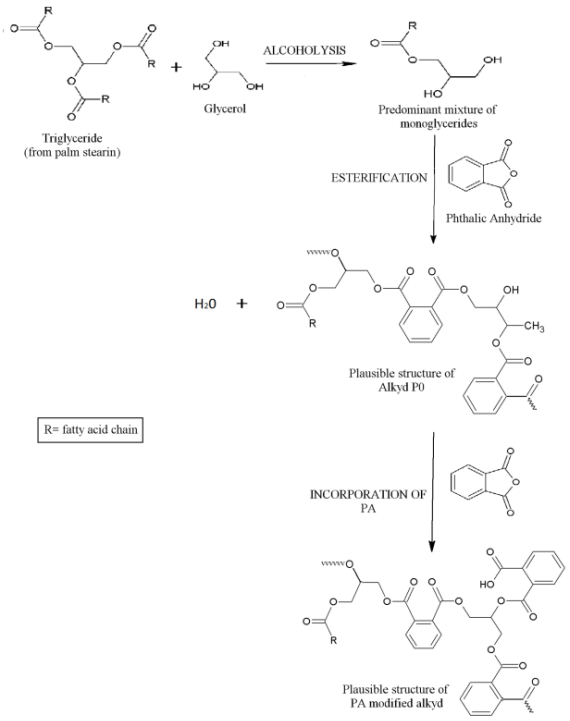

Figure 1: Preparation of alkyd resins

Figure 2 shows the normalised FTIR spectra of Alkyd P0, P1 and P2. The expanded spectra of the alkyds at 2800-3600 cm^{-1} region is shown inset in the figure. All the peaks in the

spectra were normalised against the peak at 1456 cm^{-1} for better comparison. Qualitatively, all the three alkyds show similar characteristic peaks as they were synthesised from the same raw materials but with different proportions of PA incorporated. However, there is noticeable change observed in the –OH stretching vibrations at 3476 cm^{-1}. The decrease in the peak absorbance, A_{3476}/A_{1456} from 7.2 in Alkyd P0 to 6.7 and 6.4 in Alkyd P1 and Alkyd P2 respectively suggests that the hydroxyl groups were consumed during incorporation of PA into Alkyd P0. This is consistent with the synthesis route suggested earlier (Figure 1) where hydroxyl groups from Alkyd P0 react with the incorporated PA to form half ester and free –COOH groups was generated as side chain in the alkyd.

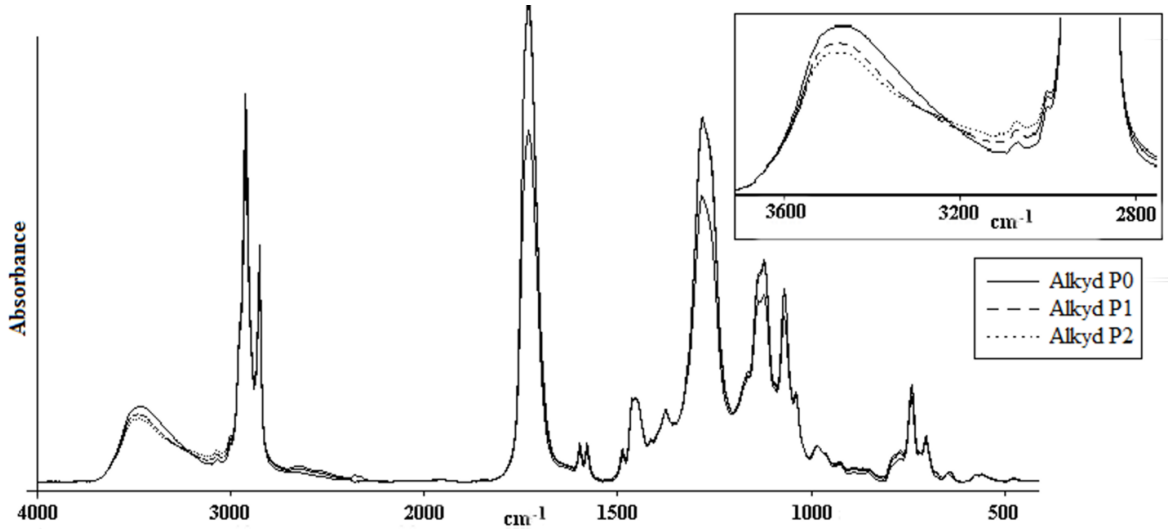

Figure 2: Normalised FTIR spectra of Alkyd P0, P1 and P2.

ENR 50/Alkyd blends

Solvent casting technique was used to blend ENR 50 and alkyd in a common solvent, toluene. 3 sets of blends, ENR50/AlkP0, ENR50/AlkP1 and ENR50/AlkP2, were prepared by stirring ENR 50 with Alkyd P0, Alkyd P1 and Alkyd P2 respectively for a period of 4 h at room temperature. Visual observation shows that the viscosities of the blends increased with blending time. The blends were then left to dry in vacuum oven at room temperature and dried films were obtained.

FTIR analysis of ENR 50/Alkyd blends

Figure 3 shows the FTIR spectra of ENR 50, Alkyd P2 and ENR50/AlkP2 blend. From the spectra, it can be observed that ENR50/AlkP2 blend contained peaks from both ENR 50 and Alkyd P2.

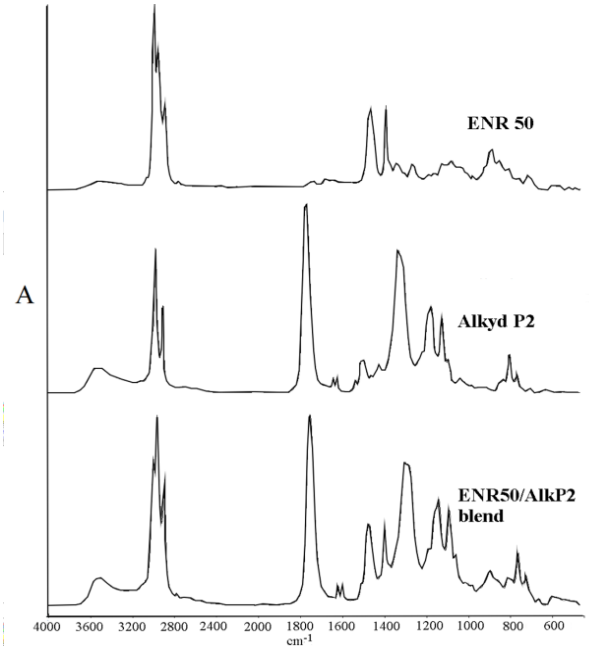

Figure 3: FTIR spectra of ENR 50, Alkyd P2 and ENR50/AlkP2 blend

Reaction between ENR 50 and alkyds were studied by monitoring the changes in the epoxy ring stretching peak at 873 cm^{-1}. FTIR peak absorbance ratio of the blends at 873 cm^{-1} to a reference peak at 1599 cm^{-1} (A_{873}/A_{1599}) was calculated, and summarized in Table 2. These ratios were then compared with those of the initial blends (blending time = 5 min).

Table 2: FTIR absorbance ratio, A_{873}/A_{1599}, of ENR 50/Alkyd blends after blending for 5 min and 4 h

Blend	A_{873}/A_{1599}		% decrease in A_{873}/A_{1599}
	Blending time = 5 min	Blending time = 4 h	
ENR50/AlkP0	4.4	4.3	3.3
ENR50/AlkP1	4.3	4.0	7.8
ENR50/AlkP2	3.5	3.0	11.9

As observed from Table 2, the ratio of A_{873}/A_{1599} decreased in each blend. It suggests that ring opening of the epoxide groups in ENR has taken place during the blending. The change in A_{873}/A_{1599} also reflects the extent of reaction between the epoxide groups of ENR 50 with -COOH groups of alkyd. ENR50/AlkP2 blend experienced the highest extent of reaction, followed by ENR50/AlkP1, and ENR50/AlkP0 blend. This is attributed to the amount of -COOH groups present in the alkyds.

Swelling % of ENR 50/Alkyd blends in toluene

The crosslink density in the ENR 50/Alkyd blend is reflected by the % of swelling in toluene. Blend with higher crosslink density tends to have higher swelling resistance. Table 3 summarized the swelling capacities of ENR50/AlkP0, ENR50/AlkP1 and ENR50/AlkP2 blends in toluene.

Table 3 : Swelling capacities of ENR50/AlkP0, ENR50/AlkP1 and ENR50/AlkP2 blend in toluene

Blend	Swelling Capacities / %
ENR50/AlkP0	1198
ENR50/AlkP1	536
ENR50/AlkP2	380

Both ENR 50 and alkyds are soluble in toluene. However, their blends showed reduction in solubility in toluene, presumably due to the presence of crosslinks in the blend matrix. From the swelling capacities of the blends, ENR50/AlkP2 has the highest amount of crosslinks, followed by ENR50/Alkyd P1, and ENR50/Alkyd P0 blend. The results are in agreement with FTIR analysis where crosslink density of the blend is proportional to the amount of -COOH groups present in the alkyd prior to blending.

DSC analysis

DSC analysis was conducted on the blend constituents and the dried film of the blend samples. T_g was obtained by taking the temperature at the midpoint of the inflection in DSC curves and the results are shown in Table 4.

Table 4: Glass transition temperature of blend constituents and ENR 50/Alkyd blends as determined by DSC

Sample	Blending time / h	T_g / °C
ENR 50	-	-18.2
Alkyd P0	-	-21.8
Alkyd P1	-	-20.4
Alkyd P2	-	-17.4
ENR50/AlkP0	0.08	-25.9
	4	-25.1
ENR50/AlkP1	0.08	-23.7
	4	-22.5
ENR50/AlkP2	0.08	-22.8
	4	-18.0

With reference to Table 4, all the blend samples exhibited single T_g and this reflects the miscibility of ENR 50 and alkyds when they are blended at 50:50 weight ratios at ambient temperature. Alkyds with different amount of -COOH produced blends with different T_g. There is only marginal increase in the T_g values of ENR50/AlkP0 blend, from -25.9°C to -25.1°C after 4 h of blending. This is due to the fact that there is relatively lower amount of -COOH groups present in Alkyd P0 to participate in the formation of crosslinks. However, PA-modified alkyds could produce blends with higher T_g. For example, Alkyd P2 which has the highest amount of -COOH groups resulted in blend with the highest T_g.

It is noteworthy that the increase in T_g of the blend may not be solely due to the formation of crosslink between the epoxide groups of ENR and -COOH groups of alkyds. Other factors such as presence of polar hydroxyl groups in the ring-opened structure of ENR/`Alkyd blend, which responsible for the occurrence of inter- and intra- molecular hydrogen bonding could have contributed to the increase in T_g as well [4].

Conclusion

Three alkyds with different –COOH contents were synthesised from palm stearin, glycerol and PA. FTIR characterization of the alkyds shows that Alkyd P2 contains the highest -COOH followed by Alkyd P1 and Alkyd P0. The success of the incorporation of alkyds into ENR 50 chain is shown from the changes in the FTIR peaks of the blends. DSC analysis confirms the miscibility of ENR 50 and alkyd, where all the blends exhibit single T_g. The extent of crosslinking in the blend is proportional to the -COOH content in alkyd. Alkyd with higher amount of -COOH groups resulted in blend with lower swelling percentage in toluene, and higher T_g.

Acknowledgements

This work was financially supported by University of Malaya PPP Grant (PS353-2010A)

References

[1] Choo, Y.M. 2011. *Overview of the Malaysian Oil Palm Industry 2010*. Source: http://econ.mpob.gov.my/economy/Overview%202010_final.pdf

[2] Cuillo, A.P. 1996. *Industrial minerals and their uses: a handbook and formulary*. New Jersey: Noyes Publications.

[3] Deligny, P. & Tuck, N. 2000. *Resins for surface coatings: Alkyds & polyester*. London: John Wiley & Sons Inc.

[4] Gan, S.N. & Burfield, D.R. 1989. *Polymer.* 60: 1903-1908.

[5] Gelling, I.R. 1991. *Journal of Natural Rubber Research,* 6(3): 184-205.

[6] Gunstone, F. 2004. *The Chemistry of Oils and Fats: Sources, Composition, Properties and Uses*. Oxford: Blackwell Publishing Ltd.

[7] Manoj,N.R., De, S.K., De, P.P. and Peiffer, D.G. 1994. *Journal of Applied Polymer Science*. 53: 361-370.

[8] Mukhopadhyay, S. & De, S.K. 1990. *Journal of Material Science.* 25: 4027-4031.

[9] Pire, M., Norvez, S., Iliopoulos, I., Rossignol, B. L. and Leibler, L. 2010. *Polymer.* 51: 5903-5909.

[10] Ramesh, P. and De, S.K. 1991. *Journal of Material Science*. 26: 2846-2850**.**

THE EFFECTS OF TERT-BUTYL PERBENZOATE ON THE TENSILE AND FLEXURAL PROPERTIES OF SUGARCANE BAGASSE REINFORCED POLYESTER COMPOSITES

M.Z. Salihin, L. Musa, N.Z. Noriman & A.M. Mustafa Al Bakri

Center of Excellence Geopolymer & Green Technology (CEGeoGTech), School of Materials Engineering, Universiti Malaysia Perlis (UniMAP), Kompleks Pengajian Jejawi 2, 02600 Arau, Perlis, Malaysia

Abstract

The effects of tert-butyl perbenzoate (TBP) as catalyst at elevated temperature 110°C on the mechanical properties of sugarcane bagasse reinforced polyester (SBRP) composites were investigated. Sugarcane bagasse fibers were alkalized with different sodium hydroxide (NaOH) solution 1, 3 and 5% combined with different fiber loading formulation 0, 20, 30 and 40 php, and hot-pressed to form natural fibers composite were prepared. The results indicated that incorporation of bagasse fiber composites alkalized with 3% NaOH solution improved the tensile strength (TS) and tensile modulus (TM) of reinforced composites meanwhile the untreated bagasse gave the lowest value. However, the elongation at break (E_b) decreased steadily with increasing bagasse fiber content in both composites. The similar trend was obtained for the flexural strength (FS) and flexural modulus (FM). The scanning electron microscopy (SEM) observations on the flexural surface of composites showed the surface modification of the fiber occurred thus improved fiber-matrix adhesion.

Keywords: *Flextural properties, NaOH, SBRP composites, tensile properties, tert butyl perbenzoate (TBP).*

Introduction

Fiber–reinforced plastic composites have played a dominant role for a long time in a variety of applications for their high specific strength and modulus. Fiber incorporated plastics have been very popular due to their flexibility, their lightness and the ease of fabrication of complicated shapes with economic savings in contrast to fiber reinforced metals/ alloys. In addition, these composites can easily substitute for conventional materials in several areas such as the building industry, transportation and consumer goods. Some of the attempts made in recent times for the utilization of natural fibers through composite material technology have indicated their potential as substitutes for conventional materials such as wood and glass fiber reinforced plastics (GFRP) in many applications [1].

In recent years, organic fillers, such as cellulose-based fibers have slowly taken root in the market to replace synthetic materials [2]. Cellulose-based fibers (natural fibers) come from renewable and relatively inexpensive resources, and also by the addition of natural fibers, such as wood fibers, flax or sisal to polymeric matrices can result in feasible composites concerning mechanical and economic points of view [3]. Composites based on natural fibers are environmentally superior to those based on synthetic fibers, such as fiberglass. Recent studies reported that the incineration of components with natural fibers uses 45% less energy, and results in lower air emissions [4].

Among the agro-industrial residue diverse, sugarcane bagasse is detached to be a residue widely generated in high proportions and contains cellulose (46.0%), hemicellulose (24.5%), lignin (19.95%), fat and waxes (3.5%), ash (2.4%), silica (2.0%) and other elements (1.7%) [5]. Bagasse is a vegetable fiber mainly constituted by cellulose, that is a glucose-polymer with relatively high modulus, often found as fibrillar component of many naturally occurring composites (wood, sugarcane straw and bagasse) in association with lignin [6].

Alkali treatment is viewed as one of the widely employed chemical treatment techniques for surface modification of cellulosic fibers for the purpose of improving their adhesion properties with various thermosetting binders [7, 8, 9]. This treatment involves partial removal of the cementing materials (hemicellulose and lignin) and other impurities from the fiber surfaces [10]. A similar change due to alkali treatment at limited concentrations of NaOH has been reported to improve some of the mechanical properties of phenol formaldehyde bonded composites [7]. Alkali treatment of cellulosic fibers, also called mercerization, improves the fiber surface adhesive characteristics by removing natural and artificial impurities, thereby producing a rough surface topography.

To the best of our knowledge, the effects of tert-butyl perbenzoate (TBP) as catalyst on properties of sugarcane bagasse reinforced polyester (SBRP) composites were not reported yet. Therefore in this work, the effects of tert butyl perbenzoate (TBP) as catalyst at elevated temperature 110°C on the tensile and flexural properties of sugarcane bagasse reinforced polyester (SBRP) composites were carried out. The scanning electron micrograph of the surface of untreated and treated bagasse fiber was also examined.

Materials and Method

Materials and preparation of composites

Materials and their characteristics used in this study are shown in Table 1.

Table 1: Materials Description

Materials	Descriptions	Sources
Sugarcane bagasse fiber	Averages sizes average of 1.18 mm and 600 μm	Kilang Gula Felda Perlis Sdn. Bhd. (KGFP)
Tert-butyl perbenzoate ($C_{11}H_{14}O_3$)		Sigma-Aldrich
Sodium hydroxide pellets extra pure		Hamburg Chemicals
Zinc strearate ($C_{36}H_{70}O_4Zn$)		Sigma-Aldrich

Bagasse fibers were soaked in each 1, 3 and 5% NaOH solution at room temperature for 1 h, maintaining a liquor ratio of 20:1. Then the fiber were washed several times with distilled water to remove any NaOH solution sticky to the fiber and the fibers were oven dried at 70°C for 72 h [11]. The bagasse fibers then keep in desiccators before compounding.

All materials were weighted by following the formulation to produce composite with percentage fiber that stated in Table 2. The composites were prepared by mixing bagasse fiber, unsaturated polyester, tert-butyl perbenzoate and zinc stearate with different fiber loading using high dispersion impeller. Catalyst was put in the mixer followed by the resin. The mixer was switched on to start the mixing process. After that, lubricant was put in the mixer followed by the fiber to get a homogenous compound. The mixing process is conducted for 30 min. After that, the homogenous compounds were put into the mold for the hot pressing process.

After preparation, the samples were hot pressed by using hydraulic hot press machine Technopress 50HC – β model. The compression was done at 110°C for 5 min, and the samples were allowed to cool for 5 min by cooling process. The pressure was set at 150 psi. In the compression molding, a hollow rectangular mold was used which the dimension is 170 mm × 135 mm × 3 mm.

Table 2: Composites Formulation

Materials	Untreated	Treated with NaOH
Unsaturated Polyester (php)	100	100
Sugarcane Bagasse (php)	0, 20, 30, 40	0, 20, 30, 40
Zinc Stearate [a]	6	6
Tert-Butyl Perbenzoate [b]	1	1
NaOH [c]	-	1, 3, 5

[a] 6 php from weight of unsaturated polyester
[b] 1 php from weight of unsaturated polyester
[c] 1, 3, 5 php from weight filler

Tensile Test

An *Instron 5569* tensile tester was used for the tensile analysis of the samples using ASTM D638 at room temperature. The rectangular test specimens were stretched at a speed of 5 $mm \cdot min^{-1}$ under a cell load of 2500 N. At least 8 samples for each formulation were tested to ensure persistence.

Flexural Test

Three-point flexural tests were performed in accordance to ASTM D790. The support span was set at 50 mm. Tests were conducted at a crosshead speed of 2 $mm \cdot min^{-1}$ on the same *Instron 5569* tensile testing machine used for tensile tests. At least 8 samples for each formulation were tested to ensure persistence.

Morphology Study

The tensile fracture surface of the composites sample was studied with scanning electron microscopy (SEM) model *JOEL JSM- 6460LA*. The objective of this analysis is to study the mode of failure of the composite system. The surface of specimens was sputter coated with a thin layer of gold (2 nm) to avoid electrostatic charging during examination.

Results and Discussion

Tensile Properties

Figure 1 shows the effect of NaOH solution concentration at 20, 30 and 40% (w/w) on tensile strength of sugarcane bagasse reinforced unsaturated polyester, respectively. It is observed that the use of treated bagasse fiber improved the tensile strength of the polyester composites compared to the untreated bagasse fiber. This implies that, most of the fats, lignin and pectin covered the fiber surface are removed after alkali treatment, in the combination with the matrix improved the fiber adhesive character.

From the results, it is observed that all treated fibers have higher tensile and flexural strength than those of untreated fibers, with obvious higher properties shown in 3% NaOH solution concentration treated fibers. The fibrillation of fibers created a superior interfacial adhesion in the composites [12]. Fiber fibrillation is breaking down the composite fiber bundle into smaller fibers, increasing the effective surface area available for contact with the wet matrix [13]. However, for the 5% NaOH treated fiber composites, the mechanical properties decreased with the greater fibrillation owing to the relatively larger fiber ends available for crack initiation. This could lower the effective stress transfer at the interface [12]. The maximum improvement in tensile strength was observed in the 3% NaOH treated fiber composites. It was believed that better interfacial adhesion along with better fibrillation of these fibers contributed effectively to the enhancement in tensile strength.

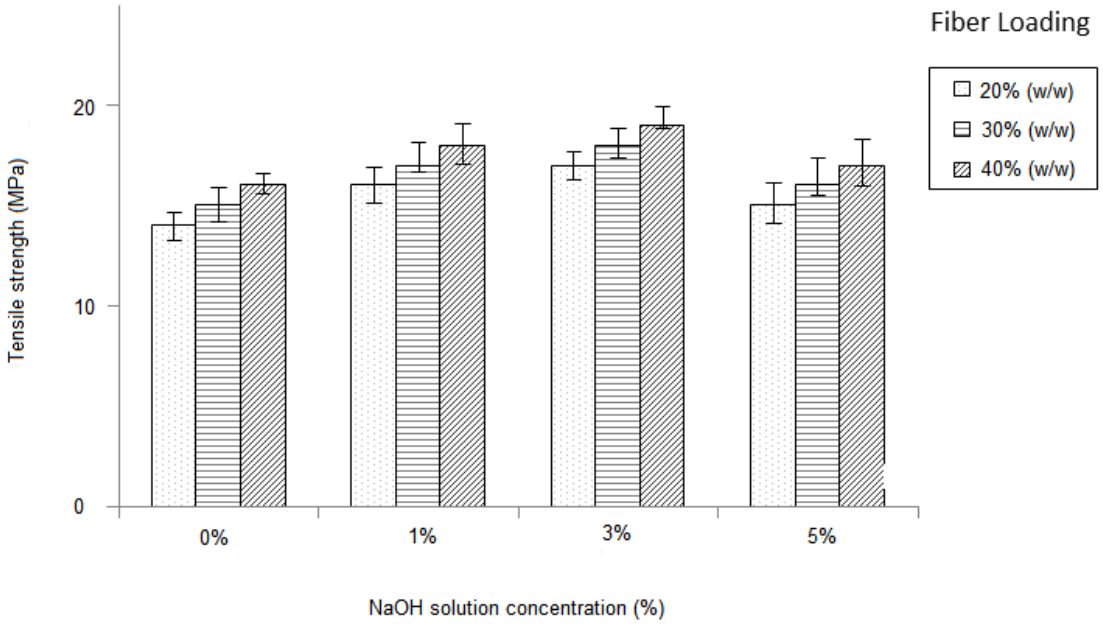

Figure 1: The effect of different NaOH solution concentration on tensile strength of sugarcane fiber reinforced unsaturated polyester composites with different fiber loading

The effect of NaOH solution concentration at 20, 30 and 40% (w/w) on elongation at break of sugarcane bagasse reinforced unsaturated polyester composites are illustrated in Figure 2. It can be seen that the elongation at break for the sugarcane bagasse reinforced unsaturated polyester decreases steadily with increasing bagasse fiber content in both composites. From the graph, indicates that elongation at break of treated bagasse fiber composites shows the lower value compared to untreated composites. Two hypotheses can be considered; (A) fibers are failed points that can generate a crack, and (B) there is a sliding of the fibers in relation to the matrix. The elongated materials present ductile fracture and the failed points in composites exhibit the brittle fracture [14]. This was probably due to the fact that modified fibers were rendered more hydrophobic and thus enhanced compatibility between fiber and matrix resin consequently. The improvement of fiber-matrix bonding would increase the strength, stiffness and interfacial adhesion of the composites. Moreover, this also was due to the improved fiber-matrix adhesion (to give more stiffness to the composites) and because modified fiber were prone to split and fall apart, so that, fiber was more brittle after modification. Consequently, we can conclude that in this case improved wetting of the treated fibers by the matrix was responsible [15].

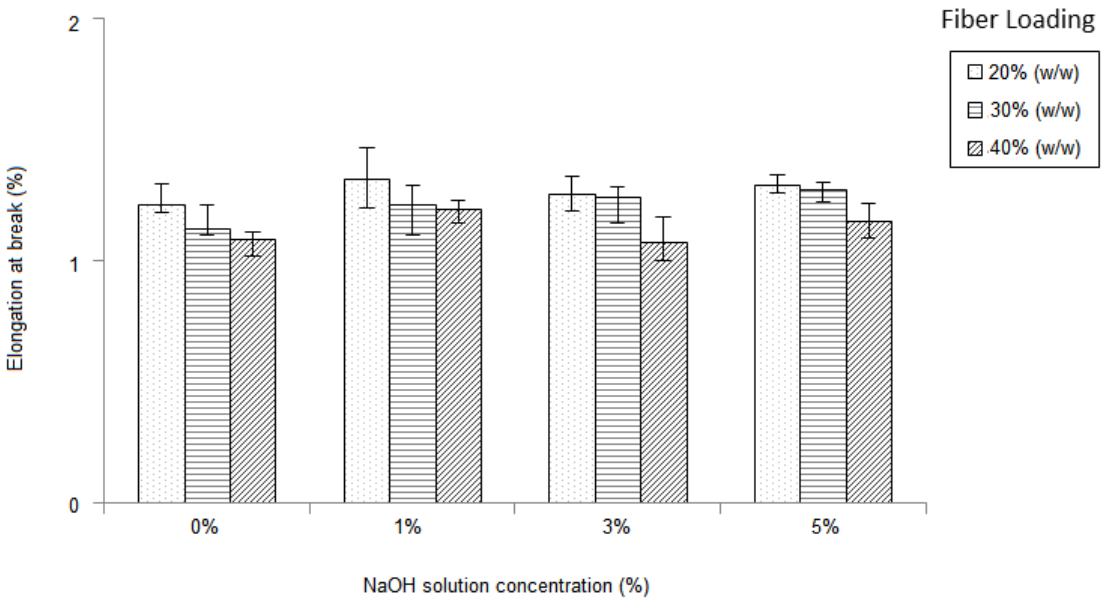

Figure 2: The effect of different NaOH solution concentration on elongation at break of sugarcane fiber reinforced unsaturated polyester composites with different fiber loading.

Figure 3 shows the effect of NaOH solution concentration at 20, 30 and 40% (w/w) on modulus of elasticity of sugarcane bagasse reinforced unsaturated polyester composites. The Young's modulus of the composites increased with increasing the filler loading and NaOH solution concentration. The increase in Young's modulus with increase in filler loading is expected since the addition of filler increase the stiffness of the composites. It can be seen that 40% (w/w) of bagasse fiber of 3% NaOH solution concentration have the highest value of modulus of elasticity. Here 40 volume % treated bagasse fiber with 3% NaOH solution concentration – reinforced composites showed 28% of increase in Young's modulus. However, for the 5% NaOH treated fiber composites, the mechanical properties decreased with the greater fibrillation owing to the relatively larger fiber ends available for crack initiation. This could lower the effective stress transfer at the interface [12].

This variation can be explained as follows: During mercerization, the NaOH reacts with hydroxyl groups of the cementing material hemicelluloses, and it brings the destruction of the cellular structure and thereby the fibers split into filaments. This phenomenon is termed as fibrillation, which breaks the untreated fiber bundle down into smaller ones by the dissolution of the hemicelluloses. This fibrillation increases the effective surface area available for contact with the matrix [12]. The removal of lignin and hemicelluloses affects the tensile characteristics of fibers. When the hemicelluloses fractions are removed, the interfibrillar region is likely to be less dense and rigid which can make the fibrils more capable of rearranging themselves along the direction of tensile deformation. The alkaline treatment on sisal fibers causes fibrillation and a collapse of the cellular structure due to the removal of the cementing materials was reported [16]. Mercerization also increases the percentage of crystallinity index of fibers because of the removal of cementing materials, which leads to a better packing of cellulose chains.

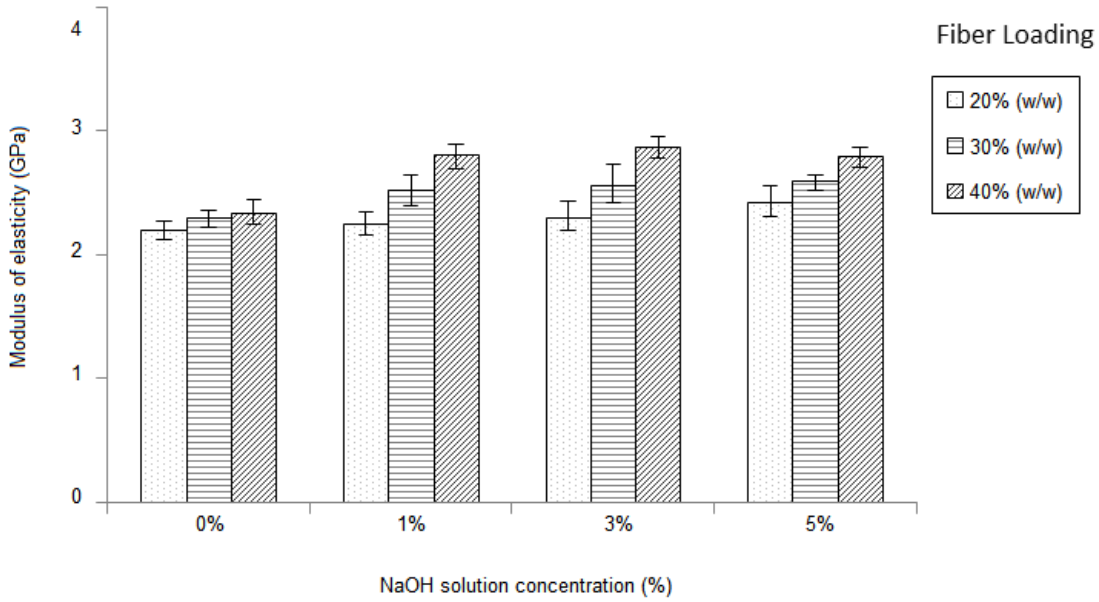

Figure 3: The effect of different NaOH solution concentration on modulus of elasticity of sugarcane fiber reinforced unsaturated polyester composites with different fiber loading

Flexural Properties

The flexural strength and modulus of bagasse fiber reinforced polyester composite are shown in Figure 4 and 5. From the figure, it can be seen that the flexural strength of the composites increase with the increasing filler loading and NaOH solution concentration. The poor flexural properties shown by the composites were attributed to the weak fiber/ matrix bonding. In production of fiberboard, poor wetting was expected due to inadequate compatibility between polar bagasse fiber and non-polar unsaturated polyester resin that lead to the weak interfacial region. These weak interfacial regions would reduce the efficiency of stress transferred between resin and fiber, thus poor strength properties can be anticipated. The quality of interfacial bonding was determined by several factors, such as, the nature of the fiber and binder as well as their composition, the fiber aspect ratio, the types of mixing procedures, processing conditions employed and on the treatment of the polymer or fiber with various chemicals, coupling agent, compatibilizer, etc [15].

The results in Figure 4 also showed that composites with 3% NaOH solution concentration higher flexural strength than other concentration. The fibrillation created a superior interfacial adhesion in the composites thus increases the flexural strength compared to the greater fibrillation of 5% NaOH solution concentration owing to the relatively larger fiber ends available for crack initiation.

Figure 5 illustrates that the flexural modulus of the composites increased due to the NaOH solution concentration. The effect on flexural modulus was more significant than on the flexural strength because the incorporation of modified fiber was still able to impart stiffness to the composites. The composites with 3% NaOH solution concentration displayed higher stiffness as compared to those with NaOH modification. This might due to the increased compatibility between the resin and the fiber. The increased compatibility results in the formation of a continuous interfacial region, which permitted a better and efficient stress transfer in the samples [15].

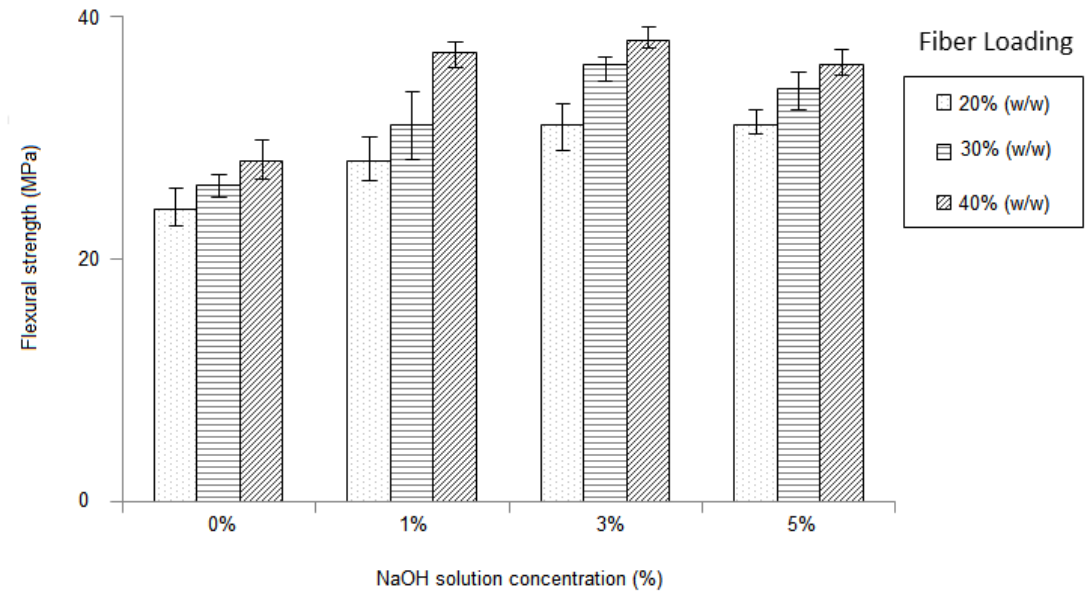

Figure 4: The effect of different NaOH solution concentration on flexural strength of sugarcane fiber reinforced unsaturated polyester composites with different fiber loading

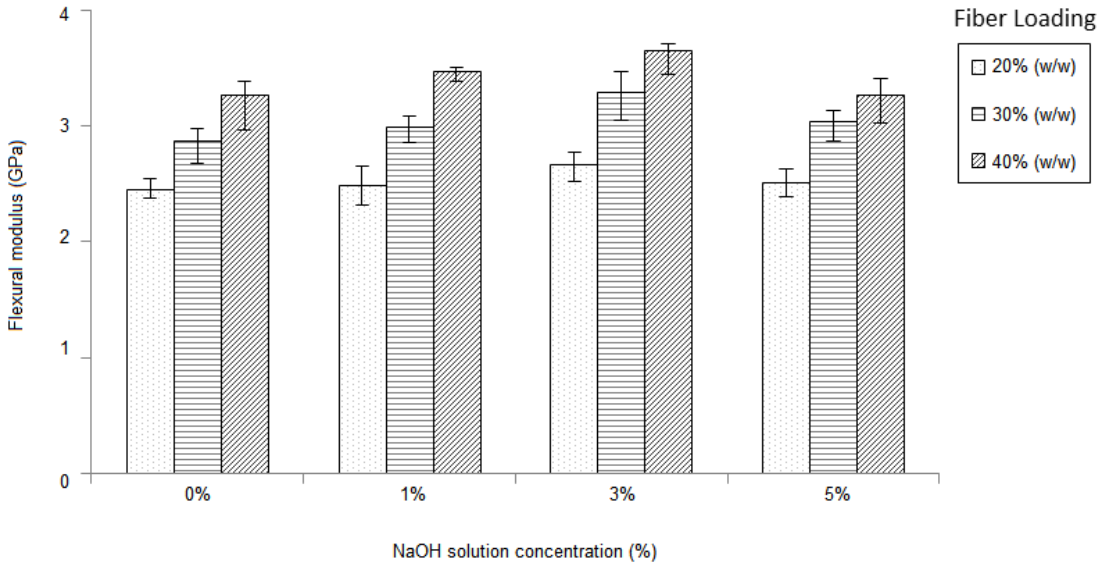

Figure 5: The effect of different NaOH solution concentration on flexural modulus of sugarcane fiber reinforced unsaturated polyester composites with different fiber loading

Morphology

Figure 6 is the SEM micrograph of the cross-section of untreated bagasse fiber. The micrograph exhibits the cellular structure of the fiber, which indicates the porous structure. According to [17] in general all natural cellulose fibers are multi cellular, where a bundle of individual cells bound by natural polymers such as lignin and pectin. The fiber used in this study refers to a bundle of individual cell. The hollow cavity called lumen exists in unit cell of the biofibers. The presence of the hollow lumen decreases bulk density of the fiber and acts as acoustic and thermal insulators [11].

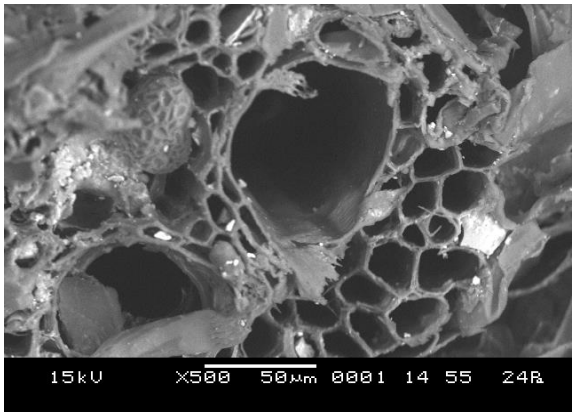

Figure 6: SEM micrographs of the cross-section of untreated bagasse fiber.

The difference between the fiber before and after alkali treatment is exhibited in Figure 7 (a) and (b). It was observed that the filaments in the untreated fiber were packed together but got split after the alkali treatment. This phenomenon is termed as fibrillation, which breaks the untreated fiber bundle down into smaller ones by the dissolution of the hemicellulose. The fibrillation increases effective surface area available for contact with the matrix [12] and hence the interfacial adhesion was improved. It can be observed that presence of waxy substances on the untreated fiber surface. According to [18], such waxy substance contributed to ineffective fiber–matrix bonding and poor surface wet out.

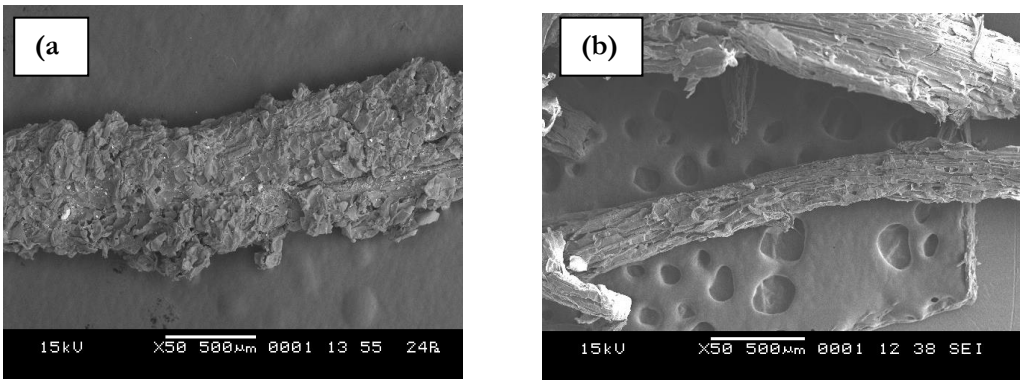

Figure 7: SEM micrographs of a bagasse fiber. (a) untreated fiber and (b) 3% NaOH treated bagasse fiber.

Conclusions

The following conclusion can be drawn from this study;

a. Tensile strength, Young's modulus, and flexural strength value were increased with increasing solution concentration of NaOH. However, 5% NaOH solution concentration modification shows the decreasing value of tensile strength, Young's modulus and flexural properties of the composites.

b. Elongation at break for the sugarcane bagasse reinforced unsaturated polyester composites decreased with increasing bagasse fiber content in both composites.

c. SEM micrograph prove that the interfacial adhesion between the bagasse fiber and unsaturated polyester matrix was enhanced when NaOH are used as surface modifier.

References

[1] Satyanarayana, K.G., Sukumaran, K., Mukherjee, P.S., Pavithran, C., & Pillai, S. G. K. 1990. *Cement and Concrete Composites*. 12(2): 117-136.

[2] Pandey, A., Soccol, C. R., Nigam, O., & Soccol, V.T. 2000. *Bioresource Technology.* 74: 69–80.

[3] Luyt, A.S., & Malunka, M.E. 2005. *Thermochim Acta.* 426: 101–107.

[4] Joshi, S.V., Drzal, L.T., Mohanty, A.K., & Arora, S. 2004. *Composite Part A: Applied Science Manufacturing*. 35: 371–376.

[5] Sene, L., Converti, A., Felipi, M.G.A., & Zilli, M. 2002. *Bioresource Technology.* 83: 153–157.

[6] Alonso, P.W., Garzone, P., & Cornacchia, G. 2007. *Waste Management*, 27: 869–885.

[7] Ndazi, B.S., Karlsson, S., Tesha, J.V., & Nyahumwa, C.W. 2007. *Composites Part A*. 38: 925-935.

[8] Ray, D., & Sarkar, B.K. 2001. *Journal of Applied Polymer Science.* 80: 1013-1020.

[9] Bisanda, E.T.N., & Ansell, M.P. 1991. *Composite Science and Technology.* 41(2): 165-178.

[10] Albano, C., Ishazo, M., Gonzalez, J., Delgado, M., & Poles, R. 2001. *Material Research Innovation.* 4: 284-293.

[11] Vilay,V., Mariatti, M., Mat Taib, R., & Todo,M. 2008. *Composites Science and Technology*. 68(3-4): 631-638.

[12] Cao, Y., Shibata, S.S., & Fukumoto, I. 2006. C*omposites Part A: Applied Science and Manufacturing*. 37(3): 423-429.

[13] Lai, Y.Z. 1996. *Chemical modification of lignocellulosic materials*, In Hon, D. (Ed). New York: Marcel Dekker Inc.

[14] Sawyer, L. C., & Grubb, D. T. 1996. *Polymer microscopy*. London: Chapman & Hall.

[15] Khalil, H.P.S.A., Issam, A.M., Ahmad, S.M.T., Suriani, R. & Awang, A.Y. 2007. *Industrial Crops and Products.* 26: 315-323.

[16] Vazquez, A., Dominguez, V.A., Kenny, J. M. 1999. *Journal of Thermoplastic Composite Materials.* 12: 477-497.

[17] Reddy, N. & Yang, Y. 2005. *Trends in Biotechnology*, 23(1): 22-27.

[18] Mohanty, A.K., Wibowo, A., Misra, M., Drzal, L.T. 2003. *Composites part A: Applied Science and Manufacturing.* 35(3): 363-370.

THERMOPLASTIC STARCH COMPOSITES REINFORCED BY RICE HUSK CELLULOSE NANOCRYSTALS

Nurain Johar & Ishak Ahmad*

Polymer Research Center, Faculty of Science and Technology,
School of Chemical Sciences and Food Technology, Faculty of Science and Technology,
Universiti Kebangsaan Malaysia, 43600 Bangi, Selangor, Malaysia.

Abstract

Rice husk cellulose nanocrystals-reinforced thermoplastic starch composite was prepared by solution casting technique. Rice husk was undergo alkali treatment, bleaching process and sulphuric acid hydrolysis before cellulose nanocrystals can be produced. Characterization on rice husk fibers were done to investigate the properties of the fiber that to be used as filler to reinforce glycerol plasticized starch in the preparation of composites. The rice husk cellulose nanocrystals content varies from 0% to 10% (w/w). Transmission electron microscopy (TEM) was used to determine the diameter and length distribution of cellulose nanocrystals. FTIR spectra showed that certain components in chemical composition of rice husk which are hemicelluloses, lignin, and pectin were removed during chemical treatment. X-ray diffraction analysis (XRD) results revealed that the crystallinity index was increased from raw fibers to cellulose nanocrystals. Tensile strength and Young's modulus of the starch/rice husk cellulose nanocrystals composite films were enhanced by the incorporation of the cellulose nanocrystals. Rice husk cellulose nanocrystals at the optimal 6% filler loading level exhibited a higher reinforcing efficiency for plasticized starch plastic than any other filler loading level.

Keywords**:** *Cellulose nanocrystals, rice husk, solution casting, thermoplastic starch.*

Introduction

There was growing interest in preparing the biodegradable materials through the years. Researchers are trying to develop the products which called biodegradable 'green' composites by combining natural fibres with biodegradable resins [1]. This was due to the promising result showed by these composite which that they are environmentally-friendly, fully degradable and sustainable. At the end, they can easily dispose or decomposed without harming the environment and create pollution.

Several studied had been carried out and starch is the best candidates among the natural polymers to be used as raw materials in the production of biodegradable composites. Starch is natural renewable polymer obtained from variety of crops. The major attraction about the starch is that it is cheap materials, easily to find and has fast biodegradation rate. In recent years, starch has been used to produce biodegradable plastics. Starch itself is not the true thermoplastics but in the presence of plasticizers and under high temperature and shear, starch can be processed into a mouldable thermoplastic, known as thermoplastic starch (TPS).

Thermoplastic starch (TPS) may have several disadvantages when compared to the certain plastics that currently been used nowadays. TPS shows some drawbacks which were water sensitive and have poor mechanical properties. This was due to the hydrophilic nature and thus their sensitivity to moisture content. Several studies that have been carried out showed that the addition of water [2] and the glycerol as plasticizers [3] can be considered as one way to improve the mechanical properties. Other than that, the mechanical properties and its water resistance can be improved by mixing it with certain synthetic polymers [4], adding crosslinking agents [5, 6] or adding lignin [7].

Furthermore, another approach to overcome the material weaknesses is to use fibers as reinforcement for TPS. The fibers described in the literature for this purpose are cellulosic microfibrils [8]. The introduction of organic filler such as cellulose fibers to a polymer matrix

increases its strength and stiffness which then can enhance the mechanical properties of the composites. The use of natural fibers in the nanoscale size to reinforce TPS and other biodegradable material can resulted in obvious improvements in the mechanical properties of the composites. This was due to the homogenous distribution of the filler as the large aspect ratio (L/d) can be achieved which can contribute to better dispersion and strong interactions between the polymer matrix and the reinforced agents.

In this present work, cellulose nanocrystals (CNC) from rice husk have been prepared and characterized by transmission electron microscopy (TEM), x-ray diffraction (XRD), and Fourier Transform Infrared (FTIR) spectroscopy. This CNC was then subjected to be used as reinforcing agent in the preparation of TPS. Three stages of fiber treatment were use as filler which are raw fibers, cellulose fibers and cellulose nanocrystals. The reinforcing effect of filler loading from rice husk fibers on TPS is evaluated to compare the mechanical properties of the composites.

Materials and Method

Materials

The rice husk that was used as raw materials had been obtained from the Bernas Malaysia Sdn. Bhd. Native cassava starch was supplied by Thye Huat Chan Sdn. Bhd. Sodium hydroxide, acetic acid, sulphuric acid and glycerol were purchased from System ChemAR. Sodium chlorite (80%) was purchased from Sigma-Aldrich.

Preparation of cellulose nanocrystals from rice husk

Cellulose nanocrystals from rice husk were extracted via acid hydrolysis method. Briefly, the mixture of ground rice husk and 4% (w/w) of alkali solution (NaOH) was undergo the reflux process under mechanical stirring at a temperature range of 100-120°C for 2 h. The reflux process of bleaching treatment took place by adding acetate buffer, aqueous chlorite [1.7% (w/w)] and distilled water at a temperature of 110-130°C for 4 h and repeated for 4 times. Acid hydrolysis process was conducted on the cellulose particles at a temperature of 45°C with 65% (w/w) of sulphuric acid (heated) for 40 min under mechanical stirring. Fiber content for the hydrolysis treatment was in the range of 4-6% (w/w). The hydrolyzed cellulose was then centrifuge several times at 10.000 rpm and 10°C for 10 min. The suspension was dialyzed against distilled water for several days until constant pH in the range of 5-6 was reached.

Preparation of thermoplastic starch (TPS) film

Fabrication of TPS films was based on solution casting technique and evaporation process [9]. Cassava starch was first mixed with the plasticizers (glycerol) and the filler (rice husk fibers) in distilled water and heated at 100°C under continuous stirring until the mixture gelatinized. The filler loading from three types of fibers which are raw fibers, cellulose fibers and cellulose nanocrystals was varied from 2%, 4%, 6%, 8% and 10% for the production of TPS. The mixture was then cast in a petry dish and dried at 60°C overnight to obtain the TPS films with a thickness of approximately 0.20 mm. A neat matrix of TPS film was also prepared via the same process mentioned above excludes that there is no filler added to the composites. The films were kept at room temperature in conditioning desiccators at 30% relative humidity before tests.

Characterization

Transmission electron microscopy (TEM)

The dimensional image of cellulose nanocrystals from rice husk was determined using transmission electron microscopy *(Philips CM 12)* with an accelerating voltage of 80 kV. A drop of diluted suspension [1% (w/w)] was dispersed on the surface of a copper grid and coated

with a thin carbon film. To enhance contrast in TEM, the cellulose nanocrystals were negatively stained in a 2% (w/w) solution of uranyl acetate (a heavy metal salt) in deionized water for one minute and dried at ambient temperature. TEM analysis was carried out to determine the length and diameter range of cellulose crystal in nanometer scale.

Fourier Transform Infrared (FTIR) spectroscopy

Fourier transform infrared spectra were recorded using a *Perkin-Elmer* FTIR spectrometer. The samples which have finely ground and mixed with potassium bromide, KBr were tested in the spectroscopic analysis. The mixture then compressed until a form of pellets produced. FTIR spectral analysis was performed and the samples were recorded within the wavenumber range of 400-4000 cm^{-1}.

X-ray diffraction and crystallinity measurement

X-ray diffraction techniques used to characterize the crystallinity of the rice husk fibers. Each fiber in the form of milled sample powder was placed on the sample holder and levelled to obtain total and uniform X-ray exposure. The sample was analysed using X-ray diffractometer *(D8-Advance Bruker AXS GmbH)* at ambient temperature by step scanning using monochromatic CuKα radiation source (λ = 0.1539 nm) in the step-scan mode with the angle of 2θ range: 10° to 50° with a step size of 0.04 and scanning rate of 5.0°C·min^{-1}.

In order to measure the crystallinity value for those samples, the crystallinity index of cellulose, C_{Ir} was calculated based on the reflected intensity data following the method of Segal et al. (1959):

$$C_{Ir(\%)} = [\ (I_{002} - I_{am}) / I_{002}\ ] \times 100 \qquad (1)$$

where I_{002} is the peak intensity corresponding to both the amorphous and crystalline regions of cellulose and I_{am} is the peak intensity of the amorphous region.

Tensile tests

Mechanical performance of the films was evaluated through tensile strength and Young's modulus using universal testing machine *(Instron model 5560)* at room temperature with crosshead speed of 50 mm·min^{-1}. The average value of five replicate for each sample was taken.

Results and Discussion

Morphology of the cellulose nanocrystals

The transmission electron micrograph for the cellulose nanocrystals of rice husk obtained after the hydrolysis with sulphuric acid is shown in the Figure 1a. In the cellulose fibers, the sulphuric acid hydrolysis usually could cleave the amorphous region of microfibrils transversely. This was eventually will reduce the size of the fibers from micron to nanometers [10]. The diameter distribution and aspect ratio of 100 samples of cellulose nanocrystals from rice husks was illustrated in Figure 1b. The maximum diameter of cellulose nanocrystals were between 15-20 nm with the total of 35% while the highest aspect ratio for cellulose nanocrystals were found in the range of 10-15 nm at 39%.

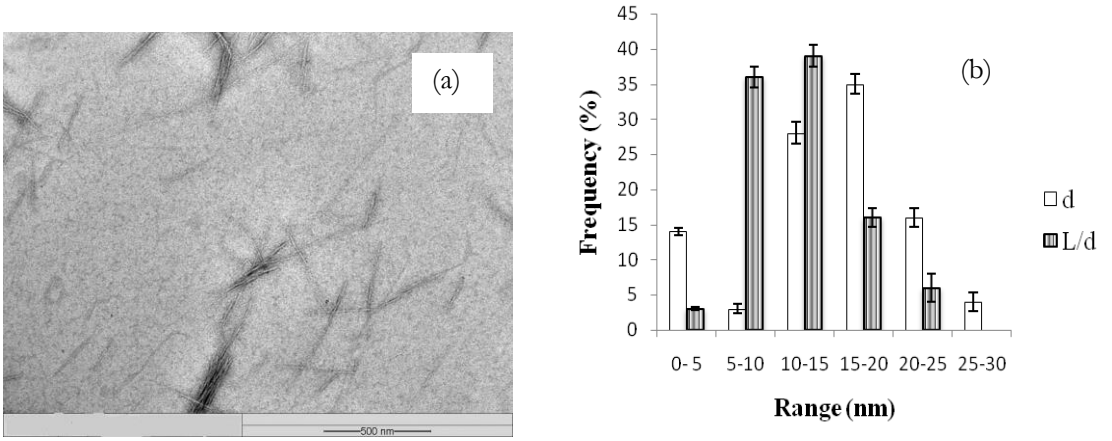

Figure 1: (a) TEM micrograph of cellulose nanocrystals from rice husk and (b) Diameter distribution and aspect ratio of the cellulose nanocrystals from rice husk

Spectroscopic analysis (FTIR)

Figure 3 shows FTIR spectra of raw fibers, cellulose fibers, and cellulose nanocrystals from rice husk. Peak at a wavelength at around 3440-3400 cm^{-1} and 1640 cm^{-1} which can be seen in all of the three spectra were representative of O-H groups and referred to the absorption of water respectively. The absorption peaks in the range of about 3400 cm^{-1} and 1640 cm^{-1} showed the stretching of the hydrogen bond and bending of the hydroxyl (O-H) that was bound to the cellulose structure.

There was a prominent peak at around 1700 cm^{-1} showed in the spectrum of raw fibers. It represents acetyl groups and ester groups in hemicelluloses or carboxylic acids group of ferulic and *p*-coumeric in lignin. The same was also reported by Alemdar and Sain [11] and Sun et al. [12] that the peak in the range of 1700 cm^{-1} showed by the spectrum of untreated wheat straw and soy hulls in the FTIR analysis represents the acetyl group and ester group in hemicelluloses or likely to be network groups of carboxylic acids of ferulic and *p*–coumaric in lignin. However, the shoulder peak was not visible in the spectrum of rice husk after the chemical treatment. The disappearance of this peak was referred to the removal of hemicellulose after the chemical treatment.

The peak in the range of about 1300 cm^{-1} in the two spectra of rice husk that has been treated was representing a change in the symmetry of the C-H [12]. Absorption at around 1266-1200 cm^{-1} in the spectrum of cellulose and cellulose nanocrystals refers to the bending frequency of C-H, O-H, or CH_2, while the absorption at around 1060-1050 cm^{-1} and 890 cm^{-1} that was shown by all spectra refers to the C-H stretching and C-O vibration of the cellulose component [11].

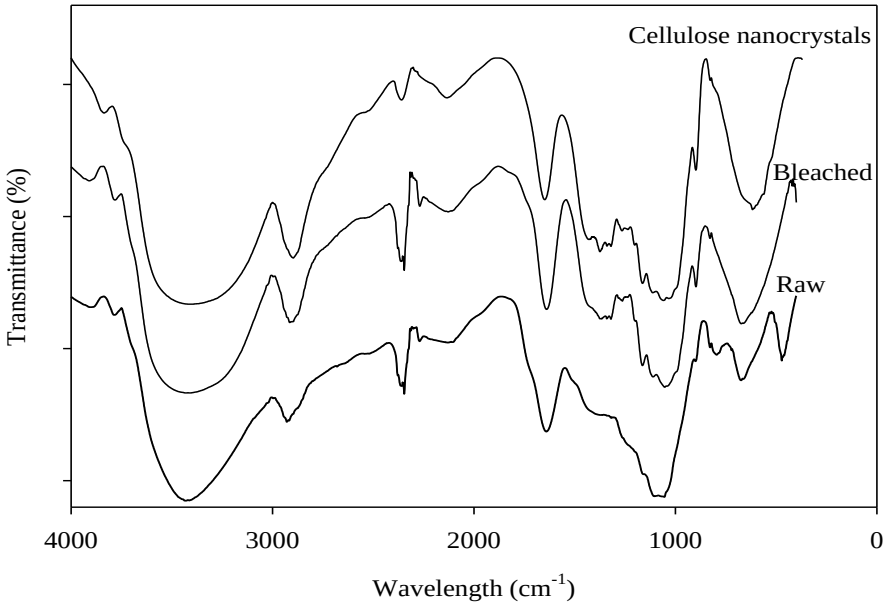

Figure 3: Combination of FTIR spectra of raw fiber, cellulose fiber and cellulose nanocrystals from rice husk.

X-ray diffraction (XRD)

Crystallinity index of rice husks fibers at all stages of chemical treatment were measured through x-ray diffraction analysis. The crystallinity index of the untreated rice husks fibers, bleached rice husks fibers, and cellulose nanocrystals obtained after hydrolysis with acid were calculated and showed in Table 1.

The increase in the crystallinity of the fibers associated with the removal of non-cellulosic components during chemical treatment. This will contribute to the high crystallinity value of bleached fibers and cellulose nanocrystals compared to raw fibers. During the hydrolysis process, hydronium ions could also penetrate into the amorphous region of the cellulose molecules that allow the hydrolytic cleavage of glycosidic bonds which then can eventually produce the individual crystallites [13]. In addition, during the preparation of cellulose nanocrystals, formation and realignment of monocrystals may occur in parallel and thus can improve the crystallinity of cellulose nanowhiskers [14]. Thus, the crystallinity index of cellulose nanocrystals is higher than bleached fibers.

With the increase in the crystalline cellulose structure, the stiffness and rigidity of the fibers increases. The higher value of crystallinity of chemically treated cellulose fibers was related to the higher tensile strength of the fibers. Thus, the expected mechanical properties of composite materials can be improved by using cellulose fiber as filler in the production of composites [15, 16].

Table 1: Crystallinity index of rice husk fibers at different stages of treatment.

Samples	Crystallinity index (%)
Untreated rice husks	46.8
Bleached rice husks fibers	56.5
Cellulose nanocrystals	59.0

Tensile test

Tensile test was carried out to get the data of tensile strength (MPa), tensile strain at break (%), and modulus (MPa) for TPS films loaded with rice husk fibers as filler. Mechanical properties of composites were strongly influenced by adhesion between the matrix and the fibers. The differences on the mechanical properties of biocomposites were due to the types and size of the fibers used as filler in the production of TPS films.

The effect of tensile strength (MPa) as a function of fibers loading and the effect of modulus (MPa) on the composite for TPS films were shown in Figure 4 and 6. It was found that the tensile strength for TPS films were lower for all composition of raw fibers loading compared to the neat matrix (2.5 MPa) while, for cellulose fibers and cellulose nanocrystals, the tensile strength were increased with the increase of the filler composition. This similarity also shown by the tensile modulus of the composites as the value increased for all filler composition of all types of fiber. However, a decreased in tensile strain at break (Figure 5) is observed for all composites when compared to the neat matrix.

The treated fibers which were cellulose and cellulose nanocrystals gives better tensile strength and modulus result compared to the untreated fibers which is raw fibers. The maximum value of tensile strength for cellulose fibers TPS films is 3.0 MPa obtained at 6% filler loading while for cellulose nanocrystals the maximum value achieved at 6% filler loading as 3.8 MPa. The maximum value of modulus was 46.6 MPa at 6% for cellulose nanocrystals filler loading. As for tensile test, the best result for mechanical properties was showed by TPS films with 6% of cellulose nanocrystals.

The matrix-filler interface and adhesion is greater with cellulose fibers and cellulose nanocrystals compared to raw fibers. This was due to the removal of amorphous part during the chemical treatment as the presence of lignin on the surface of the raw fibers which are less polar than cellulose [17], decrease the adhesion and interaction of fiber with the matrix. Furthermore, the tensile strength for raw fibers composites was lower due to the uniformity of the filler size. The size of raw fiber was varied as it is still in the particulate form which leads to the lower value of aspect ratio (L/d) for the fibers. Consequently, the interaction between fibers and polymer matrix was not enhanced and resulted in the lower tensile strength.

Furthermore, the reduction size of filler also affect the tensile strength and modulus result as the cellulose nanocrystals showed higher value compared to cellulose fibers. As the nano sized of filler used in the preparation of TPS films, the aspect ratio (L/d) of the fibers increased which allowed better dispersion and interaction between polymer matrix and the fibers. Moreover, as reported by Mohanty et al. [18], chemical treatment reduces fiber diameter and thereby increase the aspect ratio, improving mechanical properties of the composites.

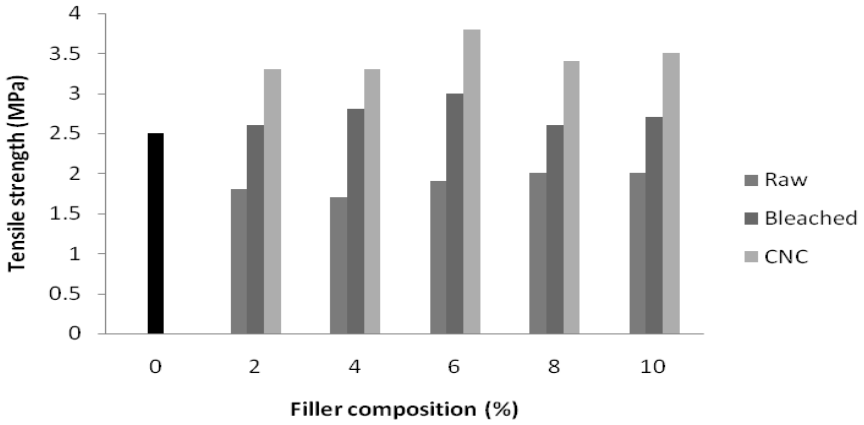

Figure 4: Graph of tensile strength (MPa) versus filler composition (%)

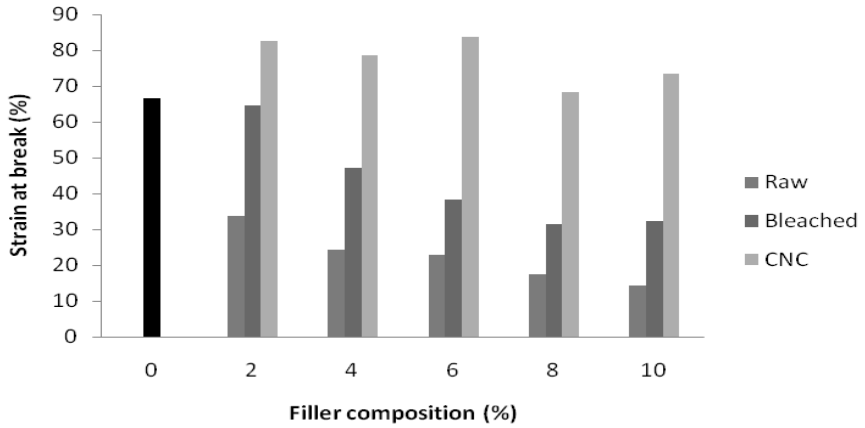

Figure 5: Graph of tensile strain at break (%) versus filler composition (%)

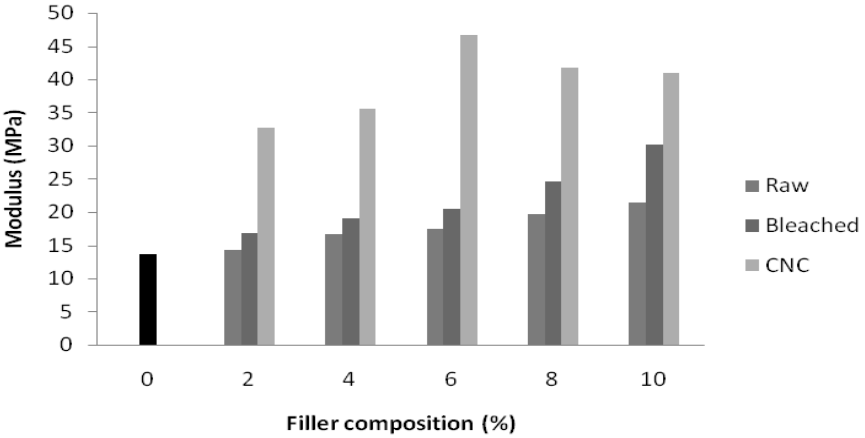

Figure 6: Graph of modulus (MPa) versus filler composition (%)

Conclusion

Cellulose nanocrystals from rice husks had been successfully isolated using acid hydrolysis method. The average length and highest aspect ratio value of the 100 samples of nanocellulose recorded by transmission electron microscope (TEM) are 15-20 nm and 10-15 nm respectively. FTIR spectroscopy and x-ray diffraction analysis confirmed the removal of non-cellulosic material during chemical treatment performed to the rice husk fibers. Thermoplastic starch (TPS) films with fibers from rice husk used as filler were prepared via solution casting technique. Reinforcement effect of filler was investigated by associating different filler loading (2%, 4%, 6%, 8% and 10%) and different types of fibers used with the matrix polymer. It was found that TPS nanocomposites film showed enhancement in the mechanical properties with 6% of cellulose nanocrystals loading showed the optimum result for tensile stress values of 3.6 MPa and 41.7 MPa for modulus.

Acknowledgements

The research work reported in this paper was funded by the Ministry of Science, Technology and Innovation, Malaysia and Universiti Kebangsaan Malaysia (UKM).

References

[1] Netravali, A. N. & Chabba, S. 2003. *Mater Today*. 6: 22-29.

[2] Hulleman, S. H. D., Janssen, F. H. P. and Feil, H. 1998. *Polymer*. 39: 2043-2048.

[3] Fishman, M. L., Coffin, D. R., Konstance, R. P. and Onwulata, C. I. 2000. *Carbohyd Polym.* 41, 317-325.
[4] Avérous, L. & Fringant, C. 2001. *Polym Eng Sci*. 40: 727-734.
[5] Chatakanonda, P., Varavinit, S. and Chinachoti, P. 2000. *Food Sci Technol.* 33: 276-284.
[6] Shogren, R. L., Lawton, J. W., Tiefenbacher, K. F. and Chen, L. 1998. *J Appl Polym Sci*. 68: 2129-2140.
[7] Baumberg, S., Lapierre, C., Monties, B. and Della Valle, C. 1998. *Polym Degrad Stabil*. 59: 273-277.
[8] Dufresne, A. & Vignon, M. R. 1998. *Macromolecules.* 31: 2693-2696.
[9] Lu, Y., Weng, L. & Cao, X. 2006. *Carbohyd Polym.* 63: 198-204.
[10] Azizi Samir, M. A. S., Alloin, F. and Dufresne, A. 2005. *Biomacromolecules*. 6: 612-626.
[11] Alemdar, A. & Sain, M. 2008. *Bioresource Technol*. 99: 1664-1671.
[12] Sun, X. F., Xu, F., Sun, R. C., Fowler, P. and Baird, M. S. 2005. *Carbohyd Res.* 340: 97-106.
[13] de Souza Lima, M. M. and Borsali, R. 2004. *Macromol Rapid Comm*. 25: 771-787.
[14] Li, R., Fei, J., Cai, Y., Li, Y., Feng, J. and Yao, J. 2009. *Carbohyd Polym.* 76: 94-99.
[15] Bhatnagar, A. & Sain, M. 2005. *J Reinf Plast Comp.* 24, 1259-1268.
[16] Rong, M. Z., Zhang, M. Q., Liu, Y., Yang, G. C. and Zeng, H. M. 2001. *Compos Sci Technol.* 61: 1437-1447.
[17] Pouteau, C., Dole, P., Chatala, B., Avérous, L. and Boquillon, N. 2003. *Polym Degrad Stabil.* 81: 9-18.
[18] Mohanty, A. K., Misra, M. and Drzal, L. T. 2001. *Compos Interface.* 8: 313-343.

EFFECT OF TETRAETHYLAMMONIUM BROMIDE ON TENSILE PROPERTIES AND MORPHOLOGY OF EPOXIDIZED SOYBEAN OIL BASED THERMOSET

S.G. Tan, Z. Ahmad & W.S. Chow*

School of Materials and Mineral Resources Engineering, Engineering Campus, Universiti Sains Malaysia, 14300 Nibong Tebal, Pulau Pinang, Malaysia

Abstract

In the present study, a novel epoxidized soybean oil (ESO)-based thermoset was prepared using casting method. ESO resin was thermally cured by methylhexahydrophthalic anhydride (MHHPA), in the presence of tetraethylammonium bromide (TEAB) catalyst. The effects of TEAB catalyst concentration (0.3-0.8 phr) on the tensile properties of ESO thermosets were investigated. ESO thermoset containing low TEAB catalyst concentration (i.e. 0.3–0.6 phr) experienced ductile deformation; on the other hand the ESO thermoset consisting of high TEAB concentration (i.e. 0.7–0.8 phr) fractured in brittle mode. The morphological properties of the ESO thermoset were investigated using field-emission scanning electron microscope (FESEM). Fibrous patterns and crack arrest lines revealing a ductile fracture were found on the fractured surface of ESO thermoset catalyzed with low TEAB concentration; whereas the waviness and closely placed line patterns indicating a brittle fracture were observed on the highly TEAB-catalyzed ESO thermoset. It was determined that the tensile properties of the ESO thermoset were governed by the concentration of TEAB, which can be associated to their gel content and degree of crosslinking.

Keywords: *Epoxidized soybean oil, gel content, morphology, thermoset, tensile properties.*

Introduction

Synthesis of biopolymers from vegetable oils is gaining much attention in recent years. This is attributed to the environmental friendliness and cost effectiveness of vegetable oils. It has been documented that the unsaturated sites of vegetable oils can be epoxidized to enhance their reactivity and versatility [22]. Accordingly, the epoxidized vegetable oil can be further cured by appropriate curing agents – to produce biothermosets.

Epoxidized soybean oil (ESO) is a triglyceride constructed of a complex multi-component mixture of glycerol esters and epoxidized fatty acids. These epoxidized oleic, linoleic and linolenic fatty acids can react with suitable curing agent and lead to the formation of crosslinked biopolymer networks. It has been recognized that ESO resin can be thermal- and UV-cured [3, 4, 6, 9, 12, 13, 15, 20, 21, 24, 25, 26].

Considering the fact that ESO possesses epoxy oxirane groups with low reactivity, the resulting networks could be less densely crosslinked. As a result, epoxidized vegetable oils are commonly reinforced with fibers [10], blended with petrochemical-based epoxy resin [22], or chemically acrylated [18] in order to enhance the mechanical properties of the epoxidized vegetable oil based thermoset.

It is hypothesized that ESO thermoset with a balance of good mechanical properties can be prepared by using tetraethylammonium bromide (TEAB) catalyst. In the presence study, we investigated the effects of TEAB concentration on the tensile and morphological properties of ESO thermosets.

Materials and Method

Preparation of ESO Thermoset

ESO resin with 6.1% (w/w) epoxy content and molecular weight of 950 $g \cdot mol^{-1}$ was purchased from Shangding Longkou Londa Chemical Industry Co., Ltd., China. Methylhexahydrophthalic anhydride (MHHPA) curing agent was supplied by CAPE Technology Sdn. Bhd., Malaysia.

TEAB catalyst was purchased from Sigma-Aldrich, Malaysia. The material designation and composition of the ESO thermoset is summarized in Table 1. The ESO resin and MHHPA/TEAB mixture were mixed at a pre-determined ratio and then stirred mechanically at room temperature. The mixture was then poured into the mould cavity and subjected to thermal curing in an oven at 140°C for 3 h.

Table 1: Material designation and composition of ESO thermoset

Material designation	Concentration of TEAB catalyst (phr)
ES_0.3A	0.3
ES_0.4A	0.4
ES_0.5A	0.5
ES_0.6A	0.6
ES_0.7A	0.7
ES_0.8A	0.8

Characterization of ESO thermoset

Mechanical tests

The tensile specimens (Type IV) with 3 mm thickness were prepared using casting method. Tensile test was conducted according to ASTM D638 by using Instron machine, at a crosshead speed of 5 mm/min.

Morphology characterization

The morphology of the tensile-fractured surface of ESO thermoset was observed using field emission scanning electron microscope (FESEM, model *Supra 35*, *Zeiss*, USA). The ESO sample was gold-coated prior to FESEM to avoid electrostatic charging.

Degree of conversion

The cure characteristics of ESO thermoset was studied using differential scanning calorimeter (DSC Diamond Analyzer, *Perkin Elmer*, USA). The degree of conversion of the ESO sample was calculated based on Equation 1 [17].

$$\alpha = \frac{\Delta H_c - \Delta H_r}{\Delta H_c} \times 100\% \quad (1)$$

where α is the degree of conversion, ΔH_c is the total exothermic heat generated for a fully cured system and ΔH_r is the total residual exothermic heat generated during a specific period of time.

Gel content determination

Gel content measurement was conducted using the solvent extraction technique. The samples were initially weighed and then immersed into acetone solvent at room temperature for 1 week. The samples were removed, dried and re-weighted after 1 week. The gel content of the ESO thermoset was determined according to Equation 2.

$$Gel\ Content = 1 - \left(\frac{W_s - W_d}{W_o} \right) \quad (2)$$

where W_s is the weight of specimen being tested, W_d is the weight of dried gel, and W_o is the original specimen weight.

Results and Discussion

Figure 1 shows the stress-strain curves of the ESO thermosets. It is clear that the stress-strain behaviour of the ESO thermoset depends on the TEAB concentration. It has been documented that the TEAB is responsible for catalyzing the esterification reaction between ESO resin and MHHPA curing agent. For those ESO thermosets catalyzed with low TEAB concentration (0.3–0.6 phr), the specimen exhibited a yield point, followed by an extensive elongation. On the other hand, ESO thermoset catalyzed with higher TEAB concentration (0.7–0.8 phr) deformed elastically with stress. The tensile elongation of the ESO thermoset was very small with no yield point. One possible explanation to these findings can be associated to the increase in the crosslink density with the increasing of TEAB concentration. In our previous study [24] it was found that the degree of conversion and crosslink density of the ESO thermosets increased approximately 4.4% and 4.2%, respectively when the TEAB concentration was increased from 0.3 to 0.8 phr. Also, it is experimental determined that the gel content of the ESO thermosets increase with increasing the TEAB concentration. Specifically, an increment in gel content from 97.2% to 100% was detected when the TEAB concentration was increased from 0.3 to 0.8 phr. This is consistent with the finding reported by Lam & Chong [7] who mentioned that the yielding behaviour of DGEBA thermoset was affected by the crosslink density and curing condition.

Generally, the diluting effect imposed by the residual (e.g. un-reacted MHHPA) tends to cause the ESO thermoset to undergo yielding and to deform in a ductile manner. It can be found that no yield point was observed for the ESO thermoset catalyzed with high TEAB catalyst concentration. This is due to the fact that the diluting effect of unreacted MHHPA became less significant. Consequently, the deformation of ESO thermoset followed Hookean elastic behaviour. In other words, ESO thermosets with more intense crosslinked network structure (i.e. catalyzed with high TEAB concentration) will show a rapid elastic response if a small stress is applied onto it. However, they are prone to brittle fracture at relatively low strain via bond rupture if a larger external stress is applied. This is because ESO thermoset with very limited flexible chain segments has no way to dissipate the applied force effectively through plastic deformation when a high breaking force is applied.

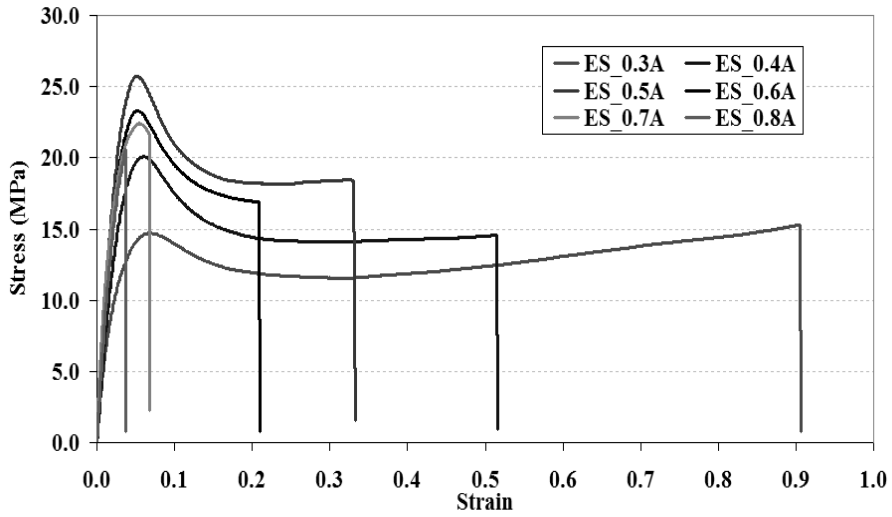

Figure 1: Stress-strain curves of ESO thermosets.

As shown in Figure 1 and Figure 2, it is found that the tensile strength of ESO thermoset increased with increasing the TEAB concentration up to 0.5 phr, after which there was a drop. The enhancement of tensile strength is due to the higher degree of cure and the

concomitant reduction of the unreacted species in crossliked network structure. Accordingly, the presence of unreacted species tends to induce a non-uniform stress distribution and microscopic stress concentration. These stress concentration areas will make the breakage of the chains around the unreacted site easier. In this respect, the progressive improvement in the tensile strength up to an optimum level is believed due to the alleviation of stress concentration as the degree of cure increases.

However, the reduction in tensile strength was detected when the TEAB concentration was increased exceeding 0.5 phr. This is presumable attributed to the build-up of residual internal stress. Particularly, the magnitude of internal stress in ESO thermosets increases with increasing TEAB concentration. This is because the highly crosslinked molecular segments are lack of time to relax and to shrink during cooling, and thereby resulting in an entrapment of these undesirable residual stresses [23]. The build-up of these internal stresses tends to deteriorate the resistance of the ESO thermoset against the large stress. This will lead to the reduction in tensile strength. This is also in line with the finding reported by Liu et al. [8] which stated that the tensile strength of epoxidized polysiloxane toughened DGEBA composites decreases with increasing of the internal residual stress.

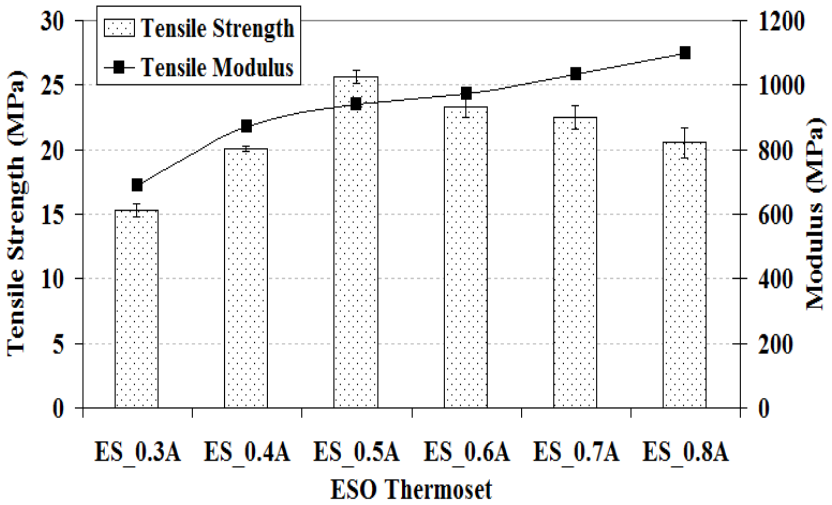

Figure 2: Tensile strength and tensile modulus of TEAB-catalyzed ESO thermoset

In addition, it is clearly shown in Figure 2 that the tensile modulus of the ESO thermoset increases with respect to TEAB concentration. A gradual decrease of elongation at break is also detected with increasing TEAB concentration, as shown in Figure 1. These findings can be reasonably explained by taking into consideration the crosslink density of ESO thermosets. Bear in mind that the number of crosslink formed in ESO thermoset increases with increasing TEAB concentration. Considering this fact, the mobility of the chains as well as the degree of slippage between the chains in ESO thermoset will be reduced with increasing the TEAB concentration from 0.3 to 0.8 phr. These will give rise to an increase in tensile modulus and a reduction in elongation at break. This finding is also in agreement to the finding reported by Pan et al. [14] which stated that the elongation at break of an epoxy-anhydride thermoset decreases with increasing of the crosslink density. Banik & Browmick [1] and Sharif et al. [19] also reported that there is a direct relationship between the tensile modulus and the crosslink density.

It was clearly observed in Figure 3 that the fracture mode for ESO thermoset gradually changed from ductile to brittle mode when the TEAB concentration was increased from 0.3 to 0.8 phr. The morphological fibrous patterns and river markings in the tensile fractured surface

of ESO thermosets catalyzed with low TEAB concentration (i.e., 0.3–0.6 phr) revealed the evidence of ductile fracture; whereas the waviness and closely placed line pattern on the fractured surface of ESO thermoset catalyzed with high TEAB concentration (i.e., 0.7–0.8 phr) showed a brittle fracture deformation mode.

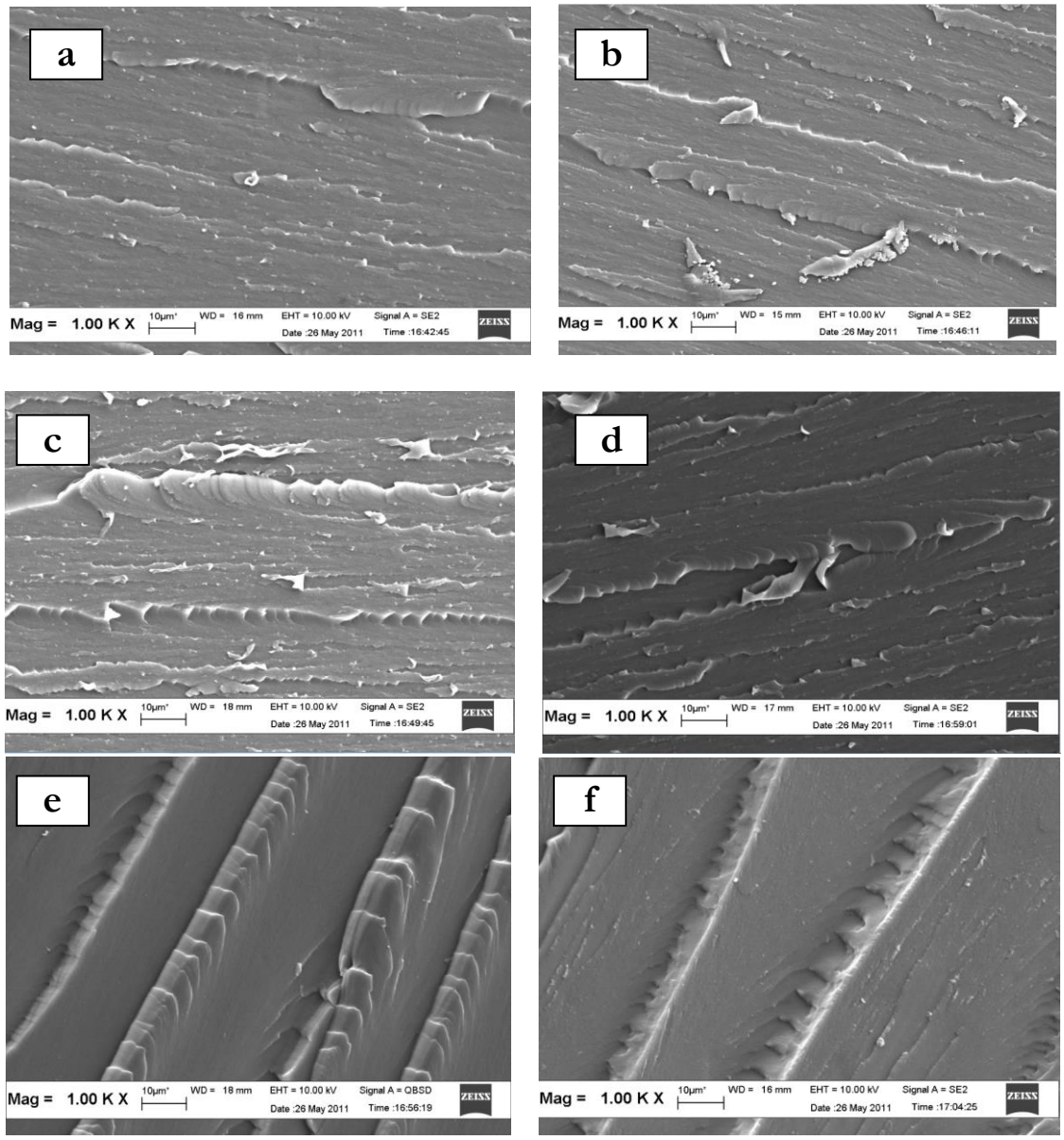

Figure 3: Tensile fractured morphologies of TEAB-catalyzed ESO thermosets (a) ES_0.3A, (b) ES_0.4A, (c) ES_0.5A, (d) ES_0.6A, (e) ES_0.7A, and (f) ES_0.8A

According to Zhang & Evans [28], the presence of fibrous and river pattern on the fractured surface indicates the evidence of ductile mode of fracture involving a relatively stable crack growth. Biju et al. [2] reported that closely placed line pattern is the characteristic feature revealing a brittle fracture deformation. Also, from Figure 3, it can be observed that the number of ridges and the ridge depth on the fracture surface of the ESO thermoset increase with the increase in TEAB concentration up to 0.5 phr. These findings show a distinguished symbolic of increased energy absorption on a large scale of deformation [27], which is account for the

increment in the tensile strength of the ESO thermosets as displayed in Figure 2. Also, it is noted that the fractured surfaces of the ESO thermosets catalyzed with higher TEAB concentration (> 0.5 phr) are smooth and their fracture paths are mainly straight. This indicates the poor ability of a material to resist crack initiation and propagation since the regular cracks on the tensile fractured surface are unable to resist crack initiation and material deformation when an external force is applied onto it [11, 15, 27]. This explains the reduction in the tensile strength of the ESO thermoset catalyzed with relatively high TEAB concentration, as shown in Figure 2.

Conclusion

Based on our present work devoted to study the effect of TEAB concentration on the tensile properties and fractured morphologies of ESO thermosets, the following conclusions can be drawn:

TEAB concentration plays an important role in influencing the tensile properties and tensile fractured morphology of the ESO thermoset. It is determined that the tensile strength of ESO thermoset can achieve a maximum value by using 0.5 phr of TEAB. ESO thermoset catalyzed with higher TEAB concentration possesses higher tensile modulus and lower percentage of elongation at break due to the increase in crosslink density and the degree of crosslink. The tensile fractured deformation mode of the ESO thermosets changes from ductile to brittle once the TEAB catalyst concentration is increased from 0.3 to 0.8 phr, gradually. In summary, the tensile properties are found to be lower than the petroleum-based thermosets [5, 16], but are comparative or even higher than those ESO/triethylenetetramine [11], ESO/terpene-based acid anhydride [21] and ESO/MHHPA [14] systems. Furthermore, the ESO thermoset with improved tensile properties can be prepared in this work using a lower curing temperature and shorter curing schedule.

Acknowledgements

This study was funded by the Universiti Sains Malaysia Incentive Grant (Grant Number: 8021013), USM Research University Postgraduate Research Grant Scheme (USM-RU-PRGS; Grant Number: 8045001), the Ministry of Higher Education, Exploratory Research Grant Scheme (MOHE, ERGS; Grant Number: 6730084) and the Ministry of Science, Technology and Innovation, National Science Foundation (MOSTI, NSF) fellowship.

References

[1] Banik, I. & Bhowmick, A.K. *J Appl Polym Sci.* 69: 2079-2087.
[2] Biju P.K., Radhakrishnan-Nair, M.N., Thomas, G.V. and Gopinathan-Nair, M.R. 2007. *Mat Sci Poland.* 25: 919-932.
[3] Gerbase, E., Perzhold, L. and Costa, O. 2002. *J Am Oil Chem Soc.* 79: 797-802.
[4] Gupta, A.P., Ahmad, S. and Dev., S. 2010. *Polym Plast Tech Eng.* 49: 657-661.
[5] Gupta, N. & Nagorny, R. 2006. *J Appl Polym Sci.* 102: 1254-1261.
[6] Jin, F.L. & Park, S.J. 2007. *J Ind Eng Chem.* 13: 808-814.
[7] Lam, D.C.C. & Chong, A.C. 2000. *Mater Sci Eng A.* 281: 156-161.
[8] Liu, W.Q., Ma, S.Q., Wang, Z.F., Hu, C.H. and Tang, C.Y. 2010. *Macromol Res.* 18: 853-861.
[9] Liu, Z. & Erhan, S.Z. 2010. *J Am Oil Chem Soc.* 87: 437-444.
[10] Liu, Z.S., Erhan, S.Z., Xu, J. and Calvert, P.D. 2002. *J Appl Polym Sci.* 85: 2100-2107.
[11] Nick, T. & Kevin, L. 2002. *An introduction to automotive composites*. UK: Rapra Technology.
[12] Ortiz, R.A., Lopez, D.P., Cisneros, M.L.G., Valverde, J.C.R. and Crivello, V. 2005. *Polymer.* 46: 1535-1541.

[13] Ozturk, C. & Kusefoglu, S.H. 2010. *J Appl Polym Sci.* 118: 3311-3317.
[14] Pan, X., Sengupta, P. and Webster, D.C. 2011. *Biomacromolecules.* 12: 2416-2428.
[15] Park, S.J., Jin, F.L. and Lee, J.R. 2004. *Macrol Rapid Comm.* 25: 724-727.
[16] Qi, B., Zhang, Q.X., Bannister, M. and Mai, Y.M. 2006. *Compos Struct.* 75: 514-519.
[17] Sanchez-Cabezudo, M., Prolongo, G., Salom, C. and Masegosa, M. 2006. *J Them Anal Calorim.* 86: 699-705.
[18] Seniha-Guner, F., Yagci, Y. and Erciyes, A.T. 2006. *Prog Polym Sci.* 31: 633-670.
[19] Sharif, J., Khairup, Z.M.D. and Wan, M.Z.W.Y. 2007. *J Mater Sci: Mater Med.* 13: 1065-1069.
[20] Shibata, M., Teramoto, N. and Makino, K. 2011*. J Appl Polym Sci.* 120: 273-278.
[21] Takahashi, T., Hirayama, K., Teramoto, N. and Shibata, M. 2008. *J Appl Polym Sci.* 108: 1596-1602.
[22] Tan, S.G. & Chow, W.S. 2010a. *Polym Plast Tech Eng.* 49: 900-907.
[23] Tan, S.G. & Chow, W.S. 2010b. *J Therm Anal Calorim.* 101: 1051-1058.
[24] Tan, S.G. & Chow, W.S. 2011a. *Express Polym Lett.* 5: 480-492.
[25] Tan, S.G. & Chow, W.S. 2011b. *J Am Oil Chem Soc.* 88: 915-923.
[26] Tanrattanakul, V. & Saithai, P. 2009. *J Appl Polym Sci.* 114: 3057-3067.
[27] Unnikrishnan, K.P. & Eby, T.T. 2005. *J Elast Plast.* 37: 347-359.
[28] Zhang, Z. & Evans, D. 2004. *Polym Eng Sci.* 43: 1071-1080.

PERFORMANCE OF RECLAIM CARBON FIBRE VIA PYROLYSIS AS FILLER IN COMPOSITE PANELS

H.F.A. Marzuki[1], E.A.E. Ubaidillah[1], N. Roslani[1], Y.M. Junos[1], M.F.Z. Abidin[1], I.N. Ismail[1], S. Omar[1] & F.M.M. Ayub[2]

[1]Composite Material Section, Advanced Material Research Centre, (AMREC), SIRIM Berhad, Lot 34, Jalan HiTech 2/3, Kulim Hi-Tech Park, 09000 Kulim, Kedah

[2]Faculty of Applied Science, University Teknologi MARA Perlis, 02600 Arau, Perlis Indera Kayangan

Abstract

Reclaiming carbon fibre from composite waste and scrap to recycle the fibre has becoming one of the global issues in the composite industry today. Many approaches have been study to reclaim the fibre in order to maintain the virgin properties of the fibres. Pyrolysis, one of the methods used to reclaim fibre, was used in this research to reclaim carbon fibres from a pre-preg waste. The waste was immersed in acetone for certain period of time and then burn in inert atmosphere at 600^{o}C. Then, the reclaim fibre was ground to obtain a uniform size of powder, which will be used as filler to reinforce composite panels. The composite panels then were fabricated and analyse to see the performance of the reclaimed fibre and comparing it with samples filled with $CaCO_3$ powders. It is observed that the reclaim fibre shows promising performance especially in compression loading condition.

Keywords: *Composite Performances, Pyrolysis, Recycle Carbon Fibre.*

Introduction

Carbon fibres, CF are the most popular and highly demanded synthetic fibres for advanced polymer composite applications. Carbon fibres reinforced polymers (CFRPs) were first used in aerospace applications in the early 1970´s. Today they are widely used in aircraft such as new Airbus 380 and Boeing 787 Dreamliner, automotive such as Formula-1 racing cars and sporting goods industry.

The increasing need of carbon fibres in the various industrial applications may cause a shortage of supply of carbon fibres. Nowadays, over 27,000 tonnes per annum of carbon fibre tow are currently being produced each year to support the needs of CF in various applications. It is reported by March 2009 that these numbers are expected to reach up to 35,000 tonnes per annum to meet the increasing demand.

However, the growth of CFRP's application has some effect towards the environmental issues. Disposal of composite structure which reaches the end of its service life to landfill or incinerator becomes a big issue. Disposing the scraps by grinding it is not a proper solution due to the non-degradability of both carbon fibres as reinforcement as well as thermosets matrix for the health and safety risks they possess. On the other hand, incineration of plastics releases toxic by-products which contribute to global warming issues. Therefore, reusing and recycling these scrap was inspired to help solving the environmental issues that arise.

The high cost of CF also leads the industry to reuse and recycle the CF scrap. It is reported that high grade CF cost up to £10,000 for each tonne. However, two-third of CF used in producing aircraft such as Dreamliner-787 and Airbus A380 resulted as scrap. The huge number of scrap which means a huge material cost was end-up as nothing if the scrap was not recycled and reuse.

Considering both environmental and economic reasons, reclaiming carbon fibre from carbon fibres composites waste and scrap for recycling purposes has attracted a lot of attention. The reclaiming intention is to stripping away the polymer matrix such as epoxy from

CF fibres in such a way as to leave most of the original fibre properties undiminished with positive environmental balance.

Pyrolysis is thermochemical decomposition method in the absence of oxygen to decompose a large compound to become a small and simpler profile [1]. Meyer et al. [2], pyrolysis can be considered as the simplest method of reclaiming recycling reinforcement material and in this case CF. Furthermore this method are appropriate to be applied on thermoset composites which cannot be remoulded. The polymeric material will be decomposed to low molecular weight products such as liquids or gases while the inorganic components that is CF will remain unmodified and therefore can be reclaimed for recycling purposes. For reclaiming the CF, the pyrolysis must be performed in an inert atmosphere or it will result producing CO and CO_2 due to decomposition of CF itself.

The purposes of this research are to reclaim the CF from the manufacturing waste that is expired pre-preg material and reused it as filler in composite material. In addition to that, the performance of CF was identified by comparing the properties of composite filled with reclaimed CF and the traditional filler that is Calcium Carbonate, $CaCO_3$.

Materials and Method

Acetone Immersion

Acetone immersion was performed as pre-removable process to separate the polymeric matrix and CF. Manufacturing waste that is expired pre-preg from Asian Composite Manufacturing Sdn. Bhd. (ACMSB) was used in this experiment. The waste was immersed in acetone and continuously stirred for 8, 16 and 24 days. This is to ensure that the decompose resin will settled at the bottom of the container and not lumped at the fibre. Thermogravimetri Analysis (TGA), was carried out on waste from each different period of immersion. Furthermore, Scanning Electron Microscopy (SEM) was also been carried on the samples immersed after 24 days to ensure the pre-removable take place.

Pyrolysis experiment

The pyrolysis process was carried on samples that were immersed after 24 days. The samples were burned at 600^{o}C in nitrogen atmosphere, using enclosed tube furnace. The nitrogen gases were purged at 15 ml·min^{-1} before the samples were heated to 600^{o}C. This is to ensure that the oxygen was totally removed and result the inert atmospheric condition in tube. After heating up to 600^{o}C, the samples were soaked for 1 hour to ensure complete removable of polymer matrix from the samples. The purging of nitrogen gases were continuing until the fibre was cooled to the room temperature to avoid oxidation reaction to take place on the samples.The reclaimed CF from pyrolysis process was milled using *RetschMultistages* Planetary Ball Mill, *PM400*. The samples were milled for 10 hours until the samples become a uniform powder form. The uniformity of powder formed was also observed under SEM.

Fabrication and testing of composite panels

The composite panels were prepared using continuous filament mat glass fibre, CFM with weight per area of 450 (CFM 450) and polyester resin, Norsodyne 3317A with Methyl Ethyl Ketone Peroxide, MEKP Butanox M-50, was used as matrix material. The panels were fabricated by press moulding techniques, using *WABASH* Hot-Press *E54 100T* Compression Machine.Three panels were prepared for this study as in Table 2.1. All the three fabricated panels were subjected to density testing, tensile and flexural test.

Table 2.1: Composite Panels Composition Details

Panels No.	Composition Details		
	Reinforcements	Matrices	Fillers
1	Glass Fibre (CFM450)	Polyester (Norsodyne 3317A+MEKP Butanox M50)	No filler
2	Glass Fibre (CFM450)	Polyester (Norsodyne 3317A+MEKP Butanox M50)	10% Wf of Calcium Carbonate ($CaCO_3$)
3	Glass Fibre (CFM450)	Polyester (Norsodyne 3317A+MEKP Butanox M50)	10% Wf of Reclaimed CF powder.

Results and Discussion

TGA

TGA was performed to detect the total of polymeric matrix removed from the acetone immersion process. From result of the analysis as in Figure 3.1, it shows that at the beginning of the experiment, the weight fraction of the matrix material are huge that is 33.37%. After 8 days of immersion, the carbonyl group from acetone that have acidic properties attack the non-cure epoxy structure in the samples and cause the decompose of the matrix material into the acetone. After 8 days of immersion, the balance of matrix material is only 5.6%. Continue with the immersion process for 16 and 24 days, it shows that the weight loss of the samples was very small that is 4.4% on the 16^{th} days and 4.19% on the 24^{th} days. This is because the samples were an expired pre-preg that contains both cured and non-cured (B-stage) epoxy resin. The small percentages of cured epoxy, that have cross-linked structure only can be removed or decompose by applying heat due to the strong bonding in the polymeric structure.

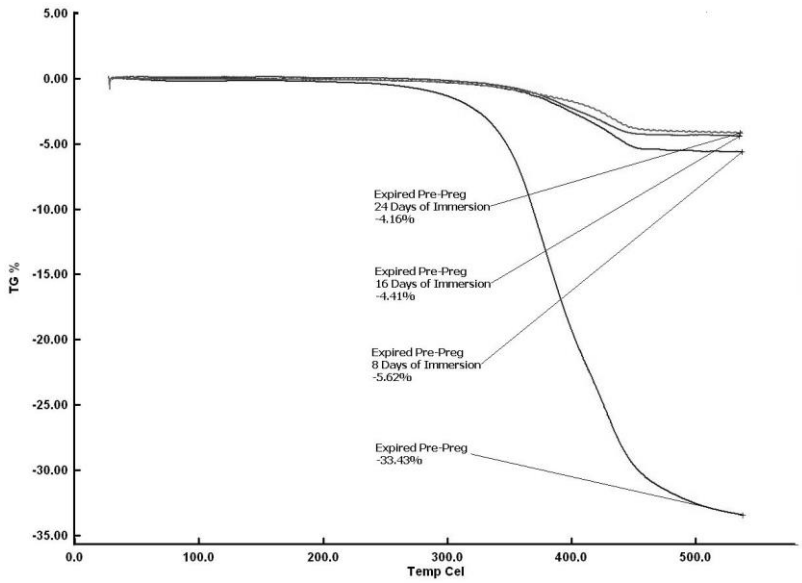

Figure 3.1: TGA graph on samples that been immersed in acetone for different period.

SEM Observation

From the SEM observation, it shows that at the beginning of the work, the diameter of the CF is 6.709 µm as shown in Figure 3.2 (a). The size of the fibre at this stage was including the size of the fibre itself as well as the epoxy resin, as a result of pre-preg condition.

After immersed in acetone for 24 days, the non-cured epoxy resin was decomposed into the acetone as result from the immersion process. The partly cured epoxy resin (because the samples were an expired pre-preg), which has the cross-linked structure remain on the fibre and show that two different diameter of fibre as shown in Figure 3.2 (b).

Pyrolysis process had been performed to totally remove the epoxy material from the samples. After the pyrolysis process, the applied heat again burned the remaining organic structure of epoxy material and result in smaller fibre diameter that is 5.732 µm as in Figure 3.2 (c). Figure 3.2 (d) shows the size and shape of the milled reclaimed CF for 10 hours. The sizes of the particles were in range of 3.5 µm to 4.5 µm with a flake shape.

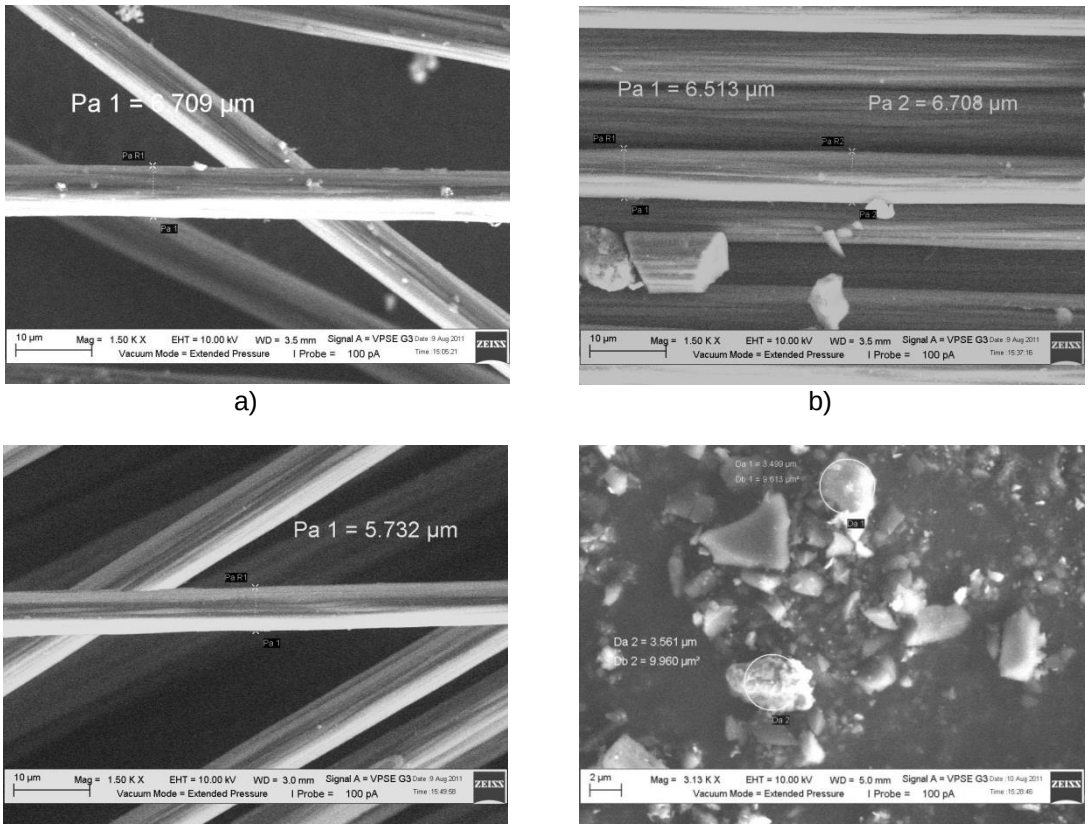

a) b)

c) d)

Figure 3.2: SEM Image of carbon fibre (a) Waste pre-preg carbon fibre before immersion in acetone, (b) Waste pre-preg carbon fibre after immersion of 24 days in acetone, (c) Reclaimed carbon fibre from waste pre-preg after pyrolysis process and (d) Reclaimed CF after milling process.

Testing of Composite Panel

Density Testing

Using the *Alfa-Mirage* Electronic Densimeter, *MD-300S*, the density of each panels was determine as shown in Table 3.1. Panel 1, an original composite panel, only contains the glass fibre and the polyester matrix. Panel 3 is filled with reclaimed CF powders which also have the same specific density of original CF that is 1.7 g·cm^{-3}. On the other hand, Panel 2 have a greater density due to the higher density of $CaCO_3$ filler that is 2.7 g/cm^3

Table 3.1: Density of Fabricated Composite Panels

Panel	Density ($g \cdot cm^{-3}$)
Panel 1: CFM450	1.44
Panel 2: CFM450+$CaCO_3$	1.56
Panel 3: CFM450+RCF	1.48

The existence of filler in panel # 2 and # 3 will increase the density of the composite panel. However, the higher density of the panel will cause a greater weight of the panels. The increasing weights of the panels are not appropriate in order to be applied in lightweight application.

Tensile and Flexural Test

As the most fundamental mechanical testing, tensile test was performed on the samples to determine its strength. Moreover, in order to determine the performances of the composites, 3-point bending test was also conducted to identify the flexural properties of the composite systems. This demonstrate the combination loading mechanism of tensile (at the lower part) and compression (at the upper) part of the tested specimen.

In the tensile test, Panel 1 shows the highest tensile modulus, followed by Panel 3 and Panel 2. From the test conducted, it shows that the tensile modulus for Panel 3 is higher by 1% compared to Panel 2. This shows that reclaimed CF in powder form can be used as filler because it demonstrated an equal performances with $CaCO_3$ filler

On the other hand, from the 3-point bending test, Panel 3 gives the lowest flexural modulus compared with Panel 1 (lower by 5.7%) and Panel 2 (lower by 2%). These result was differ compared to tensile test.

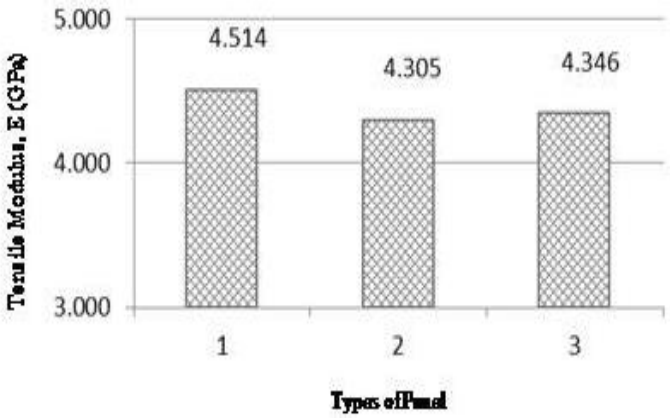

Figure 3.3: Tensile Modulus of Composite Panels

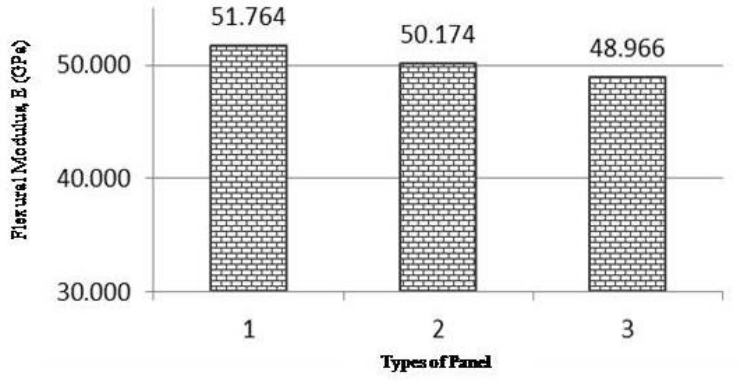

Figure 3.4: Flexural Modulus of Composite Panels

The SEM images in Figure 3.2 (d) shows the milled particle of reclaimed CF. The particles sizes was in range of 3.5 µm to 4.5 µm, a huge difference in micron scale. These may contribute to the differences performances of the Panel 3 in tensile and flexural test. Moreover, the flake shape of the milled reclaimed CF can also be the causes that contribute to the differences. According to Ahmad et al. [3], an elongated particles shape will exhibit higher flexural and tensile properties of composite systems. Moreover Suriati et al. [4] also reported that the nano-sizes particles resulted in higher tensile and flexural properties compared to micron flake particles. These show that the non-uniform sizes of milled CF as well as the flake-like shape contributes the differences in the tensile and flexural properties results.

The other properties of composite that shows it advantages are the specific modulus. From the density and mechanical testing conducted, it shows that Panel 3 has a higher specific tensile modulus compared to Panel 2 that is higher by 6.5% and the specific flexural modulus are higher by 2.8%. These was resulted from the lower density of reclaimed CF particles (refer Table 3.1 for the composite panel density) which contributes the lower density of the composite systems, as demonstrate in Table 3.2.

Table 3.2: Comparison between Modulus and Specific Modulus of Composite Panels.

Panel No	Density, ρ , $g \cdot cm^{-3}$	Tensile Modulus, E, GPa	Specific Tensile Modulus	Flexural Modulus, E, GPa	Specific Flexural Modulus
1	1.44	4.514	3.135	51.764	35.947
2	1.56	4.305	2.759	50.174	32.163
3	1.48	4.346	2.937	48.966	33.085

The specific modulus is also known as stiffness to weight ratio, which functions to determine material that will produce structure that have higher mechanical properties with minimum weight especially in designing product that have limitation in physical deformation or deflection rather that load at breaking requirement. On the other hand, these type of material also known as lightweight materials.

The needs of the lightweight material were also the other issues that demands replacement to filler that lighter but able to provide same or equal strength with the traditional filler that is $CaCO_3$. Based on the experiment it is proven that the composite panel filled with reclaimed CF powder result in an approximately equal or better specific modulus compared to composite panel filled with $CaCO_3$.

In composite industry, filler was used widely in preparing the pre-mix material such as Sheet Moulding Compound, (SMC) and Dough Moulding Compound, (DMC). These pre-mix material normally used in application that requires high strength and ability to sustain in

environmental condition such as hot-water tank, and chemical tank. Therefore, these pre-mix materials, requires a high grade of polymer matrix resin which result in higher cost on the material according to Palmer et al. [5].

The function of filler material was not only to improve the properties of composite systems but it was also to reduce the usage of expensive polymer matrix material. According to Oksman [6], the increasing percentages of filler from 10% to 30% will improve the properties i.e. strength and impact properties of the composite system. The increasing percentages of the filler, which means the increasing amount of filler, will reduce the polymeric resin consumption. This will help to help to reduce the high cost of polymer matrix material in preparing a pre-mix material for special application.

Moreover, recycling and reusing waste material issues also can be applied in this condition. CF can be reclaimed from waste and scrap from manufacturing or product that reach their end-service-life. These reclaimed CF can be processed by using pyrolysis method, a simple and cost-effective process to produce a powder particle form to become a filler material in other composite industry such as pre-mix material i.e. SMC and DMC material. These reclaimed CF was not only suitable for those applications but also resulted in better specific properties due to lower density of the CF itself compared to the traditional $CaCO_3$ powder.

Conclusion

Reclaimed CF demonstrates promising performances as filler material in composite systems. The reclaimed CF from composite waste and scrap must be treated either surface treated or uniformed grinding or milling accordingly to enable the interaction of the particles and the matrix material. The higher specific modulus of the composite panels that filled with reclaimed CF again demonstrates the capability of reclaimed CF in contributing the higher properties of composite systems as well as helping to reduce the cost in producing composite products because the recycling and reusing ability of reclaimed CF.

Acknowledgements

The authors would like to thank SIRIM Berhad as well as from Asian Composite Manufacturing Sdn. Bhd. (ACMSB) for the support and assistance in conducting this research work.

References

[1] A. Torresa, I. de Marcoa, B.M. Caballeroa, M.F. Laresgoitia, J.A. Legarretaa, M.A. Cabreroa A. Gonza´leza, M.J. Chomo´na, K. Gondrab (2000). Fuel.79: 897–902

[2] L.O. Meyer, K.Schulte, E.Grove-Nielsen 2007. *16th international conference on composite materials*. Kyoto, Japan

[3] F.N. Ahmad, M. Jaafar, S. Palaniandy, K.A.M. Azizli. (2008). *Comp. Sci. Tech.* 68(2): 346-353

[4] G.Suriati, M. Mariatti, A. Azizan. (2010). *J. Mat. Sci.: Mat. Elect.* 22(1): 56-63.

[5] J.Palmer, L.Savage, O.R. Ghita, K.E. Evans (2010). *Composites: Part A.* 41: 1232–1237

[6] K. Oksman, C. Clemons. (1997). J. Appl. Polym. Sci. : 1503-1513

EFFECT OF HEAT TREATMENT OF WOOD FLOUR ON THE WATER ABSORPTION AND MECHANICAL PROPERTIES OF RED BALAU SAW DUST/LDPE COMPOSITES

Ruth Anayimi Lafia-Araga[1,2], Aziz Hassan[1*], Rosiyah Yahaya[1] & Normasmira Abd. Rahman[1]

[1] Department of Chemistry, University of Malaya, 50603 Kuala Lumpur, Malaysia

[2] Department of Chemistry, School of Natural and Applied Sciences, Federal University of Technology, Minna 920001, Niger State, Nigeria

Abstract

Due to the hygroscopic nature of wood, its use in wood thermoplastic composites (WTC) in outdoor industrial and domestic applications is limited. Wood is usually modified to reduce this tendency. Red balau saw dust was modified by heat treatment at 180°C and 200°C for 1 hour, compounded with LDPE at 20% and 37% by weight and molded into test specimens by injection molding. Samples were immersed in distilled water at room temperature for four months. Pure LDPE did not absorb water as no weight gain was recorded throughout the experimental period. Composites containing heat treated wood flour show remarkable water resistance than those made from untreated ones. Reduced water absorption of treated wood composites relative to untreated ones indicates a degree of modification by heat treatment. Tensile and flexural tests results revealed that the untreated wood composites have poorer mechanical properties with water immersion as a result of degradation due to moisture. The mechanical properties of composites made from heat treated wood flour were not adversely affected with water absorption. Therefore, heat treatment is capable of reducing the proneness to water absorption in WTC, alleviate the detrimental effects on mechanical properties and provide a good way of improving the WTC properties in applications that poses moisture related challenges.

***Keywords**: Heat treatment, injection molding, thermoplastic composites, water absorption.*

Introduction

One of the shortcomings of using wood in thermoplastic composites production is the hygroscopic nature of wood. This leads to swelling and shrinkage due to moisture absorption and desorption, resulting in poor mechanical properties of the resultant product. As a result, the use of wood thermoplastic composites (WTC) in industrial and domestic applications is limited. In certain use, the environmental conditions can be so unfavourable that the performance of these composites is adversely affected.

Several treatment methods have been employed to checkmate these limitations and enhance better moisture resistance [1]. Heat treatment is one of the wood modification methods. In heat treatment, wood is subjected to higher temperatures than drying (160-250°C). This results in the degradation of hemicellulose which has the lowest molecular weight among the wood constituents, leading to reduction of the OH groups and the formation of O-acetyl groups. Thermal softening of cell wall matrix, mainly lignin also sets in with cross-linking occurring between carbohydrate polymers and/or between lignin and carbohydrate polymers, resulting in an increase in the crystallinity of amorphous cellulose with consequent improvement in dimensional stability and decreased hygroscopicity of wood. Also, the softened lignin flows and blocks the cell pores, thereby contributing to the reduction in moisture absorption [2]. Therefore, heat treated wood is expected to become more hydrophobic with increase in treatment temperature.

The ability of wood particles treatment to reduce the water absorption tendencies in WTC has been reported [3]. However, moisture absorption in WTC is still a major concern,

especially for their outdoor applications. It has been observed that the sorption of water by non polar polymers containing fillers depends mainly on the nature of the filler [4]. Therefore, for hydrophilic fillers such as wood particles, increase in water absorption should be expected. Another very important concern is the negative effects moisture has on physical and mechanical properties. Research has shown that mechanical properties of WTC decreased with water absorption [1]. Hence, it is necessary that this problem is tackled so that natural fillers can be seen as a viable reinforcement material in WTC.

Therefore, this paper is aimed at modifying red balau saw dust with heat treatment, compounding with LDPE and studying the effects of water absorption on the tensile and flexural properties of the resultant composites.

Materials and Method

Red balau (*Shorea dipterocarpaceae*) saw dust was obtained from a local saw mill in the Klang Valley, Selangor, Malaysia. It was milled to between 40-100 mesh (400-150 µm) sizes using a locally fabricated mill. Commercially available LDPE (Titanlene LDI300YY), with a density of 920 kg/m^3, molecular weight of 3.5-3.8 x 10^5 g·mol^{-1} and MFI of 20 g·10^{-1} min, supplied by Titan Petchem (M) Sdn. Bhd., Malaysia, were used as the matrix.

Acid insoluble lignin was determined using ASTM D-1106 [5] standard. Hemicellulose and cellulose were analyzed according to the method described by Rowel *et al.* [6].

Untreated wood sawdust was dried in an oven at 60°C for 48 hours to a moisture content of less than 2% and stored in sealed plastic bags over dried silica gel in desiccators prior to compounding. Undried wood flour was subjected to 180°C and 200°C temperatures in a vacuum oven for one hour effective treatment time.

LDPE was compounded with untreated or the heat treated wood flour at two compositions of 20% and 37% by weight (Table 1) using a twin screw co-rotating extruder (*Brabender KETSE 20/40 Lab Compounder*, Germany) at a barrel temperature of between 150-155°C along the barrel zones and screw speed of 250 rpm. The melt pressure varied between 34-39 bars depending on the wood content, while the die temperature was between 164-178°C. The compounds were extruded out through a circular die of 3 mm in diameter, cooled in a water bath and pelletized. Extruded pellets were oven dried at 80°C for 24 hours and stored in sealed plastic bags over silica gel in desiccators for injection molding.

The pellets were injection molded into tensile test bars according to size as stated in ASTM D-638 [7] standard using the *BOY 55M* (Germany) injection molding machine at a barrel temperature of between 150-155°C, an injection pressure of 100-120 bars and mold temperature of 25°C.

Water absorption tests were performed on samples cut from tensile test stripes according to ASTM D-570 [8]. Tensile tests were carried out at room temperature on dry and water soaked specimens using a universal testing machine (*Instron 5569*, USA) equipped with a load cell of 50 kN and a mechanical extensometer according to ASTM D-638 [7] at a cross-head speed of 5 mm·min^{-1}. A zero span of 50 mm was chosen for the extensometer. Minimum seven samples were tested and the average value of at least five best results was recorded.

Table 1. Formulations of the composites

Sample code	Treatment temperature (°C)	Weight of wood flour (%)	Weight of LDPE (%)
LDPE/$W_{UN/20}$	Untreated	20	80
LDPE/$W_{UN/37}$	Untreated	37	63
LDPE/$W_{180/20}$	180	20	80
LDPE/$W_{180/37}$	180	37	63
LDPE/$W_{200/20}$	200	20	80
LDPE/$W_{200/37}$	200	37	63

The same instrument used for tensile testing was used for the flexural testing but in three point bending mode according to ASTM D-790 [9]. Dry as molded and moisture saturated tensile test specimens were tested at room temperature with a span of 50 mm. Samples were tested to a maximum deflection of 30 mm at a cross-head speed of 1.28 mm·min^{-1}. Minimum seven samples were tested and the average value of at least five best results was recorded.

Results and Discussion

Chemical composition

Table 2 illustrates the percentage composition of lignin, carbohydrates, extractives and ash in the wood flour samples.

Table 2. Chemical composition of red balau saw dust [10].

Treatment temperature (^{o}C)	Lignin (%)	Hemicellulose (%)	Cellulose (%)	Extractives (%)	Ash (%)
Untreated	29	29	41	2	2
180	29	28	42	2	2
200	31	25	42	2	2

The results suggest that carbohydrates were more susceptible to thermal degradation than lignin at the treatment temperature. Hemicellulose degraded faster than cellulose as the values decreased when wood is subjected to heat treatment. This may possibly be because cellulose is more crystalline than hemicellulose which confers better resistance to thermal degradation. Zaman *et al.* [11] have suggested that cellulose (a linear homo-polysaccharide of β-D-glucopyranose) is more thermally stable than hemicellulose. On the other hand, a steady increase in lignin content was observed as the treatment temperature increased. This clearly indicates that lignin is more thermally stable than carbohydrates.

Water absorption behaviour

Water uptake, W_t, was calculated using the formula,

$$W_t = \frac{W_2 - W_1}{W_1} \times 100\ (\%) \qquad (1)$$

where W_1 and W_2 are the dry weight and weight after time t of immersion in water respectively.

A plot of moisture content against time for the different treatment temperatures and wood flour loadings is presented in Figure 1. The neat LDPE shows no water absorption as no weight increase is observed over the period of study. This is because neat LDPE is hydrophobic and has no tendency of absorbing water. However, both the untreated and the treated wood composites absorbed water to various extents. As the neat LDPE did not absorb water, it can be assumed that the wood flour is responsible for all the moisture absorbed by the composites. This is expected due to the hydrophilic nature of wood flour. It is sometimes believed that moisture is not an issue with WTC because wood is totally encapsulated by the matrix. If that is the case, the matrix would shield the wood from moisture because they are hydrophobic. Nevertheless, composites still exhibits a degree of moisture absorption tendency [12]. This seems to indicate that wood must have been exposed on the surface of the samples which may be responsible for the various degree of water absorption exhibited by the composites.

Also, it can be seen that water absorption increases with time of immersion, reaching a certain value (the equilibrium point), when the water content of the composite remained constant. LDPE/$W_{180/20}$ and LDPE/$W_{200/20}$ reached equilibrium (1.03% and 1.04% respectively) at 35 days while LDPE/$W_{180/37}$ and LDPE/$W_{200/37}$, attained equilibrium point (1.94% and 1.91% respectively) on the 49th day of immersion. This may be due to the presence of more O-H groups on the surface of the composites with higher filler content, leading to more ability to absorb water [13]. However, LDPE/$W_{UN/20}$ and LDPE/$W_{UN/37}$ exhibits a saturation point of 1.87% and 3.23% respectively on the 77th day of immersion. This is likely because of the higher number of free O-H groups on the surfaces of untreated wood composites which interact with water via hydrogen bonding. It is also possible that at 37 wt%, the wood flour is not continuously distributed and most of the wood particles may probably have contacted one another directly, in which case, complete encapsulation is not achieved (Figure 2). This could result in the higher water absorption values recorded for composites at 37 wt% wood content.

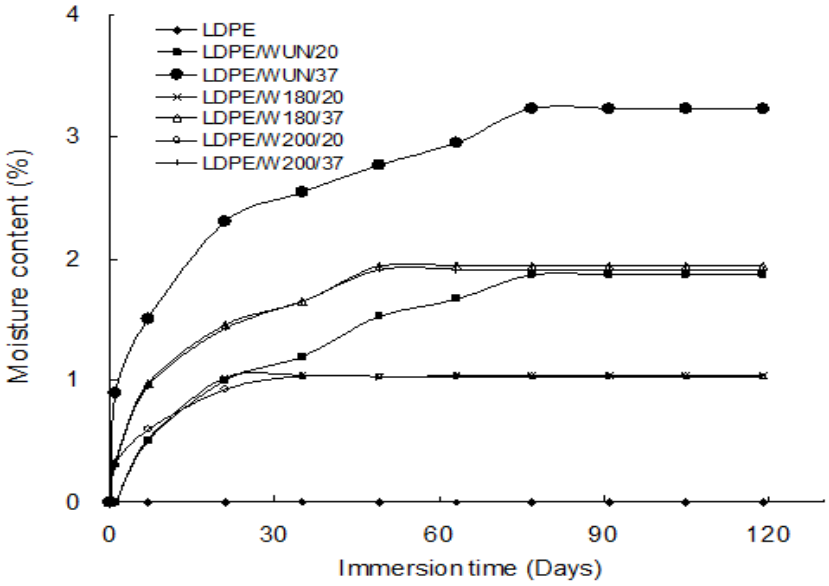

Figure 1: Water absorption curves of red balau/LDPE composites

Water absorption in WTC has been shown to not only depend on the filler particles and matrix structure, but also on the filler-matrix interface [14]. Hydrophilic fillers lead to lower filler-matrix interaction resulting in poor interface which facilitates the absorption process. This is supported by the SEM micrographs presented in Figure 2.

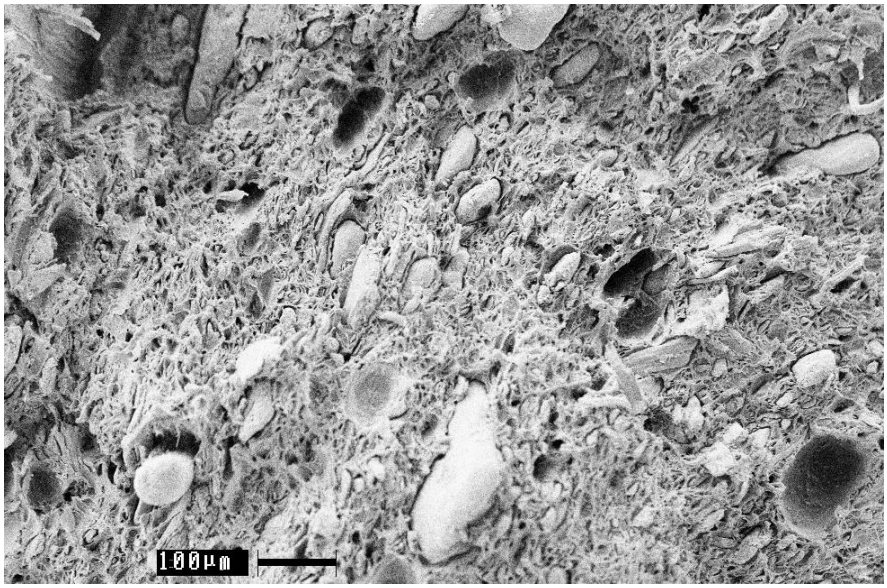

Figure 2: Untreated wood composites after moisture saturation showing flaws and gaps

It has been said that moisture can be absorbed into the composite by the dissolution of water into the polymer network, moisture sorption into the free volume, if present, in the glassy structure and by hydrogen bonding between the hydrophilic group of water and the components of the composite. Micro-cracks can also allow moisture transportation involving flow and storage of water within the cracks [14]. Untreated wood composites generally show higher water absorption than treated ones. LDPE/$W_{UN/20}$ absorbed 55% more water compared to LDPE/$W_{180/20}$ and LDPE/$W_{200/20}$ while LDPE/$W_{UN/37}$ absorbed about 40% water higher than LDPE/$W_{180/37}$ and LDPE/$W_{200/37}$. This could be attributed to the removal of the water sensitive components, hemicelluloses, in wood flour by heat treatment, thereby rendering the composites more water resistant. Reduction of hemicelluloses in heat treated wood flour was reported in our previous studies [10]. Furthermore, free hydroxyl groups of the cellulose are reduced with heat treatment. This may lead to decrease in the water absorption of the wood flour and consequently, the composites. Follrich *et al.* [15] reported that at 200°C, hydrophilicity of spruce wood decreased appreciably. This was observed as an important result for WTC compounding and inferred that it is an alternative way of increasing the adhesion between wood and hydrophobic thermoplastics without the use of compatibilizer. Composites containing 20 wt% wood flour absorbed water and reached saturation faster than that made from 37 wt% wood flour content, which attained saturation more gradually (Table 2). The fact that higher filler content means higher ability to absorb water may have resulted in delayed equilibrium moisture content attainment for both treated and untreated composites. Increase in water absorption of untreated wood composites relative to the treated ones is due to the hydrophilicity of wood imparted by the free O-H groups in the wood structure which has a high tendency for hydrogen bonding with water. It has also been reported in our previous publication [10], that the untreated wood has higher hemicellulose content which is responsible for moisture absorption. Reports revealed that the absorption of water by non polar polymers containing fillers depends mainly on the nature and the amount of the fillers. Furthermore, the amount of accessible O-H groups that can form hydrogen bonds with water molecules is another factor responsible for the degree of water absorption by composites. The higher the amount of the OH groups, the higher is the initial rate as well as the level of water uptake [4], explaining the observed trend.

Mechanical properties

Tensile properties

Figure 3 shows the tensile modulus of dry and wet specimens at equilibrium moisture content for WTC immersed in water. Tensile modulus of the composites was generally found to decrease with water immersion. The relative extent of decrease is greater in untreated wood composites relative to the heat treated ones. Composites containing 20 wt% and 37 wt% untreated wood flour present the highest reduction (38% and 23% respectively) in tensile modulus after immersion in water compared to their counterparts made from wood flour treated at 180°C (36% and 5% respectively) and those containing wood flour treated at 200°C (10% and 0.1% respectively).

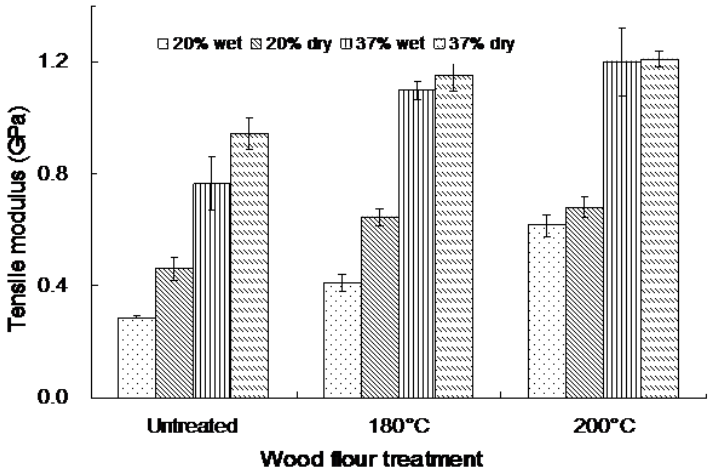

Figure 3: Tensile modulus of wet and dry as molded composites

The deteriorating effects of water molecules interacting with the wood at the composites interface due to the inherent incompatibility between the polar wood and the non polar matrix (Figure 2) may be responsible for this observation. As a result of the hydrophilic nature of wood, when WTC is exposed to water, the wood particles takes up water resulting in the swelling of the wood cell wall, leading to changes in the dimensional stability of the composites and consequently, reduced mechanical properties. Also, water molecules present at the interface reduces the interaction between the filler and the matrix which can lead to poor mechanical properties [16]. Tensile modulus of 180°C treated wood composites reduces slightly with water absorption. This may be due to the reduced hydrophilicity in heat treated wood which enhanced better compatibility between the filler and the matrix. It has been reported that water molecules can act as plasticizers to soften the wood cell wall polymers [17].

Also, the tensile modulus of a composite is determined by the stiffness of the filler and the matrix. In addition, it is a filler sensitive property in composites that is affected by moisture absorption [18]. Therefore, the lower the water uptake, the lower the amount of water molecules available to act as plasticizer to affect the tensile modulus. However, composites from heat treated wood at 200°C exhibit the lowest decrease in tensile modulus with water immersion (Figure 3). This may be due to the better wetting shown by these composites (Figure 4) and indicate that the amount of water absorbed at equilibrium moisture content has minimal effects on the stress transfer capability. On the other hand, LDPE/$W_{180/20}$ shows a significant drop in tensile modulus compared to the other heat treated composites.

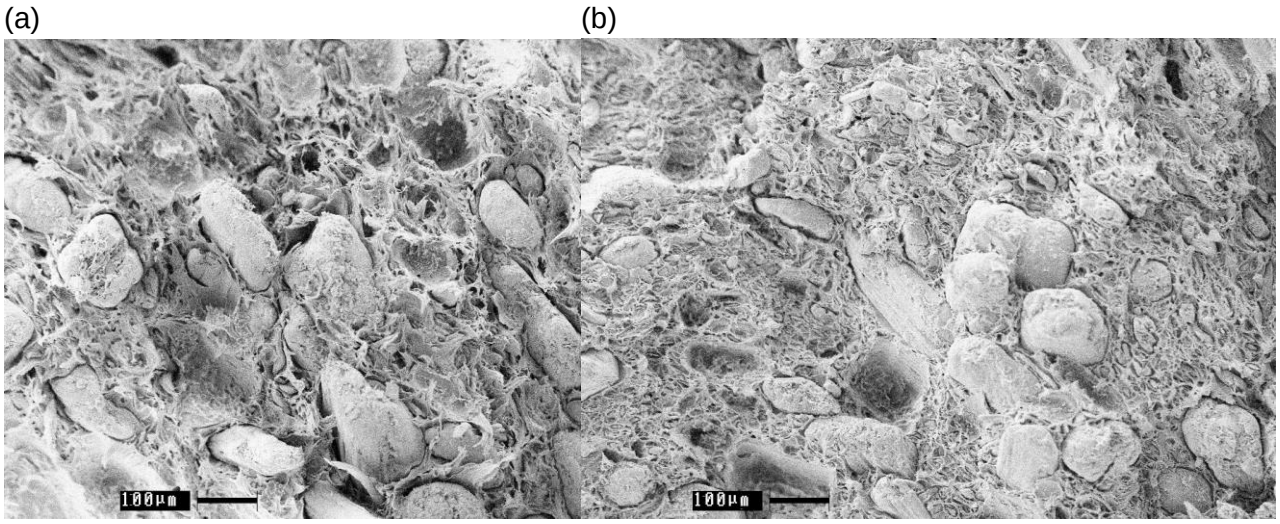

Figure 4: SEM micrograph of moisture saturated composites containing wood flour treated at (a) 180°C and (b) 200°C showing better encapsulation and lesser flaws.

Tensile strength decreases after immersion in water in the untreated wood composites (Figure 5). This may be a result of the plasticization effects of water on WTC and is in agreement with literature [19][20][21].

The absorption of moisture plasticizes the system, leading to a reduction in tensile strength. More so, in the presence of moisture, cellulose at the filler-matrix interface tends to swell. This results in a shear stress at the interface which favours ultimate debonding of the fillers, leading to a reduction in the tensile strength [1]. However, tensile strength for heat treated wood composites did not show a significant decrease. This could mean that the high interfacial adhesion in these composites due to heat treatment becomes predominant relative to the induced shear stress. The tensile strain of the wet composites decreased generally for all the composites studied relative to the dry ones. This is anticipated because of the notching effects of wood particles (Figure 6). In addition, excessive absorption of water has a pronounced effect on matrix softening and can lead to low strain.

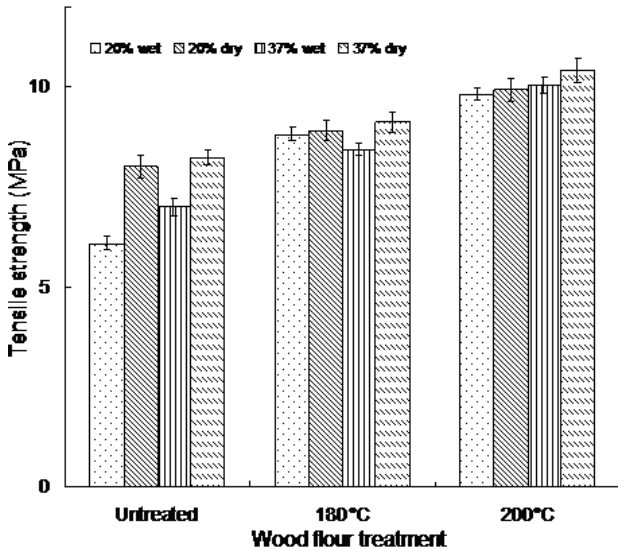

Figure 5: Tensile strength of wet and dry as molded composites

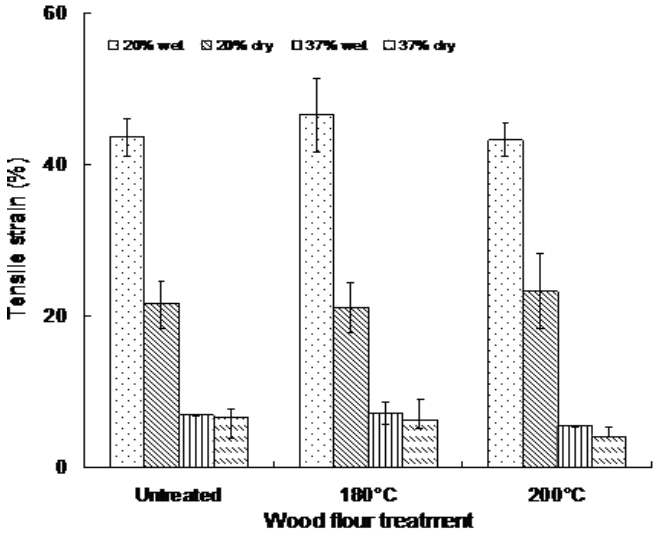

Figure 6: Tensile strain of wet and dry as molded composites

Flexural properties

Figures 7-9 presents the flexural modulus of water soaked and dry as molded composites. Water absorption seems to have no pronounced effect on the flexural modulus of wet composites compared to dry ones (Figure 7). Generally, there is a slight decrease in flexural modulus values at equilibrium moisture content. Furthermore, higher reduction in flexural modulus was observed for water soaked composites from untreated wood. Flexural modulus of heat treated wood composites was not appreciably altered with water immersion.

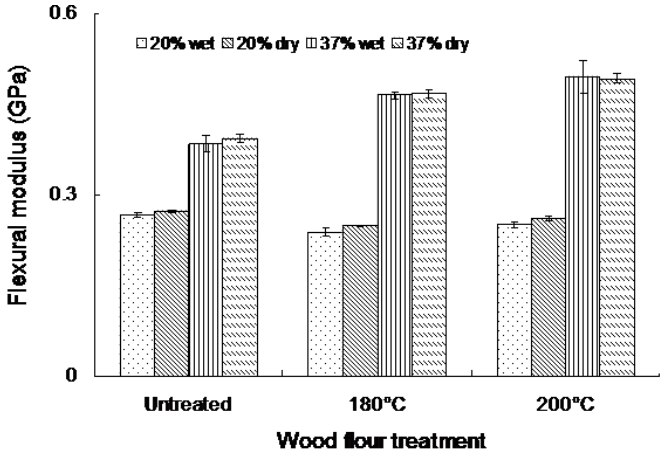

Figure 7: Flexural modulus of wet and dry as molded composites

It is possible that the better compatibility in heat treated wood composites (Figure 4) has alleviated the interfacial degradation of the filler-matrix interface, resulting in better stress transfer. This result agrees with earlier reports [18]. The flexural strength decreases marginally in wet samples relative to the dry as molded ones. Again, the rate of decrease is higher in composites made from untreated wood flour (Figure 8). However, no particular trend is observed for the flexural displacement with moisture absorption (Figure 9).

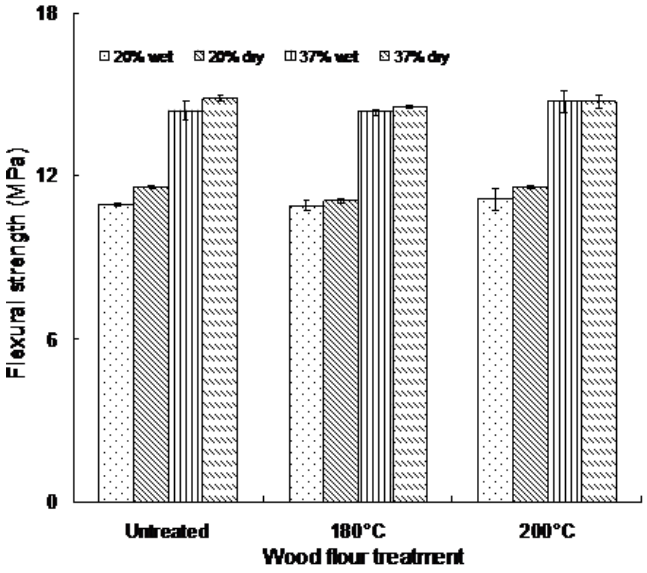

Figure 8: Flexural strength of wet and dry as molded composites

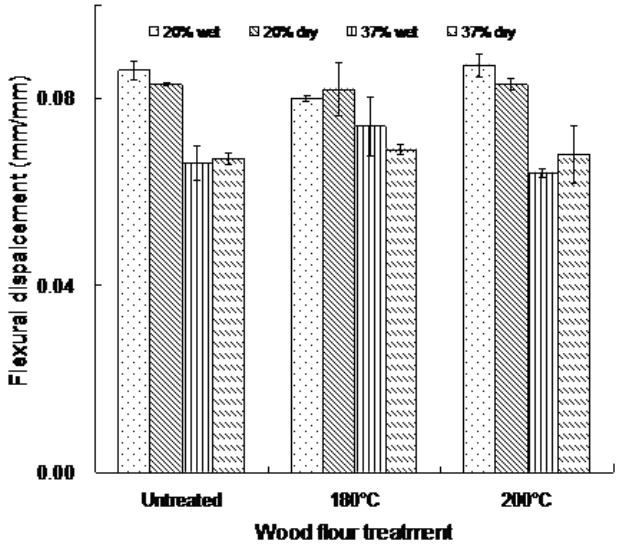

Figure 9: Flexural displacement of wet and dry as molded composites

Conclusion

All the composites were found to absorb moisture to various extents due to the hydrophilic nature of wood. However, composites from heat treated wood showed lower water absorption tendency because of the reduced hydrophylicity imparted to the wood by heat treatment. Tensile properties decreases generally with water absorption for all composites studied but the extent of decrease is more observable in untreated wood composites compared to the heat treated ones. In addition, flexural modulus and flexural strength present a marginal decrease for all the composites. Again, the heat treated composites showed a lower decrease compared to the untreated ones. However, flexural displacement presented no particular trend. From these results, it is evident that heat treatment can reduce the moisture absorbing tendency in wood leading to a more water resistant composites with the ability to retain its mechanical properties after long time exposure to moisture. It is therefore a good way of improving the WTC properties in applications that poses moisture related challenges.

Acknowledgements
The authors gratefully acknowledge the University of Malaya for supporting work reported in this manuscript through grant numbers PS347/2009C and RG150/11AFR.

References

[1] Joseph, P.V., Rabello, M.S., Mattoso, L.H.C., Joseph, K. and Thomas, S. 2002. *Compos Sci Technol. 62, 1357–1372*
[2] Tjeerdsma, B.F., Boonstra, M., Pizzi A., Tekely, P. and Militz, H. 1998. *Holz Roh-Werkst. 56, 149-153.*
[3] Demir, H., Atikler, U., BalkÖs, D. and Tıhmınlıoğlu, F. 2006. *Compos Part A.* 37, 447-456.
[4] Marcovich, N.E., Reboredo, M.M. and Aranguren, M.I. *Polymer.* 1999. *40*, *7313–7320.*
[5] ASTM standard D-1106, 1996, *ASTM International,* West Coshoshocken, PA
[6] Rowell, R.M., Pettersen, R., Han, J.S., Rowell, J.S. and Tshabala, M.A. 2005. In Rowell, R.M. (ed.). *Handbook of Wood Chemistry and Wood Composites*. Boca Raton: CRC Press. 474.
[7] ASTM standard D-638, 2003, *ASTM International,* West Coshoshocken, PA
[8] ASTM standard D-570, 1998, *ASTM International,* West Coshoshocken, PA.
[9] ASTM standard D-790, 2003, *ASTM International*, West Coshoshocken, PA.
[10] Lafia-Araga, R.A., Hassan, A., Yahya, R., Abd.Rahman, N., Hornsby, P., Heinderian, J. 2012. *J Reinf Plast Compos. 31, 215-224.*
[11] Zaman, A., Alen, R., and Kotilainen, R. 2000. *Wood Fiber Sci. 32, 138-143.*
[12] Balatinecz, J. J. and Park, B. 1997. *J Thermoplast Compos Mater. 10, 476-487*.
[13] Khalil, H.P.S.A., Shafizah Shahnaz, S.B., Ratnam, M.M., Ahmad, F., Nik Fuad N.A. 2006.
J Reinf Plast Compos. 25,1291-1303.
[14] Sreekala, M.S., Kumaran, M.G. and Thomas, S. 2002. *Compos Part A*. *33, 763-777*
[15] Follrich, J., Muller, U. and Gindl, W. 2006. *Holz als Roh Werks. 64, 373-376*.
[16] Mat Taib, R., Mohd Ishak, Z.A., Rozman, H.D. and Glasser, W.G. 2006. *J Thermoplast Compos Mater. 19, 475-489.*
[17] Stamboulis, A., Bailie, C.A., Peijis T., 2001. *Compos Part A. 32, 1105-1115*
[18] Dhakal, H., Zhang, Z. and Richardson, M. 2007. *Compos Sci Technol. 67, 1674-1683*.
[19] Nachtigall, S.M.B., Cerveira G.S., Rosa, S.M.L. 2007. *Polym Test.* 26, 619– 628.
[20] Panthapulakkal, S., Sain, M. 2007. *J Compos Mater.* 41,1871-1882.
[21] Cui, Y.H., Wang, X.X., Xu, Q., Xia, Z.Z. 2010. *J Thermoplast Compos Mater.* 24 , 65-82.

CORN STALK FILLED LOW DENSITY POLYETHYLENE BIOCOMPOSITES: EFFECTS OF COCA AS COUPLING AGENT

Azimah Ismail, Salmah Husseinsyah & Hakimah Osman
School of Materials Engineering, Universiti Malaysia Perlis, 02600, Jejawi, Perlis, Malaysia.

Abstract

Corn stalk (CS) filled low density polyethyelene (LDPE) biocomposites was prepared. The effect corn stalk loading and coconut oil coupling agent (COCA) on tensile properties and morphology of LDPE/CS biocomposites were investigated. The results show that the increasing of corn stalk content, tensile strength and elongation at break decreased while Young's modulus increased. The dispersion and interfacial adhesion between the corn stalk filler and thermoplastic were important factors affecting the tensile properties of composites system. The addition of COCA has enhanced tensile properties and interfacial interaction between corn stalk and LDPE biocomposites was proven by SEM study.

***Keywords**: Biocomposites, corn stalk, coupling agent, low density polyethylene.*

Introduction

Over the past decade there has been a growing interest in the use of lignocellulosic fibres as reinforcing elements in polymeric matrices [1,2] due to increasing environmental concerns. Biodegradable polymers have been a subject of interest for many years because of their potential to protect the environment by reducing non-biodegradable synthetic plastic waste. Biodegradation involves enzymatic and chemical degradation by living microorganisms. Agriculture is an important sector in Malaysian economy. Traditionally, agricultural materials have been shipped away for processing, or disposed of post-harvest. Diversification of the industry is crucial in encouraging economic stability and growth. Value added processing would helps in agricultural diversification. There are a lot of industrial and waste materials that are currently being thrown everywhere and one of them is agriculture biomaterials. Big amount of them occur universally as waste materials of industrial processing and other operations. They occur in various processed forms, such as pulp sludge from the manufacture of paper, commonly known as clarifier sludge, wood, sugar cane, bagasse pith, grass, coarse grass, sisal, pineapple, coir and jute [3-5]. Corn Stalk is selected as the biomass feed stock. Corn is an important crop all around world. As it is expected, after huge amount of production, huge amount of residue remain. Although corn residue may contain valuable compounds, used for animal food or retained in the field to prevent soil erosion, converting the organic matter in the residue into more valuable.

Low density polyethylene (LDPE) is widely used for manufacturing various containers, dispensing bottles, wash bottles, tubing, plastic bags for computer components, and various moulded laboratory equipment. Its most common use is in plastic bags. Made in translucent or opaque variations, it is quite flexible, tough also having a good combination properties such as excellent resistance (no attack) to dilute and concentrated acids, alcohols, bases and esters, good resistance (minor attack) to aldehydes, ketones and vegetable oils. Interfacial adhesions between the natural reinforcing filler and matrix polymers, is the most important issue associated with these composites. The compatibility problem may be due to the fact that the polyolefin is non-polar and hydrophobic, where as the natural polymer, which is a lignocellulosic material, is polar due to the –OH groups in cellulose. This results in poor adhesion and prevents the reinforcing filler from acting effectively in the composite. The good properties of these composites can be obtained by improving the compatibility between these two materials. Several strategies have been suggested in the literature describing the way to improve the compatibility of lignocellulosic fibres with thermoplastics polymers, example

physical treatment such as surface oxidation activation, and chemical modification [1,6] .In order to solve these problems, Belgacem et al. [7] studies have been performed on surface modification or treatment of filler using a compatibilising agent or coupling agent in order to reduce the hydrophilicity of the filler. Coconut oil coupling agent is the new type of coupling agent. The basic ingredient was extracted from the virgin coconut oil (VCO).The main composition of the virgin coconut oil is the lauric acid or also mentioned as fatty acid. In this study was focus to investigate the effect of filler loading of CS and Coconut Oil Coupling Agent (COCA) as coupling agent into LDPE/CS bicomposites on mechanical properties, and morphology.

Materials and Method

Materials

The Light Density Polyethylene grade LDF200YZ (film extrusion general purpose) was supplied by Titan Chemicals Corp. Bhd. The corn stalk was obtained from Kodiang Plantations, Kedah. After cleaned, the corn stalk was crushed and grinded into powder. The corn stalk powder (CSP) was dried at 80^{o}C for 24 hours. The average particle size of the CSP was 29.96 µm, by using *Malvern* Particle Size Analyzer Instrument.

Preparation of Biocomposites

The LDPE/CS biocomposites was prepared by using Brabender Plastograph mixer *Model EC PLUS* at temperature 160^{o}C and rotor speed of 50 rpm LDPE was charged into mixing chamber for two minute until it completely melts. After two minute, CS powder and COCA was added and mixing continued for six minutes. The total mixing time was eight minutes. The biocomposites was compressed into tensile bar by using compression moulding machine *model GT 7014A*. Tensile bar was reference to ASTM D638 tensile bar type IV with 1mm thickness. The compression procedure involved preheating at 160^{o}C for 4 minute follow by compressing for 1 minute and subsequent cooling under pressure for 5 minutes. The similar procedure was done for LDPE/PKS with COCA. The formulation of LDPE/CS biocomposites with and without COCA with different filler loading was shown in Table 1.

Table 1: Formulation of LDPE/CS biocomposites

Materials	LDPE/CS	LDPE/CS
LDPE(php)	100	100
CS (php)	0,10,20,30,40	10,20,30,40
COCA(php)*	-	3

*3 php from weight LDPE.

Tensile Testing

The tensile testing was done according to ASTM D638 using *Instron Machine model 5569*. The cross head speed of 50 mm.min^{-1} was used and the tests were performed at 25 ± 3 ^{o}C. Tensile properties for five identical samples of each composition were measured and the average values were reported. The tensile strength, elongation at break and Young's modulus were measured from stress-strain curve and automatically calculated.

Morphology Analysis

Scanning Electron Microscope (SEM) model *JEOL JSM-6460LA* was used to examine the dispersion of corn stalk in LDPE matrix. The fracture ends of the specimen were mounted on an aluminium stub and sputter coated with a thin layers of palladium electrostatic charging during examination.

Results and Discussion

Tensile Properties

Figure 1 shows the effect of filler loading on tensile strength of LDPE/CS biocomposites with and without COCA. The tensile strength of LDPE/CS biocomposites without COCA was decreased with the increasing of filler loading. This occurs because the weak interfacial adhesion, and poor dispersion between filler and polymer matrix. The tensile strength of LDPE/CS biocomposites with COCA higher compared to LDPE/CS biocomposites without COCA. This behaviour can be attributed to present of strong interfacial adhesion and better dispersion between filler and polymer matrix with addition COCA. The better fillers- matrix interaction was derived from the formation of hydrogen bonding between the COCA and hydroxyl groups of corn stalk. The effectiveness of COCA in increasing the strength of the composites may explained by greater wettability, dispersion and orientation of the CS and LDPE matrix. Othman et al. [8] also found the same finding in their study of the effect of palm oil fatty acid (POFA) as compatibilising agent on bentonite filled polypropylene composites. The addition of POFA has improved the interaction between bentonite and polypropylene to become more effective thus increasing the tensile strength of the composites.

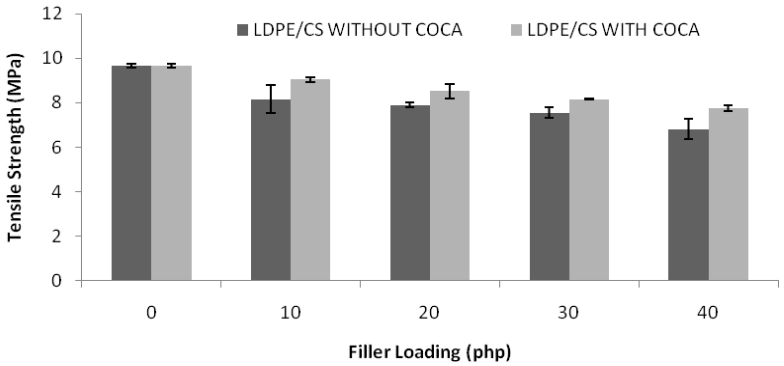

Figure1: The effect of filler loading on tensile strength of LDPE/CS biocomposites with and without COCA

Figure 2 shows that, the elongation at break of LDPE/CS biocomposites with and without COCA decreased with filler loading. The elongation at break of both biocomposites show decreasing trend with CS loading increased, due to more weak interfacial region between filler and matrix are formed. At similar filler loading, elongations at break of LDPE/CS biocomposites without COCA lower than biocomposites with COCA. The presence of COCA has increased the ductility of biocomposites.

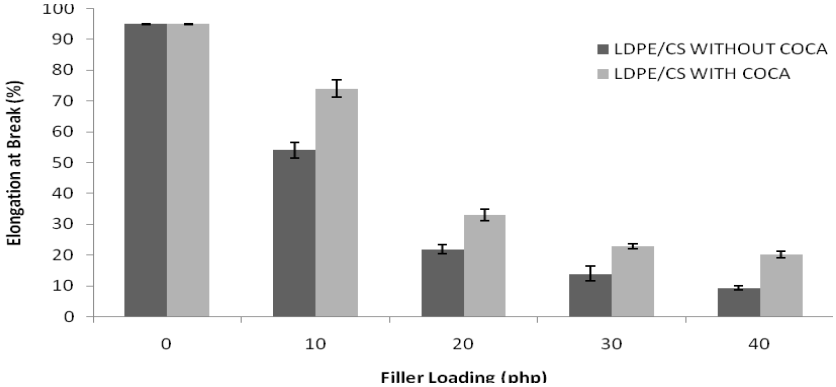

Figure 2: The effect of filler loading on elongation at break of LDPE/CS biocomposites with and without COCA.

The Young's modulus of LDPE/CS biocomposites with and with COCA was increased with the increasing of filler loading is shown in Figure 3. The Young's modulus of bicomposites without COCA composites increased with increasing filler loading. It is known that filler which has higher stiffness than matrix can increase the modulus of composites. At similar filler loading, the Young's modulus of LDPE/CS biocomposites without COCA was higher than biocomposites with COCA. These results indicates that the efficiency of COCA in improving plasticizers of LDPE/CS composites, while the polymer chain mobility inherent by the better filler-matrix interaction.

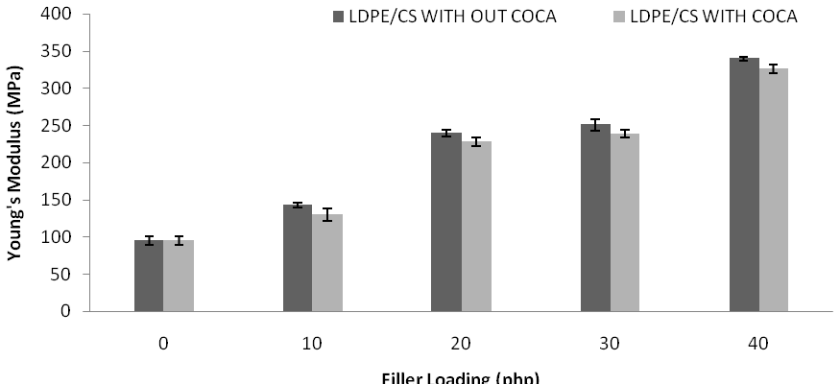

Figure 3: The effect of filler loading on Young's modulus of COCA LDPE/CS biocomposites with and without COCA.

Morphology Study

The micrograph of tensile fracture surface of LDPE/CS biocomposites without COCA at 20 and 40 php were shown in Figures 4 and 5, respectively. The micrograph of without COCA bicomposites show poor wetting of corn stalk in LDPE matrix. It can be seen that the bonding at interface of CS and LDPE matrix and CS pull out from LDPE surface, indicates a low adhesion between CS and LDPE matrix. Figure 6 and figure 7 show the ductility and plasticizers of the LDPE/CS biocomposites with COCA at 20 php and 40 php. SEM test prove that, elongation at break of LDPE/CS biocomposites with COCA is higher than LDPE/CS without COCA. Therefore, the presence of COCA enhances ductility and plasticizers properties of LDPE/CS biocomposites.

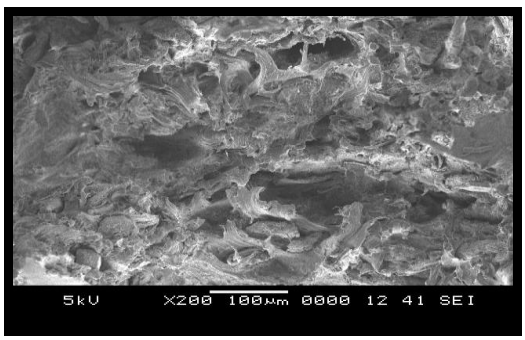

Figure 4: SEM micrograph of tensile fracture surface of LDPE/CS biocomposites without COCA (20 php) at magnification 200X.

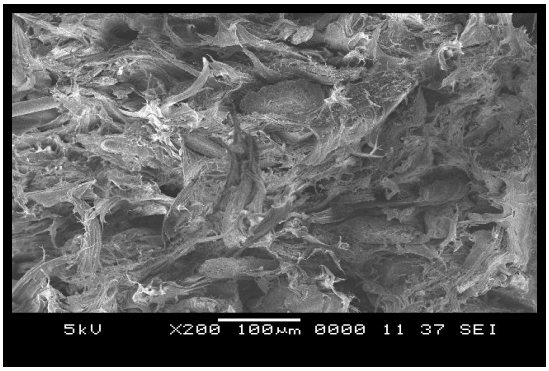

Figure 5: SEM micrograph of tensile fracture surface of LDPE/CS biocomposites without COCA (40 php) at magnification 200X.

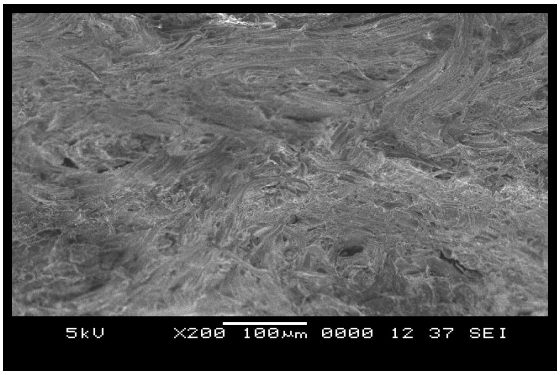

Figure 6: SEM micrograph of tensile fracture surface of LDPE/CS biocomposites with COCA (20 php) at magnification 200X.

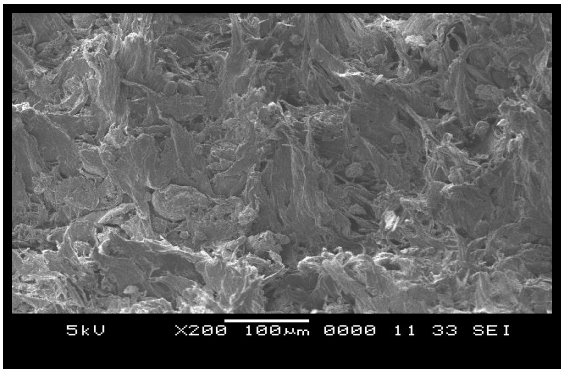

Figure 7: SEM micrograph of tensile fracture surface of LDPE/CS biocomposites with COCA (40 php) at magnification 200X.

Conclusion

The compatibility between corn stalk (CS) and LDPE matrix was improved by the addition of COCA as a coupling agent. The tensile strength, the elongation at break and the Young's modulus of LDPE/CS biocomposites with COCA were higher than biocomposites without COCA that means. The presence of COCA has increased the ductility and plasticizers of biocomposites. SEM studies indicate that the interfacial adhesion between CS and LDPE matrix improved with presence of COCA.

References

[1] Bledzki, A.K., Gassan, J. (1999). *Prog. Polym. Sci*. 24(2): 221-74.

[2] Eichorn, S. J., Baillie, C. A., Zafeiropoulos, N., Mwaikambo, L. W., Ansell, M.P., Dufresne, A. (2001). *J. Mat. Sci.* 36(9): 2107-31.

[3] Kim, H. S., Yang, H. S., Kim, H. J., Lee, B. J. and Hang, T. S. (2004). *J. Thermal Analysis Cal. 76*: 359.

[4] J.M. Krokhta, C.L.C. De Mulder-Johnston (1996). *ACS Symposium Series*. 647: 120–140

[5] Son, J., Kim, H. J. and Lee, P.W. (2001). *J. Appl. Polym. Sci. 82:* 2709.

[6] Freire, C. S. R., Silvestre A. J. D.,Neto C. P.,Belgacem, M. N.,Gandini, A. (2006). *J. Appl. Poly. Sci*.100 (2): 1093-1020.

[7] MN Belgacem, & A Gandini (2005). Composite Interfaces*. 12: 41-75*

[8] Othman, N., Ismail, H. and Mariatti, M. (2006). *Polym. Degrad. Stabil. 91: 1761-1774.*

MICROCRYSTALLINE CELLULOSE – PALM REINFORCED POLYESTER COMPOSITE: A STUDY OF MECHANICAL PROPERTIES AND THERMAL AGEING RESISTANCE OF THE COMPOSITE

M. D. Yusrina, A.R. Rozyanty, O. Maizatul, H. Salmah & A. A. Sinar
School of Materials Engineering, Kompleks Pusat Pengajian Jejawi 2, Universiti Malaysia Perlis, 02600 Jejawi, Perlis

Abstract

A study on a pineapple leaf fiber (PALF) reinforced polyester composite was carried out by the casting technique at room temperature using methyl ethyl ketone peroxide (MEKP) as a catalyst. A layer of composite (microcrystalline cellulose as the filler) was introduced to improve the mechanical properties of the composite. The effects of various parameters (i.e. fibre loading and fibre size) on the mechanical properties and thermal aging were investigated. Under aging testing, the composite samples with the presence of PALF increased the thermal aging resistance of the composite. In addition, the treated PALF composite revealed higher tensile properties as compared to the untreated PALF composite. The fibre loading between 2% and 5% in this study was low as shown in the flexural strength results. However, the increment in flexural modulus and impact strength was parallel with the increment of the fibre loading percentage.

Keywords: *Microcrystalline Cellulose, Pineapple Leaf Fiber, Polyester.*

Introduction

Lignocellulosic-unsaturated polyester composites are natural fibre-reinforced polymer composites. There are many kinds of natural fibres, such as bast fibres (flax, ramie, nettle and mesta), leaf fibres (sisal, pineapple and screw pine), seed fibres (cotton), fruit fibres (coconut husk, or coir), and stalk fibres (straw of various kinds) [1]. In addition, glass fibre can cause acute irritation of the skin, eyes, and upper respiratory tract. Concerns have been raised for long-term development of lung scarring (i.e. pulmonary fibrosis) and cancer. Natural fibres have advantages over synthetic or man-made fibres such as glass and carbon due to these reasons: low cost, low density, acceptable specific strength properties, ease of separation, carbon dioxide sequestration and biodegradability.

Nowadays, door panels, seat backs, headliners, dashboards, interior parts, package trays, furniture, packaging, building and construction materials, and even spare parts for military vehicles and aircraft are made from natural fibres. Natural fibres are renewable resources and they do not exacerbate the carbon dioxide emission problem [2]. Natural fibre-reinforced polymer composites have raised great interests among material scientists and engineers in recent years due to the need for developing environmental-friendly materials, and partly replacing currently used glass for composite reinforcement [3].

The pineapple leaf fibre (PALF) reinforced polyester composite is a natural fibre composite. Pineapple leaf fibre, which is rich in cellulose, is relatively inexpensive and abundantly available, and it has the potential to be used as reinforcement in polymer composites [3].

This paper presents the mechanical and thermal properties of a short PALF-reinforced LDPE composite. The effects of fibre loading, fibre length, chemical treatments and temperature on melt were focused in this research.

Materials and Method

Materials and Equipment

The pineapple leaf fibre (PALF) in this study was supplied by Mata Ayer Pineapple Leaf Farm, Mata Ayer, Perlis, Malaysia. The cellulose used was microcrystalline cellulose powder by Sigma-Aldrich Chemicals, US, whereas the catalyst used was methyl ethyl ketone peroxide (MEKP). Typical properties of unsaturated polyester resin and MEKP are shown in Table 1 and Table 2 below. Meanwhile, the unsaturated polyester resin and catalyst were supplied by Hasrat Bestari Sdn. Bhd.

Table 1: Typical properties of unsaturated polyester resin

Characteristics	Description
Appearance	Hazy, pinkish
Non-volatile, %	56-59
Viscosity @ 25˚C, cps	
-, #3/60	450-600
- , #3/6	900-1350
Thixotropic Index	1.5-2.8
Geltime @ 25˚C, minutes -1%MEKP	18-23
Acid Value, mgKOH/g solid resin	29-34
Specific Gravity, g/cm³	1.12
Volumetric Shrinkage, %	8

Table 2: Typical properties of MEKP

Characteristic	Description
Molecular formulation	C4H10O4
Molar mass, g/mol	122.12
Appearance, g/cm³	Colorless, high-viscosity liquid
Density, g/cm³	1.15
Melting point, ˚C	-8
Boiling point, ˚C	109

Preparation of the Pineapple Leaf Fiber (PALF)

The pineapple leaves in this study were harvested from a farm in Mata Ayer, Perlis, whereby all the thorns were separated from the leaves using a knife. A noodle mill was used to soften the pineapple leaves by removing the water content which contains chlorophyll. Retting method was used to remove the pineapple skin, in which this process took about a week. Next, air compressor was used to remove any contamination such as dust or dirt from the pineapple leaf fibre and in the same time to dry the fibre. Next, the fibre was cut into the size of 10 mm in length.

Each sample contained two layers of the composite. The first layer contained unsaturated polyester, cellulose powder and methyl ethyl ketone (MEKP), while the second layer consisted of unsaturated polyester, methyl ethyl ketone (MEKP) and pineapple leaf fibre. The formulation, as shown in Table 3 below, is in phr scale in which the total weight was 72 g per formulation.

For the first layer, the unsaturated polyester and cellulose powder were manually stirred. Then, methyl ethyl ketone was poured into the mixture and manually stirred. Next, the mixed compound was poured into the mould and homogenously spread. After 6-7 minutes of gelling time, the formulation was then prepared for the second layer. For the second layer, the

pineapple leaf fibre was dispersed and distributed on the first layer. After that, the unsaturated polyester and methyl ethyl ketone (MEKP) were manually stirred. Lastly, the mixed compound was poured onto the first layer. The mould was then closed and left for curing for about 24 hours.

Table 3: Formulation of the untreated and treated PALF unsaturated polyester resins

Composite (layer)	Untreated Composites	(phr)	Treated Composites	(phr)
First layer	Unsaturated polyester	100	Unsaturated polyester	100
	Cellulose powder	15	Cellulose powder	15
	MEKP	2	MEKP	2
Second layer	Unsaturated polyester	100	Unsaturated polyester	100
	PALF	2	PALF	2
		5		5
	MEKP	2	MEKP	2

Thermal Aging Resistance

The experiment on the thermal aging property was carried out by placing the uncut tensile specimens in an air circulating oven at 100°C for 22 hours. Then, the specimens were cooled at room temperature for at least 18 hours before testing. Relative tensile properties were calculated using the equation as shown below and they were employed to represent the thermal aging resistance of the various PALF-reinforced unsaturated polyester composite specimens.

$$\text{Relative tensile properties} = P_1 / P_0 \quad (1)$$

where P_1 and P_0 are the tensile results of the aging and non-aging specimens, respectively.

Tensile Testing

The tensile properties of the composite were determined by the *Instron* 50 kN (ID Number: *5569P7531)* electromechanical universal testing machine (UTM) with series IX control system. A standard method of ASTM D638 was chosen. The gauge length was set at 50 mm while the testing speed was set at 2 mm·min^{-1}. Rectangular samples with the thickness of 3 mm were cut from the moulded sheets of the compression moulding. Figure below shows the Instron machine that was used for gauging the tensile strength. During the tensile testing, 5 identical samples for each compound were used to determine the tensile properties. Values for the samples were reported. Other than the tensile properties (tensile strength), elongation at break (Eb) and Young's modulus were also recorded and calculated automatically by the software instrument.

Results and Discussion

Tensile Analysis

In this research, PALF was used as the fibre to reinforce the microcrystalline cellulose-PALF reinforced polyester composite. The PALF-reinforced polyester acted as a second layer for this composite. The study was based on the effect of fibre loading in order to study the optimum amount of fibre loading to be used. Tensile testing was performed, and then thermal aging resistance was done to find out the performance of PALF to enhance the properties of thermal aging of the composite. Next, the experimental study was carried out to determine whether

chemical treatment of PALF was significant to increase the thermal properties of the composite.

Figure 1 shows the results of tensile strength based on the fibre loading of PALF on the microcrystalline cellulose-PALF reinforced polyester composite. The control sample (without PALF) showed the highest tensile strength, which was 45.131 MPa. The samples with 2 and 5 phr of PALF gave the tensile strengths of 29.633 MPa and 27.234 MPa, respectively.

From the tensile strength results, it was revealed that the loading of PALF decreased the tensile strength of the composite. The observation based on the results showed a delaminating area, which occurred between the first layer and the second layer of the composite. The first layer of the PALF-reinforced unsaturated polyester composite might not be compatible with the second layer of the composite, which was the microcrystalline cellulose-reinforced polyester composite. The second reason was the increase of the void content in the composite. This would decrease the tensile strength of the composite. The third reason was due to the dispersion and distribution of the fibre in the composite. In the sample, the fibre became bulky because of the attraction between the fibres, which decreased the tensile strength of the composite.

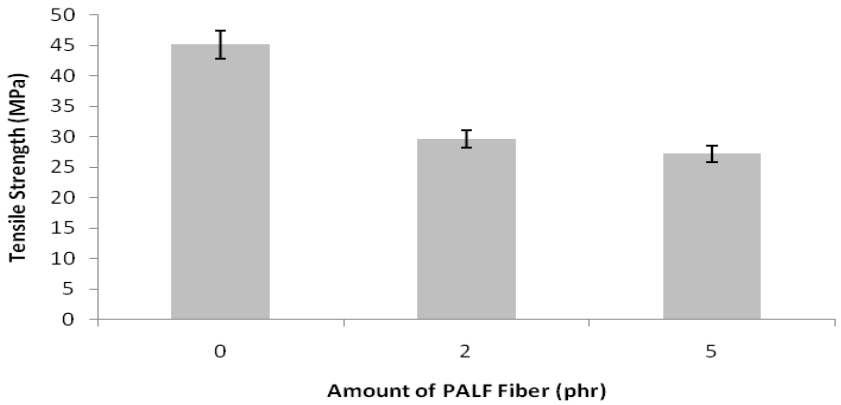

Figure 1: Tensile strength of fibre loading effect on the microcrystalline cellulose-PALF reinforced polyester composite

However, in a study done by Arib et al. [4] on the tensile behaviour of pineapple leaf fibre/polypropylene composite as a function of volume fraction, the researchers found that the tensile modulus and tensile strength of the composite were affected by the fibre content in accordance with the rule of mixtures.

Figure 2 shows the results of tensile modulus on the effect of fibre loading on the microcrystalline cellulose-PALF reinforced polyester composite. The control sample (without PALF) showed the highest modulus of elasticity, with 1.2769 GPa. The samples with 2 and 5 phr of PALF gave the values of 0.9279 GPa and 0.9665 GPa, respectively. These results were in agreement with the findings of Maya et al. [5] who found that increasing the concentration of fibres would result in the reduction of tensile strength, but this may also increase the modulus of the composite.

For elongation at break, the control sample (without PALF) gave the highest value, which was 5.2%. On the other hand, the samples that contained 2 and 5 phr of PALF gave the values of 4.2 % and 4.1 %, respectively.

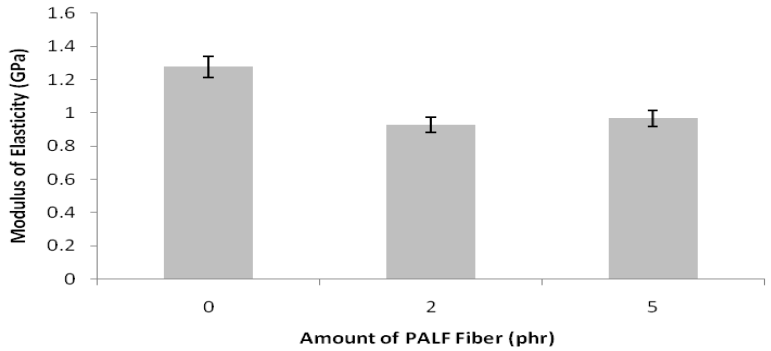

Figure 2: Modulus of elasticity of the fibre loading effect on the microcrystalline cellulose-PALF reinforced polyester composite

Thermal Aging Analysis

Table 4 shows the tensile strength results for thermal aging analysis under 100°C of the microcrystalline cellulose-PALF reinforced polyester composite. The highest reading of tensile strength was obtained from the non-aging control, with 45.13 MPa, whereas the lowest reading was obtained from the aging control sample, with 22.733 MPa. As for other samples, namely, the non-aging samples with 2 and 5 phr of PALF, as well as the aging samples with 2and 5 phr of PALF, the results were 29.633 MPa, 27.017 MPa, 27.234 MPa, and 26.613 MPa, respectively. There were a few reasons why the tensile of all types of the samples became lower. The first reason was the fibre breakage in the matrix composite, which was due to the heating of the samples during the thermal aging testing. The heat was absorbed into the fibre that broke the fibre open; and thus, the tensile strength of the samples gradually decreased after they were heated. The other reason was the breakage of the bond between the fibre and the matrix. This made the bond become weaker, and thus, resulting in low tensile strength.

Table 4 tabulates the results of tensile modulus for thermal aging resistance of the microcrystalline cellulose-PALF reinforced polyester composite. The sample of non-aging control showed the highest tensile modulus among the samples, that was 1.28 GPa. As for the aging samples, the results revealed a decrease in the tensile and modulus strength. Furthermore, the aging sample with 2 phr of PALF showed the lowest tensile modulus, with 0.9279 GPa. The other samples, namely, the non-aging control sample, the aging samples with 2 and 5 phr of PALF and the non-aging samples with 2 and 5 phr of PALF gave the tensile modulus values of 1.2769 GPa, 1.2517 GPa, 0.9665 GPa, and 1.0562 GPa, respectively. A research study done by Shinji Ochi [5] found that the thermal analysis of kenaf fibre revealed that the tensile strength decreased when it was kept at 1800°C for 60 min.

Table 4: Thermal aging resistance of the microcrystalline cellulose-PALF reinforced polyester composite

Sample	Tensile strength (MPa)	Eb (%)	Modulus of elasticity (GPa)
Control sample	45.13	5.2	1.28
Ageing	22.73	2.2	1.83
Non ageing/2 phr PALF	29.63	4.2	0.93
Ageing/ 2phr PALF	27.07	3.1	1.25
Non ageing/5 phr PALF	27.23	4.1	0.99
Ageing/ 5phr PALF	26.61	3.3	1.01

The unidirectional fibre-reinforced composite showed the tensile strength of 223 MPa. Moreover, the tensile of the kenaf fibre-reinforced composite decreased to a fibre content of

50% [6]. The results for elongation at break of the non-aging control sample showed the highest value, that was 5.2%. On the other hand, the non-aging control sample showed the lowest elongation of break, with 2.2%. The other samples, namely, the non-aging samples of 2 and 5 phr of PALF and the aging samples of 2 and 5 phr of PALF gave the elongation at break readings of 4.2%, 3.1%, 4.1%, and 3.3%, respectively. The results for the elongation at break rapidly decreased after the thermal aging resistance testing because of the increase in the void area due to sample heating. The entrapped air in the void space rapidly expanded since the heat applied to the samples was increased. Notably, the air has the capability to expand according to heat capacity. The increasing of void space would significantly affect the elongation at break of the composite samples.

Relative Tensile Analysis

Figure 3 shows the relative properties of the samples for thermal aging properties. From the bar graph, the pattern showed clearly both the tensile strength and elongation of break. The relative tensile strength increased from 0.504 for the control sample to 0.912 for the sample with 2 phr of PALF and 0.977 for the sample with 5 phr of PALF. The relative elongation of break also increased from 0.423 for the control sample to 0.738 for the sample with 2 phr of PALF and 0.805 for the sample with 5 phr of PALF. Nevertheless, for relative tensile modulus, the pattern gradually decreased from 1.435 for the control sample to 1.349 for the sample with 2 phr of PALF and 1.093 for the sample with 5 phr of PALF. This pattern proved that the presence of PALF increased the thermal aging properties of the composite. Hence, the presence of PALF can be proven to increase the thermal aging resistance of the composite.

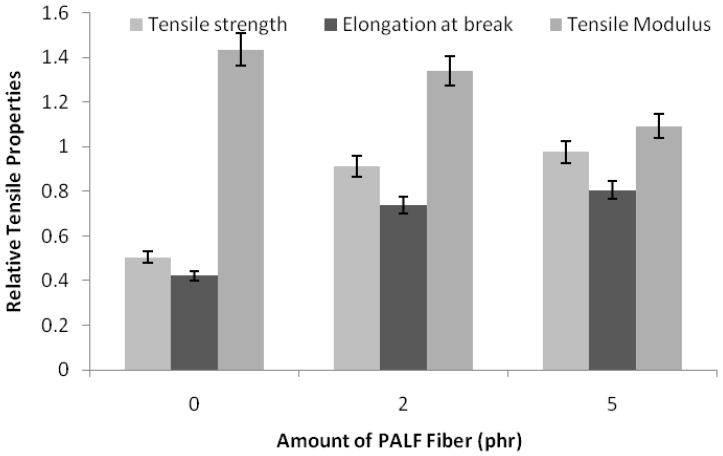

Figure 3: Relative tensile properties of the composite for thermal aging resistance

Conclusion

Pineapple leaf fibre (PALF) is one of natural fibres which can be found abundantly in Malaysia. This fibre contains very high cellulose. Based on this research, it was proven that the addition of PALF can affect the tensile properties of the microcrystalline cellulose-PALF reinforced polyester composite. The tensile done also determine the thermal aging properties of the fibre. Based on the observation on the aging test, it was found that the aging microcrystalline cellulose-PALF reinforced polyester composite provided significant data on tensile modulus results; however, the results were opposite for the tensile strength. The suitable fibre loading was 2 phr since it presented enhanced tensile modulus and quite impressive tensile strength results. Relative tensile properties of the composite sample with 5 phr of PALF were found to have higher tensile properties as compared to the composite sample without PALF.

References

[1] Klysov, A. A. (2007). *Wood-Plastic Composites*. John Wiley & Sons: New Jersey.

[2] Chawla, K. K. (1998). *Fibrous materials* (p. 56). Press Syndicate of The University of Cambridge: Cambridge.

[3] Ishak M. R., Leman Z., Sapuan S. M., Edeerozey A. M. M., & Othman I. S. (2009). Mechanical properties of kenafbast and core fibre reinforced. *National Symposium on Polymeric Material*.

[4] M.N. Arib, S.M. Sapuan, M.M.H.M. Ahmad, M.T. Paridah, H.M.D. KhairulZaman. 2006. *Materials and Design.* 27(5): 391-396.

[5] Maya Jacob, Sabu Thomas, K.T. Varughese. 2004. *Comp. Sci. Tech.* 64(7-8): 955-965

[6] Shinji Ochi. 2008. *Mech. mat.* 40 (4-5): 446-452

FRACTURE TOUGHNESS AND IMPACT STRENGTH OF HOLLOW EPOXY PARTICLES- TOUGHENED POLYESTER COMPOSITE

L.F. Low & A. Abu Bakar
School of Materials and Mineral Resources Engineering, Engineering Campus, Universiti Sains Malaysia, 14300 Nibong Tebal, Penang, Malaysia

Abstract

Hollow epoxy particles (HEP) serving as reinforcing fillers were prepared using the water-based emulsion method in this present study. HEP was incorporated into the polyester matrix at various loading, ranging from 0 wt % to 9 wt %, to toughen the brittle polyester thermoset. The polyester composites were prepared using the casting technique. The fracture toughness and impact strength of the polyester composites increased with increasing the HEP loading up to 5 wt %, after which there was a drop. The improvement in fracture toughness and impact strength is attributed to the good polymer-filler interaction. This finding was further supported by the scanning electron microscopy (SEM) micrograph, in which it has shown that the polyester resin was interlocked into the pore regions of the HEP filler. The reduction in fracture toughness and impact strength of the polyester composite were believed to be attributed to the filler agglomeration. This filler-filler interaction would create stress concentration areas, and eventually weakened the interfacial adhesion between the polymer matrix and the filler particles. Hence, lower fracture toughness and impact strength of the highly HEP-filled polyester composites (above 5 wt %) were detected.

Keywords*: Filler loading, fracture toughness, hollow epoxy particles (HEP), impact strength, water-based emulsion.*

Introduction

Polyester resin has been utilized as the matrices for the composite materials and these advanced composite materials will eventually be used in a variety of industrial applications, such as in the aerospace, automobile and marine industries [1-3]. However, the brittleness of the polyester limits most of their applications that require toughness. Hence, plenty of efforts have been implemented to overcome the brittleness problem of the polyester matrix.

One of the methods is to incorporate the fillers into the thermoset matrix to enhance the impact resistance and fracture toughness of the composites. For example, rigid inorganic fillers such as calcium carbonate, clay, talc, and kaolin are commonly introduced into the thermoset matrix to enhance the toughness of the composites. It is owing to the fact that these fillers are economic and is able to toughen the composites. Specifically, Astruc et al. [4] introduced kaolin into the thermoset matrix to enhance the toughness of the composite. Johnsen et al. [5] also found that the modulus and fracture toughness of the thermoset composite can be increased when a small amount of silica nano-particles is added into the thermoset matrix.

On the other hand, recent work investigated by Watanabe et al.[6] and Yuan et al. [7] also found that the hollow spheres particles have been utilized as filler to reinforce materials. Zhao et al. [8] and Huang et al. [9] stated that hollow microspheres are commonly used as low weight fillers for most materials since their low density and hollow structures are able to give rise to the “micro-package” effect. Apart from that, Liang & Li [10] also proved that the smooth spherical surfaces of hollow microspheres do not generate undesirable stress concentration area between the polymer-filler interface. Considering these advantages as mentioned, much efforts have been made to synthesize, develop and utilize the hollow microspheres in various filler applications. For example, hollow calcium carbonate particles is used in the paper filler application, whereas hollow mesoporous silica spheres is used in the membranes for the

purpose of improvement in water absorption properties [6,7,11]. Although plenty of research works have been done to investigate the applicability of various hollow spheres particles to toughen the thermoset matrix, to our knowledge, there are still very limited research studies focused on hollow epoxy particles which are prepared using water-based emulsion technique in filler reinforcing applications. Hence, in this present study, the hollow epoxy fillers (HEP) were prepared. The effect of HEP filler loading on the fracture toughness and impact properties of polyester-based composites were investigated.

Experimental

Materials

The epoxy resin 331 [diglycidyl ether of bisphenol A (DGEBA)] with the epoxide equivalent weight of 182-192 g/mol and polyamide hardener A026 used in this present study were supplied by Euro Chemo-Pharma Sdn. Bhd. Polyester resin (RP 9509GP) and methyl ethyl ketone peroxide (MEKP) catalyst with the density of 1.08 g/cm^3 were purchased from Zarm Scientific & Supplies Sdn. Bhd. (Malaysia). The calcium carbonate ($CaCO_3$) with the density of 2.71 g.cm^{-3} and hardness of 3 Mohs scale was provided by Malaysian Calcium Corporation Sdn. Bhd.

Preparation of hollow epoxy particles (HEP)

The water-based emulsion was used to prepare hollow epoxy particle (HEP). At the predetermined ratio, the epoxy resin (DGEBA) and calcium carbonate ($CaCO_3$) were stirred together using mechanical stirrer at 300 rpm for 5 minutes. After that, the polyamide hardener was mixed into the epoxy mixture and stirred continuously for 2 minutes until homogeneous mixture was obtained. The epoxy mixture was then poured into the water medium and the emulsion process was conducted using homogenizer at the speed of 15,000 rpm for 9 minutes. Finally, the mixture was placed in an oven at 80^{o}C for 24 hours for further curing process. The fine powder of HEP filler could be produced after the cured epoxy sample was grinded.

Preparation of HEP-filled polyester composites

Polyester composites were prepared using casting method. Firstly, the HEP powders were incorporated into the polyester resin at different loading, ranging from 0 wt % to 9 wt %. The epoxy mixtures were stirred homogeneously before the MEKP catalyst was added. After that, the epoxy mixtures were poured into rubber mould and subjected to thermal curing in an oven at 80^{o}C for 3 hours.

Mechanical Characterization of HEP-filled composites

To investigate the effect of HEP filler loading on the mechanical properties of polyester based composite, fracture toughness test were conducted according to ISO 13586: 2000 standard method using *Instron machine model 3366*. The dimension of the specimen was about 60 mm $\times$ 12 mm $\times$ 3 mm with the crack length-to-width ratio (*a/W* ratio) of 0.5. The initial crack was introduced on the specimen using razor blade before the fracture toughness test. The fracture toughness test was conducted at a crosshead speed of 10 mm·min^{-1}. The fracture toughness values, K_{IC} of the polyester composites with different HEP loading were determined using Equation (1) and Equation (2)

$$y = 1.93 - 3.07\left(\frac{a}{W}\right) + 14.53\left(\frac{a}{W}\right)^2 - 25.11\left(\frac{a}{W}\right)^3 + 25.8\left(\frac{a}{W}\right)^4 \quad (1)$$

$$K_{IC} = \frac{3PSa^{1/2}y}{2tw^2} \quad (2)$$

where *y* is a geometrical correction factor, *a* is the notch length (mm), *W* is the specimens width (mm), *S* is the span length (mm), *P* is the load at peak (N) and *t* is the specimen thickness (mm).

The fractured surfaces of the HEP-reinforced epoxy composites after fracture toughness testing were observed using a field-emission scanning electron microscope (FESEM) *model Ziess Supra 35VP* (USA). The sample was coated with platinum/gold prior to FESEM characterization.

The impact test was conducted using impact test machine (*Zwick Impact tester*) according to ASTM D 256. The Charpy method was carried out using notched samples with the dimensions of 60 mm x 12 mm x 3 mm and notch length of 2 mm. The impact strength of composites specimens were calculated in unit kJm^{-2} according to Equation (3)

$$Impact\ Strength = \frac{W}{b_n \times h} \quad (3)$$

where *W* is the impact energy absorbed (J), b_n is the width of sample minus notch length (mm) and *h* is the thickness of sample (mm).

Results and Discussion

Figure 1 exhibits the effect of the HEP filler loading on the fracture toughness of the polyester composite. It was found that the fracture toughness of the composite increased with the increase of HEP filler loading up to 5 wt %. The continuous increment in fracture toughness of composite is believed to be due to the capability of the filler particle to resist the crack propagation before fracture taken place. The HEP filler particles will act as an obstacle to the applied force through the crack-pinning mechanism. It can increase the crack path length as the cracks are forced to be propagated by bowing around the filler particle. Hence, the increment in the line energy will lead to the enhancement of the fracture toughness of the polyester composites. This is particularly in line with the finding reported by Wetzel et al. [12] and Fu et al. [13] who mentioned that the toughness of the polymer system can be improved since the crack pinning mechanism give rise to an increase in the line energy. In addition, the highest fracture toughness of the 5 wt % HEP-filled composite is due to the good interaction between HEP filler and polymer matrix. This is attributed to the fact that the interlocking of the polyester resin into the pores region of the HEP filler as shown in Figure 2(b) can raise the capability of the composite to absorb more energy before fracture initiates. This incident will give rise to the decrease in crack propagation rate and increase the resistance against crack deformation in the composite. Therefore, the improvement in the fracture toughness of polyester composite at the optimum HEP loading is justified in Figure 1.

However, the fracture toughness of the composite decreases as the filler loading exceeds 5 wt %. This phenomenon might be due to the agglomeration of the filler particles as illustrated in Figure 2(c). The poor dispersion of the HEP filler particles throughout the polymer matrix and the formation of larger cluster of filler agglomeration will act as stress concentration areas. This will result in the reduction of the resistivity of the composite against the crack propagation and subsequently deteriorate the fracture toughness of the composite. Hence, a decrease in fracture toughness of the polyester composites filled with relatively high HEP filler loading is detected.

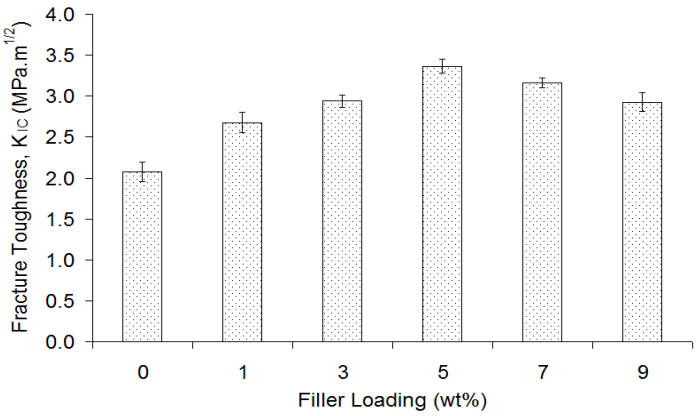

Figure 1: Fracture toughness of the polyester composite reinforced with different HEP filler loading

Figure 2 displays the fracture surface of the neat polyester, 5 wt % HEP-filled polyester composite and 9 wt % HEP-filled polyester composites after the fracture toughness test. The fracture behaviour of each composite can be explained based on their fractured morphologies. Accordingly, a relatively smooth fracture surface of the neat polyester [c.f. Figure 2(a)] indicates the catastrophic brittle fracture of the resin. This will lead to the lower resistance of the neat polyester against the crack propagation and deformation. In contrast to the neat polyester, a more tortuous and rougher surface is observed on the fractured surface of the 5 wt % HEP-filled polyester composite as shown in Figure 2(b). A number of cavitated holes as a results of the HEP fillers 'pulled' out from the polyester matrix with the external forces applied, are dispersed throughout the fractured surface of the composite. This incident gives rise to the increase in resistance against the deformation and subsequently reduces the crack propagation rate throughout the polyester matrix. Therefore, higher fracture toughness of the composite is contributed. However, at higher HEP filler loading which exceeding the optimum loading, agglomeration and the presence of small gap between the polyester matrix and HEP filler are observed in Figure 2(c). Poor polymer-filler interaction and the creation of stress concentration area due to agglomeration will reduce the fracture resistance of the composite. Thus, a decrease in fracture toughness properties of the polyester composite is observed as the filler loading exceeds 5 wt %.

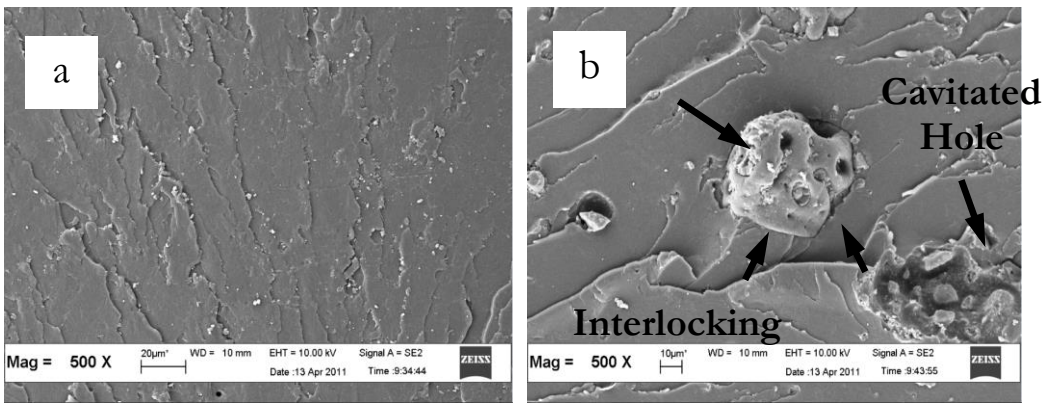

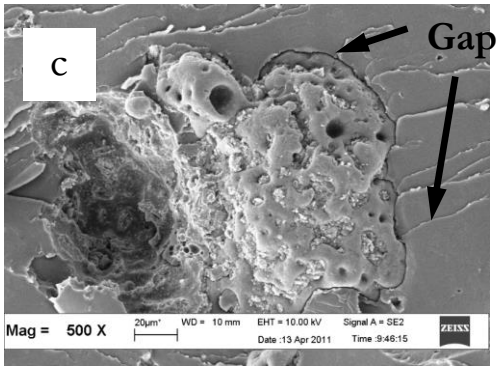

Figure 2: SEM micrographs of the fracture surface of (a) neat polyester, (b) 5 wt% HEP-filled polyester composite and (c) 9 wt% HEP-filled polyester composite

Figure 3 shows the impact strength of the polyester composite filled with different HEP filler loading, ranging from 0 wt % to 9 wt %. It is noticed that the polyester composite possesses the highest impact strength if it is filled with 5 wt % HEP loading. The improvement in impact strength with HEP loading up to its optimum filler loading is attributed to the aforementioned good polymer-filler interaction. The interlocking as well as the penetrating of the polymer matrix into the pore regions of the HEP fillers gives rise to a good interaction between the polymer and the filler. This will help to resist and eventually stop the crack propagation throughout the polymer matrix when the composite is subjected to an impact load. The increment in the crack length path is also due to the filler particles which will increase the ability of the composites to absorb greater energy before failure. Gupta et al. [14] also reported in their research study that the presence of fillers will resist crack propagation and prolong the crack length path.

However, a reduction in the impact strength is observed when the HEP filler loading added is greater than that of the optimum loading. This is mainly due to the filler-filler interaction that will caused agglomeration, which leads to the poor interaction between the HEP filler and the polymer matrix [15,16]. These undesirable polymer-filler interaction and the existence of weak interface region in the polymer matrix may attribute to the reduction in the resistance against the crack propagation of the system. Shivamurthy et al. [17] also agreed that this filler-filler aggregation will act as a stress concentrator in altering the impact properties of the composite. Therefore, the ability of the composite to absorb external applied force reduces due to the presence of stress concentrators. So, lower impact strength is obtained for those composite filled with high HEP loading.

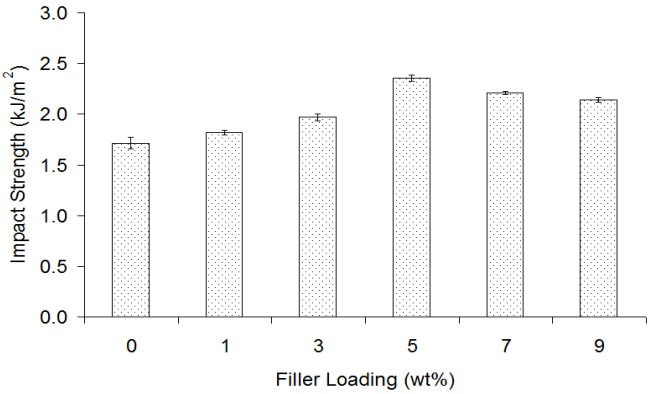

Figure 3: Impact strength of the polyester composite reinforced with different HEP filler loading

Conclusion

Hollow epoxy particle (HEP) are produced using water-based emulsion technique. The fracture toughness and impact strength of the polyester composites increase with increasing the HEP filler loading up to 5 wt %. The enhancement in toughening on the polyester composite is mainly attributed to the good polymer-filler interaction since the polyester resin interlocks into the pores regions of the HEP fillers. The fracture toughness and impact properties of the polyester composite will be deteriorated if the HEP filler loading incorporated into the polyester matrix exceeding the optimum HEP filler loading. Filler-filler interaction which leads to agglomeration is one of the factors giving rise to the reduction of the mechanical properties of the HEP-filled polyester composite.

Acknowledgements

The authors wish to acknowledge the Universiti Sains Malaysia for the research university postgraduate research grant scheme (Grant number: 1001/PBAHAN/8033016), short term grant (Grant number: 6039037) and fellowship grant that have made this research work possible.

References

[1] Kosar, V. and Gomzi, Z. 2010. *App. Math. Model. 34: 1586-1596.*

[2] Visco, A. M., Calabrase, L. and Cianciafara, P. 2008. *Compos. Part A 39: 805-814.*

[3] Apicella, A., Migliaresi, C., Nicolais, L., Iaccarino, L. and Roccotelli, S. 1983. *Composites 14: 387-392.*

[4] Astruc, A., Joliff, E., Chailan, J. F., Aragon, E., Petter, C. O. and Sampaio, C. H. 2009. *Prog. Org. Coat. 65: 158-168.*

[5] Johnsen, B. B., Kinloch, A. J., Mohammed, R. D., Taylor, A. C. and Sprenger, S. 2007. *Polymer 48: 530-541*

[6] Watanabe, H., Mizuno, Y., Endo, T., Wang, X. W., Fuji, M. and Takahashi, M. 2009. *Adv. Powder Technol. 20: 89-93.*

[7] Yuan, J. J., Zhou, G. B. and Pu, H. T. 2008. *J. Membr. Sci. 325: 742-748.*

[8] Zhao, H., Li, Y., Liu, R. J., Zhao, F. Y. and Hu, Y. Q. 2008. *Mater. Lett. 62: 3401-3403.*

[9] Huang, Y. F., Xiao, H. N., Chen, S. G. and Wang, C. 2009. *Ceram. Int. 35: 905-907.*

.

[10] Liang, J. Z. and Li, F. H. 2007. *Polym. Test. 26: 1025-1030.*

[11] Chen, Z. M., Li, S. J., Xue, F. F., Sun, G. N., Luo, C. G., Chen, J. F. and Xu, Q. 2010. *Colloids Surf. A 355: 45-52.*

[12] Wetzel, B., Rosso, P., Haupert, F. and Friedrich, K. 2006. *Eng. Fract. Mech. 73: 2375-2398*

[13] Fu, S. Y., Feng, X. Q., Lauke, B. and Mai, Y. W. 2008. *Compos. Part B 39, 933-961.*

[14] Gupta, N., Brar, B. S. and Woldesenbet, E. 2001. *Bull. Mater. Sci. 24: 219-223.*

[15] Suresha, B., Kumar, B. N. R., Venkataramareddy, M. and Javaraju, T. 2010. *Mater. and Des. 31: 1993-2000.*

[16] Zaini, M. J., Fuad, M. Y. A., Ismail, Z., Mansor, M. S. and Mustafah, J. 1996. *Polym. Inter. 40: 51-55.*

[17] Shivamurthy, B., Siddaramaiah and Prabhuswamy, M. S. 2009. *J. Miner. Mater. Charact. Eng. 8: 513-530.*

MECHANICAL PROPERTIES IN HYBRID SURFACE TREATED-OIL PALM EMPTY FRUIT BUNCH (OPEFB)/ TALC-FILLED POLY (VINYL CHLORIDE) (PVC) COMPOSITES

Noor Izyan Syazana Binti Mohd Yusoff, Aznizam Bin Abu Bakar & Azman Bin Hassan

Abstract

The PMMA-g-OPEFB/talc-filled PVC hybrid composites with good stiffness and strength than OPEFB single filler composites have been investigated. Therefore, the aim of this study is to enhance the mechanical properties of hybrid composites by improving the filler-matrix interaction. To obtain good filler-matrix interaction, the graft polymerization of PMMA onto OPEFB was carried out under the nitrogen atmosphere using free radical initiation technique and H_2O_2/Fe^{2+} as an initiator in aqueous medium to produce PMMA-g-OPEFB fibres. The grafted OPEFB/talc and ungrafted OPEFB/talc hybrid composites with various filler loading from 0 to 20 phr were incorporated into PVC. The effect of grafted and ungrafted OPEFB/talc with various loading on flexural and impact strength has been studied. Any differences on the surface morphology impact fracture of the composites have been investigated using SEM. The presence of PMMA functional group at peak around 1733.65 cm^{-1} in FTIR spectrum proved that PMMA was successfully grafted onto OPEFB surface.

Keywords*: Composite, graft copolymer, hybrid, oil palm empty fruit bunch*

Introduction

PVC resin had become of the major component for polymer composites manufacturing especially for construction parts, pipes and hose, electric cables, and packaging material .It offers several unique properties and advantages which include excellent chemical and weathering properties, nonflammable, and also cheaper compared to others plastic [3]. However, PVC can be brittle under high deformation rate and concentrated stress. This drawback can be overcome by adding additives into the PVC blend to meet the required properties. There are also other ways to improve properties, such as by incorporating organic and inorganic filler into the composites. Previous study done by Abu Bakar et al. [1] showed that there is a new trend in polymer composite technology by adding natural fibre which is oil palm empty fruit bunch (OPEFB) as filler in PVC. Furthermore, PVC is widely used on plastic; therefore strengthening the mechanical properties of the composite will bring more benefits into those industries.

OPEFB fibre is one of the demanding natural fibres to be used as reinforcing filler in polymer composite. OPEFB consists of three main parts; hemicelluloses, cellulose and lignin which known as lignocellulosic [6]. The seed oil from the oil palm is being extracted then the waste materials after the extraction are known as OPEFB.OPEFB was generally used as mulch for oil palms, converted to bunch ashes or discarded as waste. In order to minimize the abundance of this industrial waste and the environmentally problem, therefore new applications are urgently required for OPEFB to be more useful. Therefore, due to its low cost factor and availability, OPEFB had been utilized as fillers in polymer composite technology.

Previous research reported that upon increasing of OPEFB fillers loading, the impact strength of composites decreased linearly [2].Thus, surface modification has to be done onto the surface of the OPEFB to increase the compatibility of phases between the PVC and OPEFB. Recent studies by Abu Bakar et al. [5] showed that PMMA has successfully been grafting onto OPEFB fibre at the optimum conditions. The fibre length used in their study was less than 75 µm.

A study that had been done on comparison between the fibre loading of 20 phr of grafted and ungrafted OPEFB fibres filled PVC composite. The elongation at break and tensile strength increased while on the other hand the stiffness of the composites were decreased for both grafted and ungrafted OPEFB [4]. Talc as reinforcing filler and hybridization with OPEFB tended to give the ultimate properties of the composites. Hybrid is the combination of two types of filler or fibre or hybrid fillers or fibres in the polymer and it is a current trend in order to strike the balance properties of composites.

Rozman et al. [11] prepared polypropylene (PP) hybrid composites using OPEFB and glass fibre as reinforcing filler. The incorporation of the both fibre showed the reduction of flexural and tensile strength. While for the properties of flexural and tensile modulus were improved by increasing the level loading of the fibre. Meanwhile, Leong et al. [9] have studied hybrid polypropylene (PP) composites filled talc/$CaCO_3$. The thermal and mechanical properties of the polypropylene composites were investigated. PP composites with hybrid fillers showed a good performance on flexural strength and impact strength compared to single-filler PP composites. The tensile modulus decreased gradually with increasing of talc filler compared to the $CaCO_3$. The same trend is showed by flexural modulus; this was because talc has the tendency to melt parallel to the flow path throughout the fabrication.

In this study, the talc filler will be used as reinforcement to enhance the stiffness of OPEFB-grafted-PMMA filled PVC composites. The use of hybrid filler system that is combination of grafted and ungrafted OPEFB fibre and talc filler in PVC composite should be possible to produce composites with good combination of strength and stiffness properties.

Materials and Method

Suspension PVC resin used in this study with solution viscosity K-value 66 and trade name MH-66 was produced by Industrial Resin Malaysia (IRM) Sdn. Bhd., Tampoi, Johor, Malaysia. The specifications of PVC used are summarized in Table 1. OPEFB fibre used in this study is in powder form with the length less than 30 µm. This OPEFB was purchased from Sabutek Sdn. Bhd., Teluk Intan, Perak, Malaysia. Talc was purchased from Sigma Aldrich, Malaysia in the white powder form with the size less than 10 µm. Methyl methacrylate (MMA) monomer supplied by Merck Schuhardt OHF, Hohenburnn Germany. This monomer underwent purification process before being used. Hydrogen peroxide (H_2O_2) as initiator of AR grade was purchased from QRëC, Malaysia. Ammonium ferrous sulphate catalyst was obtained from Sigma-Aldrich, Malaysia.

Table 1: Specifications of PVC Suspension Resin MH-66

Specification	Resin MH-66
Appearance	White powder
Degree of Polymerization	1000 ± 50
K-value	66
Specific gravity	1.4
Bulk density (g/cm^3)	0.50 ± 0.05
Volatile matter (max) (%)	0.5
Foreign matter (grain/100 g)	15
Particle size (retained on 250 µ) (max) (%)	0.3

Preparation of PMMA-grafted-OPEFB

The preparation of the PMMA-grafted-OPEFB was done using free-radical initiation techniques in the nitrogen atmosphere. Three necked beaker flask was submerged in a thermostated warm water bath at 50°C with reflux condenser and nitrogen inlet tube. Next, 1 g of OPEFB

and 100 mL distilled water was transferred into the flask. Then, nitrogen gas was purged into the flask for 30 min to remove oxygen and followed by adding 2 mL of the initiator, hydrogen peroxide and the mixture was left for 5 min. Next, 0.1 g of iron (II) ammonium sulphate was added and was allowed to settle for 5 min. Afterwards, 5 mL of purified MMA was added into the mixture and stirred continuously under nitrogen atmosphere at 50°C for 60 min. After the reaction was completed, the PMMA-g-OPEFB was obtained. Then it was filtered off using vacuum pump and lastly the filtered product was dried in the oven at 60^{o}C until it reaches a constant weight. Finally, the last product was further treat using soxhlet extraction technique. This technique was done to remove the homopolymer content. The procedure of grafting was explained in detailed from the study by Abu Bakar et al. [3].

Preparation of the ungrafted OPEFB, grafted OPEFB, talc, ungrafted OPEFB/talc and grafted OPEFB/talc filler filled PVC composites

One hundred part per hundred resin (phr) of PVC with the addition of additives such as tin stabilizer 2 phr, calcium stearate 0.5 phr, stearic acid 0.6 phr, acrylic processing aid 1.5 phr, titanium oxide 4 phr and various loading from 10 to 20 phr of untreated OPEFB, PMMA-g-OPEFB, talc and also the hybrid filler of untreated OPEFB/talc, PMMA-g-OPEFB/talc was blended in a laboratory high-speed mixer for 10 min. The dry-blended formulation then was melt mixed and sheeted by using a two roll mill at 175°C for 10 min. The sheeted-formulation prepared was then moulded into flexural and impact test specimens by compression moulding at 190°C and 1.2 kPa for 10 min. The mould was cooled for 5 min before the composite being removed from the mould cavities.

Mechanical testing

The flexural test in this study was done using ASTM D 790-97. This testing was conducted on *Instron Machine (4301)*. Three point loading method with specimen dimensions of 125 mm × 13 mm × 3 mm and 51 mm support span. The flexural strength and flexural modulus were measured. The *Izod impact* test was carried out at room temperature on a notched specimen according to ASTM D256-88 with the dimension of 62.5 mm × 13 mm × 13 mm and notched at depth and angle of 2.6±0.02 mm and 45° respectively using notch cutter. The swing angle of 149° was used.

Fourier transforms infrared (FTIR) spectroscopy

A Fourier transform infrared spectrometer (*Nicolet 5700 FTIR*) was used to indicate the related functional groups of composites. A few grams of the sample are mixed with potassium bromide (KBr) in the powder form to form a thin disc. Then, the thin disc was scanned 16 times in the range of 4000 cm^{-1}- 370 cm^{-1}.

Scanning electron microscopy (SEM)

SEM test has been done using *JOEL Model JSM-5600 LV* to determine the surface morphology of the single and hybrid composites. A small portion of sample was mounted on the copper stub and sputter-coated with platinum to prevent electric charging throughout the process.

Results and Discussion

The performance of the single filler and hybrid filler filled PVC composites in flexural strength and modulus are shown in Figure 1 and 2, respectively. The result shows that the results of the flexural strength are decreased with increasing filler contents from 0 to 20 phr. This is a common trend found in conventional lignocellulosic-thermoplastic composites [11]. Even though the surface modification had been done on the OPEFB surface, the grafted OPEFB filled PVC also showed a similar trend as ungrafted OPEFB. However, the flexural strength of

grafted OPEFB is slightly lower than the ungrafted OPEFB which is contradicted with the result obtained by Abu Bakar et al. [4]. This may due to the fibre length used in this study is shorter than the previous study that might lead to catastrophic failure caused by too much interaction at interface. As expected, by adding talc into PVC matrix and also into hybrid filler filled composites does not impart greater differences into the composites. However, hybrid OPEFB/talc and grafted OPEFB/talc show an improvement than OPEFB single filler in flexural strength since talc is reinforcing filler which its platy nature and posses ability to orient to the polymer flow during processing [9].

The flexural modulus of the composites increased with increasing loading of OPEFB, grafted OPEFB, talc and hybrid filler as shown in Figure 2. The result shows that the stiffness of the composite is increased. The chemical treatment of OPEFB surface increases the compatibility of phases between the PVC and OPEFB fibre. The improved fibre matrix interaction also enables more stress to be transferred from the matrix to the filler during external load. Hybrid filler of OPEFB/talc and grafted OPEFB/ talc shows increasing in stiffness compared to single filler of fibre which according to Leong et al. [9] the platy filler have high aspect ratio and also increase the wettability of the filler by the matrix that creating fewer microvoids.

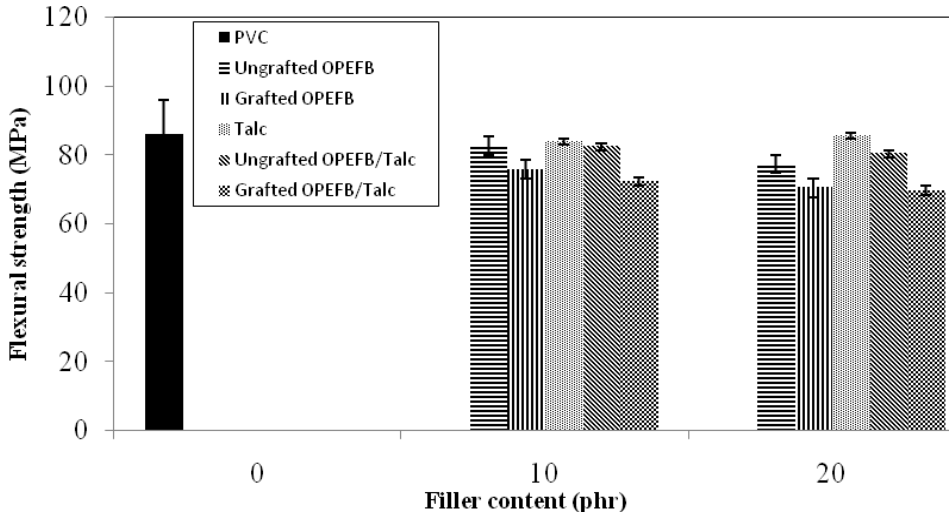

Figure 1: Flexural strength for single filler and hybrid filler filled PVC composites

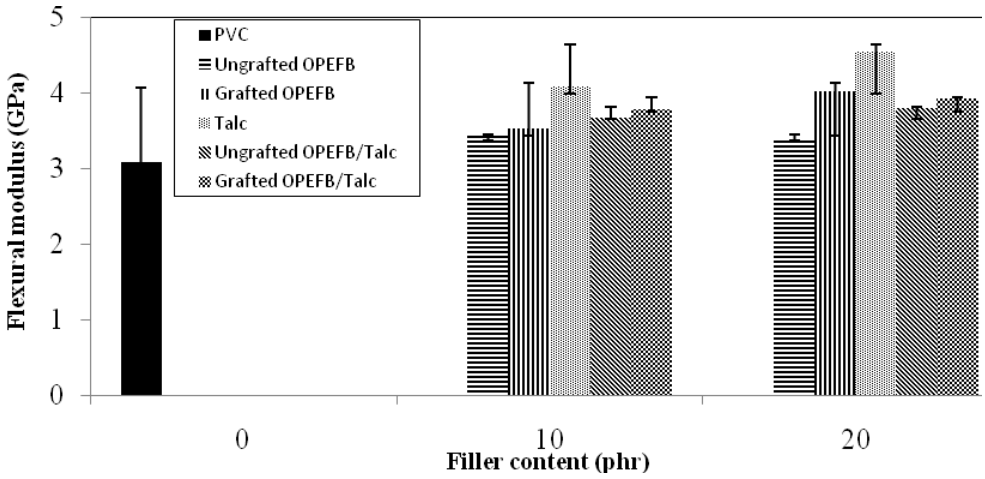

Figure 2: Flexural modulus for single filler and hybrid filler filled PVC composites

The impact strength decreases upon the addition of ungrafted and grafted OPEFB fibre as expected are shown in Figure 3. This is due to poor wetting of fibre by PVC matrix, which leads to poor fibre-matrix interfacial adhesion [10]. The addition of grafted OPEFB, the impact strength of PVC composite appeared to be lower than the blend incorporated with ungrafted OPEFB. This may be associated with good improvement in the fibre-matrix interaction. If the interfacial adhesion between the fibre and matrix is very good, it can also result in poor impact strength, as it will lead to catastrophic brittle failure [12]. Khalid et al. [8] had also reported similar reason in their studies on the effect of compatibilisers on PP biocomposites. The great interaction between fibre and matrix could lead to poor impact strength because the strong adhesion between fibres and polymer matrix cannot stop the crack growth propagating through the matrix and the crack can easily penetrate into fibres leading to catastrophic brittle failure. Similar observation was also made by Raju et al. [10] they observed that at above 5% fibre loading, the impact properties of grafted composite appear to be lower than the blend incorporated with ungrafted fibre.

The impact strength of talc and hybrid OPEFB/ talc and PMMA-g-OPEFB filled PVC showed better improvement than single filler of untreated and treated OPEFB composites. This is due to the fine size of talc that contributes to the improvement of the impact strength of the composite. According to Bakar et al. [5] better filler dispersion would have obviously reduced the stress concentration site, which is very sensitive to impact loading.

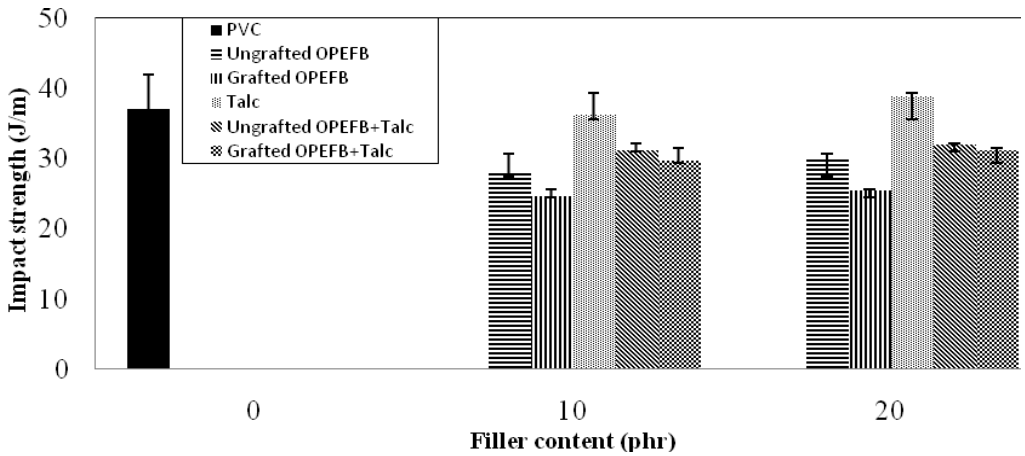

Figure 3: Impact strength for single filler and hybrid filler filled PVC composites

SEM micrographs of impact fractured surface are shown in Figure 4. As can be seen in Figure 4 (a) and 4 (c), the ungrafted OPEFB fibre are pulled-out (indicated by arrows) can be found in the fracture surface of the composites. Abu Bakar et al. [4] have also indicated the existence of fibre pulled-out in the fracture surface which indicated that most of the fibres come out without breaking during the fracture. Figure 4 (b) and (d) show the grafted OPEFB fibre is rather breakage than pulled-lout compared to the ungrafted OPEFB. It is due to the good interfacial adhesion between the fibre and matrix. Figure 4 (c) and (d) show the surface composites of hybrid ungrafted OPEFB/talc and grafted OPEFB/talc. These particles are in the plate like structure [5].

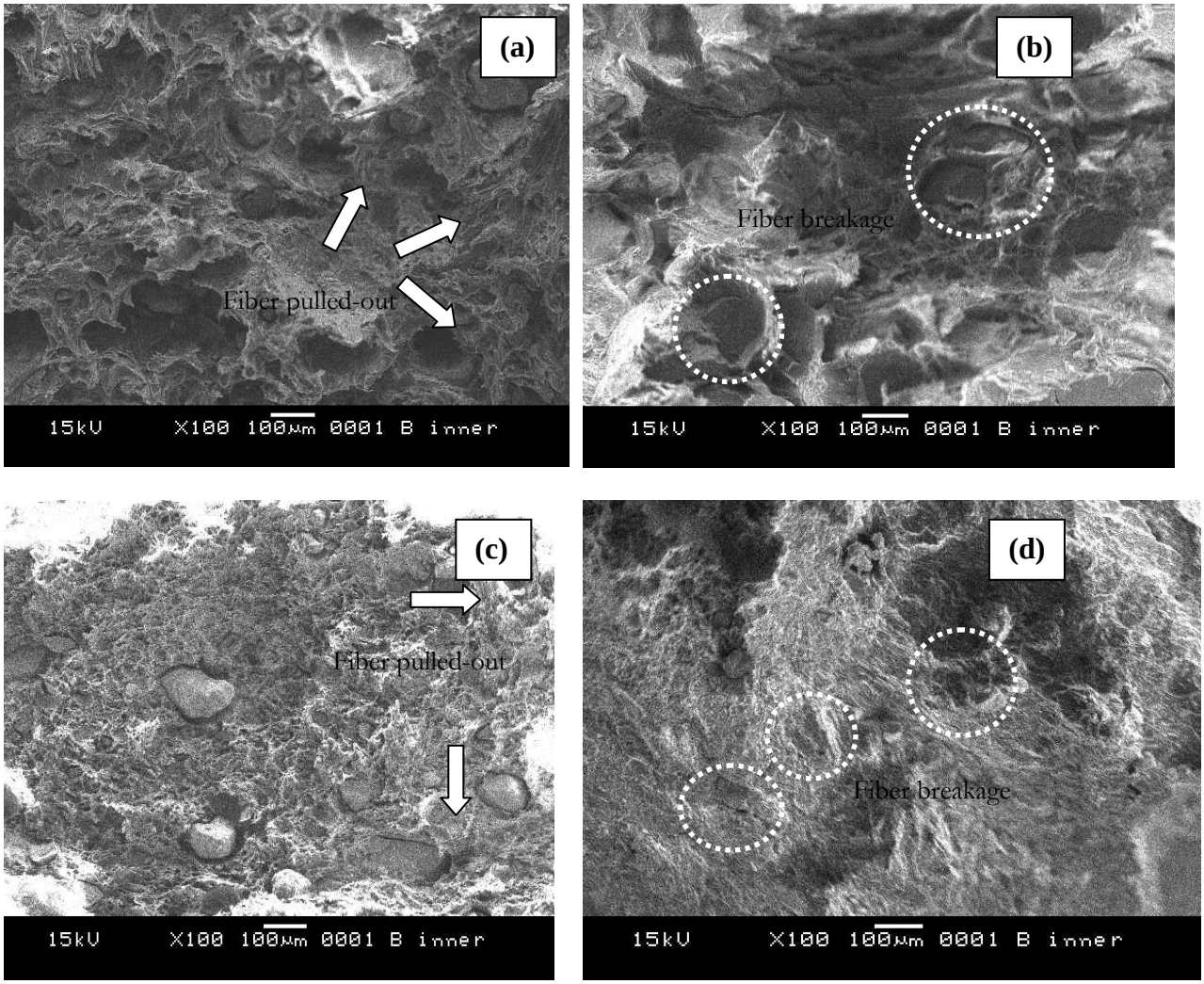

Figure 4: SEM micrographs of impact fractured surface of (a) ungrafted OPEFB filled PVC, (b) grafted OPEFB filled PVC, (c) ungrafted OPEFB/talc filled PVC, (d) grafted OPEFB/talc filled PVC

Figure 5 shows the FTIR spectra of OPEFB and PMMA-g-OPEFB to verify the existence of the PMMA onto the fibre. The absorption band on both spectra with peaks at 3430.41 cm^{-1} and 3435.32 cm^{-1} attributes to hydroxyl group in which the O-H bond existed from the cellulose and lignin constituent of OPEFB [7]. The absorption band in the 1638.31 cm^{-1} region may be attributed to the presence of aromatic or benzene rings in lignin comprising of C=C bond. Meanwhile, the existence of PMMA onto the OPEFB was verified by the presence of the peak near 1733.65 cm^{-1} in PMMA-g-OPEFB indicates that the presence of an ester group with a C=O bond from MMA and provides strong evidence of grafting. Another characteristic that shows the evidence of grafting was found at absorption peak 1290 cm^{-1} [3]. This peak correlated with $CO\text{-}OCH_3$ which is the stretching of PMMA.

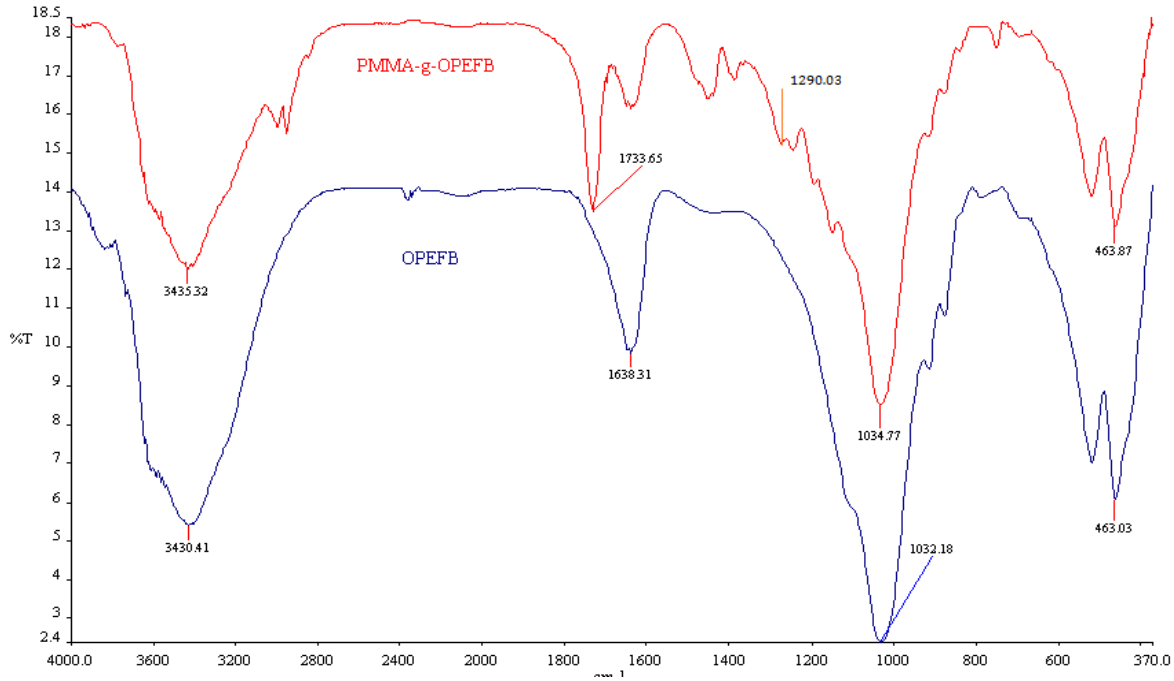

Figure 5: FTIR spectra of OPEFB and PMMA-g-OPEFB

Conclusion

This study investigated effect of single and hybrid filler of ungrafted, grafted OPEFB, ungrafted OPEFB/talc and grafted OPEFB/talc filled PVC composites. The flexural strength and impact strength of the single and hybrid filler are lower than the PVC composites. This is due to the shorter fibre length used. This might lead to failure due too much interaction between the fibre and matrix that caused the improvement of the interfacial adhesion between the fibre and matrix. The flexural modulus of the single and hybrid filler are higher compared to the PVC composites. The improvement of interfacial adhesion between the PMMA and OPEFB fibre is confirmed by the FTIR and SEM analysis.

Acknowledgements

The authors would like to thank the Ministry of Higher Education of Malaysia and Research Management Center, Universiti Teknologi Malaysia for the financial support under the Fundamental Research Grant Scheme (Vot. 78612).The authors wish to thank Mr. Mohd Azri and Mr Izad from Polymer Testing Laboratory Faculty of Chemical Engineering Universiti Teknologi Malaysia, Mr. Tarmizi from Department of Material Science Universiti Tun Hussien Onn and Idemitsu Petrochemical Sdn Bhd for their support during testing.

References

[1] Abu Bakar, A., Hassan, A. and Mohd Yusof, A. F. 2005a. *Polymer and Polymer Composites*. 13(6):1-8

[2] Abu Bakar A., Hassan A., Mohd Yusof A. F. 2005b. *Composites.Polymer-Plastics Technology and Engineering*. 44: 1125-1137

[3] Abu Bakar A., Nik Mat N.S. & Isnin M.K. 2008. *Journal of Applied Polymer Science*. 110: 847-855

[4] Abu Bakar A., Tham B. K. & Hassan, A. 2010. *Journal of Applied Polymer Science*. 115: 91-98

[5] Bakar M.B.A., Leong Y.W., Ariffin A. and Mohd Ishak Z.A. 2008. *Journal of Applied Polymer Science.* 110: 2770-2779

[6] Hassan A., Salema A. A., Ani F. N. & Abu Bakar A. 2010*. Polymer Composites.*

[7] Ibrahim N. A., Wan Yunus W. M. Z., Abu-Ilaiwi F. A., Rahman M. Z. A., Ahmad M. B. & Dahlan K. Z. M. 2003. *Journal of Applied Polymer Science.* 89: 2233 – 2238

[8] Khalid M., Salmiaton A., Ratnam C. T. & Luqman C. A. 2008. *Journal of Engineering Science and Technology*. 3(2): 153-162

[9] Leong Y.W., Mohd Ishak Z.A.& Ariffin A.2004. *Journal of Applied Polymer Science.* 91 (5): 3327-3336

[10] Raju G., Ratnam C. T., Ibrahim N.A., Ab. Rahman M.Z. & Wan Yunus M.Z. 2008. *Journal of Applied Polymer Science*.110 (1): 368-375

[11] Rozman H.D., Tay G.S., Kumar R.N., Abusamah A., Ismail H. & Mohad Ishak, Z. A. 2001. *European Polymer Journal*. 37:1283-1291

[12] Sain M., Suhara P., Law S. & Bouilloux A. 2005. *Journal of Reinforced Plastics and Composites*. 24(2): 121-130

THE EFFECT OF ELECTRON BEAM (EB) IRRADIATION IN THE PRESENCE OF TMPTA CO-AGENT ON MECHANICAL PROPERTIES OF POLYPROPYLENE / RECYCLED ACRYLONITRILE-BUTADIENE RUBBER/ RICE HUSK POWDER (PP/NBR/RHP) COMPOSITES

S.Ragunathan[1], H. Ismail[1], C. T. Ratnam[2] & K.Hussin[3]

[1]School of Materials and Mineral Resources Engineering, Engineering Campus, Universiti Sains Malaysia

[2]Radiation Processing Technology Division, Malaysian Nuclear Agency, Bangi,

[3]School of Environmental Engineering, Kompleks Pengajian Jejawi 3, Universiti Malaysia Perlis, Malaysia

Abstract

The effects of electron beam (EB) irradiation on the mechanical properties and morphology of PP/NBRr/RHP composites were investigated. The PP/NBRr/RHP composites were prepared at 100/0/15, 80/20/15, 70/30/15, 60/40/15 and 40/60/15 composite ratio with and without the presence of a polyfunctional monomer, trimethylolpropane triacrylate (TMPTA) at constant ratio 4 phr. Melt mixing techniques was employed using a *Haake Polydrive* internal mixer at 180 °C for 9 min and 50 rpm rotor speed. Results indicated tensile strength and tensile modulus decrease with NBRr content but elongation at break increased. All tensile properties at all composite ratio for irradiated PP/NBRr/RHP composite at 60 kGY with the presence of TMPTA was found to be improved. Scanning electron microscopy proved the enhancement in tensile properties when TMPTA were added in PP/NBRr/RHP where the irradiated tensile fracture surfaces demonstrate more irregularity with increasing crack branching (fracture planes are located at different heights) due to the increased filler matrix interaction.

Keywords*: Acrylonitrile butadiene rubber, mechanical properties, polypropylene, trimethylolpropane triacrylate*

Introduction

The amount of plastic waste generation increases as a result of rapid growth in polymeric material production. Acrylonitrile butadiene rubber(NBR) has been used to greater extent because of its superior strength, excellent resistance to abrasion, water, alcohols and heat besides non-existence of leachable allergenic proteins unlike in natural rubber latex. Hence, production trend of glove manufacturing has slowing shifting towards nitrile gloves. They are currently used widely in many areas such as medical, food industries, automotive industries, chemical industries and so on. These gloves are primarily used for single application and discarded as waste after usage. As a result, significant quantities of nitrile glove waste are generated worldwide daily. Therefore appropriate method to recycle and reuse these waste materials has drawn much interest among researchers.

Rice husk (RH) is natural fibre produced as waste product from agricultural sector mainly from paddy plantation. It is the outer covering of paddy and accounts for 20 % of its weight [16]. Currently, it has been disposed by open burning after removing the rice grains from them. The potential of RH usage as fillers in polymer may serve as an alternative to utilize the waste material [14,24]. It is expected that lignocellulosic composites have several advantages over the composites produced from synthetic fibres. The advantages of natural fibre made composite are its low density, recyclable, low production cost of moulded products and biodegradability [14].

The incorporation of NBRr and RH in plastic material was done by adding crystalline plastics such PP, PE, HDPE, LLDPE and etc with them. Polypropylene is most likely to be

used because of its low density, easy processing, good melt behavior besides it cheap cost. However, PP and NBR are highly incompatible due to poor physical, mechanical, and chemical interactions across the phase boundaries [10]. Addition of compatibilizing agents is a common method used to overcome the incompatibility [3]. Several compatibilizing systems for PP/NBR have been studied and reported by many researchers [6,8,9,13]. Cross-linking of elastomeric phase of such a composite system is another method that can be used to defeat a lack of stability in some thermoplastic elastomeric composites [3]. Cross-linking can be done either by dynamic vulcanization or by high energy radiation [4].

Electron-beam irradiation of polymers results in the formation of a three dimensional network structure through the combination of free radicals which are formed by dissociation of the excited state or by ion molecular reaction [2,7]. The cross-linked structure could reduce the interfacial tension and provide a material with improved final properties [4]. Electron-beam modification has certain advantages over conventional grafting processes such as the absence of catalyst residue, bringing about uniform crosslinking, consuming less energy, complete control of the temperature, a solvent free system and accurate reproducibility [2,21]. Nevertheless, irradiation of polymers by electron-beam results in simultaneous formation of cross-links and chain scission. Therefore; the final properties of the material depend on the ratio of cross-links to chain scission [4]. NBR is an unsaturated amorphous polymer and belongs to crosslinking type rubber when exposed to high energy radiation. But NBR is required high irradiation dose to reach the desired crosslink density. However, high irradiation doses can adversely affect the mechanical properties of the material due to degradation induced by radiation. Desired crosslink density can be obtained at lower irradiation dose by addition of appropriate polyfunctional monomers (PFMs) into polymer matrix [20].

Many researchers [21,23], have been studied on co-agents such as,N,N'-methylene bisacrylamide (MBAAm), Trimethylol propane trimethacrylate (TMPTMA), TMPTA and etc. (TMPTMA).They have found that TMPTMA is more effective in enhancing the mechanical and physical properties of NBR/HDPE vulcanized composites [23]. However in this study TMPTA was utilized to investigate the effect of electron beam irradiation on tensile properties and morphology of polypropylene/recycled acrylonitrile butadiene rubber/rice husk powder (PP/NBRr/RHP) composites.

Materials and Method

Materials

Polypropylene (PP) used in this work was supplied by Titan PP Polymers (M) Sdn, Bhd, Johor, Malaysia (code 6331) having melt flow index and density of 14 g/10 min at 230^{o}C and 0.9 g.cm^{-3} respectively. Recycled acrylonitrile butadiene rubber (rNBR) was produced in house by grinding nitrile rubber gloves obtained from Juara One Resources Sdn Bhd, Penang, Malaysia. The range of particle size of rNBR used was 300-500 μm and the density of rNBR was 1.015 g.cm^{-3} trimethylolpropane triacrylate TMPTA, a trifunctional coagent was purchased from UCB Asia Pacific Ltd, Malaysia

Preparation of the composites

Two types of composites; namely PP/NBRr/RHP-Control (non-irradiated) and PP/rNBR/RHP-IC (Irradiated) were prepared from PP/NBRr/RHP having compositions 80/20/15, 70/30/15, 60/40/15, 50/50/15, 40/60/15. For PP/NBRr/RHP-IC composites, 10 phr of TMPTA was added during the composite preparation. The composites were prepared by melt mixing in a Haake Rheomix Polydrive R 600/610 mixer at 180^{o}C with the rotor speed of 60 rpm. The PP was charged into the mixing chamber and melted for 3 min followed by the addition of NBRr. The RHP is added at 6min and mixing was continued for another 3 min. For PP/rNBR/RHP-Irradiated composites; PP was melted 3 min and then rNBR was added and continued mixing

for another 3 min. TMPTA was added into the composite together with the RHP powder at the 6^{th} min. The total mixing time was 9 min.

Compression molding

Samples of the composites were compression molded in an electrically heated hydraulic press. Procedure of moulding of both composites involved preheating of the sample for 7 min at 180 ^{o}C, followed by compressing the mould for 2 min at the same temperature and subsequently cooling under pressure for another 2 min.

Irradiation

The molded sheets of PP/rNBR/RHP-TMPTA composite were irradiated using a 3 MeV electron beam accelerator NHV EPS-3000 at a dose of 60 kGy. The acceleration energy, beam current and dose rate were 2 MeV, 2 mA and 20 kGy per pass, respectively.

Tensile properties

Tensile tests were carried out according to ASTM D638 standard method using Instron tensile machine model no. 3366. One millimeter thick dumbell tensile specimens were cut from the molded sheets with a Wallace die cutter model S6/1/16 A. A cross head speed of the tensile machine was maintained at 5 $mm.min^{-1}$ and tests were performed at 25 ± 3 ^{o}C. Tensile strength, Young's modulus and elongation at break were measured.

Fourier transforms infrared (FTIR) spectroscopy

The FTIR spectra of non-irradiated and irradiated composites were obtained using a Perkin-Elmer 2000 series instrument. The spectrum resolution was 4 cm^{-1} and the scanning range was from 550 to 4000 cm^{-1}.

Morphological study

The morphology of the tensile fractured surfaces of the samples was examined and analysed using the *SUPRA36VP-24-58* Field Emmission Scanning Electron Microscope (FESEM). The fractured ends of the specimens were mounted on aluminum stub and sputter-coated with a thin layer of gold to avoid electrostatic charging during examination.

Results and Discussion

Stabilization torque

Stabilization processing torque for both composites with and without TMPTA co-agent is obtained at the end of 9 min mixing time. Figure 1 shows stabilization value of PP/rNBR/RHP-Control and PP/rNBR/RHP-TMPTA composites. The stabilization torques increased with increasing NBRr composition in the composite. The possible reason for this phenomenon is the increase in melt viscosity of the composites at higher NBRr composition. Similar finding have been reported by Ruksakulpiwat et al. [15] on natural fibre-polypropylene composite by using natural rubber and EPDM. However, the addition of TMPTA co-agent did not significantly influence the processing torque, whereby both composites are having almost same stabilization torque value for all the examined composites.

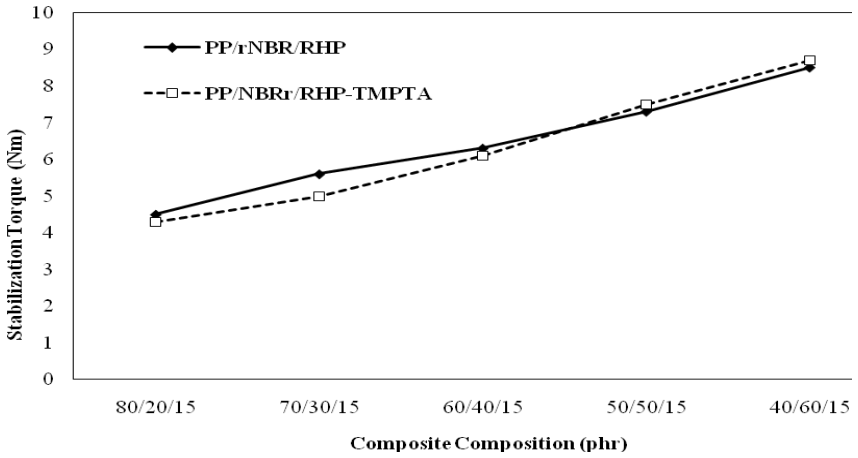

Figure 1: Stabilization torque of PP/rNBR/RHP and PP/rNBR/RHP-TMPTA composites

Tensile properties

Figure 2-4 shows the tensile properties such as tensile strength, Young's modulus and elongation at break of PP/NBRr/RHP-Irradiated and PP/NBRr/RHP-Controlcomposites as a function of composite composition. Results showedthe tensile strength and the Young's modulus for all composite composition increased with irradiation. The radiation-induced cross-linking was believed to be responsible for increase in the tensile strength and the Young's modulus. Youssef et al. [22] reported that electron beam irradiation enhanced the tensile strength of composite of short polyethylene terephthalate fiber (PET) filled NBR composites.

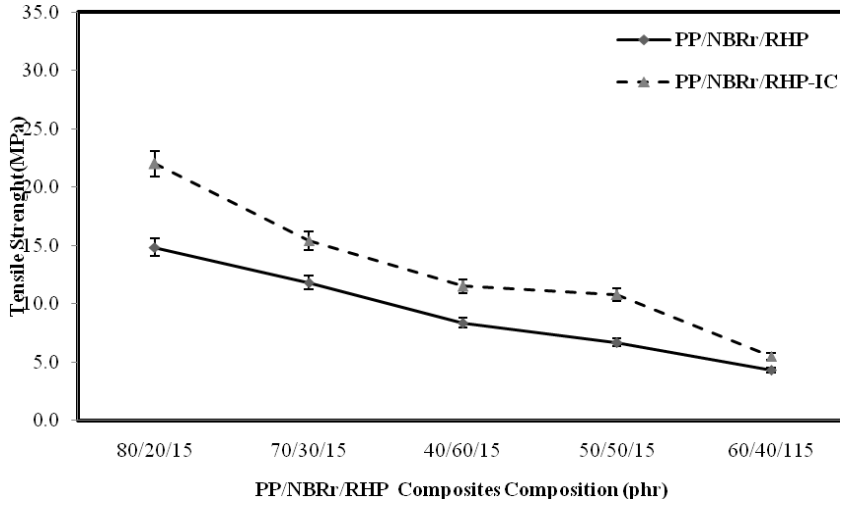

Figure 2: Tensile strength vs composite composition of PP/NBRr/RHP and PP/NBRr/RHP-IC composites

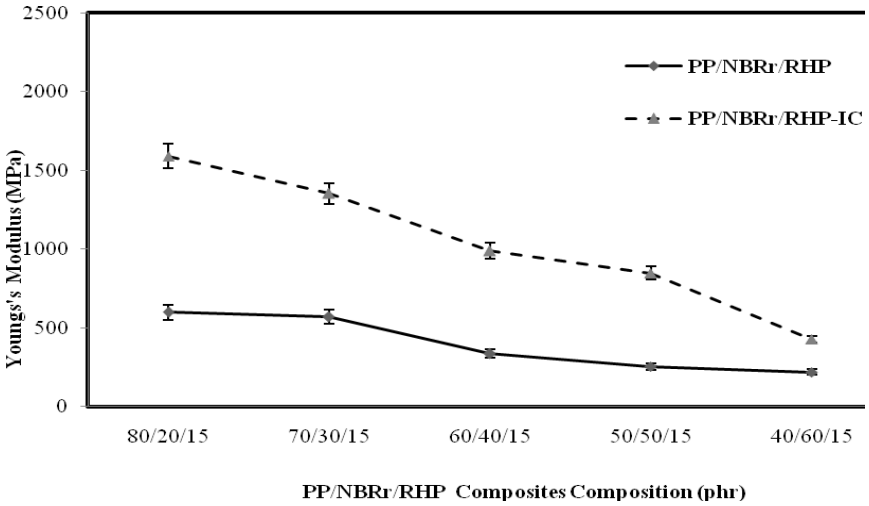

Figure 3: Young's modulus vs composite composition of PP/rNBR and PP/rNBR-IC composites

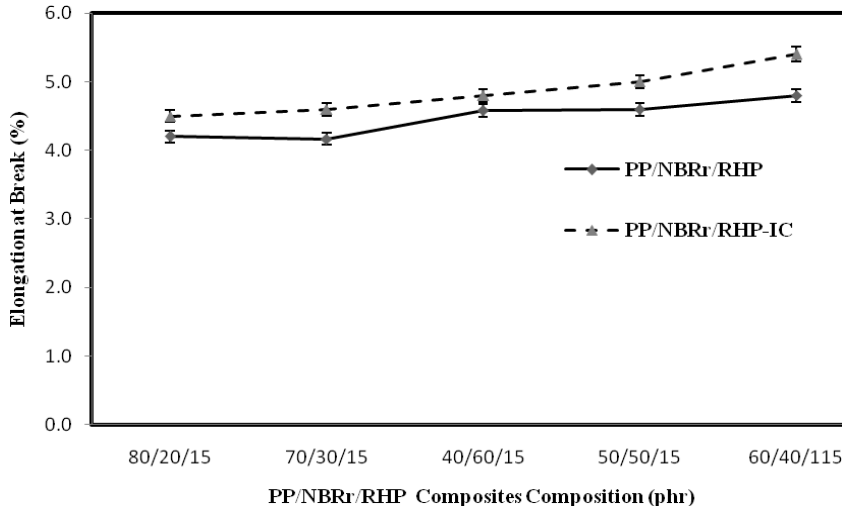

Figure 4: Elongation at break vs composite composition of PP/NBRr/RHP and PP/NBRr/RHP-IC composites

However, in contrary decreasing trend in the tensile strength and the Young's modulus was observed with increasing NBRr composition. This probably was due to decreasing amount of crystalline PP structure in the PP/NBRr/RHP composites [1,19].In addition, stress transfer across the composites is highly attributed to RHP distribution in NBRr and PP matrices. At higher NBRr composition poorer RHP distribution was observed as shown later in the morphological study.

Figure 4 shows the elongation at break for composites at different NBRr compositions. A slight enhancement in elongation at break (E_b) was noticeable for irradiated composites. Irradiation promoted cross-links in the composite are the possible reason for increasing elasticity of the composite, resulting in higher elongation at break(E_b).The increasing trend of E_b at higher NBRr composition is attributed to increasing content of elastic rubbery material in the composites that further elongate prior to failure. Shaltout et al. [17] reported that electron beam irradiated NBR/HDPE blends showed improved tensile properties compared to control blends.

FTIR Spectroscopy analysis

It is well known that NBRr is a polar polymer based on its existing nitrogen groups. TMPTA is an initiator which also exhibits polar properties. There is an interaction between the polar sites of NBR with polar site of the initiator. The oxygen from the carbonyl groups of TMPTA tends to form hydrogen bonding with nitrogen groups of NBR to form a three dimensional network structure through the union of *in situ* generated macroradicals. Figure 5 shows FTIR spectra of PP/NBRr/RHP-Control and PP/NBRr/RHP-IC (Irradiated) composites. The FTIR analysis reveals broader peak appearing at around 1600-1650cm^{-1}which indicates the presence of C=C bond of NBR in the PP/NBRr/RHP composite. It can be seen that the existence of sharper and bigger C=C peak in the PP/NBRr/RHP spectrum compared to that of PP/NBRr/RHP-IC (Irradiated). This is a good indication of the formation of cross links between NBRr and TMPTA as well as within the NBRr molecules.

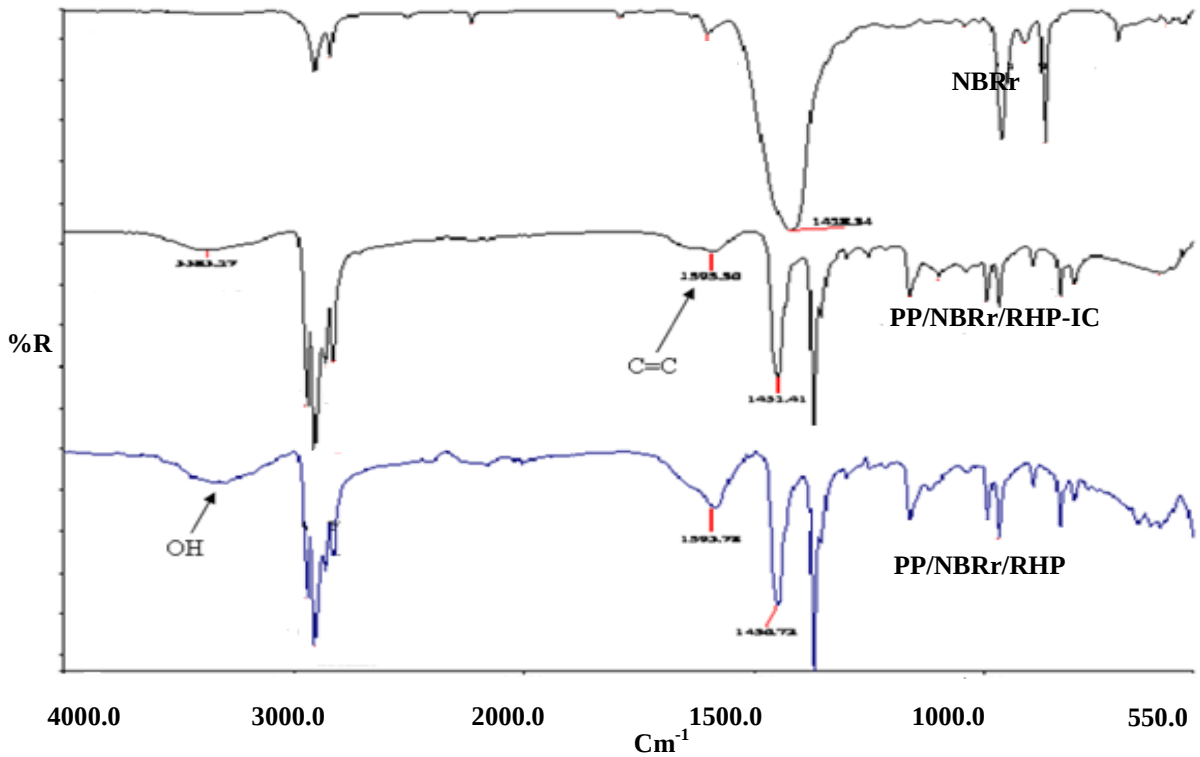

Figure 5: FTIR spectra of PP/NBRr/RHP and PP/NBRr/RHP-IC composites

Polyfunctional monomer (PFMs) such as TMPTA is able to achieve cross-linking in polymer matrices [12]. The free radical generated on the carbon atoms of polymers may react with each other or grafted with PFMs followed by crosslinking. Similarly polypropylene may also undergo cross linking and grafting through radical formation when exposed to radiation. This explains why better tensile properties were observed in irradiated composites. However no significant role of RHP was identified with electron beam radiation on PP/NBRr/RHP composites with TMPTA co-agent.

Morphological study

The SEM micrographs of tensile fractured surface of control and irradiated composites at different composite composition i.e, 80/20/15, and 40/60/15 of PP/NBR/RHPare illustrated in Figure7 (a-d), respectively. In comparison to the SEM micrographs of tensile fractured surfaces of control PP/NBRr/RHP composites, a considerable improvement in adhesion

between the PP and NBRr phases can be observed in the irradiated composites. Further, more tear lines and less detachment of NBRr from PP matrix which indicate higher strength properties. Such changes in morphology could be attributed to radiation- induced cross-linking of the dispersed NBRr phase. In our previous studies we have also reported similar finding on PP/NBRr blends with electron beam radiation at 40 kGy [8].

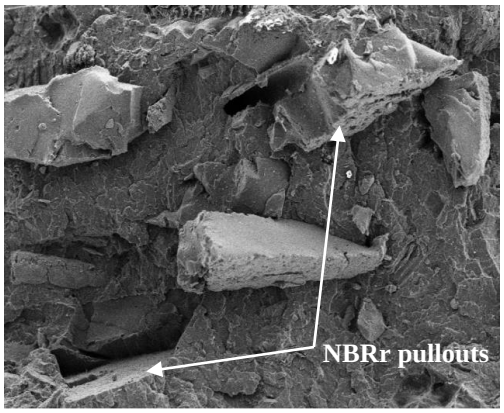

7a) PP/NBRr/RHP:80/20/157

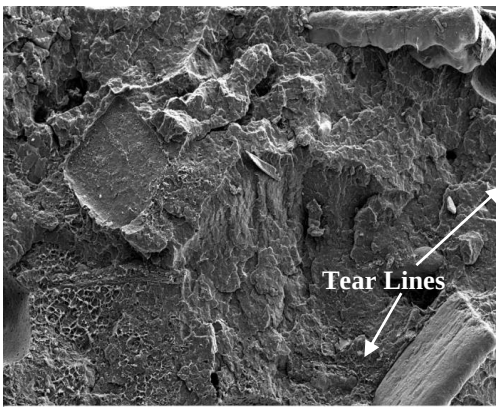

c)PP/NBRr/RHP-IC:80/20/15

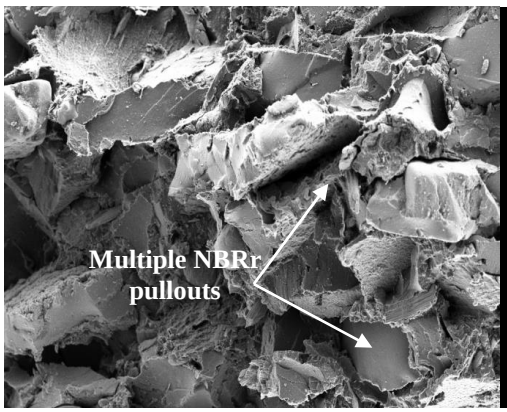

7b) PP/NBRr/RHP:40/60/157

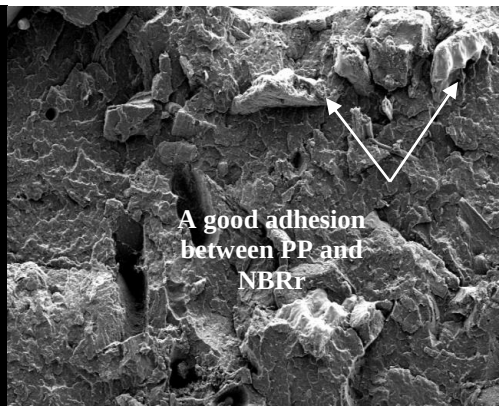

d) PP/rNBR/RHP-IC:40/60/15

Figure 7: Scanning electron micrograph of tensile fractured surface of (a,b) non-irradiated composites (PP/rNBR) and (c-d) irradiated composites (PP/rNBR-IC) (% w/w) at magnification of 100×.

Conclusions

The mixing torque and stabilization torque increased with addition of more NBRr into the PP matrix due to higher viscosity of NBRr**.** There was no significant effect with the addition of TMPTA on the melt viscosity of PP/NBRr/RHP control composites. Tensile properties and oil resistance of the composites were enhanced by the electron beam irradiation. The morphology results indicated that the electron beam irradiation has enhanced the adhesion between PP and NBRr phases of the PP/NBRr/RHP composites.

Acknowledgement

We would like to acknowledge Dr. C.T. Ratnam and the staff, MINT staff for their assistance during the electron irradiation of the samples and the Universiti Malaysia Perlis for the study leave granted for Mr. S. Ragunathan.

References

[1] Awang, M., Ismail, H., & Hazizan, M.A. 2008. *Polym. Test.* 27: 93-97

[2] Chattopadhyay, S., Chaki, T.K., & Bhowmick, K. 2001. *J. of Appl. Polym. Sci.* 81: 1936-1950

[3] Dyke, J.D.V., Gnatowski, M., & Buruczyk, A. 2008. *J. Appl. Polym. Sci.*109: 1535-1546

[4] Das, P.K., Amnatkar,S.U., Sarma, K.S.S., Sabharwal, S., & Banerji, M.S. 2006. *Polym.Inter.* 55: 118 123

[5] George, G., Joseph, R., & Thomas, S.1995. *Polymer.* 36: 4405-4416

[6] George,S., Prasannakumari, L., Koshy, P., Varughese, K.T., & Thomas, S.1996. *Mater. Lett.* 26: 51- 58

[7] Hafezi, M., Khorasani, S.N., Ziaei, F., & Azim, H.R. 2007. *J. Elastom*. *and Plast*. 39: 151-163

[8] Ismail, H., Galpaya, D., & Ahmad, Z. 2010(a). *J. Vinyl Addit. Technol.* 16(2): 141-146

[9] Ismail, H., Ragunathan, S., & Hussin, K. 2010(b). *Polym. Plast. Technol. Eng.* 49,13: 1323-1328

[10] Joseph, A., George, S., Joseph, K., & Thomas, S. 2006. *J. Appl. Polym. Sci.* 102: 2067- 2080

[11] Naderi,G., Nouri, M.R., Mehrabzadeh, M., & Bakhshandeh, G.R.1999. *Iran. Polym. J*. 8:
37-42

[12] Noriman, N.Z., Ismail, H., Ratnam, C.T., & Rashid, A.A. 2010. *Polym. Plast. Technol. Eng.* 49: 228-236

[13] Ragunathan, S., Ismail, H., & Hussin, K. 2011. *Key Eng. Mater*. 471-472: 478-483

[14] Razavi-Nouri, M., Jafarzahed-Dogouri, F., Oromiehie, A., & Langroudi, A.E. 2006. *Iran. Polym. J*. 15: 757- 766

[15] Ruksakulpiwat, Y., Sridee, J., Suppakarn, & N., Sutapun, W. 2009. *Comp. Part B*. 40: 619-622

[16] Satyanarayana, K.G., Arizaga, G.G.C. , & Wypych, F. 2009. *Prog. Polym. Sci*. 34: 982-1021

[17] Shaltout, N.A. 2010. *J. Macromolec. Sci. Part A*. 47:2: 160-165

[18] Soares, B.G., Almeida, M.S.M., Deepa Urs M.V., Kumaraswamy,G.N., Ranganathaiah, C., & Siddaramaiah, Mauler, R. 2006. *J. Appl. Polym. Sci*. 102: 4672-4681

[19] Soares, B.G., Almeida, M.S.M., Ranganathaiah, C., Deepa Urc, M.V., & Siddaramaiah. 2007. *Polym. Test.* 26: 88-94

[20] Yasin, T., Ahmed, S., Yoshii, F., & Makuuchi, K. 2002. *React. and Funct. Polym.* 53: 173-181

[21] Yasin, T., Ahmed, S., Ahmed, M., & Yoshii, F. 2005. *Radiat. Phys. and Chem*. 73: 155-158

[22] Youssef , H.A., Shaltot, N.A., El Nemr, K.F., & El Miligy, A.A. 2009. *J. Polym. Research* 16: 199–212

[23] Zeid, M.M.A., Shaltout, A.S., Khalil, A.M., & Miligy, A.A.E. 2008. *Polym. Comp*. 29: 1321-1327

[24] Zurina, M., Ismail H., & Bakar, A.A. 2004. *J. Appl. Poly.Sci.* 92: 3320-3332

MODIFICATION OF NR/PVC BLENDS BY ELECTRON BEAM RADIATION

Chantara Thevy Ratnam[1], Lee Kah Heng[2], Sivanesan Appadu[1] & Azizan Ahmad[3]
[1]Radiation Processing Technology Div., Malaysian Nuclear Agency
[2]College of Engineering, Universiti Tenaga Nasional
[3]School of Chemical Sciences & Food Technology,
Faculty of Science and Technology
Universiti Kebangsaan Malaysia, Selangor, Malaysia

Abstract

Electron beam initiated crosslinking on the 50/50 poly(vinyl chloride), PVC/ natural rubber (NR) blend was studied in the absence and presence of 4 phrtrimethylolpropanetriacrylate (TMPTA). The 50/50 NR/PVC blend was prepared by mixing in a Brabender Plasticoder at 150 °C. The blend was then irradiated by using a 3.0 MeV electron beam machine at doses ranging from 0 to 200 kGy in air and room temperature. The changes in gel fraction, tensile properties, flexural modulus, impact strength and hardness of the blends were investigated. A gradual increase in mechanical properties of the blends with irradiation dose was observed. The gel fraction results indicate that electron beam irradiation causes crosslinking in the NR/PVC blend. The addition of TMPTA was found to be effective in the acceleration of the radiation-induced cross linking.

Keywords: *Enhancement, natural rubber/poly(vinyl chloride) blend, properties, radiation-induced crosslinking*

Introduction

The blending of polymers for property enhancement or for economic purposes has become increasingly important in the last decade. In this respect, poly(vinyl chloride) (PVC) and epoxidized natural rubber (ENR) has attracted the attention of many researchers [3,4,17]. Numerous studies [2,3,4,17] showed that PVC/ENR blends exhibit a single glass transition temperature, T_g which lies between that of PVC and ENR indicating compatibility at molecular level. A number of reports indicated that the physical and mechanical properties of the blend could be enhanced by electron beam irradiation [7-9,10,11,12-15]. Other miscible blends of PVC include its blends with chlorinated polyethylene and nitrile butadiene rubber. The blends of natural rubber, NR and PVC show separate T_g which indicate that they are not compatible [5]. A more recent work by Radhakrishnan et al. [6] revealed that the enhancement in the compatibility between NR and PVC could be achieved by using NR/polyurethane block copolymer.

However, to date, no information has been published on the effect of high-energy irradiation on the NR/PVC blends to the best knowledge of the authors. Thus, the present study focuses on the effect of electron beam irradiation on the physical properties of NR/PVC blends. In this study, the effect of irradiation on 50/50 NR/PVC blend was studied with particular attention to irradiation-induced crosslinking in the presence of a radiation sensitizer, trimethylolpropanetriacrylate (TMPTA).

Materials and Method

Materials

Standard Malaysian Rubber (SMR L) was obtained from Malaysian Rubber Board; poly(vinyl chloride), PVC with a K- value of 66 (Mn of 66,000), grade “MH66, 6519” was purchased from Industrial Resin (M) Ltd. The PVC stabilizer used, tribasic lead sulfate (TS-100M) was purchased from Lonover Scientific Suppliers Ltd., London. They were used as received.

Formulations
The 50/50 NR/PVC blends were prepared by mixing 50 wt-parts of PVC with 50 wt-parts of SMRL, 2 wt-parts of heat stabilizer and 4 wt-parts of TMPTA. The blend without the addition of TMPTA was used as control.

Blend Preparations
PVC and the stabilizer were premixed at room temperature in a tabletop high-speed mixer at 1200 rpm for 10 min. Melt blending was carried out at 150 °C and 50 rpm rotor speed in a *Brabender Plasticorder Model PL 2000* with a mixing cam attachment. The blending was done as follows. When the desired temperature was reached, the SMR was charged into the mixing chamber and mixed for 1 min. The PVC compound was then added, and the blending was continued for a further 9 min. The blends obtained from the Brabender Plasticorder were then compression molded into 1 and 5 mm thick sheets under a pressure of 14.7 MPa at 150 ^{o}C for 3 min. The sheets were immediately cooled between two plates of a cold press at 25 ^{o}C. Dumbbell-shaped test pieces were cut from these sheets in accordance with BS6746 standard. The molded sheets and dumbbell test pieces were irradiated using a 3 MeV electron beam accelerator at a dose range of 0-200 kGy. The acceleration energy, beam current, and dose rate were 2 MeV, 2 mA and 10 kGy/pass respectively.

Gel Fraction
The gel fraction was determined by extraction in tetrahydrofuran (THF) at 50±2 ^{o}C. The blends were solvent extracted with THF for 24 h and the extracted samples were dried to constant weight. The gel fraction was calculated as:

$$\text{Gel Fraction} = \left(\frac{W}{W_0}\right) \times 100 \quad (1)$$

where W and W_0 are the weight of the dried sample after extraction and the weight of the sample before extraction respectively.

Measurement of Tensile Properties
The tensile strength (Ts), modulus at 100% elongation (M100) and elongation at break (Eb) were measured with an Instron *Universal Testing Machine* using a crosshead speed of 50 mm.min^{-1} in accordance to BS6746 standard. Eight samples were used for the tensile test and an average of six results was taken as the resultant value (the maximum and minimum data being discarded).

Hardness
The Shore A hardness test was carried out according to ASTM D2240-89 standard using the Zwick 7206 hardness tester. Sheets of 5 mm thickness were used for hardness measurement.

Flexural Modulus
The flexural modulus was determined by using an *Instron Model 4301* machine in accordance with ASTM D 790-97 standard. Five rectangular bar shaped specimens are tested for each composition with a thickness of 3 mm and their average values were calculated.

Impact Strength
The Izod impact test was performed using a 4 J hammer on notched samples by a *Universal Digital Pendulum Model CEAST* machine in accordance to ASTM D 256-97 standard. A total of

seven samples were used for the tensile test and an average of five results was taken as the resultant value.

Results and Discussion

Gel Fraction

Studies over the past two decades have established that irradiation can be very useful in the processing of polymer blends [16]. Improvement of blend properties has been achieved through several different approaches, including: crosslinking, scission, compatibilisation, and morphology stabilization. The extent of irradiation–induced crosslinking of polymers can be estimated from gel fraction determination. Figure 1 shows the effect of irradiation on the gel fraction of 50/50 NR/PVC blend. It is clear from Figure1 that the gel fraction increases with the increase in radiation dose, indicating that the radiation-induced crosslinking has occurred in the PVC/NR blend similar to PVC/ENR blend system [7,9,12,13]. The higher gel fractions observed upon irradiation of the NR/PVC blend in the presence of TMPTA indicate the acceleration of the irradiation-induced crosslinking by the acrylate. Similar acceleration of crosslinking by the addition of polyfunctional monomers was observed for PVC/ENR blend compounds [7,9].

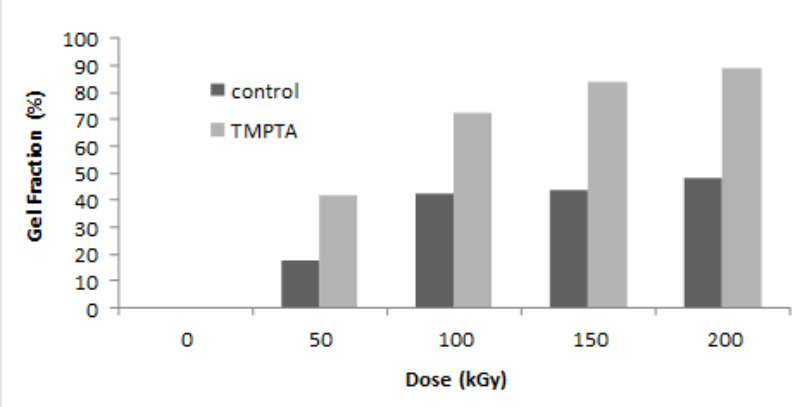

Figure 1: Effect of irradiation on the gel fraction of 50/50 NR/PVC blend

Tensile and flexural properties

The effect of radiation on the Ts, flexural modulus, and M100 and Eb of 50/50 NR/PVC blend are illustrated in Figure 2-5, respectively. Figures 2-4 clearly show that an enhancement in the Ts M100 and flexural modulus of the NR/PVC blend has occurred upon irradiation. Upon irradiation the Ts, M100 and flexural modulus of the blends incorporated with TMPTA show higher values as compared to the control. Such trend of results is attributed to the formation of radiation induced crosslinking and acceleration of the radiation-induced crosslinking by the TMPTA in the blend as observed from the gel fraction data. In contrast, Figure 5 depicts that increasing the irradiation dose causes a reduction in the elongation at the break. This observation is attributed to the increasing brittleness of the blend as a consequence of the increase in number of crosslinks as the absorbed dose increases. Ratnam et al. [12-15] working with electron beam radiation of PVC/ENR blends have reported similar observations. Besides that, it is also important to note that, the enhancement in the NR/PVC blend properties with radiation dose could be associated with the increase in the compatibility of the blend system upon radiation. In view of this, studies on dynamic mechanical properties of PVC/ENR binary system showed that the compatibility of the blend improved upon irradiation [12,13].

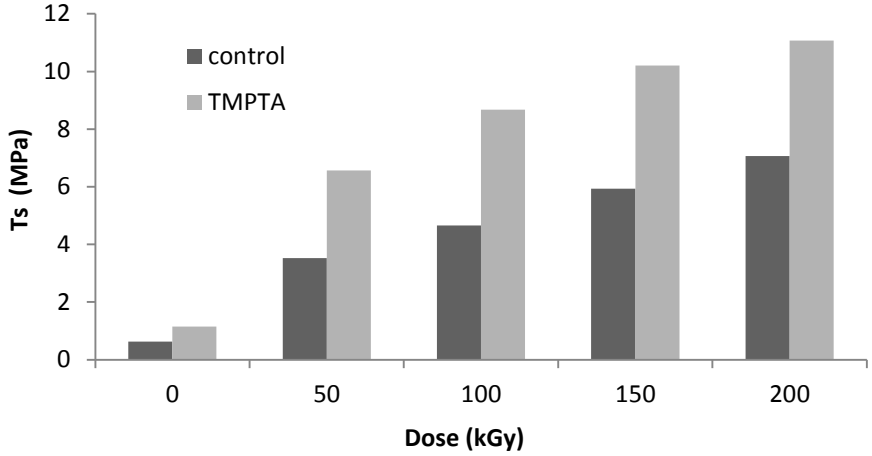

Figure 2: Effect of irradiation on the Ts of 50/50 NR/PVC blend

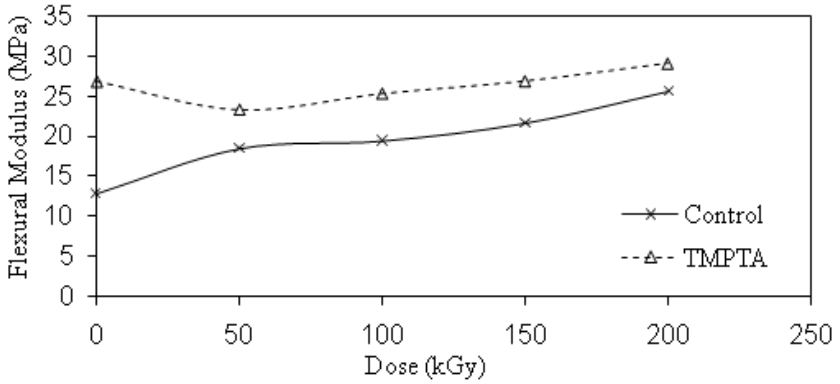

Figure 3: Effect of irradiation on the flexural modulus of 50/50 PVC/NR blend

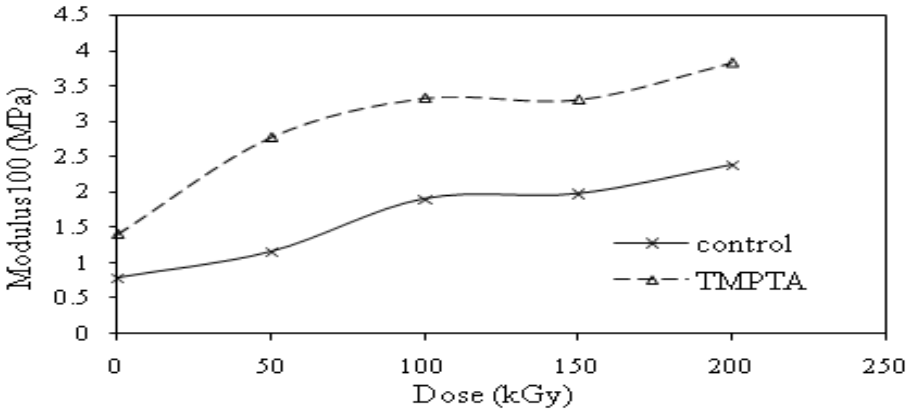

Figure 4: Effect of irradiation on the M100 of the 50/50 NR/PVC

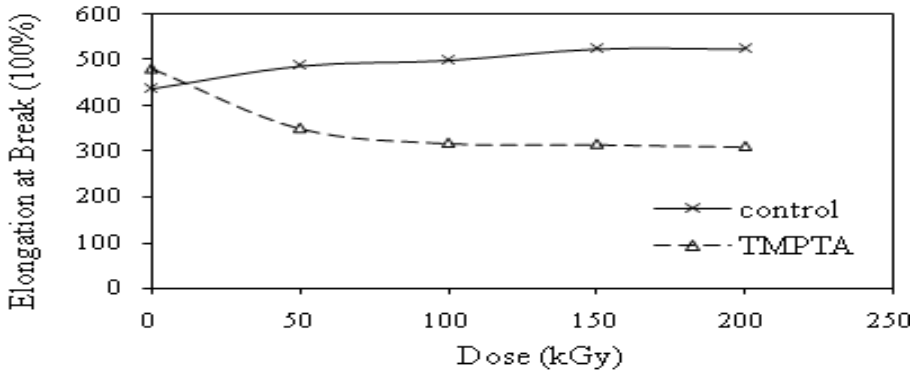

Figure 5: Effect of irradiation on the elongation at break of 50/50 PVC/NR blend

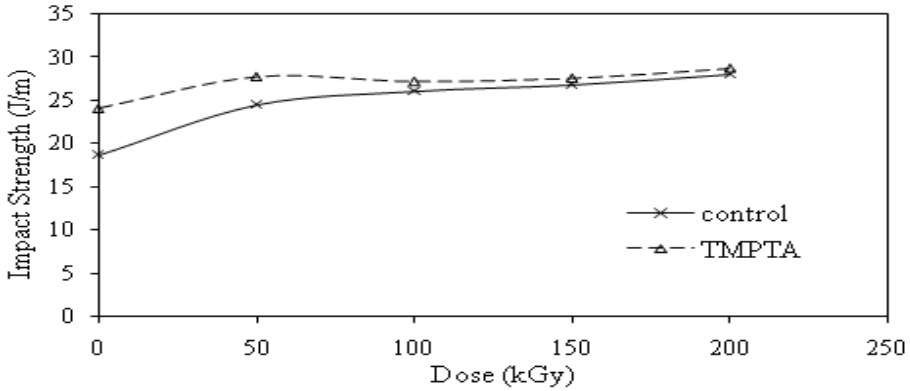

Figure 6: Effect of irradiation on the impact strength of 50/50 NR/PVC blend

Figure 6 depicts the effect of radiation on the impact strength of 50/50 NR/PVC blend. The impact strength of the blend shows a gradual increase with the increase in radiation doses. The impact properties of polymeric materials are directly related to the overall toughness of the material. Thus, the enhancement in impact strength of NR/PVC blend with EB irradiation and a further increase with the addition of TMPTA is attributed to the increase in crosslink density of the blend which increases the ability of the system to absorb energy during fracture propagation.

Hardness

The effect of TMPTA on the hardness of the 50/50 NR/PVC blend with increasing irradiation dose is illustrated in Figure 7. Apparently, formation of the three dimensional network as a result of irradiation induced crosslinking has successfully increased the resistance of the NR/PVC blends to local deformation which in return improved the hardness of the blend. The further enhancement in the hardness of the blend upon irradiation in the presence of TMPTA again indicates the accelerating effect of the additive on the occurrence of radiation -induced crosslinking. Therefore the hardness further confirms the observation obtained on the tensile, flexural and impact properties.

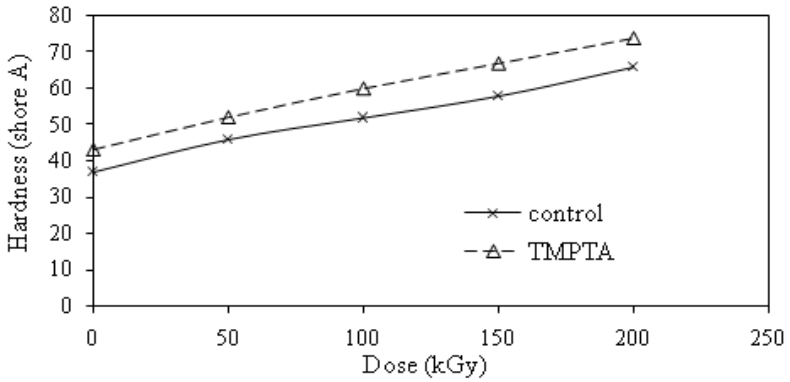

Figure 7: Effect of irradiation on the hardness of 50/50 NR/PVC blend

Conclusion

The effect of electron beam irradiation on the gel fraction and mechanical properties of 50/50 NR/PVC blend has been studied. It was observed that irradiation-induced crosslinking occurs in the NR/PVC blend. Addition of TMPTA can significantly accelerate the irradiation-induced crosslinking in the blend.

Acknowledgements

The authors wish to thank the Ministry of Science Technology and Innovation for sponsoring this work under IRPA Grant (IRPA 03-01-03-0013 EA001). The cooperation given by ALURTRON staff of Nuclear Malaysia during the irradiation is appreciated.

References

[1] Ishiaku, U. S., Nasir, M. & Mohd. Ishak, Z. A. 1995. *J. Vinyl Additive Technol.* 1(2): 66-70

[2] Ishiaku, U.S., Nasir, M. & Mohd.Ishak, Z.A. 1994. *J. Vinyl Technol*. 16: 226-230

[3] Margaritis, A. G., Kallitsis, A. K. & Kalfoglou, N. K. 1987. *Polym.* 28: 2122-2129

[4] Nasir, M. & Ratnam, C. T. 1989. *J. Appl. Polym. Sci.* 38: 1219-1229

[5] Popovic, R.S & Popovic, R.G. 1999. *Kautschuk und Gummi, Kunststoffe*. 54(4): 254-260

[6] Radhakrishnan Nair, M.N. & Gopinathan Nair, M.R. 2006. *Polym. Bull*. 56(6): 619-631

[7] Ratnam C.T. & Zaman, K.1999a. *Polym. Deg. and Stab.* 65: 99-105

[8] Ratnam, C. T. & Zaman, K.1999b. *Polym. Deg. and Stab*. 65: 481-490

[9] Ratnam, C. T. & Zaman, K.1999c. *Nuclear Instrument and Method B*. 152: 335-342

[10] Ratnam, C.T. 2001. *Polym. Intern.* 50: 1132-1137

[11] Ratnam, C.T. & Zaman K. 1999d. *Angew.Makromole.Chemie.* 269: 42-48

[12] Ratnam, C.T. Nasir, M., Baharin, A. & Zaman, K. 2001a. *J. Appl. Polym. Sci.* 81: 1914-1925

[13] Ratnam, C.T., Nasir, M., Baharin, A. & Zaman, K. 2001b. *Polym. Intern.* 50: 503-508

[14] Ratnam, C.T., Nasir, M., Baharin, A. & Zaman ,K. 2000a. *Nuc. Instr. Method B.* 171(4): 455-464

[15] Ratnam, C.T., Nasir, M., Baharin, A. & Zaman K. 2000b. *Polym. Intern.* 49: 1693-1703

[16] Spanadel, L.1979. *Radiat. Phys. Chem*. 14: 683-697

[17] Varughese, K.T. & De, P. P.1989. *J. Appl. Polym. Sci*. 37: 2537-2548

TENSILE AND FLEXURAL PROPERTIES OF KENAF-POLYPROPYLENE COMPOSITE WITH MAPP COUPLING AGENT

A.R Noor Leha & N.A Nordin
Faculty of Mechanical Engineering, University of Technology MARA Shah Alam, Selangor, Malaysia

Abstract

Biocomposite from kenaf powder and polypropylene was fabricated by compression molding technique. The objective of this study was to evaluate the rheological behavior and mechanical properties of kenaf compounded with polypropylene. 3 % of Maleic Anhydride Polypropylene (MAPP) was used as coupling agent. The size of kenaf powder is limited to 150 μm with different ratio of 10% (w/w), 20% (w/w) and 30% (w/w) of kenaf. Tensile and flexural tests were done to characterize its mechanical properties. It was observed that the strength of kenaf-polypropylene was increased by 17 % with increasing amount of kenaf powder [1]. This could be attributed by the strong interaction between kenaf and MAPP. In addition, the flexural strength shows the highest value at 30% (w/w) kenaf [2]. The surface morphology which was characterized by optical microscope showed that the surface fracture without MAPP has severe defect compared to the specimen with MAPP. This indicates that the addition of MAPP would modify the surface characteristic and give an effective interaction between kenaf and polypropylene. It was found that kenaf-polypropylene can be a good candidate to be used in many engineering applications.

Keywords: *Flexural properties, kenaf, maleic anhydride polypropylene, polypropylene,tensile properties*

Introduction

Issues with decomposition and recycling are a major problem in many countries especially in managing millions of tons of post-consumer plastic. Plastic films, packaging containers, durable goods and other items which made from petro based polymer such as glass fibers composite are difficult to recycle or decompose. Glass fibers are widely used in many applications especially in automotive interior part due to their low cost and good mechanical properties. Because composites are made using two dissimilar materials, they cannot be easily recycled or reused. Some countries are attempting to overcome this problem by incinerating the waste; however the quantum of waste which is incinerated is small and incineration is not without its problems. Current disposal methods for these materials are garbage dump or burning, but issues with overflowing landfill sites become another problem. Besides, two main environmental problems arise as a result of landfill which is toxic gasses emission release into atmosphere and ground water pollution. A possible solution to minimize the amount of waste going into landfill is by making a composite interior part using biodegradable materials, so that the automotive interior part can be recycle completely or disposed without environmental hazard.

The new composite material, fiber reinforced polymer (FRP) composite is introduce to overcome the matter by replacing it to some of plastic products nowadays. The low cost of this composite material as comparing to the other composite material available in market is the advantage in developing the new material.

Recent studies have investigated the development of biodegradable composite materials using natural fibres such as flax [3,4], bamboo [5], pineapple [6-7], jute [8] and kenaf [1] as a reinforcement for biodegradable plastics. These studies have examined molding conditions, mechanical properties, and interfacial bonding. Natural fibre based composite have increase the growth of new applications in market such as construction, transportation

including automotive, marine and aerospace. The advantages of natural fibre over traditional reinforcing material are: acceptable specific strength properties, low cost, low density, high toughness, good thermal properties, reduced tool wear, reduced dermal and respiratory irritation, ease of separation, enhance energy recovery, and biodegradability [9]. Natural fibre also gives cost advantages and benefits associated with processing, as compared to synthetic fibre such as glass, nylon, and carbon. On the other hand, natural fibre also can recycle, biodegradable and this will save energy use and good for environment.

Kenaf, an annual hibiscus fibre plant and filament lengths longer than 1 m are common. These filaments consist of discrete individual fibre, generally 2 to 6 mm long, which are themselves, composite of predominantly cellulose, lignin and hemicelluloses [10]. The kenaf has been found to be an important source of fibre for composite and other industrial applications. The kenaf bast fibre has high potential as reinforces fibre in thermoplastic composites because of its superior toughness and high aspect ratio in comparison with other fibre [11]. A single fibre of kenaf can have tensile strength and modulus as high as 11.9 GPa and 60.0 GPa respectively. These properties can vary depending on the source, age, and separating technique of the fibre [9].

Most of the studies relating to the kenaf fiber reinforced polymer composite investigated the mechanical properties [2,12-13,], and properties of kenaf plastic composites under various conditions such as investigation on influences of processing methods and fibre length on kenaf fibre-reinforced soy based biocomposites [14] and rheological behaviour of kenaf hybrid composite [15]. Few studies have been done to improve the mechanical properties of natural fibre composites.

Materials and Method

Kenaf powder and polypropylyne (PP) were obtained from Lembaga Tembakau Negara, Kelantan and Propylen (M) Sdn Bhd. Maleic anhydride grafted polypropylene (MAPP) was used as coupling agent.

Kenaf powder was mixed with PP with three different mixing ratios of 10 %, 20 % and 30 % of kenaf by weight. Kenaf powder was sieved by using powder was sieved by using *Fritsh Vibratory Sieve Shaker Machine* for 10 min with 15 amplitudes of vibration. MAPP was used as a coupling agent at 3 % of total composite weight to improve the compatibility and adhesion between the fibers and matrix. Kenaf powder, PP and MAPP were mixed by dispersion mixer where the only source of heat is generated through the kinetic energy of rotating blades. The compounded materials were then ground with a crusher to prepared granules and were hot pressed molded using 25 ton hydraulic hot press. The pressure is in the range of 150-400 psi and the temperature of 190 ºC. The pressing time is about 15 min. The specimen was allowed to cure in room temperature for the 20 min and was cut into different shape.

Tensile and flexural test were carried out according to BS EN ISO 527 and EN ISO 178 standards using Instron machine (*Instron 8500*) at a constant displacement rate of 2 $mm.min^{-1}$ to evaluate the tensile behavior and flexural properties of the materials. Observations were performed on fracture surface after tensile and flexural test using stereomicroscope and image analyzer to observe fracture surface characteristics.

Results and Discussion

The mechanical properties of tested samples are listed in Table 1. The measured tensile properties were tensile or elastic modulus and tensile strength, whereas the measured flexural properties were flexural modulus and flexural strength. Each value given in Table 1 is the result of six measurements.

Table 1: Result of mechanical tests on various PP-Kenaf composite blends

Material	Kenaf Powder (% w/w)	Tensile Strength (MPa)	Modulus (GPa)	Flexural Strength (MPa)	Modulus (GPa)
PP only	0	11.62	1.5	34.8	1.3
Kenaf-PP without MAPP	10	11.32	2.37	32.41	2.77
	20	12.83	2.40	25.02	1.81
	30	13.99	2.79	29.36	2.63
Kenaf-PP with 3% MAPP	10	16.46	2.27	26.56	1.37
	20	17.57	2.18	24.00	1.73
	30	19.65	2.58	41.62	3.45

The effects of MAPP on the tensile properties of composites

The results of the tensile tests are shown in Table 1 and Figure 1. It can be seen that the present reinforcement has significantly enhanced the tensile strength for both composite with and without MAPP. The increase of tensile stress with the additional of kenaf powder is in good agreement with any filled polymer composites including natural fiber filled polymer composite [16]. The increased is due to the restrained of polymer chains movement by the kenaf powder during load applications. Thus the stress transfer can be done efficiently between the kenaf powder and PP because there is good bonding between kenaf and PP molecular structure. Generally the increased in tensile modulus and strength with increasing of kenaf powder were in good agreement with a study on kenaf filled PP which found out the similar trends [9].

The variation of tensile strength with and without coupling agent with different percentage of kenaf composition was shown in Figure1. The strength of composite with MAPP is found to be increase with increasing fibre mass proportion and always higher than kenaf–PP composite without MAPP. The anhydride group present in the MAPP can covalently bond to the hydroxyl group of the surface. This will improve the interaction and adhesion between the kenaf powder and PP which leads to better stress transfer [16].

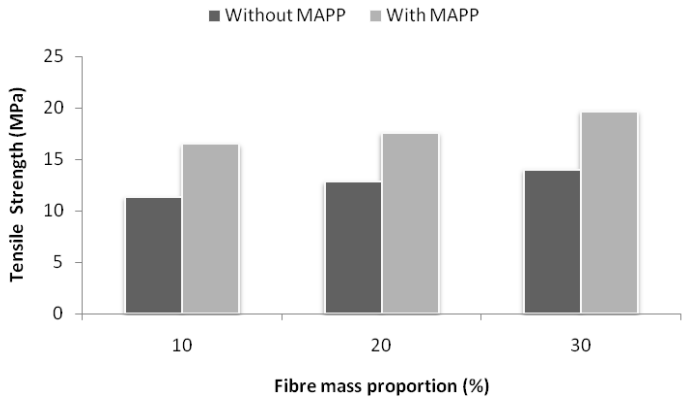

Figure 1: Tensile strength of the composites versus fibre mass proportion

The effects of MAPP on the flexural properties

The variation of flexural strength and modulus as a function of kenaf powder mass proportion are shown in Table 1 and Figure 2. The flexural strength seems has to decrease with the

increasing percent of kenaf powder. However it increases again with the increasing of 30% (w/w) kenaf. The inconsistent trend might be due to the poor dispersion of kenaf powder in PP [17]. However, it is observed that the 30% (w/w) kenaf with MAPP shows the best result with higher flexural strength and modulus.

Generally, the flexural modulus seems to follow the same trend as the tensile modulus with increasing of kenaf powder [3]. The addition of 30% (w/w) kenaf with MAPP had a dramatic effect on the higher flexural strength and modulus of kenaf/PP composite by approximately about 50 % of PP alone. Where the enhancement of composite stiffness is expected due to the higher modulus of the filler compared to its matrix. Besides that, the addition of coupling agent has dramatically enhanced the flexural properties. Again, the anhydride group present in the MAPP can covalently bond to the hydroxyl group of the surface. The improved interaction and adhesion between the kenaf powder and PP leads to better stress transfer.

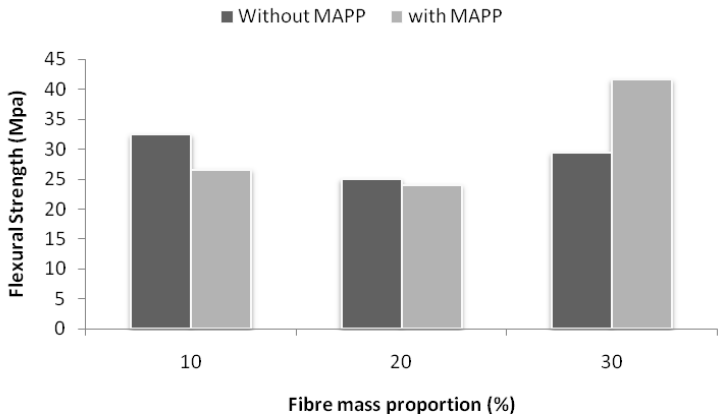

Figure 2: Flexural strength versus fiber mass proportion

Fracture Surface

The surface morphology of the specimens after tensile test was examined with optical microscope to observe the surface tensile fracture surface of kenaf/PP composite. Figure 3 shows the surface fracture for a composite without MAPP and Figure 4 shows for a composite with MAPP. From both figures, the defect such as holes and crack can be observed. This defect may reduce the tensile properties when the loading is applied. However, the additional of MAPP and kenaf powder will produce modification in the matrix surface by breakage of the fibers as shown in Figure 5 and Figure 6. The MAPP content gives an effective interaction between the kenaf fiber and PP/MAPP matrix. The fiber-related failure mechanisms operating in kenaf/PP defect in the fracture of the composite are the fracture mechanisms associated with poor bonding between kenaf powder and PP. There was fiber delamination which indicated by the white arrow while the black arrow represent the defect in the fracture area of the composite. This fracture mechanism is associated with poor bonding between kenaf powder and PP.

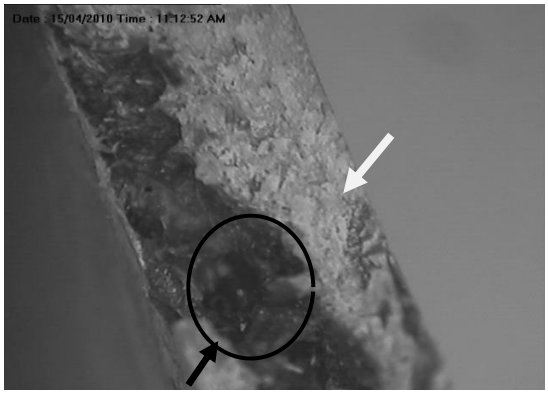

Figure 3: Surface fracture of kenaf/PP without MAPP

Figure 4: Surface fracture of kenaf/PP with MAPP

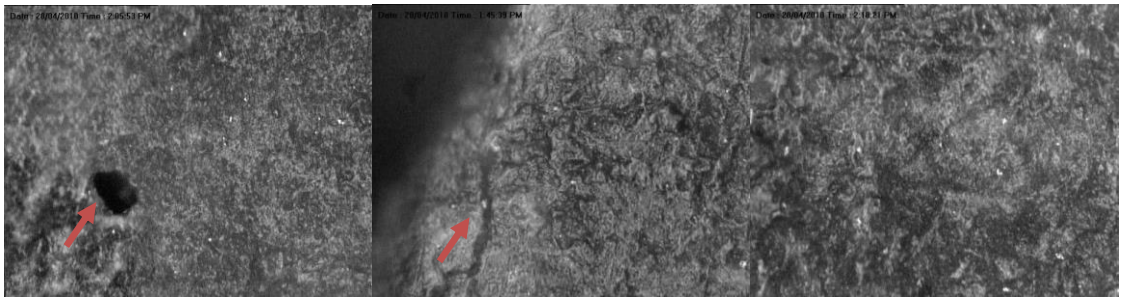

(a) (b) (c)

Figure 5: Fracture observation of different composite without MAPP: (a) 10% w/w kenaf; (b) 20% w/w kenaf and (c) 30% w/w kenaf

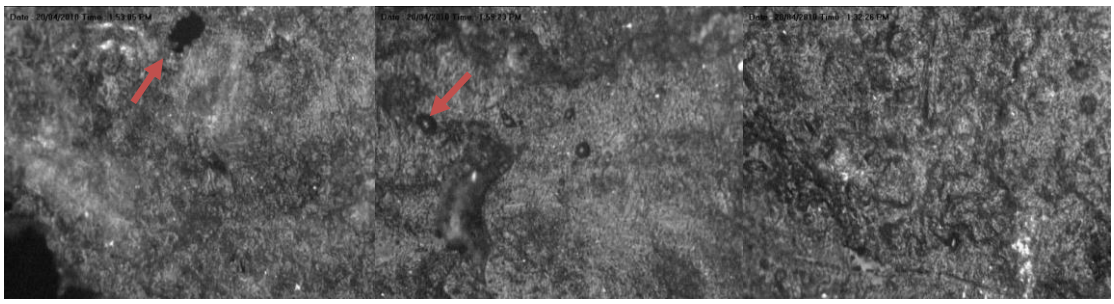

(a) (b) (c)

Figure 6: Fracture observation of different composite with MAPP (a) 10% (w/w) kenaf (b) 20% (w/w) kenaf (c) 30% (w/w) kenaf

Conclusion

The results presented in this work indicate that in term of mechanical properties, strength increased with the greater percent of kenaf powder. Composite with an additional of coupling agent exhibited higher mechanical properties than a composite without coupling agent. Fracture surface observation revealed that the failure mainly due to fiber delamination in addition to ductile failure of PP. It is shows that the mechanical properties of composites are highly depending on its internal structure.

Acknowledegment

The financial support from Excellence Fund award 600-RMI/ST/DANA 5/3/Dst (146/2011), “A study on the rheological behavior and mechanical properties of kenaf/PP composite”, is gratefully acknowledged.

References

[1] T. Nishimo, K. Hirao, M. Kotera, K. Nakamae & H. Inagaki. 2003. *Composite Science And Technology*. Volume 63, Issue 9: 1281-1286

[2] Shinji Ochi. 2008. *Mechanics of Materials*. Volume 40, Issues 4-5: 446-452

[3] T. Stuart, Q. Liu, M. Hughes, R.D. McCall, H.S.S. Sharma & A. Norton. 2006. *Composites part A Applied Science and Manufacturing*. 37**:** 393–404

[4] K. Oksman, M. Skrifvars & J.F. Selin. 2003. *Composites Science and technology*. 63: 1317-1324

[5] S.Lee & S.Wang. 2005. *Composites part A: Appl. Science and Manufacturing.* 37: 80-91

[6] W. Liu, M. Misra, P. Askeland, L. Drzal & A.K Mohanty. 2005. *Polymer.* 46: 710-721

[7] S. Luo & A.N. Netravali. 1999. *Journal of Materials Science.* 34: 3709-3719

[8] D. Plackett, T.L. Andersen, W.B. Pedersen & L. Nielsen. 2003. *Composites science and Technology. 63*: 1287-1296

[9] Rajeev Karnani, Mohan Krishnan & Ramani Narayan. 1997. P*olymer Engineering and science.* 37: no.2

[10] A.R Sanadi & D.E Caulfield. 2000. *Composite Interfaces.* vol.7, No. 1: 31-43

[11] Muhammad Pervaiz & Mohini M. Sain. 2003. *Resource, Conservation and Recycling* 39: 325-340

[12] H. Anuar, & A. Zuraida. 2010. *Composite Part B: Engineering*

[13] M. Bernard, A. Khalina, Aidy Ali, R. Janius, M. Faizal, K.S. Hasnah & A.B. Sanuddin. 2010. *Materials & Design*. Volume 32, Issue 2: 1039-1042

[14] W. Liu, L.T. Drzal, A.K. Mohanty & M. Misra. 2007. *Composites Part B*. 38: 352-359

[15] Ismaeil Ghasemi, Hamed Azizi & Navid Naeimian**.** 2008. *Iranian Polymer Journal*. 17 (3): 191-198

[16] Roger M. Rowell, Anand R, Sanadi, Daniel F. Caulfield & Rodney E. Jacobson. “Utilization of Natural Fibers in Plastic Composites: Problems and Opportunities”, University of Wisconsin

[17] Kalam, A., Berhan, M.N & Ismail, H. 2009. *Journal of Mechanical Engineering:An International Journal.* vol 6 No.2: 27-40

DIELECTRIC BEHAVIOUR SUDIES OF PROTON CONDUCTING POLY (VINYL) CHLORIDE (PVC) BASED GEL POLYMER ELECTROLYTES

Siti Khatijah Deraman[1], N.S. Mohamed[2] & R.H.Y. Subban[1]

[1] Faculty of Applied Sciences, Universiti Teknologi MARA,Selangor,

[2] Centre for Foundation Studies in Science, University of Malaya, Kuala Lumpur, Malaysia

Abstract

Poly(vinyl) chloride (PVC)-NH_4I-EC films have been prepared by solution cast technique. The sample containing 30% (w/w) NH_4I exhibited highest room temperature conductivity of 4.60×10^{-7} S.cm^{-1}. The conductivity increased to 1.08×10^{-6} S.cm^{-1} when 15% w/w of ethylene carbonate (EC) was added to 70% (w/w) PVC – 30% (w/w) NH_4I. Fourier Transform Infrared (FTIR) spectroscopy showed evidence of polymer–salt complexation while DSC showed decrease in glass transition temperature (T_g) of PVC -NH_4I - EC polymer electrolytes. The conductivity behavior of the studied system could be accounted by the changes in T_g values. The effects of ethylene carbonate (EC) on the frequency dependent dielectric properties of PVC based electrolytes were also investigated by electrochemical impedance spectroscopy (EIS) at room temperature. Analysis of the ac conductivity data revealed the electrolytes to be of the non-Debye type.

Keywords: *Dielectric properties, gel polymer electrolyte, non-Debye type, proton conductivity*

Introduction

A proton conductor is an electrolyte, typically a solid electrolyte, in which movable ions like H^+, H_3O^+ or NH_4^+ are the primary charge carriers. Proton conductors are interesting materials due to their potential application as solid electrolytes in ionic devices such as fuel cells, batteries, electrochromic glasses, etc. [1,2]. A few groups of researchers have studied proton conducting electrolytes using strong inorganic acids such as H_3PO_4, H_2SO_4 and HCl as the doping salts [3,4]. However proton conducting polymer electrolytes containing inorganic acids suffer from chemical degradation and have poor mechanical integrity and thus are unsuitable for practical applications [5]. Other than complexation with inorganic acids, proton conducting polymer electrolytes can also be prepared by complexation with ammonium salts which are considered as good proton donors to polymer matrices [6,7]. In such systems, the charge carriers may come from ammonium ions and H^+ ion. The conduction of H^+ ions occur via the Grotthus mechanism, where conduction occurs through exchange of ions between complexed sites [8,9]. PVC has been studied as a host polymer for the development of lithium ion conducting electrolytes [10,11,12,13]. However, no studies employing this host polymer for proton conducting electrolytes have been done. Therefore, in this work, PVC based proton conducting polymer electrolytes were prepared employing NH_4I as the doping salt. The samples were characterized by electrochemical impedance spectroscopy (EIS), Fourier Transform Infrared (FTIR), Different Scanning Calorimetry (DSC) and the dielectric properties of the electrolytes are presented and discussed.

Materials and Method

PVC and NH_4I of required mass were dissolved separately in tetrahydrofuran (THF) after which they were mixed and stirred for several hours at room temperature. Appropriate amounts of EC were added to form solutions which were later cast into petri dishes, and left to dry by evaporation at room temperature to form films. The films were further dried in a vacuum oven at 40 °C for 24 h. PVC and NH_4I weight ratios was maintained at 70:30 since this weight formed the highest conducting polymer-salt film while the amount of EC dispersed was

expressed as a weight percent (% w/w) with respect to the total weight present in the system. Complex impedance measurements were carried out using *HIOKI 3532-50 LCR Hi Tester*. FTIR were taken using *Perkin-Elmer FTIR Spectrometer* in the wave region from 400 cm^{-1} to 4000 cm^{-1} with a resolution of 4 cm^{-1}. Differential scanning calorimetry (DSC) was carried out using *TA DSC Q200* under nitrogen flow at a heating rate of 10°C.min^{-1} up to 100 °C.

Results and discussion

Conductivity studies

Figure 1 depicts the room temperature conductivity as a function of weight percent of NH_4I for the salted polymer electrolytes. It is apparent from the figure that the conductivity increased rapidly from 10×10^{-10} S.cm^{-1} for pure PVC system to 4.60×10^{-7} S.cm^{-1} for PVC - NH_4I system when 30% (w/w) of NH_4I was added and decreased slowly with further increase in NH_4I content. This system is then chosen to be added with EC. Figure 2 shows the variation of room temperature conductivity with weight percent EC for the plasticized proton conducting electrolytes. In the case of plasticized electrolytes, the conductivity increased to a maximum of 1.08×10^{-6} S.cm^{-1} when 15% (w/w) of EC was added to 85% (w/w) (PVC - NH_4I). This means that the conductivity increased by one order of magnitude when EC is added to PVC - NH_4I system. At higher plasticizer concentration a decrease in conductivity is observed. These results are in agreement with those described in the literature [14, 15, and 16]. According to these reports, the initial increase in conductivity is attributed to increase in the number of mobile ions upon addition of plasticizer. The plasticizer acts as an agent to cause more salt to be dissociated. The amount of ions increases and so does the conductivity. Beyond 15EC, addition of more plasticizer caused aggregation of ions which impedes the movement of mobile ions consequently reducing conductivity [14].

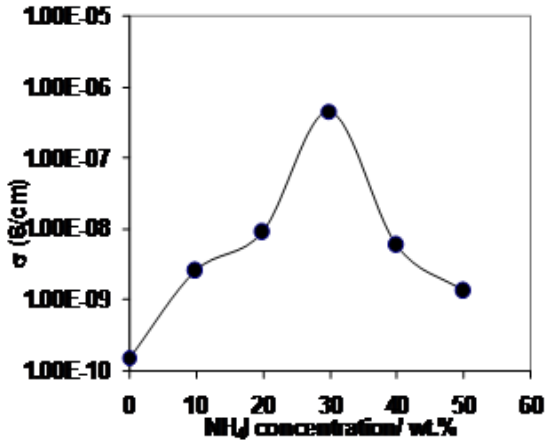

Figure 1: Variation of room temperature conductivity with weight percent NH_4I

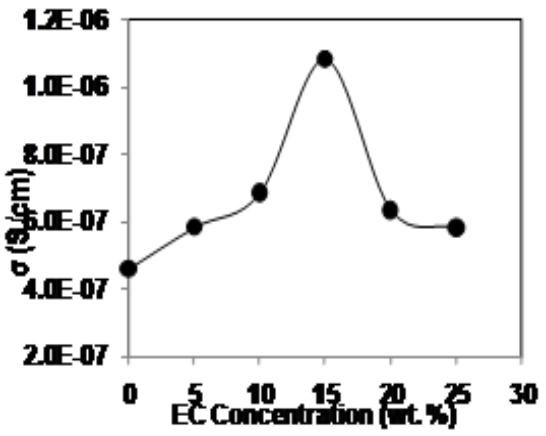

Figure 2: Variation of room temperature conductivity with weight percent EC

Fourier Transformation Infrared studies

FTIR spectra of pure PVC, pure NH_4I, pure EC, 70% (w/w), PVC–30% (w/w) NH4I and 85% (w/w) (PVC- NH_4I) – 15% (w/w) EC are shown in Figure 3. Pure PVC exhibits vibrational bands at 615 cm^{-1}, 634 cm^{-1},703 cm^{-1}, 968 cm^{-1}, 1103 cm^{-1}, 1264 cm^{-1}, 1342 cm^{-1}, 1437 cm^{-1} which are attributed to cis-CH wagging, C-Cl stretching, C-Cl stretching, CH_2 rocking , C-C stretching,C-H deformation of CHCI, C-H deformation of CHCI and CH_2 (wagging) deformation respectively [17]. Pure NH_4I shows vibrational bands at 1358 cm^{-1} due to N-H bending and 3054 cm^{-1} due to N-H stretching [18]. EC shows vibrational bands at 711 cm^{-1}, 763 cm^{-1}, 888

cm^{-1}, 1050 cm^{-1}, 1226 cm^{-1}, 1386 cm^{-1} , 1417 cm^{-1} and 1484 cm^{-1} , which are ascribed to C=O bending, CH_2 in phase rocking, skeletal breathing, skeletal symmetric stretching, CH_2 out of phase twisting, CH_2 out of phase wagging, CH_2 wagging and CH_2 bending respectively [19]. C-Cl stretching of PVC is shifted from 634 cm^{-1} to 639 cm^{-1} with decreased intensity upon addition of NH_4I indicating interaction between Cl group of PVC with NH_4I probably through interaction between Cl^- and H^+ ions. In the case of the plasticized samples, the C-Cl stretching band has further shifted to 643 cm^{-1} upon addition of EC to PVC-NH_4I indicating that there is interaction between them (Figure 3a). N-H bending is shifted from 1358 cm^{-1} to 1370 cm^{-1} with decreased intensity upon addition of NH_4I to PVC and 1418 cm^{-1} upon addition of EC to PVC-NH_4I (Figure 3b) giving further evidence of interaction between NH_4I, PVC and EC probably through the interaction between Cl^- ion of PVC and H^+ of NH_4I . It is also observed that the C=O band at 711 cm^{-1} and CH_2 in phase rocking at 768 cm^{-1} of EC seem to have broadened with decreased intensity in PVC-NH_4I- EC system (Figure 3a). The broadening of the C=O band in the plasticized polymer-salt complexes indicates that the plasticizer just interacts physically with the polymer and salt [20].

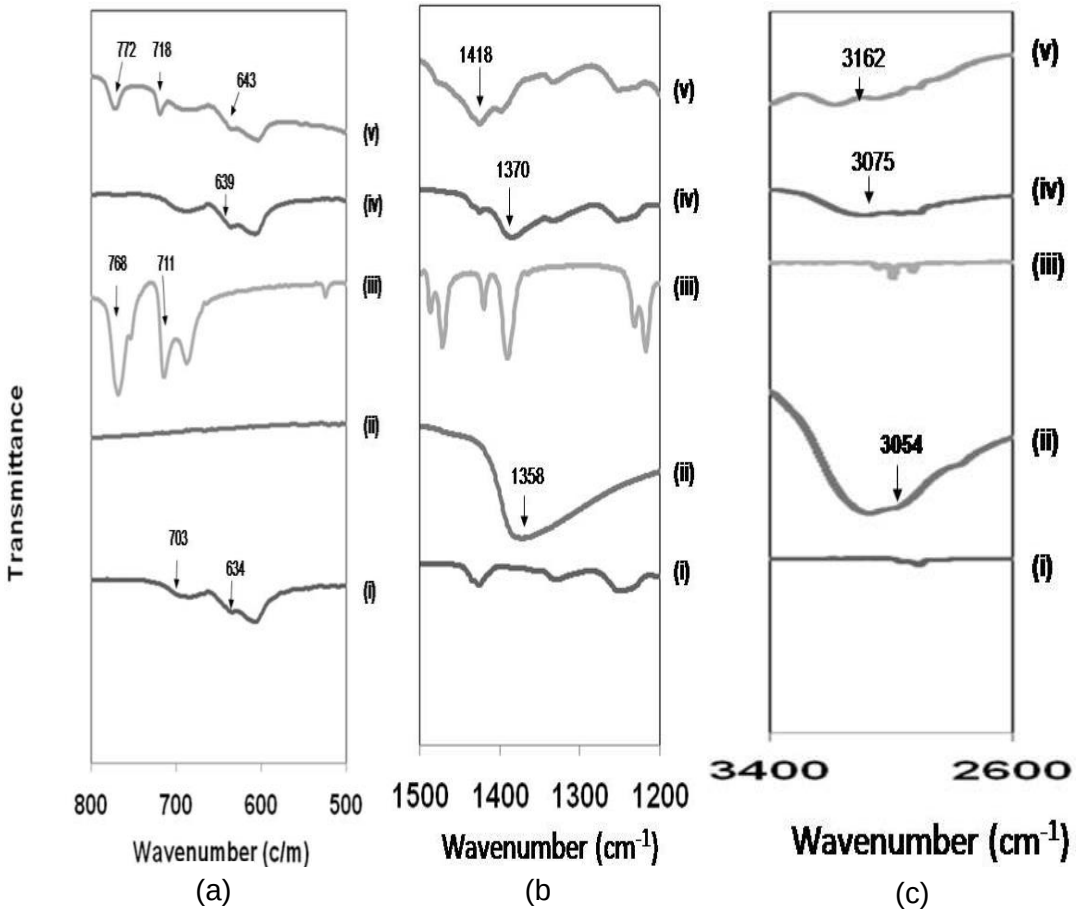

Figure 3: FTIR spectra of (i) Pure PVC, (ii) Pure NH_4I (iii) Pure EC, (iv) 70% (w/w) PVC-30% (w/w) NH4I, (v) 85% (w/w) (PVC- NH_4I) -15% (w/w) EC at different wavenumbers

Not much change is observed in the bands of EC indicating that EC has weak interaction with either NH_4I or PVC. This means that the plasticizer is mixed into the system without much interaction making the system a mixed phase electrolyte system. Apart from that, it is also observed that N-H stretching of NH_4I at 3054 cm^{-1}, is shifted with reduced intensity to 3075 cm^{-1} and 3162 cm^{-1} in the salted and plasticized system respectively (Figure 3c). This provides

further evidence for the presence of weak salt-plasticizer and polymer-plasticizer interactions. In other words the plasticizer just acts like a lubricant [21] to provide aid in conduction of ions.

Thermal studies

Figure 4 presents the DSC thermograms of unplasticized and plasticized systems from which the T_g values obtained are 56 °C and 50 °C respectively, while the T_g of pure PVC is 52 °C (DSC thermogram not shown). This means that T_g is increased when NH_4I is added to PVC, and when EC is added to PVC-NH_4I, the T_g subsequently decreased. The increase in T_g in PVC-NH_4I complex is due to the formation of cross-links between the cation of the salt with surrounding chain segments. The increase in T_g with addition of salt to polymer has also been observed by other researchers [22]. In their work, the conductivity was also observed to increase with increase in T_g. These authors attributed the increase in conductivity to an increase in number and migration rate of ions. Meanwhile, the decrease in T_g with addition of plasticizer is due to the lubricating effect of the plasticizer [23]. This means that the plasticizer not only caused more salt to dissociate giving rise to more ions but also increases the flexibility of the polymer chain which aids in ion conduction through the electrolyte. Similar decrease in T_g for plasticizer added salted-polymer systems have also been reported elsewhere [24, 25].

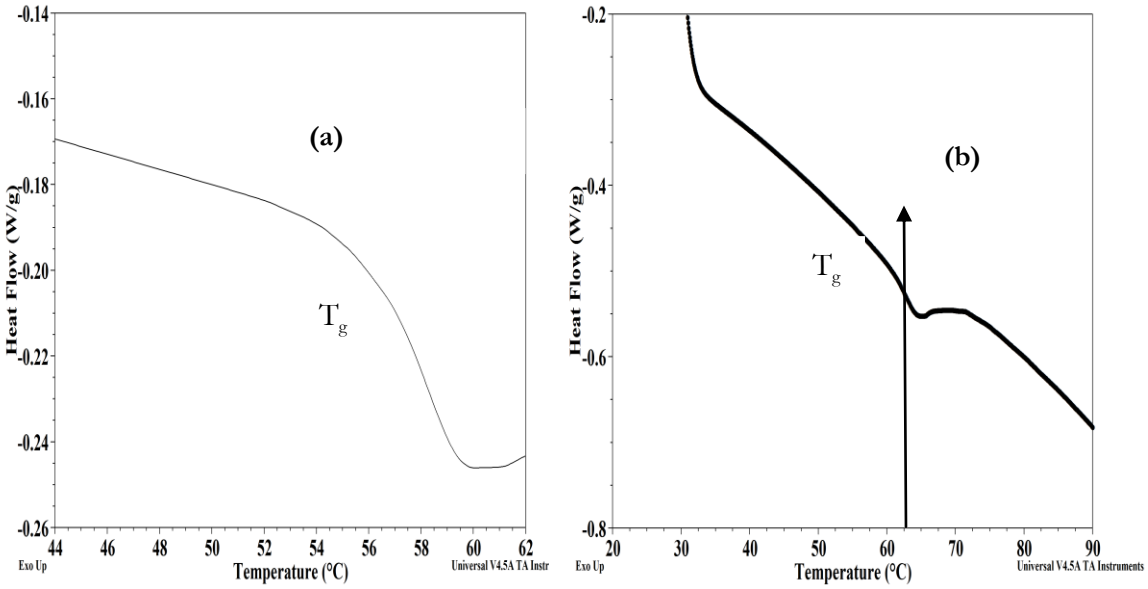

Figure 4. DSC thermogram of the (a) 70% (w/w) PVC-30% (w/w) NH_4I, (b) 85% (w/w) (PVC- NH_4I)-15% (w/w) EC polymer electrolytes

Dielectric properties

Dielectric relaxation studies are a vital tool to show the relaxation of dipoles in polymer electrolyte. The imaginary part (ε_i) and real part (ε_r) of dielectric permittivity curves for unplasticized and plasticized samples are shown in Figure 5 and 6 respectively. The observed variation in ε_r with frequency could be attributed to the formation of a space charge region at the electrode and electrolyte interface. This behaviour is known as the non-Debye type of behavior, where diffusion of ions occur in the space charge regions with respect to frequency [27]. The low frequency dispersion region corresponds to the contribution of charge accumulation at the electrode–electrolyte interface. The highest value of ε_r for 15% (w/w) EC is due to the enhanced charge carrier density at the space charge accumulation region, which causes equivalent capacitance to be enhanced [26]. The plot demonstrates that the dielectric

constant is high at low frequencies, and gradually decreases slowly and approaches zero at high frequency. At high frequencies, the periodic reversal of the electric fields occurs so fast that there is no excess ion diffusion in the direction of the field. The polarization due to the charge accumulation decreases, which caused the decrease in the value of ε_r [28].

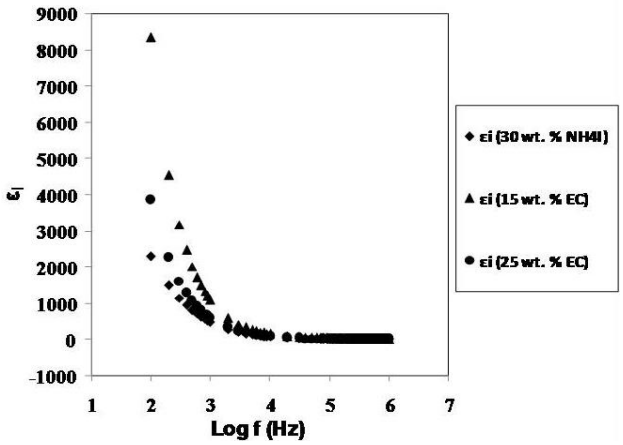

Figure 5: Variation of the imaginary part of dieletric constant with frequency for selected unplasticized and plasticized samples at 303 K

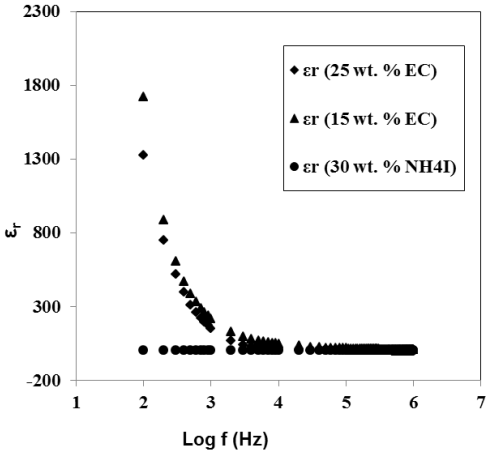

Figure 6: Variation of the real part of dieletric constant with frequency for selected unplasticized and plasticized

Modulus studies

The dielectric modulus can be understood by relying on the formulation of a dielectric modulus, which has been used to understand the conductivity relaxation. Figure 7 and 8 shows the frequency variation of the imaginary (M_i) and real (M_r) part of modulus formalism respectively. It shows that M_i and M_r increase towards high frequencies and give a long tail at low frequencies. The peaks in the modulus formalism at high frequencies show that the polymer electrolyte films are ionic conductors. The reason for the peak curving at higher frequencies is attributed to bulk effects [29]. It is observed from the plots that M_i and M_r decrease towards low frequencies. This is due to the electrode polarization phenomenon which makes a negligible contribution. The plots also show long tails at low frequencies and these are probably due to their large capacitance values of the electrodes. The modulus spectral formalism has facilitated the process of identification and separation of electrode effects from the bulk relaxation phenomena occurring within the plasticized polymer electrolyte system with higher content of EC [29].

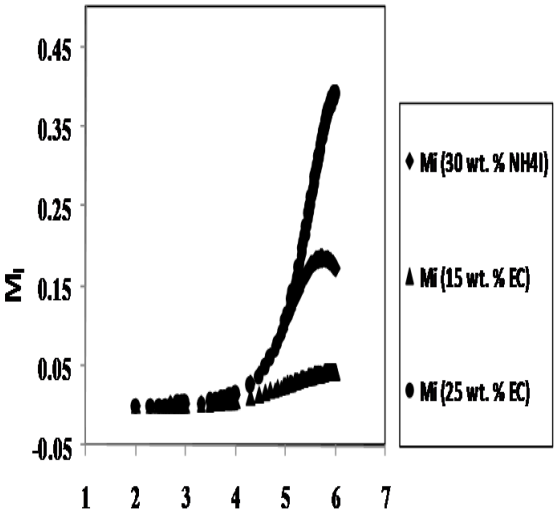

Figure 7: Variation of the imaginary part of modulus with frequency for selected unplasticized and plasticized samples at 303 K.

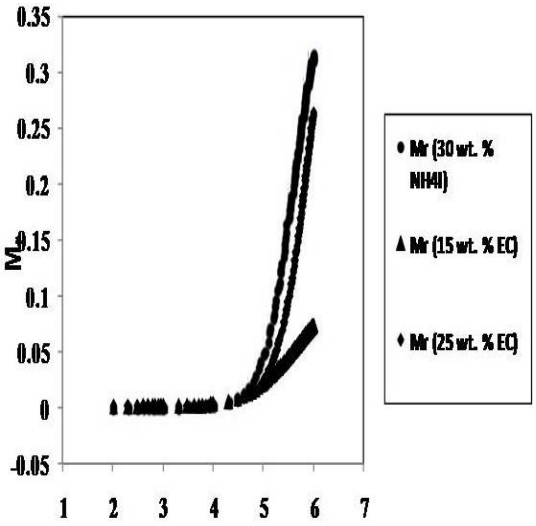

Figure 8: Variation of the real part of modulus with frequency for selected unplasticized and plasticized samples at 303 K.

Conclusion

The addition of plasticizer (EC) to PVC-NH_4I polymer electrolytes increased the ionic conductivity. The increase in ionic conductivity may be due to the presence of a large number of ions and increase in their rate of migration. The decrease in conductivity beyond the optimised concentration could be attributed to lower mobility of ions due to the presence of a higher concentration of ions that impedes the movement of ions. Complex formation in PVC-NH_4I-EC has been confirmed from FTIR studies. T_g was observed to decrease with addition of plasticizer to salted-polymer system. Analysis of the ac conductivity data revealed the electrolytes to be of the non-Debye type.

Acknowledgement

The authors would like to thank the staffs of Ionics, Color and Coating (ICC) Laboratory, Institute of Science (IOS) and Faculty of Applied Sciences, University Technology MARA (UiTM) for the sponsorship awarded.

References

[1] K.D. Kreuer. 1996. *Chem. Mater.* 8:610

[2] A.J. Appleby, in: D. Doughty, B. Vyas, T. Takamura, & J.R. Huff (Eds.). 1995.*Material for Electrochemical Energy Storage and Conversion-Batteries, Capacitors and Fuel Cells*, Vol.393. *Material Research Society*, Pittsburgh, Pennsylvania. *11*

[3] A. Bozkurt & W. H. Meyer. 2001. *Solid State Ionic.* 138: 259-265

[4] J. C. Lassegues, J. Grondin, M. Hernadez & B. Maree. 2001. *Solid State Ionic*. 145**:** 37-45

[5] M. Hema, S. Selvasekerapandian, A. Sakunthala, D. Arunkumar & H. Nithya. 2008. *Physica B*. 403**:** 2740-2747

[6] A. M. M. Ali, N. S. Mohamed & A. K. Arof. 1998. *Journal of Power Sources*. 74**:** 135-141

[7] C. S.Ramya, S. Selvasekarapandian, T. Savitha, G. Hirankumar & P. C. Angelo. 2007. *Physica B.* 393**:** 11-17

[8] S. A. Hashmi, Ajay Kumar, K. K. Maurya & S. Chandra*. 1990. J. Phys D; Appl. Phys. 23:* 1307-1314

[9] M.F.Z. Kadir, S.R. Majid, A.K. Arof. 2009. *Electrochimica Acta, In Press*.

[10] R.H.Y. Subban, A.K. Arof. 2004. *European Polymer Journal.* 40: 1841-1847

[11] S.Rajendran & T. Uma. 2001. *Ionics. 7*: *122-125*

[12] S. Rajendran, Ravi Shanker Babu & P.Sivakumar. 2008. *Journal of Membranes Science 315*: *67-73*

[13] A. Mary Sukeshini, Atsushi Nishimoto & Masayoshi Watanabe.1996. *Solid State Ionics 86-88*: *385-383*

[14] M.H. Buraidah, L.P.Teo, S.R.Majid & A.K. Arof. 2009. *Physica B.* 404: 1373-1379

[15] R.H.Y. Subban. 2003. *J. New. Mat. Electrochem. System.* 6: 197-203

[16] B.Choi & K. Shin.1996. *Solid State Ionics.* 86: 303

[17] M. Beltran & A. Marcilla. 1997. *European Polymer Journal.* 33(8): 1271-1280

[18] W.O.George & P.S. Mcintyre, edited by David J. Mowthorpe. 1990. *Infrared Spectroscopy*

[19] *Chintapalli* S. & *French* R. *1996*. *Solid State Ionic.* 86–88: 341–346

[20] S. Ramesh & G.P. Ang. 2010. *Ionics.* 16: 465-473

[21] J. Liu, J. Portier, B. Tanguy, J.J. Videau & C.A. Angell. 1989. *Solid State Ionics.* 34: *87–92*

[22] S.F Mohamad, Razali Idris & N.S. Mohamed. *Advanced Material Research.* Vol (129-131) 561-565.

[23] E. Morales & J.L Acosta. 1997. *Solid State Ionics.* 96: 99-106

[24] Ghiya, V.P., Dave, V., Gross, R.A. & McCarthy, S.P. 1996. *J. Macromol. Sci. A*. 33: 627–638

[25] Zainal, N., Idris, R., & Mohamed, N. S. 2011. *Advanced Materials Research*. 287-290, 424–427.

[26] S. Ramesh & Ong Poh Ling. *2010. Polym. Chem.* 1: 702–707

[27] R. Baskaran, S. Selvasekarapandian, N. Kuwata, J. Kawamura & T. Hattori. 2006. *Mater.Chem.Phys.* 98: 55–61

[28] S. Ramesh & M. F. Chai. 200. *Mater. Sci. Eng. B.*139: 240–245

[29] S. Austin Suthanthiraraj, D. Joice Sheeba & B. Joseph Paul*. 2009. Mater. Res. Bull.* 44:1534–1539

IONIC CONDUCTIVITY AND TRANSFERENCE NUMBER STUDIES OF PVDF-HFP/PMMA-(EC+PC) GEL POLYMER ELETROLYTES CONTAINING LITHIUM SALT

K. B. Md Isa, L. Othman, M. Mansor & Z. Osman
Department of Physics, University of Malaya, Kuala Lumpur, Malaysia.

Abstract

Blend gel polymer electrolytes composed of poly(vinylidene fluoride co-hexafluoropropylene) (PVDF-HFP) and poly(methylmethacrylate) (PMMA) as polymers, the mixture of EC+PC as plasticizers and lithium percholorate, $LiClO_4$ as dopant salt have been prepared by the solution casting technique with varying salt concentrations. The ionic conductivity of the samples has been determined by a.c impedance spectroscopy. The highest conductivity was obtained from the sample containing 25% (wt/wt) of $LiClO_4$ salt, i.e. 4.71×10^{3} $S\cdot cm^{-1}$. The increase in the conductivity with increasing salt concentration is due to the increase in the number of mobile charge carriers. The conductivity-temperature dependence obeys the VTF rule. The pseudo-activation energy can evaluated from the plot of log $\sigma T^{1/2}$ versus $1000\cdot(T-T_o)^{-1}$. The ionic transference number estimated from dc polarization method revealed that the conducting species in the blend gel polymer electrolyte samples are ions.

Keywords: *Gel polymer electrolytes, ionic conductivity, lithium percholorate, poly(methylmethacrylate), poly(vinylidene fluoride co-hexafluoropropylene), transference number.*

Introduction

Various research works in the field of material sciences have been committed to the development of gel polymer electrolytes. This type of electrolytes has several advantages such as high energy density, structural stability and low volatility. To date, many attempt have been done to improve its ionic conductivity, one of them is blending of two polymers. Major advantage of the blend gel polymer electrolytes is ease of sample preparation [1]. Blend gel polymer electrolytes system exhibit better mechanical strength and higher room temperature ionic conductivity compare with unblended polymer electrolytes system.

The most commonly polymer used in polymer electrolyte systems is poly(methyl methacrylate) (PMMA). Appetecchi et al. [2] reported that the strong effects of PMMA on the interface between the electrodes. Two decade ago, Iijima et al. [3] were investigated the use of PMMA as a polymer matrices in the plasticized-polymer electrolytes. Then, Bohnke [4] reported the studies electrodes in gel electrolytes based on PMMA. In order to enhance the performance of PMMA based gel electrolytes, one of the approaches is blend the PMMA with another polymer since this technique seems to give combination advantages of ease in control of various factors which affect the electrical, mechanical and thermal properties of the polymer electrolytes. Poly(vinylidene fluoride-hexafluoropropylene), PVDF-HFP, copolymer is well-known for having good mechanical stability and easy film formation. Therefore, this material becomes a good candidate to blend with PMMA. Recently, Saikia and Kumar [5] reported gel polymer electrolyte using PVDF-HFP/PMMA blend polymer and the conductivity achieved is 4.5×10^{-4} $S\cdot cm^{-1}$.

In the present study, the investigation of ionic transport in PVDF-HFP/PMMA + (EC+PC) + $LiClO_4$ gel polymer electrolytes will be reported. The inorganic salt, $LiClO_4$ is used as dopant salt because it shows smaller dissociation energy [6]. Ethylene carbonate (EC) and propylene carbonate (PC) are used as plasticizing solvents. Ionic conductivities and the transference number of the gel polymer electrolyte will be measured by a.c impedance spectroscopy and dc polarization method, respectively.

Materials and Method

Preparation of the blend gel polymer electrolyte films

PVDF-HFP (Aldrich, m.w. ~400000 g·mol^{-1}) and PMMA (Aldrich, m.w. ~996000 g·mol^{-1}) were dissolved in a solvent of acetone and THF solvents. After complete dissolution, the lithium perchlorate salt $LiClO_4$ and the plasticizers EC + PC with mass ratio of 2:1 were added to the mixed polymer solution. The solution was stirred and heated continuously for several hours until the homogenous solution was obtained. The blend gel polymer electrolyte films were prepared by varying the salt from 5% (wt/wt) to 30% (wt/wt). Then, the solutions of different salt concentrations were cast on to glass petri dishes and allowed to evaporate at room temperature until the gel films were obtained.

Impedance Spectroscopy

The complex impedance of gel polymer electrolytes were measured from 50 Hz to 1 MHz using a computer – interfaced HIOKI 3532 LCR. The resistance, R_b (Ω) of each sample was determined from the Cole-Cole plot and the values of conductivity can be calculated using:

$$\sigma = \frac{\mathrm{t}}{\mathrm{R_b A}} \tag{1}$$

where *t* is a thickness of the sample in cm and *A* is the effective contact area of the electrode in cm^2. The conductivity - temperature dependence study of the highest room temperature conducting sample was carried out in the temperature range from 303 K to 393 K.

Transference Number

The transference numbers of the gel polymer electrolyte films was measured by direct current (dc) polarization method. In this method, the fixed voltage (~1.0 V) was applied to the sample that sandwiched between two blocking electrodes and the current was monitored as a function of time. The electronic transference number (t_e) and ionic transference number (t_i) can be evaluated from the following equation;

$$t_e = \frac{\sigma_e}{\sigma_T} = \frac{i_e}{i_T} \tag{2}$$

and

$$t_i = 1 - \frac{i_e}{i_T} = 1 - t_e \tag{3}$$

Where i_e and i_T are the electronic and total current, and σ_e and σ_T is refer to electronic and total conductivity, respectively.

Results and Discussion

Ionic conductivity measurement

Figure 1 shows the variation of conductivity of PVDF-HFP + PMMA + EC + PC films with different amounts of $LiClO_4$ in the weight percentage. For the blend gel polymer electrolyte film without salt, the value of conductivity is 3.31×10^{-8} S·cm^{-1}. On the addition of salt, the conductivity value increases to ~10^{-3} S·cm^{-1} and continuously increases until 25% (wt/wt) of $LiClO_4$ is added and the conductivity decrease with further addition of salt. The maximum conductivity achieved is 4.71×10^{-3} S·cm^{-1}. As the salt content increase, the number of free ions also increases thus increases the conductivity value. At higher salt concentrations, the decrease in conductivity value can be explained by aggregation of ions, leading to the formation of ion cluster, thus decreasing the number of mobile ions [7].

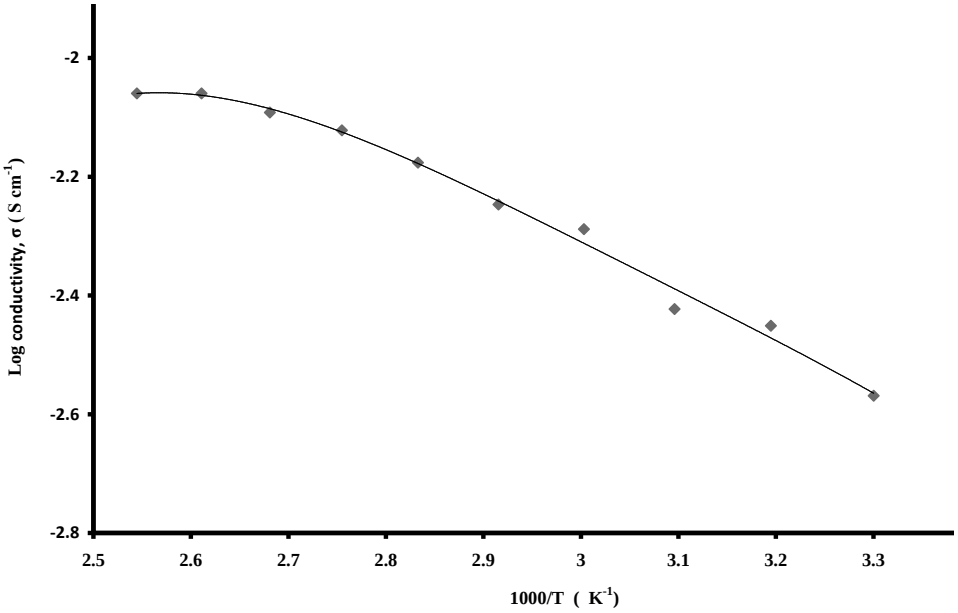

Figure 1: Variation of ionic conductivity with $LiClO_4$ salt in blend of gel polymer electrolytes.

Figure 2 shows the temperature variation of the conductivity for the highest room temperature conducting blend gel polymer electrolytes sample. It can be observed that as temperature increases the conductivity also increases.

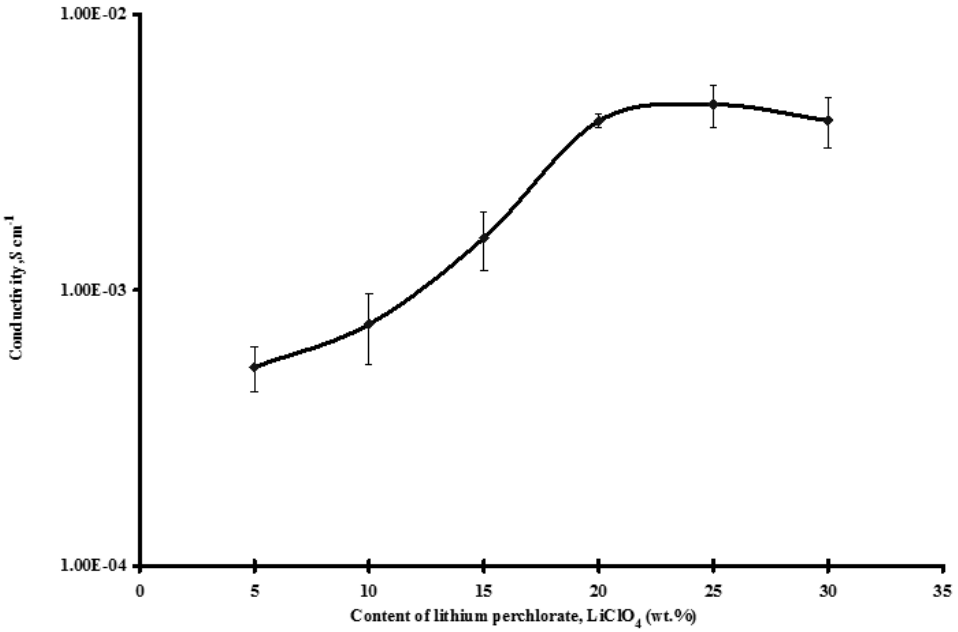

Figure 2: Log σ versus 1000/T plot for the highest conductivity sample of (PVDF-HFP + PMMA) blend gel polymer electrolyte containing $LiClO_4$ salt

The non-linearity in this plot implies that ion transport in the gel polymer electrolytes is dependent on polymer segmental motion. This result can be explained by the concept of free volume [8,9]. In order to obtain a better insight into the conductivity-temperature dependence the data have been fitted to the Vogel-Tamman-Fulcher (VTF) equation [10,11].

$$\sigma = AT^{-\frac{1}{2}} e^{\frac{B}{k(T-T_o)}} \quad (4)$$

where *A* is a fitting constant proportional to the number of charge carriers, *B* is the pseudo – activation energy associated with the motion of the polymer segment, *k* is the Boltzmann constant and T_o is the equilibrium temperature of the system corresponding to zero configuration entropy. $T_o=T_g-T$, where T_g is the glass transition temperature. In order to extract the parameters *A* and *B*, the value of the glass transition temperature, T_g of the sample has been measured using Differential Scanning Calorimetry (DSC) and is found to be -20 ^oC. In this work, T_o is equal to T_g -50 K. Linear plot can be obtained by plotting log $\sigma T^{1/2}$ versus $1000\cdot(T-T_o)^{-1}$ as shown in Figure 3. The calculated value of *A* and *B* is 0.841 $S\cdot cm^{-1}$ $K^{1/2}$ and 0.025 eV,, respectively. This result is similar that reported by Karan *et al.* [9].

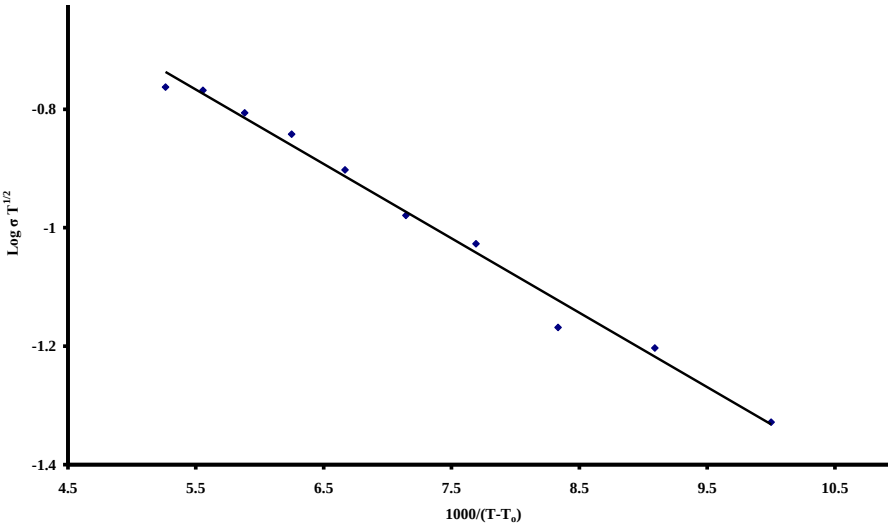

Figure 3: Log $\sigma T^{1/2}$ against $1000\cdot(T-T_o)^{-1}$ plot for the highest conducting sample of blend gel polymer electrolyte containing $LiClO_4$ salt.

Transference number measurements

The electronic and ionic transference numbers of the gel polymer electrolyte samples containing 5% (wt/wt), 25% (wt/wt), and 30% (wt/wt) have been evaluated from the plot of normalized polarization current versus time by using (2) and (3) respectively as shown in Figure 4. It can be observed that value of ionic transference number is 0.57, 0.71 and 0.70 for sample containing 5% (wt/wt), 25% (wt/wt), and 30% (wt/wt), respectively. These results indicate that the conductivity of blend gel polymer electrolyte is due to ionic carriers and the values obtained are consistent with conductivity results where the highest conducting gel polymer electrolyte film shows the highest t_i value.

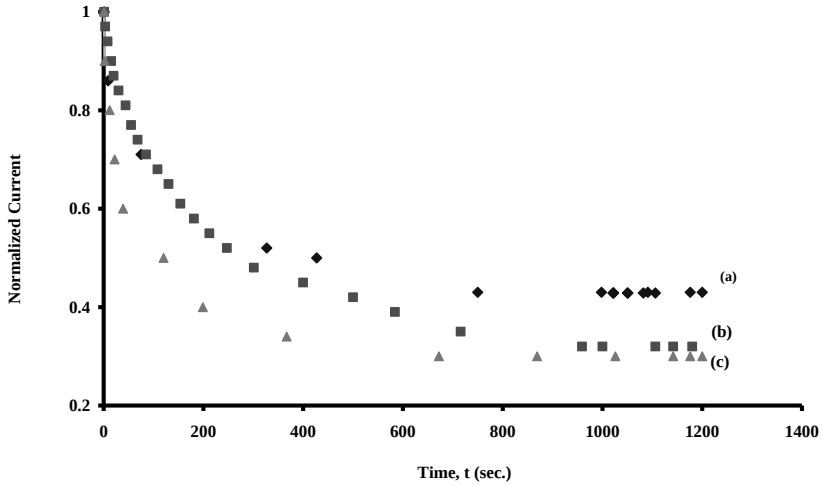

Figure 4: Normalized current versus times plots for the samples that containing (a) 5% (wt/wt), (b) 25% (wt/wt) and (c) 30% (wt/wt) of $LiClO_4$ salt

Conclusion

The blend gel polymer electrolytes of PVDF-HFP + PMMA containing various concentrations of $LiClO_4$ have been prepared and studied. The maximum ionic conductivity for this gel polymer electrolyte system at room temperature is found to be 4.71 x 10^{-3} $S{\cdot}cm^{-1}$ and was obtained from the sample containing 25% (wt/wt) of $LiClO_4$. High ionic conductivity could be attributed to the increase of mobile charge carriers. The temperature dependence of ionic conductivity of the highest conductivity film exhibited VTF behavior. The pseudo-activation energy and number of charge carriers is found to be 0.025 eV and 0.841 $S{\cdot}cm^{-1}$ $K^{1/2}$, respectively. The transference number measurements revealed the charge transport in the blended gel polymer electrolytes are mainly due to ions. This result is consistent with the conductivity values.

Acknowledgement

The authors would like to thank the University of Malaya for the grants awarded.

References

[1] Rocco, A.M., Pereira, R.P., Felisberti, M. I., 2001. Polymer 42: 5199-5205

[2] Appetecchi, G.B., Croce, F., Scrosati, B., 1995. *Electrochimica Acta* 40: 991-997

[3] Iijima, T., Toyoguchi, Y., Eda, N., 1985. *Denki Kogaku* 53: 619

[4] Bohnke, O., Frand, G., Rezrazi, M., Rousselot, C., Truche, C. 1993. *Solid State Ionics* 66:97

[5] Saikia, D., Kumar, A., 2005. *Europian Polymer Journal* 41: 563-568

[6] Tsuchida E., Ohno H., Tsunemi K., 1983. *Electrochimica Acta* 28:591-595

[7] Ramya, C. S., Selvasekarapandian, S., Savitha, T., Hirankumar, G., 2007. *Physica B* 393:2672-2677

[8] Baskaran, R., Selvasekarapandian, S., Kuwata, N., Kawamura, J., Hattori, T. 2006. *Materials Chemistry and Physics* 98: 55-61

[9] Karan, N.K., Pradhan, D.K., Thomas, R., Natesan, B., Katiyar, R.S. 2008. *Solid State Ionics* 179: 689-696

[10] Ratner, M.A.,1987. In J.R. MacCallum and C.A Vinant, (eds.). *Polymer Electrolytes Reviews,* 173-232 Elsevier, London.

[11] Ratner, M.A., & Shriver, D. F, 1988. *Chemistry Reviews*, 88: 109-124.

STUDIES OF MAGNESIUM ION CONDUCTION IN PMMA-BASED GEL POLYMER ELECTROLYTES

Z. Osman & N. H. Zainol
Department of Physics, University of Malaya, 50603, Kuala Lumpur, Malaysia.

Abstract

Investigation on magnesium-ion conducting in gel polymer electrolytes has attracted much attention since it has such advantages as it is free from hazards, its stability is high and its natural resources are plenty. In this research work, gel polymer electrolytes (GPEs) based on polymethylmethacrylate (PMMA) have been prepared by using magnesium triflate through the solution casting technique. The mixture of ethylene carbonate (EC) and propylene carbonate (PC) were used as the plasticizing solvents. The highest conductivity, σ of the GPE was obtained from the sample containing 0.6g of $Mg(CF_3SO_3)_2$ salt, i.e. 1.61×10^{-3} S cm^{-1} and shown that it follows the Arrhenius behavior with activation energy of 0.18 eV. The ionic transference number estimated by dc polarization technique revealed that conducting species are predominantly ions.

Keywords: *Gel polymer electrolytes, Ionic conductivity, magnesium triflate, polymethylmethacrylate, transference number*

Introduction

Polymer electrolytes have been widely studied and developed for battery applications because the use of a polymer electrolyte makes the fabrication of safe batteries possible and permits the development of thin batteries with design flexibility [1-6]. Gel polymer electrolytes (GPEs) are alternatives to both solid polymer electrolytes (SPEs) and liquid electrolytes in view of its potential application in solid state rechargeable batteries. SPEs possess good mechanical strength but its conductivity at room temperature is low than GPE which is in the range of ~10^{-5} to ~10^{-4} S·cm^{-1} [7].

Many of the research works on GPEs have focused on lithium salt systems [8]. To date, the works on GPEs using magnesium salt has not been widely reported [9]. The need for high performance and environmental friendly rechargeable batteries has attracted attention of researchers to the magnesium-based rechargeable battery systems. This is because magnesium possesses important characteristics, which make it attractive as a negative electrode material for high energy density batteries as it has a high charge density (a low electrochemical equivalence of ~12.15 g·eq^{-1}), considerably negative electrode potential (-2.3 V versus SHE), high melting point (649 °C), low cost, high safety, ease of handling, and low toxicity which allows for urban waste disposal [10-12]. However, development of rechargeable Mg batteries has not been accelerated mainly due to the lower reversibility of the electrode/electrolyte charge transfer and the lack of suitable Mg^{2+} ion conducting non-aqueous electrolytes [13].

In this work, we have prepared a gel polymer electrolyte system comprising PMMA, propylene carbonate (PC), ethylene carbonate (EC), magnesium triflate ($Mg(CF_3SO_3)_2$) and characterized by using impedance spectroscopic technique and transference number measurements. The impedance spectroscopy technique will be used to study the variation of ionic conductivity with various concentrations of $Mg(CF_3SO_3)_2$. Transference number measurements of the GPE will reveal the contribution of one ionic species to the ionic conductivity.

Materials and Method

Materials

Polymethylmethacrylate (PMMA) with molecular weight of 9.96×10^5 $g\cdot mol^{-1}$, propylene carbonate (PC), ethylene carbonate (EC), and magnesium triflate, $Mg(CF_3SO_3)_2$ were purchased from Sigma-Aldrich.

Method

The gel polymer electrolyte samples will be prepared by using the solution-casting method. Magnesium triflate was slowly dissolved with continuous stirring, in a required amount of the mixture of PC and EC. This solution was heated at 60 °C for several hours to ensure complete dissolution. Then, PMMA was added to this solution and the mixture was stirred thoroughly well. This solution was subsequently casted on a petri dish and allowed to dry at room temperature. For the purpose of arriving at an appropriate composition, several GPE films will be prepared by varying the quantities of $Mg(CF_3SO_3)_2$ in a constant quantity of PMMA and (PC+EC).

Impedance Spectroscopy

The ionic conductivity of the GPE films was evaluated using ac impedance spectroscopy over the frequency range from 50 Hz to 1 MHz using HIOKI 3532 LCR. The ionic conductivity temperature dependence studies will be carried out at temperature range from 303 K to 373 K on the sample that has highest σ at room temperature. The conductivity, σ can be calculated using the following equation

$$\sigma = t/R_bA \quad (1)$$

where t is the sample thickness, R_b is the bulk resistance and A is the contact area

Transference number

The transference number of the selected sample was measured by using dc polarization method. In this method, the dc current is monitored as a function of time on the application of fixed dc voltage (1.0 V) across the sample with stainless steel blocking electrodes. If the electrical conductivity of the polymer electrolytes is predominantly ionic, the current will decrease with time. The electronic and the ionic transference number can be determined by using the following equations;

$$t_e = \sigma_e/\sigma_T = i_e/i_T \quad (2)$$

and

$$t_i = 1- i_e/i_T = 1- t_e \quad (3)$$

where t_e and t_i are the electronic and ionic transference numbers, respectively, with σ_e and σ_T refer to the electronic and total conductivity while i_e and i_T are the electronic and total current, respectively.

Results and Discussion

Ionic Conductivity Studies

The GPE of PMMA exhibits a high ionic conductivity due to the presence of $Mg(CF_3SO_3)_2$ dissolve in liquid components, PC and EC as solvents [14]. The ionic conductivity increases with the salt concentrations in the gel polymer electrolytes. The increased in ionic conductivity is due to both the enhancement of the ionic mobility and the number of charge carriers ions

[15]. Subsequent to optimization of the weight ratio of (PC+EC) to PMMA, several GPE films were prepared by varying the concentrations of $Mg(CF_3SO_3)_2$.

The variation of conductivity of GPE with $Mg(CF_3SO_3)_2$ concentrations is shown in Figure 1. The value of σ increases with an increase of $Mg(CF_3SO_3)_2$ concentration and reaches a maximum at 1.61×10^{-3} S·cm^{-1} for sample containing 0.6 g of $Mg(CF_3SO_3)_2$ salt. This is due to an increase in the concentration of Mg^{2+} ions in the GPE. The value of σ decreases with further increase of $Mg(CF_3SO_3)_2$ concentration due to ion pair formation, which reduces the number of charge carriers. The GPE exhibits ionic conductivity due to the presence of $Mg(CF_3SO_3)_2$ dissolved in PC and EC, which encapsulated in the matrix of PMMA. The appropriate composition of the GPE in the weight ratio of PMMA, PC, EC, and $Mg(CF_3SO_3)_2$, thus is 2:2:2:0.6. This result is quite similar to the result that has been reported by Girish Kumar [16].

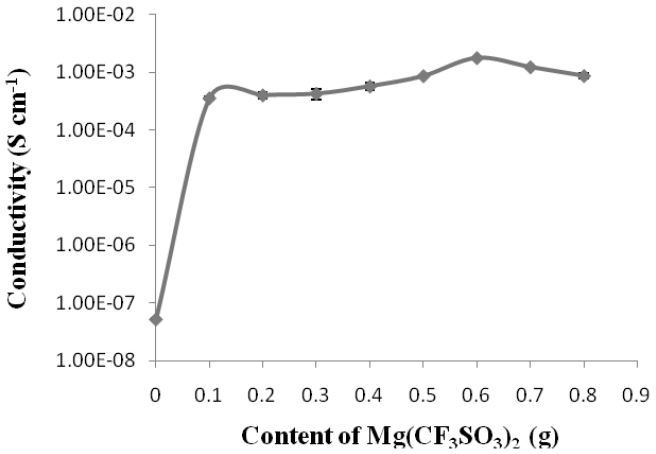

Figure 1: Variation of conductivity with amounts of $Mg(CF_3SO_3)_2$ in PMMA-based GPE

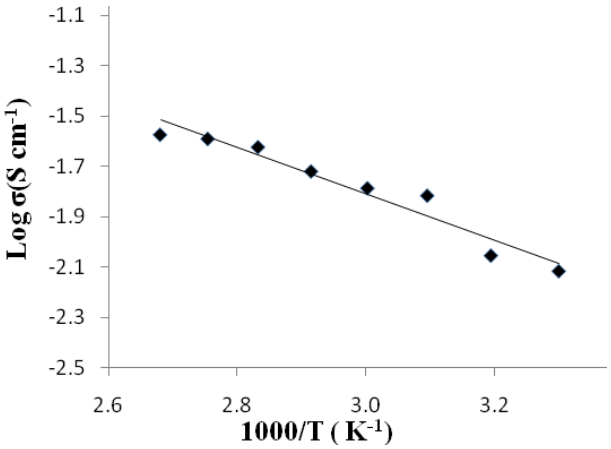

Figure 2: Arrhenius plot of the highest conducting sample

The SS/GPE/SS cells with GPE of the highest conducting sample are subjected to a.c impedance measurement at several temperatures between 30 °C and 100 °C. The σ values, thus obtained were used to construct Arrhenius plot as shown in Figure 2. The plot is fairly linear suggesting that liquid like conduction of $Mg(CF_3SO_3)_2$ in PC and EC as the electrolyte [17]. The energy of activation (E_a) obtained for this composition is 0.18 eV.

Transference number

The transference number measurements of the selected GPE samples have been measured using dc polarization technique or also called Wagner's polarization method. In this method, the dc current is monitored as a function of time on the application of fixed dc voltage i.e. 1.0 V across the sample with stainless steel blocking electrodes. Figure 3 shows the results of normalized current versus time plot at room temperature for GPE samples containing 0.1 g, 0.6 g and 0.7 g $Mg(CF_3SO_3)_2$ salt. The values of ionic transferences number have been calculated from this plot using Eq. (2) and (3). It is found that the ionic transference number for samples containing 0.1 g, 0.6 g, and 0.7g $Mg(CF_3SO_3)_2$ salt is 0.92, 0.95, and 0.94 respectively with highest conducting sample shows the highest ionic transference number, t_i=0.95. Hence, this result reveals that the charge carriers in these gel polymer electrolyte films are predominantly ions.

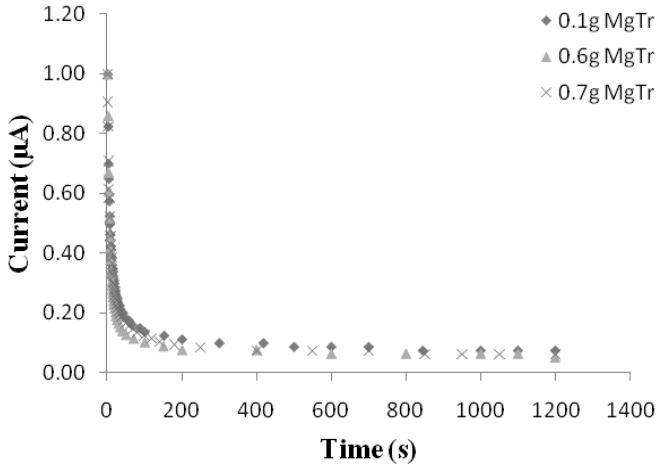

Figure 3: Normalized current versus time plots for sample containing 0.1g, 0.6g, and 0.7g of $Mg(CF_3SO_3)_2$ salt.

Conclusion

The GPE samples of PMMA containing $Mg(CF_3SO_3)_2$ salt have been prepared. This study indicates that the sample containing 0.6 g of $Mg(CF_3SO_3)_2$ exhibits the highest room temperature ionic conductivity of 1.61×10^{-3} S·cm^{-1} which shown the highest ionic transference number of 0.95. The ionic transference number estimated by dc polarization method revealed that the conducting species in the GPEs are predominantly ions. The conductivity of temperature-dependence studies follows the Arrhenius behavior with activation energy of 0.18 eV.

Acknowledgement

The authors would like to thank University of Malaya for the grant, RG 088/10AFR.

References

[1] Gregory, T.D., Hoffman, R.J., Winterton, R.C., (1990), J. Electrochem. Soc. 137, 775.
[2] Scrosati, B., (Ed.), Application of Electroactive Polymers, Chapman and Hall, London, 1993.
[3] Gray, F.M., Polymer Electrolytes, The Royal Society of Chemistry, Cambridge, 1997.
[4] Park, C H., Sun, Y-K., Prakash, J., Kim, D-W., (2003), Solid State Ionics 159 111-119
[5] Van Schalkwijk, W.A., Scrosati, B.A., (Eds.), Advances in Lithium-ion Batteries, Kluwer Academic/Plenum Publishers, New York, 2003.
[6] Park, C H., Sun, Y-K., Kim, D-W., (2004), Electrochimica Acta 50 375-378

[7] Girish Kumar, G., and Munichandraiah, N., (2002), Electrochimica Acta 47, 1013-1022.
[8] Manuel Stephan, A., (2000), European Polymer Journal 42, 21-42.
[9] Yoshimoto, N., Yokushiji, S., Ishikawa, M., Morita, M., (2002), Solid State Ionics, 152-153, 259-266.
[10] Pandey, G.P., Agrawal, R.C., and Hashmi, S.A., (2010), J. Phys. D: Appl. Phys. 43, 255501.
[11] Oh, J.S., Ko, J.M., Kim, D.W., (2004), Electrochimica Acta 50, 903-906.
[12] Novak, P., Imhof, R., Haas, O., (1999), Electrochim. Acta 45, 351.
[13] Aurbach, D., Suresh, G.S., Levi, E., Mitelman, A., Mizrahi, O., Chusid, O., and Brunelli, M., (2007), Adv. Mater. 19, 4260.
[14] Girish Kumar, G., and Sampath, S., (2005), Solid State Ionics 176, 773-780.
[15] de Freitas, J.N., Nogueira, A.F., and de Paoli, M.A., (2009), Journal of Materials Chemistry 19, 5279-5294.
[16] Girish Kumar, G., and Munichandraiah, N., (2000), Solid State Ionics 128, 203-210.
[17] Yoshimoto, N., Yokushiji, S., Ishikawa, M., Morita, M., (2003), Electrochimica Acta 48, 2317-2322.

LI-ION CONDUCTION AND STRUCTURAL STUDIES OF GEL POLYMER ELECTROLYTES BASED ON POLY (METHYLMETHACRYLATE)

Siti Mariam Samin, Lisani Othman, Khairul Bahiyah Md Isa & Zurina Osman
Physics Department, University of Malaya, 50603 Kuala Lumpur, Malaysia

Abstract

The gel polymer electrolytes (GPEs) composed of PMMA and $LiClO_4$ salt dissolved in the mixture of EC and PC have been prepared by solution casting technique. The GPE samples are prepared by varying the salt concentrations from 5% (w/w) to 30% (w/w). AC impedance spectroscopy measurement has been carried out to determine the ionic conductivity of the samples. The sample containing 20% (w/w) of $LiClO_4$ salt exhibits the highest room temperature ionic conductivity of 3.34×10^{-3} $S\cdot cm^{-1}$. The amorphous nature and structural changes between $LiClO_4$ salt, EC and PC in the PMMA based GPEs have been validated using XRD and FESEM analysis.

Keywords: *field emission scanning electron microscopy, gel polymer electrolytes, ionic conductivity, poly(methylmethacrylate), x-ray diffraction*

Introduction

Since the recognition of potential applications of polymer electrolyte in lithium batteries and electrochemical devices [1-3], a remarkable research effort has been dedicated to find the optimal combination of host polymer and dopant salt for fast ionic transport. Primary work on polymer electrolytes was solid polymer electrolytes (SPEs) which are mainly based on complexes of PEO with various lithium salts. These systems failed to show enviable ionic conductivity due to their high degree of crystallization [4,5]. There have been various attempts to prepare polymer electrolytes with properties similar to those liquid electrolytes [6]. One of the successful approaches that can achieve this requirement is by adding polymer matrix into the system to form “gel-type” polymer such as polymethylmethacrylate (PMMA) [7,8]. The gel polymer electrolytes (GPEs) have many advantages compared to solid polymer electrolytes because they inherited the important properties of liquid electrolyte including enhancement on ionic conduction, electromechanical stability on anode and other metal oxide cathode materials, safety against electrical and mechanical abuse [5,7,8]. Chandra et al. [9] has been reported that polymer only act as a stiffener and not taking part in conduction process. Among lithium salts used in GPEs, lithium perchlorate ($LiClO_4$) is more favorable due to its highly soluble in organic and even water, less hygroscopic and does not undergo oxidation on the anode [10,11]. In order to increase the amorphous phase and the conductivity value, different plasticizers like ethylene carbonate (EC) and propylene carbonate (PC) were added to these polymer electrolytes.

In this work, the samples of gel polymer electrolyte using poly(methylmethacrylate), PMMA mixed with fixed amount of the mixture of EC and PC as plasticizing solvent with varied amounts of lithium perchlorate, $LiClO_4$ have been prepared. Ionic conductivities of these samples have been measured by complex impedance spectroscopy. XRD and FESEM have been carried out to investigate the structural and complexation features of the GPE samples.

Materials and Method

Gel polymer electrolyte (GPE) samples were prepared using high purity lithium perchlorate, $LiClO_4$ salt that obtained from Aldrich ranging from 5% (w/w) to 30% (w/w) was dissolved in a plasticizing solvent of ethylene carbonate (EC) and propylene carbonate (PC). The mixture of EC:PC is fixed at 2:1. The amount of the polymer host, PMMA with an average molecular weight of 9.96×10^{-1} $g\cdot mol^{-1}$ was then added accordingly into the electrolyte solution. The

mixture was continuously stirred for several hours with magnetic stirrer at 60 °C until clear and transparent mixture was obtained. The solutions were then cast onto glass petri dishes and continue heating for additional 24 h at 80 °C. To prevent contact with air and moisture, the samples were kept in desiccator until characterizations were carried out. AC impedance spectroscopy for the samples was conducted by using a computer controlled HIOKI 3532 LCR operating in the frequency range of 50 Hz to 1 MHz. In order to study the structural properties of GPE samples, XRD patterns of the samples were recorded using D500 diffractometer which employed Cu-K_α X-radiation. FESEM is used to study the surface morphology of GPE samples. The FESEM model used is FEI Quanta 200 with a magnification of 12000×.

Results and Discussion

Ionic conductivity measurements

It is observed that conductivity has increased when salt concentrations increase from 5% (w/w) to 20% (w/w) as shown in Figure 1. From the Cole-Cole plot obtained, the bulk resistance, R_b of each sample was determined and hence the conductivity (σ) of the samples was then calculated using:

$$\sigma = t / R_b A \quad (1)$$

where t is the sample thickness (cm), A is the effective contact area of the electrode and the sample (cm^2), and R_b is the bulk resistance (Ω). The highest conductivity at room temperature obtained was 3.34×10^{-3} $S\cdot cm^{-1}$ from the sample containing 20% (w/w) of $LiClO_4$ salt. The conductivity decreased as concentrations of salt were added more than 20% (w/w) This is most likely due to aggregation of the ions, leading to formation of ion cluster which reduces the number of mobile charge carriers as reported by MacCallum et al. [12] and Subba Reddy et al. [13]. The addition of the mixture of EC and PC into the electrolyte solution also helps to increase the ionic conductivity of gel polymer electrolyte. This reflects that the synergistic effect of the physicochemical properties of solvent with high dielectric constant (ε_{25}= 95.3) and low viscosity (η_{40}= 1.87 $kg\cdot(\underline{s}\cdot\underline{m})^{-1}$) of EC and low freezing point of PC (-40 °C) along with good plasticizing characteristic greatly enhance the conductivity performance as reported by Selvasekarapandian et al. [2].

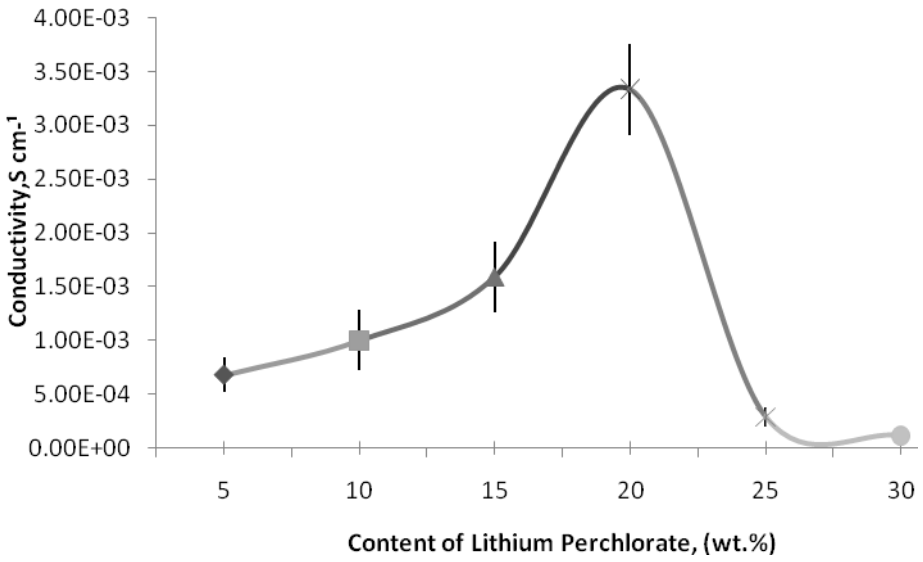

Figure 1: The variation of conductivity with $LiClO_4$ salt for the gel polymer electrolytes films.

X-ray Diffraction (XRD) studies

Figure 2 illustrates the x-ray diffractogram of pure $LiClO_4$ and GPE samples with and without salt. The intensity of salted GPE samples is significantly lower than the sample without salt. According to Jingyu et al. [14], the characteristic diffraction peaks of semi-crystalline sample of pure PMMA become weaker and broader when Li salt is introduced in PMMA based polymer electrolyte, suggesting that the coordination interactions between the C=O groups of PMMA, the plasticizing solvent and Li^+ can decrease the crystallinity of pure polymer sample. The sample containing 20% (w/w) of $LiClO_4$ has the highest conductivity at room temperature. It can be observed that this film is more amorphous compared to the other films. The disappearances of sharp peaks correspond to $LiClO_4$ salt which leads to the dominant presence of an amorphous phase confirm that the complexation between PMMA and the salt has occurred. This also indicates that the complete dissolution of excess salt in the PMMA complexes as reported by Stephan et al. [8].

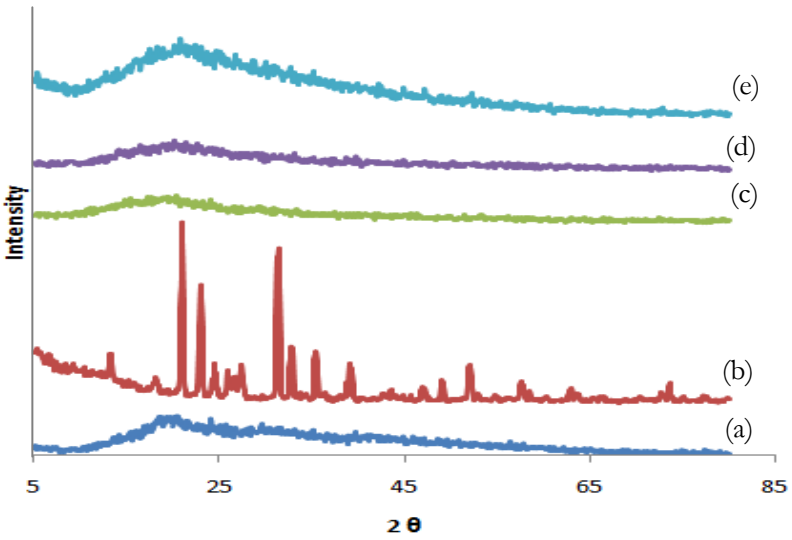

Figure 2: X-ray diffractogram of (a) PMMA-EC-PC (b) $LiClO_4$ (c) PMMA+EC+PC+5 wt.% $LiClO_4$ (d) PMMA+EC+PC+20 wt.% $LiClO_4$ (e) PMMA +EC+PC+ 30 wt.% $LiClO_4$.

Field Emission Scanning Electron Microscopy (FESEM)

The FESEM micrographs for PMMA-EC-PC samples with and without salt are depicted in Figure 3. The surface morphology of the film without salt is clear and smooth indicates an excellent dissolution and the complexation between PMMA and the plasticizing solvent EC and PC has occurred. Figure 3(b) shows white spherulites from the doping of liquid electrolytes have been observed. According to Ramesh [15], these white spherulites are formed mainly due to the entrapments of liquid electrolyte which are being retained in the polymer matrix. The surface morphology for the highest conducting film appeared to be smoother and homogenous reveals that the complexation between the PMMA polymer, plasticizing solvent and $LiClO_4$ salt has occurred. The amorphous phase of the film can be observed in accordance with XRD patterns as shown in Figure 3. The $LiClO_4$ salt is distributed more evenly inhibits the ionic transportation among the polymer electrolyte, thus enhance the conductivity of the GPE sample. In Figure 3(d), it can be seen the agglomerate of salt, EC and PC in the PMMA based GPE due to saturate of $LiClO_4$ salt concentration compared to sample containing 20% (wt/wt) $LiClO_4$ salt. As a result, the conductivity of GPE sample is decreased as well as the amorphous phase.

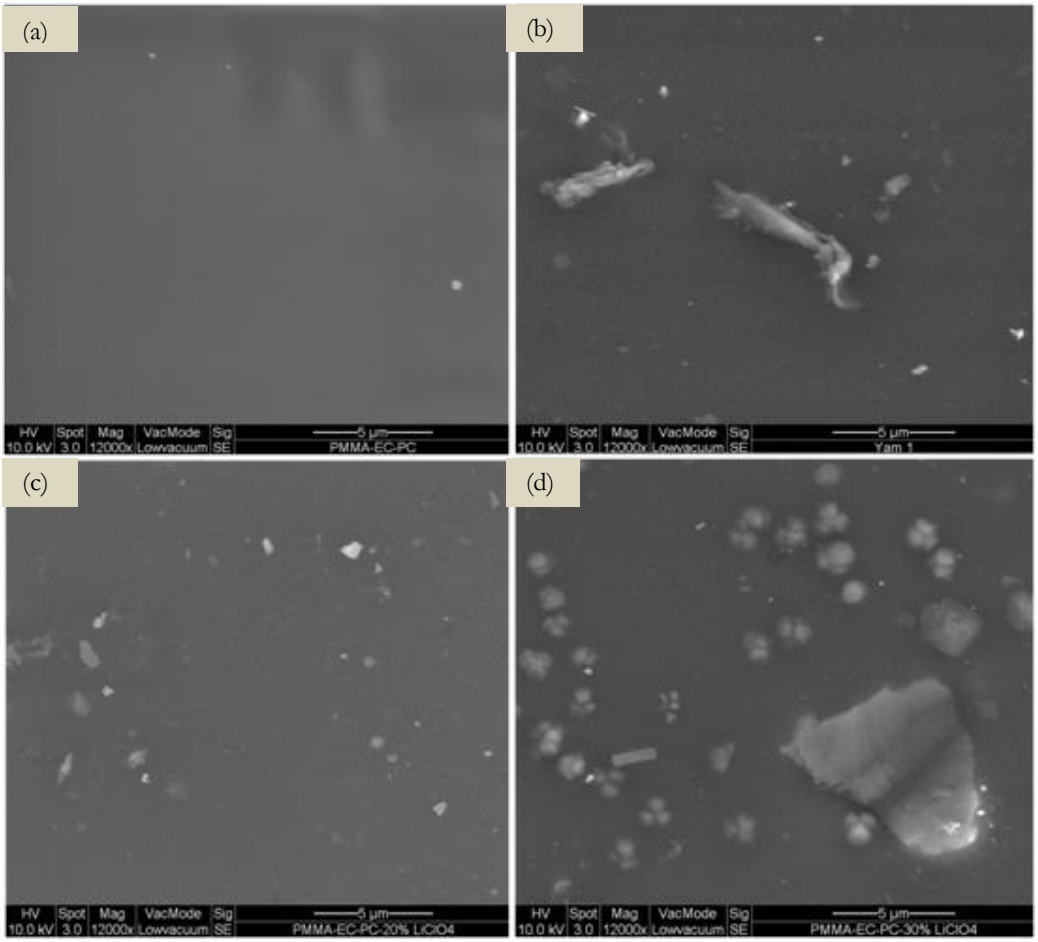

Figure 3: The FESEM micrographs of (a) PMMA-EC-PC (b) PMMA+EC+PC+5 wt% $LiClO_4$ (c)PMMA+EC+PC+20 wt% $LiClO_4$ (d) PMMA+EC+PC+30 wt% $LiClO_4$.

This study has demonstrated that the addition of an optimum content of inorganic lithium salt mixed with EC+PC solvent in PMMA based gel polymer electrolyte produced highly conductive gel polymer electrolyte. The highest room temperature conductivity obtained from the sample containing 20% (w/w) of $LiClO_4$ salt is 3.34×10^{-3} $S\cdot cm^{-1}$. Increasing the concentration of salt will result in increasing of the numbers ion charge carrier, thus the ionic conductivity. XRD studies showed that the conductivity is increased when crystallinity of the film is reduced. The FESEM studies showed that $LiClO_4$ salt is distributed more evenly for the highest conductive samples; hence lithium ions can traverse through the sample easily and thus enhance the conductivity of the GPEs sample.

Acknowledgement
The authors would like to thank University of Malaya for the grant, UM.C/625/1/HIR/008.

References

[1] Ahmad, S., 2009. Ionics *15, 309 – 321.*
[2] Selvasekarapandian, S., Baskaran, R., Hema M., 2005. *Physics B. 357, 1234-1240.*
[3] Kumar, R. Sekhon, S. S., 2008. *Ionics 14, 509-514*.
[4] Meneghetti, P. , Qutubuddin, S., Webber A. C., 2004. *Electrochimica Acta 49, 4923-4931*.

[5] Ahmad, S., Agnihotry, S. A., 2005. *Journal Power Sources 140, 151-156.*
[6] Kumar, D., Hashmi, S.A., 2010. *Solid State Ionics 18, 416-423.*
[7] Vondrak, J., Reiter, J., Velicka J., Sedlarikova, M., 2004. *Solid State Ionics 170, 79-83.*
[8] Manual Stephan, A., Thirunakaran, R., Renganathan, N. G., Sundaram, V., Pitchumani, S., Gangadharan, N. Ramamoorthy, M., P., 1999. *Journal of Power Sources 81-82, 752-758.*
[9] Chandra, S., Sekhon, S.S, Arora N., 2000. *Ionics 6, 112-118.*
[10] Silva, M. M., Barros, S. C., Smith, M. J., MacCallum, J. R., 2002. *Journal of Power Sources 111, 52-57.*
[11] Deepa, M., Sharma, N., Agnihotry, S. A., Chandra, R., Sekkhon, S.S., 2002. *Solid State Ionics 148, 451-456.*
[12] MacCallum, J.R., and Vincent, C.A. 1987. (eds), in "*Polymer electrolytes Reviews - 1*", Elsevier, New York.
[13] Subba Reddy, Ch. V., Xia Han, Quan-You Zhu, Li-Qiang Mai, Wen Chen, 2006. *European Polymer Journal 42, 3114-3120.*
[14] Jingyu Xi**,** Xiaozhen Tang, 2005. *Electrochimica Acta, 50, 5293-5304.*
[15] Ramesh, S., Chiam-Wen Liew, Ramesh, K., 2011*. Journal of Non-Crystalline Solids 1-11.*

IONIC CONDUCTIVITY AND GLASS TRANSITION TEMPERATURE OF METHYL-GRAFTED NATURAL RUBBERS AND LITHIUM PERCHLORATE COMPLEXES

Mohd Azizi Nawawi[1], Sim Lai Har[2] & Chan Chin Han[1]
[1] Faculty of Applied Sciences, Universiti Teknologi MARA, Shah Alam, Selangor, Malaysia.
[2]Centre of Foundation Studies, Universiti Teknologi MARA, Puncak Alam, Selangor, Malaysia.

Abstract

Conductivity and glass transition temperature (T_g) of methyl-grafted natural rubbers (MGNR30 and MGNR49) and lithium perchlorate complexes were investigated by impedance spectroscopy (IS) and differential scanning calorimetry (DSC), respectively. The complexes were prepared via solution casting method with a proper heat treatment. Maximum conductivities recorded at mass fraction of salt, W_s=0.130 for both MGNR30 and MGNR49 complexes are 8.66×10^{-8} and 1.66×10^{-8} $S\cdot cm^{-1}$, respectively. MGNR30 and MGNR49 exhibit two T_g values. The one corresponding to PMMA segment of the modified natural rubber increases with ascending salt concentration while the other corresponding to the natural rubber (NR) show otherwise. This result indicates a selective localization of Li^+ ion at the PMMA segment of the methyl-grafted natural rubbers.

Keywords*: Glass transition temperature, ionic conductivity, modified natural rubber, polymer electrolyte*

Introduction

Solid polymer electrolytes formed by polymer-salt solutions have attracted a great deal of scientific interest in the past 30 years [1-3]. The ionic conduction in polymer electrolytes is due to the mobility of the cation from the salt that acts as the charge carrier. The polymer plays a role as an immobile solvent. Solid polymer electrolyte offers simplification with respect to fabrication, ruggedness, safety, thin-profile geometry, flexibility and elasticity [4]. There is no danger of flammability because no liquid or gelled electrolyte is used. Natural rubber (NR) and other chemically modified NRs are elastomers. Modification of NR aims at improving its properties and characteristics. Several techniques such as epoxidation, grafting, blending and etc have been adopted by scientists to modify the properties of the NRs [5,6]. Modified NRs which possess low glass transition temperature, good mechanical properties and moderate ionic conductivity coupled with their elastomeric characteristics are ideal candidates to be used as polymer host in polymer electrolyte [7].

One of the commercially available modified NR is methyl-grafted natural rubber (MGNR) in which different mole percent of poly(methylmetacrylate) (PMMA) are grafted to NR. MGNR30 and MGNR49 which possess 30 and 49% (mol/mol) of PMMA, respectively in NR are hard, relatively stiff and non-tacky at ambient temperature. Due to the fact that MGNRs softened upon heating, thus, they can be easily processed individually or as blends with other NRs. Besides, all MGNRs acquire excellent adhesive properties because the polymer chains possess both the polar (PMMA) and non-polar rubber hydrocarbon components [8]. Figure 1 shows the chemical structure of MGNR.

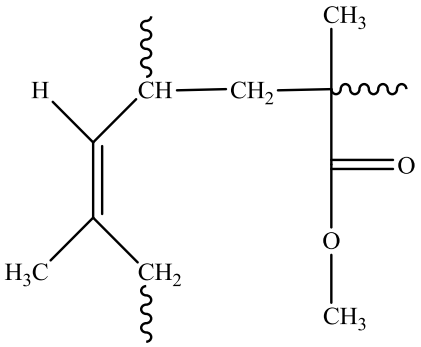

Figure 1: Chemical structure of MGNR

Materials and Method

Materials

30% (mol/mol) methyl-grafted natural rubber (MGNR30), 49% (mol/mol) methyl-grafted natural rubber (MGNR49) and deproteinised natural rubber (DPNR) were used after purification and the anhydrous lithium perchlorate ($LiClO_4$) with purity ≥ 99% (Acros Organics) was vacuum dried for 24 h at 120 °C. All the modified natural rubbers were supplied by Green HPSP.

Method

The thin electrolyte films were prepared via solution casting technique. Different mass fraction of $LiClO_4$ (W_S) ranging from 0.0476 to 0.167 was added to MNR in tetrahydrofuran solution. The mass fraction of salt is defined as in equation 1.

$$W_s = \frac{\text{Mass of salt}}{\text{Dry mass of polymer} + \text{salt}} \quad (1)$$

Polymer films were dried for 24 h at room temperature before further drying in a vacuum oven for 48 h at 50 °C.

Conductivity Measurements

Ionic conductivity (σ) at 30 ^{o}C was determined from ac-impedance measurements using a Hioki 3532-50 Hi-Tester over the frequency range between 100 Hz to 1 MHz. Films of polymer electrolyte were sandwiched between two stainless steel disk electrodes. The value of bulk electrolyte resistance (R_b) was extracted from the Cole-Cole plot of complex impedance data and σ was calculated using the equation (2).

$$\sigma = L/(R_b \cdot A) \quad (2)$$

Quantities L and A denote thickness of the polymer electrolyte film and its surface area in contact with the stainless steel disk electrodes, respectively.

Thermal Characterisation

Glass transition temperature (T_g) of the polymer electrolytes was determined by DSC TA Q200. Sample was annealed at 80 ^{o}C for 1 min followed by quenched cooling to -90 ^{o}C. Afterwards, sample was reheated up to 80 ^{o}C with a rate of 20 ^{o}C·min^{-1}. T_g was extracted from the midpoint of the difference in heat capacity at the second heating run.

Results and discussion

Conductivity

Impedance analysis was performed on as prepared neat MGNR30, neat MGNR49, neat DPNR, MGNR30-$LiClO_4$, MGNR49-$LiClO_4$, and DPNR-$LiClO_4$. The thickness of the thin electrolyte film was measured using digital caliper by averaging three measurements taken at three different spots. The surface area of the film in contact with the electrodes is equals to 3.142 cm^2. Three impedance measurements were carried out for each sample and the average σ value was applied for the following discussions.

Figure 2 represents the variation of σ as a function of mass fraction of $LiClO_4$ doped into different MNR at 30 ^oC. Neat DPNR and neat MGNR49 exhibit low σ of ~10^{-10} $S{\cdot}cm^{-1}$ while neat MGNR30 recorded a slightly higher conductivity of ~10^{-9} $S{\cdot}cm^{-1}$. Upon addition of the inorganic salt, the conductivities for MGNR30-$LiClO_4$ and MGNR49-$LiClO_4$ complexes increase steadily with increasing salt concentration and reach the maximum values of 8.66×10^{-8} and 1.66×10^{-8} $S{\cdot}cm^{-1}$, respectively at around W_s = 0.130. Further increase in the salt concentration results in a marked drop in σ for both the complexes. The decrease in σ is probably due to ion pair formation that reduces the number of free mobile Li^+ cations.

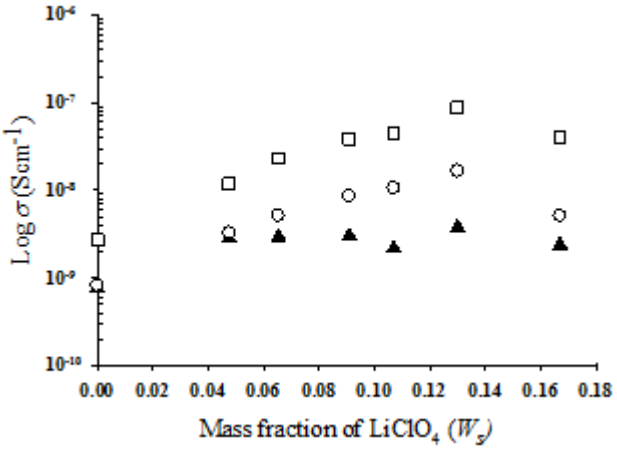

Figure 2: Log ionic conductivity versus mass fraction of $LiClO_4$ for (▲) DPNR-$LiClO_4$, (○) MGNR49-$LiClO_4$ and (□) MGNR30-$LiClO_4$ complexes at 30°C

However, incorporation of the salt to DPNR exerts little influence on its conductivity as the conductivity of the DPNR-$LiClO_4$ complex remains relatively constant at all salt concentration. In addition, it was observed that at W_s>0.167, $LiClO_4$ begins to precipitate out during the preparation of the electrolyte films for all the samples of the MNR-$LiClO_4$ complexes studied. Therefore, no relevant discussion on variation of the conductivity can be made for all the MNR-$LiClO_4$ complexes at W_s>0.167.

Glass Transition Temperature

There are two T_g observed for the samples of both the methyl grafted NRs (MGNR30 and MGNR49) as tabulated in Table 1.

Table 1: Glass transition temperature of DPNR, MGNR30 and MGNR49

Mass fraction of $LiClO_4$, W_s	T_g (°C)				
	DPNR	MGNR30		MGNR49	
0.0000	-43.0	-15.4	-64.2	-14.9	-66.4
0.0476	-42.8	-15.0	-64.7	-14.1	-66.2
0.0654	-42.6	-13.6	-64.4	-13.6	-66.5
0.0910	-42.5	-13.4	-64.9	-13.5	-67.4
0.1070	-43.1	-12.2	-65.5	-13.2	-67.8
0.1300	-43.3	-12.1	-65.4	-12.8	-69.3
0.1670	-42.8	-11.7	-65.8	-12.7	-69.5

The lower T_g values for MGNR30 are in the range of -65.8 to -64.2 °C and that of MGNR49 are in the range -69.5 to -66.4 °C. These T_g are most probably attributed to that of the natural rubber segment of the polymer. On the other hand, the higher T_g values for MGNR30 and MGNR49 are in the range of -15.4 to -11.7 °C and -14.9 to -12.7 °C respectively. These T_g corresponding to the PMMA segment of the elastomer. There is a progressive increase in the T_g values of the MGNR30 and MGNR49 from -15.4 to -11.7 °C and -14.9 to -12.7 °C, respectively with ascending salt concentration.

However, the lower T_g values in the rubber segment of the polymer demonstrated otherwise with ascending salt content. These results show that the Li^+ ions prefer to coordinate with the carboxyl groups of the PMMA as compared to the C=C group of NR. The T_g values of MGNR49 at all salt concentration as shown in Figure 3 and Table 1 are relatively higher than those of the MGNR30 suggesting that MGNR30 with less PMMA grafted to NR exhibits higher segmental motion, hence, enhancing fast ion transport resulting in higher ionic conductivity of the elastomer as compared to MGNR49. The T_g of DPNR remains relatively constant with ascending $LiClO_4$ content due to poor coordination between the Li^+ ions and the C=C group of the elastomer.

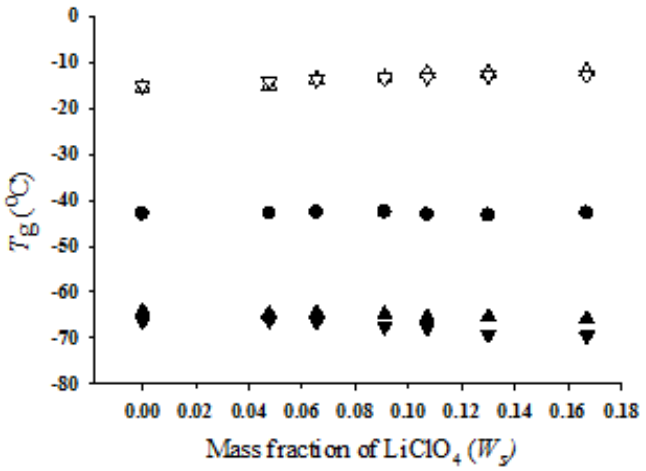

Figure 3: T_g as functions of W_s . ●: T_g of DPNR; ▲, ∆: T_g of MGNR30; ▼,▽: T_g of MGNR30

Conclusion

Thin electrolyte films of MGNR30-$LiClO_4$ and MGNR49-$LiClO_4$ complexes were prepared by solution casting technique. Ionic conductivity increases with ascending salt concentration until W_s = 0.130. Ionic conductivity decreases significantly at W_s > 0.130 due to ion pair formation that reduces the number of free mobile Li^+ cations. The T_g value corresponding to the PMMA segment of both MGNR30 and MGNR49 increase with increasing salt concentration contrary to that exhibit by the NR segment of the elastomer. This indicates that the Li^+ ions prefer to interact with the PMMA segment rather than with the NR segment of the MGNR30 and MGNR49 samples.

Acknowledgment

This research is supported by Excellent Fund, Research Management Institute, Universiti Teknologi MARA, Malaysia. Research grant no. 600-RMI/ST/DANA5/3/Dst (130/2010).

References

[1] Fenton, D. E.; Parker, J. M.; Wright, P. V. *Polym* 1973, *14*, 589.
[2] MacCallum, J. R.; Vincent, C. A. *(Eds.) Polymer Electrolyte Reviews 1*, Elsevier: London, 1987; Vols. 1.
[3] Gray, F. M. *Polymer Electrolytes*; The Royal Society of Chemistry: Cambridge, 1997.
[4] Dissanayake, M. A. K. L.; Careem, M. A. *Solid State Ionics* 1998, *28*, 1093.
[5] Glasse, M. D.; Idris, R.; Latham, R. J.; Linford, R. G.; Schlindwein, W. S. *Solid State Ionics* 2002, *147*, 289.
[6] Li, W.; Yuan, M.; Yang, M. *Eur Polym J* 2006 *42*, 1396.
[7] Idris, R.; Glasse, M. D.; Latham, R. J.; Linford, R. G.; Schlindwein, W. S. *J Power Sources* 2001, *94*, 206.
[8] Alias, Y.; Ling, I.; Kumutha, K. *Ionics* 2005, *11,* 414.

SOLUBILITY OF LI-SALT IN SOLID POLYMER ELECTROLYTES BASED-ON MODIFIED NATURAL RUBBER

S.N.H.M. Yusoff[1], L.H. Sim[2], C.H. Chan[1], H.W. Kammer[3]

[1] *Faculty of Applied Sciences, Universiti Teknologi MARA, Shah Alam, Selangor, Malaysia*

[2]*Centre of Foundation Studies, Universiti Teknologi MARA, Puncak Alam, Selangor, Malaysia*

[3]*University of Halle, Mansfelder Str. 28, D-01309 Dresden, Germany*

Abstract

Solid solutions of Epoxidized Natural Rubber (ENR) with 25 and 50 % (mol/mol) epoxidation added with $LiClO_4$ were prepared by solution casting technique. T_g values obtained using differential scanning calorimetry (DSC) and the ionic conductivity evaluated from bulk resistance (R_b) determined using the impedance spectroscopy point towards the higher solubility of the lithium salt in ENR-50. Restricted segmental motion due to the higher degree of Li^+ ion coordination to the polar epoxy oxygen of the ENR-50 leads to a lower ionic conductivity as compared to ENR-25. Besides, FTIR results agree very closely to the conclusion that the ionic salt is more soluble in ENR-50 than in ENR-25.

Keywords*: Conductivity, epoxidized natural rubber, fourier transform infrared spectroscopy, glass transition temperature, polymer electrolytes*

Introduction

Since the discovery of ion-conducting polymer by Fenton et al. [1] followed by the application of polymer electrolyte in lithium batteries by Armand et al. [2], solid polymer electrolyte (SPE) has been widely studied especially on the enhancement of ionic conductivity. To date, SPE has become the focus of extensive researches in pursue for a new generation of power source to cater for the latest development in electrochemical devices. Polymer electrolyte is a complex formed by dissolving an inorganic salt in a polymer matrix with polar groups acting as an immobile solvent.

It is generally accepted that the charge carrier density and ion mobility are the two important parameters contributing to the ionic conductivity of a SPE [3-5]. For SPE with a semi-crystalline polymer matrix like poly (ethylene oxide) (PEO), ion mobility is attributed to the segmental motion of the amorphous phase of the macromolecular chain. Epoxidized natural rubber is derived from natural rubber by converting different percent of the carbon-carbon double bonds on the macromolecule backbone to the polar epoxy groups. ENR has good potential to be polymer host in SPE because of their distinctive characteristic such as low glass transition temperature (T_g), soft elastomeric characteristics at room temperature and good electrode-electrolyte adhesion [3]. Furthermore, the highly flexible macromolecular chain and the polar epoxy oxygen provide excellent segmental motion and coordinating sites for Li^+ ion transport, respectively in ENR-based polymer electrolytes [4-5]. However, Chan and Kammer [6], in their study on the properties of PEO/ENR/$LiClO_4$ solid solutions concluded that the solubility of the ionic salt is comparatively higher in PEO than in ENR. Therefore, the conductivity mechanism as well as the role of the oxirane ring in the dissociation of ionic salt in ENR-salt complex will be investigated in detail. Other than ENR with 25 and 50% (mol/mol) of epoxidation (ENR-25 and ENR-50), deproteinized natural rubber (DPNR) will be used as a polymer reference [7].

Materials and Method

Material

Epoxidized Natural Rubber, ENR-25 and ENR-50 purchased from Malaysian Rubber Research Institute (Sungai Buloh, Malaysia), were used after mastication. The chemical structures of the two elastomers were shown in Figure 1. Deproteinized Natural Rubber (DPNR) was supplied by Green HPSP (M) Sdn Bhd (Petaling Jaya, Malaysia). $LiClO_4$ was purchased from Acrōss Organic Company (Geel, Belgium) and the solvent tetrahydrofuran was purchased from Merck.

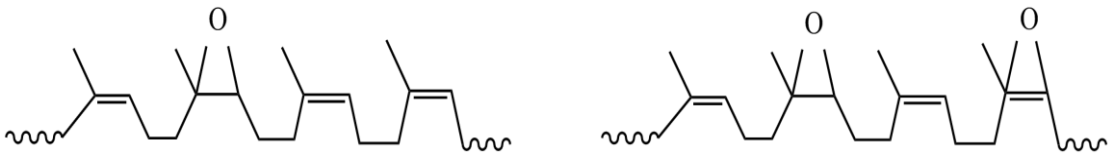

Figure 1: Chemical structure of (i) ENR-25, (ii) ENR-50

Sample preparation

The solid polymer electrolytes with ENR-25 and ENR-50 as the polymer host were prepared by solution casting technique. Appropriate amount of the rubber and $LiClO_4$ was dissolved in tetrahydrofuran by stirring with a magnetic stirrer at 50°C until a homogeneous solution was obtained. The $LiClO_4$ content (*Y*) added was varied in a range from 0.02 to 0.2 of the dry weigh of the polymer. It can be represented by

$$Y = \frac{\text{mass of salt}}{\text{mass of polymer}} \times 100\% \quad (1)$$

The electrolyte solution were cast into a Teflon dish and left to dry overnight at room temperature to form a thin film. The electrolyte films were dried in an oven for 24 h at 50°C before heating for another 24 h in nitrogen gas atmosphere at 80°C. This is to ensure a good interaction between the salt and the elastomer. The free standing film were put in vacuum oven at 50°C for another 24 h before storing in desiccators for further characterization.

Impedance measurements

The ionic conductivity measurements were performed using the HIOKI 3532-50 LCR Hi-Tester interfaced to a computer. The samples were scanned at frequency range from 100 Hz to 1 MHz at room temperature. The thin film samples were sandwiched between two stainless steel block electrodes of 20 mm diameter. The conductivity (σ) of each sample was calculated using the equation $\sigma = t / (R_b A)$, where t is the thickness of the sample, R_b is the bulk resistance and A is the cross-section area of the film. The R_b values were obtained from the Cole-cole plot which is the intersection at the x-axis. The average of the thickness, t was calculated from five measurements of the thickness of the thin film by using Mitutoyo Digimatic Caliper (Japan).

Differential Scanning Calorimetry

TA Q200 DSC which is calibrated with indium standard was used to study the thermal properties of the sample. For estimation of the T_g, approximately 10-12 mg of the sample was applied for each analysis. The samples were subjected to the following thermal history.

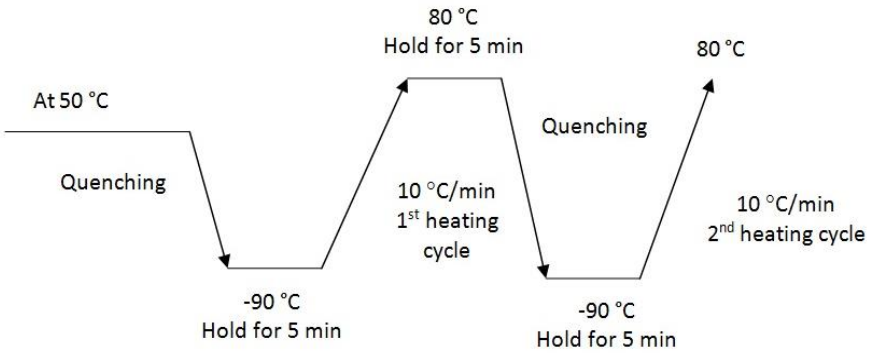

Figure 2: Thermal procedure for the determination of T_g by DSC

ATR-FTIR

Infrared spectra of all samples were obtained using ATR-FTIR Perkin Elmer at room temperature with frequency range of 4000 - 600 cm^{-1}. For each sample, 32 scans were taken at resolution 4 cm^{-1} using the Ge crystal plate.

Results and Discussion

Glass transition temperature

The glass transition temperature of a polymer observed as an endothermic shift from the baseline of a thermogram obtained using a differential scanning calorimetry (DSC), is governed mainly by the heating and cooling rates used in the DSC run. The T_g values, for all the three rubber samples, ENR-25, ENR-50 and DPNR, extracted from the second heating runs were presented in Figure 3. Among all the three salt-free rubber samples, DPNR recorded a much lower T_g value of -65°C compared to -42°C and -21°C for ENR-25 and ENR-50, respectively. An increase in the epoxidation level of ENR decreases the free volume of the chain phases leading to stiffening of the molecular chain structure is well documented [8].

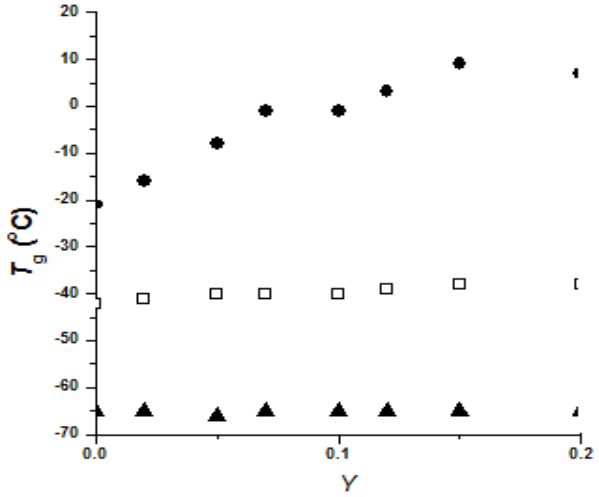

Figure 3: Glass transition temperature versus concentration of salt for (□) ENR-25, (●) ENR-50 and (▲) DPNR

Furthermore, Figure 3 depicts that the T_g values of the three rubber samples increase with ascending salt content from Y = 0 to 0.2. Similar result was also reported by Idris et al. [4].

The stiffening of the polymer chain upon addition of the ionic salt is caused by the coordination of the Li^+ with the epoxy oxygen of the oxirane group in the ENR. Therefore, ENR-50 with more epoxy oxygen in its macromolecule backbone as coordination sites for the Li^+ ion experienced a larger increase in T_g values from -21 to 9°C as the salt content increases from *Y*=0 – 0.2. On the other hand, there is only a slight increase in the T_g values of ENR-25 and DPNR with the incorporation of the same amount of salt. Increase in the T_g values of the modified natural rubber with the addition of salts suggests that the Li-salt is soluble in the rubber samples due to the complexation between Li^+ and the epoxy oxygen.

Conductivity

Ionic conductivity for ENR-25, ENR-50 and DPNR evaluated at different concentrations of Li-salt at room temperature were reported in Figure 4. The ionic conductivity of salt-free ENR-25 at room temperature is 2.1×10^{-8} S·cm^{-1} but increases to a maximum value of 2.7×10^{-7} S·cm^{-1} at *Y* = 0.15 as shown in Figure 4. Meanwhile, the conductivity for pure ENR-50 at room temperature is about 8.6 x 10^{-9} S·cm^{-1} and the conductivity increases to a maximum value of 5.3×10^{-8} S·cm^{-1} at the same salt concentration as ENR-25 (*Y* = 0.15). As the concentration of salt increases, the number of charge carrier will also increase, thus increases the conductivity of the polymer electrolytes. This is because the amorphous region in ENR promote the transportation of more free-charge carriers of lithium ion [9].

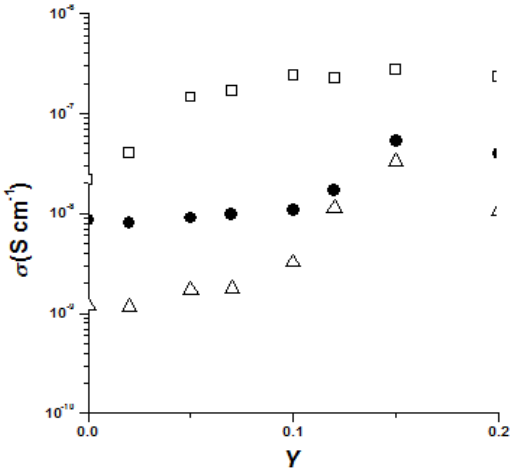

Figure 4: Ionic conductivity of (□) ENR-25, (●) ENR-50 and (Δ) DPNR as function of $LiClO_4$ at room temperature

Figure 4 shows that the ionic conductivity of both ENR-25 and ENR-50 increase with ascending salt content due to an increase in the number of charge carriers. Being a non-crystalline elastomer, the segmental motion of the macromolecular chain promote ion transport of the free-charge carriers of lithium ions within the polymer [9]. As mention in the discussion on T_g, the flexibility and the segmental motion of the polymer chain decreases with ascending salt concentration. Therefore, the ionic conductivity of ENR-50 is observed to be lower than that of ENR-25 at low salt concentration. A decline in the ionic conductivity is observed when the salt concentration, *Y* > 0.15 which is attributed to the increasing stiffness of the macromolecular chain which restricts ion transport within the polymer host [10]. The ionic conductivity of the solid solution of ENR-25 is the highest at all salt concentration, about one order in magnitude higher than ENR-50 and two orders in magnitude higher than DPNR. Therefore, the conductivity is higher with the less amount of epoxy content.

ATR-FTIR

The FTIR spectroscopy was used to determine the effect of the interaction between ENR-25, ENR-50 and DPNR with the lithium salt. The functional group and their wave numbers were tabulated in Table 1 [11].

Table 1: Functional group used in this study and their associated wave numbers

	ENR-25, cm^{-1}	ENR-50, cm^{-1}	DPNR, cm^{-1}
C-H stretching	2961, 2920, 2854	2961, 2919, 2853	2959, 2917, 2853
C=O stretching	1715	1711	1730
C=C stretching	1627	1626	1628
CH_2 scissoring, wagging, twisting	1448, 1377, 1309	1449, 1378, 1324	1447, 1375, 1305
Epoxy whole ring stretching	1248	1250	-
C-O-C stretching	1093, 1068	1069, 1071	-
Epoxy: half ring stretching	869	873	-

Figure 5 shows that the FTIR spectra for the deformation of CH_2 for ENR-25, ENR-50 and DPNR with various concentration of salt. The characteristic bands of saturated aliphatic C-H bonds are observed for C-H stretching and also the bending modes of CH_2 scissoring, CH_2 wagging, CH_2 twisting and C=C stretching mode confirmed the presence of the polyisoprene in the polymer matrix [12]. Not many changes have been observed in these bands mentioned above for all the three rubber samples.

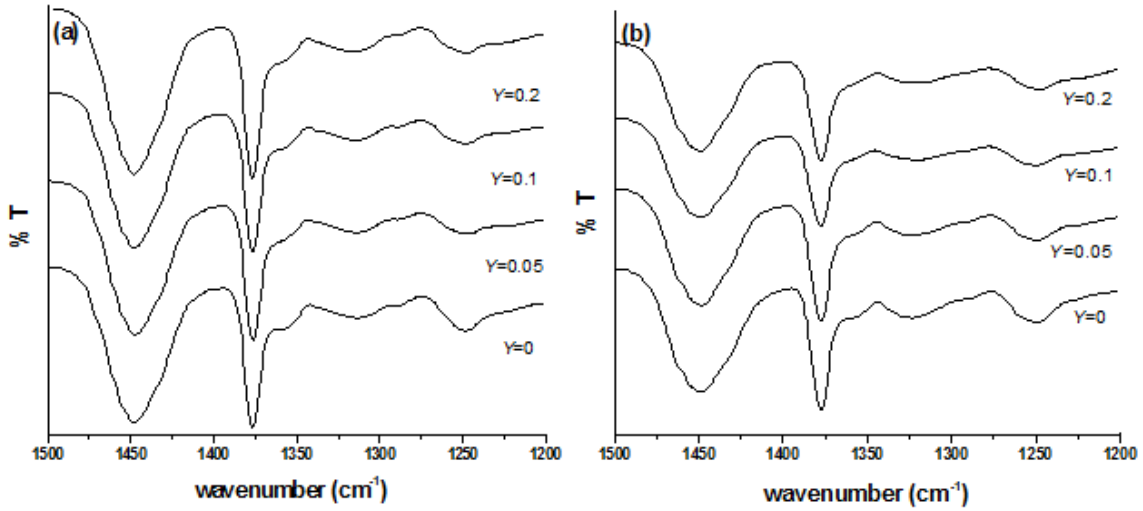

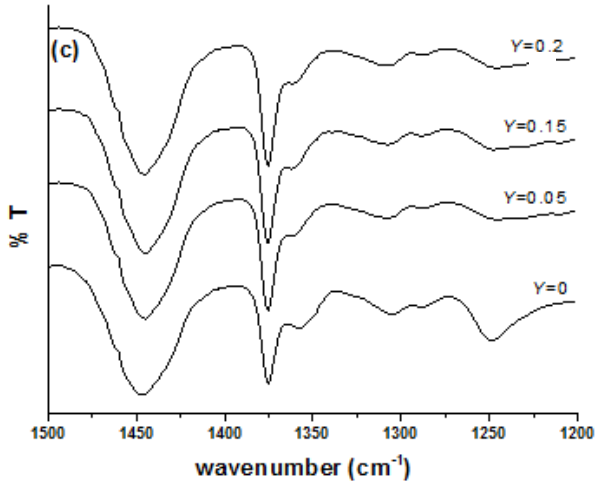

Figure 5: FTIR spectra of (a) ENR-25 (b) ENR-50 and (c) DPNR with different concentration of $LiClO_4$, *Y*; CH_2 scissoring, CH_2 wagging, CH_2 twisting

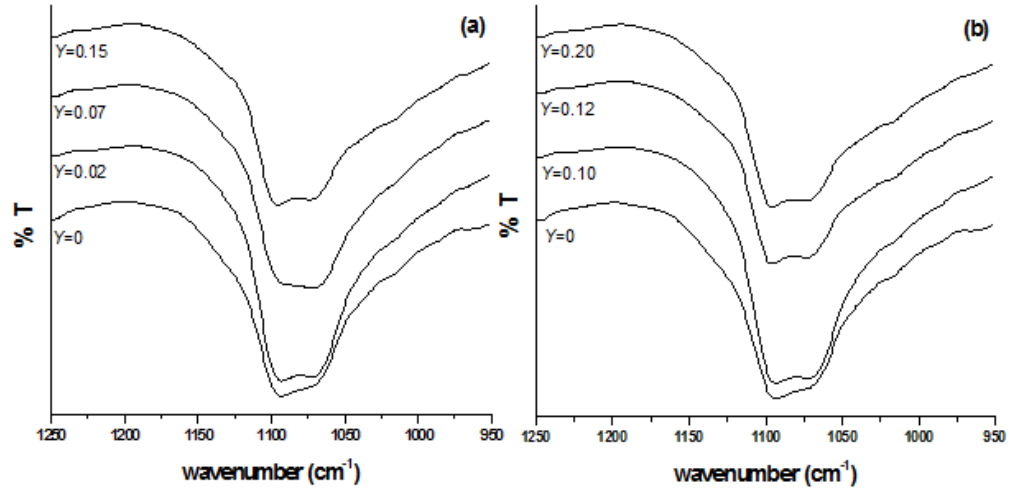

Figure 6: FTIR spectra of (a) ENR-25 and (b) ENR-50 with various concentration of $LiClO_4$, *Y*

for C-O-C stretching

The broad absorption band with the centre at 1080 cm^{-1} is assigned to the C-O-C stretching mode of the oxirane group in both ENR-25 and ENR-50 as shown in Figure 6. As the salt content in ENR-25 from *Y* = 0 to 0.15, there is a slight up shifting of the band. Moreover, Figure 6(a) demonstrated that the C-O-C absorption band becomes sharper and splits into two bands at 1094 and 1072 cm^{-1}. Similar behaviors are observed in the spectra of ENR-50. However, the salt-free C-O-C absorption band is much broader but becomes sharper and split into two peaks at 1069 and 1071 cm^{-1} as the salt concentrate on increases from *Y* = 0 – 0.15. At *Y* = 0.20, the C-O-C absorption peak downshifts to a moderately sharp peak at 1065 cm^{-1} with a broad shoulder at 1100 cm^{-1}. The changes observed in the spectra of ENR-50 suggest that more ionic salt has been coordinated to the oxirane groups of ENR-50 as compared to ENR-25. This result correlates with the higher T_g values observed in ENR-50 as discussed in the T_g section.

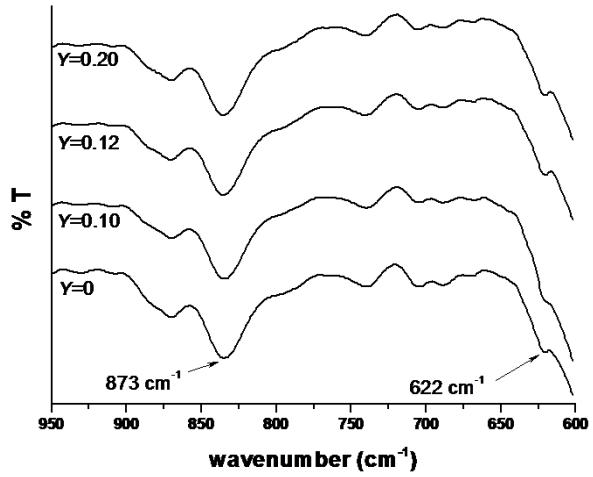

Figure 7: FTIR spectra of ENR-50 with different concentration of $LiClO_4$, *Y*

Besides, the absorption peak at 869 - 873 cm^{-1} corresponding to the oxirane ring of both ENR-25 and ENR-50 as shown in Figure 7 decreases in size when the salt content increases. Meanwhile, the sharpness of the peak at 622 cm^{-1} which is assigned to the spectroscopically free ClO_4^- ion increases as the concentration of salt increases in ENR-50 indicative of higher solubility of the salt in ENR-50.

Conclusions

Solid polymer electrolytes of ENR-25/$LiClO_4$, ENR-50/$LiClO_4$ and DPNR/$LiClO_4$ with various concentration of $LiClO_4$ were successfully prepared using solution casting technique. The effect of $LiClO_4$ on the conductivity, thermal properties and polymer-salt interaction of ENR-25 and ENR-50 were investigated by AC Impedance Spectroscopy, Differential Scanning Calorimetry and ATR-FTIR. The T_g values show that dissociation of the ionic salt is higher in ENR-50 with more epoxy oxygen which reduces the flexibility of the macromolecular chain, thus, decreases its segmental motion in ion transport resulting in a decrease in ionic conductivity as compared to that of ENR-25. In addition, the variation in the T_g values with increasing salt content correlates with the ion-dipole interaction observed in the FTIR result which conclude that the ionic salt is more soluble in ENR-50 as compared to ENR-25.

Acknowledgement

The authors would like to thank Faculty of Applied Sciences, UiTM for sample preparation and characterization.

References

[1] Fenton, D.E., J.M. Parker, and P.V. Wright, *Complexes of alkali metal ions with poly(ethylene oxide).* Polymer, 1973. 14(11): p. 589-589.

[2] Armand, M.B., M.J. Duclot, and P. Rigaud, *Polymer solid electrolytes: Stability domain.* Solid State Ionics, 1981. 3-4: p. 429-430.

[3] Latif, F., et al., *The Coagulation Impact of 50% Epoxidised Natural Rubber Chain in Ethylene Carbonate-Plasticized Solid Electrolytes.* Macromolecular Symposia, 2009. 277(1): p. 62-68.

[4] Idris, R., et al., *Polymer electrolytes based on modified natural rubber for use in rechargeable lithium batteries.* Journal of Power Sources, 2001. 94(2): p. 206-211.

[5] Latif, F., et al., *The role and impact of rubber in poly(methyl methacrylate)/lithium triflate electrolyte.* Journal of Power Sources, 2006. 159(2): p. 1401-1404.

[6] Chan, C.H. and H.W. Kammer, *Properties of solid solutions of poly(ethylene oxide)/epoxidized natural rubber blends and LiClO4.* Journal of Applied Polymer Science, 2008. 110(1): p. 424-432.

[7] Klinklai, W., et al., *Ionic conductivity of highly deproteinized natural rubber having epoxy group mixed with alkali metal salts.* Solid State Ionics, 2004. 168(1-2): p. 131-136.

[8] Gelling, I., *Modification of Natural Rubber Latex with Peracetic Acid.* Rubber Chem. Technol., 1985. 58(1): p. 86.

[9] Ali A M M, Y.M.Z.A., Bahron H and S.R.H. Y, *Electrochemical studies on polymer electrolytes based on PMMA-grafted natural rubber for lithium polymer battery.* 2006. 12(4-5): p. 303.

[10] Rahman, M., A. Ahmad, and S. Wahab, *Electrical properties of a solid polymeric electrolyte of PVC–ZnO–LiClO4.* Ionics, 2009. 15(2): p. 221-225.

[11] Van Zyl, A.J.P., et al., *Monitoring the grafting of epoxidized natural rubber by size-exclusion chromatography coupled to FTIR spectroscopy.* Journal of Applied Polymer Science, 2003. 88(10): p. 2539-2549.

[12] Pavia, D.L., G.M. Lampman, and G.S. Kriz, *Introduction to spectroscopy: a guide for students of organic chemistry*. 2001: Brooks/Cole.

THE EFFECT OF SILANE AS COMPATIBILIZER ON DISPERSION OF ORGANOCLAY AND CURING BEHAVIOR OF NR/BR/ORGANOCLAY NANOCOMPOSITES

Zahra Amini[1], Azam Jalali-Arani[2]
[1]*Polymer Engineering group, Mahshahr Branch,*
Amirkabir University of Technology
[2]Department of Polymer Engineering& Color Technology,
Amirkabir University of Technology, Tehran Iran

Abstract

In this work, nanocomposites based on NR/BR/Clay (60/40/5) were prepared by melt blending in an internal mixer, at a temperature of 80 °C and rotor speed of 60 rpm. bis(3-triethoxysilyl propyl) tetrasulfide in the name of Si75 was used as a compatibilizer and its effect on dispersion of organoclay and the curing behavior of prepared nanocomposites was investigated. Curing behavior of nanocomposites was evaluated by rubber process analyzer (RPA) equipment. The obtained results showed a slight decrease in the scorch and also cure times of nanocomposites by employing of silane. Minimum torque of rheometry (M_L) of nanocomposites was decreased in presence of silane; however the difference between maximum and minimum torque of rheometrey (M_H-M_L) was increased which was attributed to increasing of crosslink density. Nanocomposites exhibited higher tensile properties with the incorporation of silane due to the more intercalation of silicate layers by the rubber which was shown in the X-ray diffraction (XRD) patterns.

Keywords: *Cure, nanocomposite, organoclay, rubber,silane*

Introduction

Nanocomposites are defined as materials in which the particle size of the dispersed phase, at least in one dimension, is in the nanometer range. The addition of even low amount of organoclay in a rubber compound increases its tensile properties, decreases permeability and swelling in the solvents, and also it improves the abrasion and flame resistance of the vulcanized nanocomposite [1]. Montmorillonite (MMT) is the most commonly used layered silicate (clay) because of its natural occurrence and beneficial properties. The clays are hydrophilic and less compatible with organic polymers. Then for majority of polymers, owing to their hydrophobic character, the clay must be modified to enhance its compatibility with polymers. The clays can be modified with various alkylammonium salts [3].Modification expands interlayer distance of the layered silicate, reduces the surface energy [4-6] and enhances penetration of polymers into the galleries. It is well known that the mechanical, thermal, rheological, and barrier properties of the rubber/clay nanocomposites are extremely affected by two important factors: the degree of dispersion of the nano-filler in the matrix and the compatibility between the nano-filler and rubber.

The blend of Natural rubber (NR) and cis-1, 4-polybutadiene (BR) is widely used in the tire industries and the reinforcing of this blend is so important. In this study attempts have been made to prepare nanocomposite based on NR/BR/organoclay in presence of bis(3-triethoxysilyl propyl), Si75, as a compatibilizer. Different amounts of Si75 were used in the compounds and their effects on structure, curing behavior and mechanical properties of the nanocomposites were investigated and reported.

Experimental

Materials

NR, (SMR GP grade) with a Mooney viscosity of 61 (ML (1+4) at 100°C), was provided by Malaysia and BR, (BR1220) with a Mooney viscosity of 45 (ML (1 + 4)100°C), was obtained from Arak Petrochemical Co, Ltd (Arak, Iran). The used coupling agent, bis(3-triethoxysilyl propyl) tetrasulfide by the name of Si75 was obtained from Degussa company of Germany. Sulfur was supplied by Tesodak, zinc oxide by Sanaye Rangineh Pars, stearic acid by Unichema and accelerator and antioxidant by Bayer company. Organically modified montmorillonites (organoclays) was purchased from Southern clay products (Gonzales, TX) under the trade name of cloisite 15A. This organoclay has been modified by dimethyl dihydrogenated tallow quaternary ammonium.

Preparation and testes of the samples

The formulation of the compounds is given in Table 1. A brabender internal mixer (*PL 2200,* Germany) was employed to mix the ingredients of the compounds. Vulcanization characteristics of the compounds were measured according to ASTM D2084 test method with a rubber process analyzer *(RPA 2000).* Then, these compounds were cured at 150°C in an electrically heated hydraulic press according to their cure times (t_{90}) determined by the RPA test. Strength properties of the vulcanized compounds were measured on dumbbell shaped specimens in accordance with ASTM D412 test method, through using tensile testing equipment (*Instron 5800*, UK) at a crosshead rate of 500 $mm \cdot min^{-1}$. A *Philips*(Munich, Germany) model of wide-angle X-ray diffraction (XRD) equipment with Ni-filtered Cu$K\alpha$ radiation was used to study the expansion of the clay interlayer distance. The diffractogram was scanned in the 2θ range from 1 to 10^{o}.

Table 1: Formulation of the prepared nanocomposites

Material↓	S(0)	S(0.1)	S(0.2)	S(0.3)	S(0.4)
NR	60.0	60.0	60.0	60.0	60.0
BR	40.0	40.0	40.0	40.0	40.0
Silane (Si75)	-	0.1	0.2	0.3	0.4
Organoclay	5.0	5.0	5.0	5.0	5.0
Zinc oxide	5.0	5.0	5.0	5.0	5.0
St.A	2.0	2.0	2.0	2.0	2.0
Antioxidant	1.0	1.0	1.0	1.0	1.0
Sulfure+Accelarator	3.0	3.0	3.0	3.0	3.0

Results and Discussion

Cure characteristics

The effect of silane as a compatiblizer on the difference between maximum and minimum torque of rheometry for prepared nanocomposites is shown in Figure 1. Minimum torque is related to the viscosity of nanocomposites before curing .As can be seen in this figure incorporation of silane decreases the minimum torque, slightly.

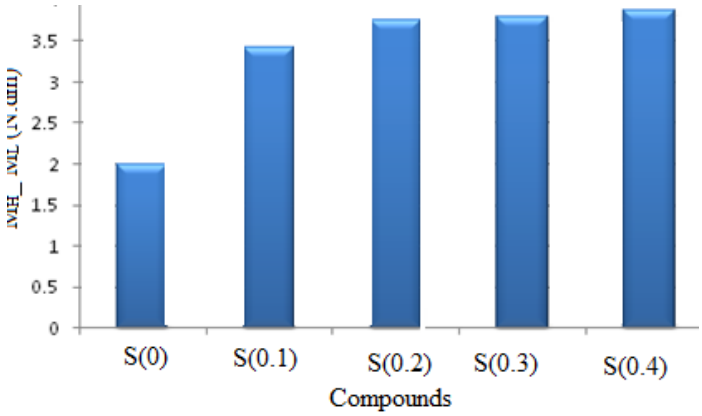

Figure1: The effect of silane amount on the (M_H _ M_L) of nanocomposites

This leads to a better process ability of the blend. M_H_ M_L is a measure of the dynamic shear modulus, which it relates to the crosslink density of the nanocomposites. M_H_ M_L is increased by using silane (Si75), which may be attributed to the presence of sulfur in the structure of Si75. This sulfur may affect the activation/crosslinking process. So, using of silane yields changes in the network density and clay dispersion, both of which influence the stiffness of the vulcanizates.

Figure 2 shows that the scorch and cure times of the compound decreases slightly by using Si75.This also may be due to presence of sulfur atoms in the structure of the used silane. Moreover, it can be said that as the silane causes more intercalation of the polymer chains in to the gallery between the layeres of organoclay, therefore facilitates the contribution of amine groups (come from intercalant) in the curing reaction.

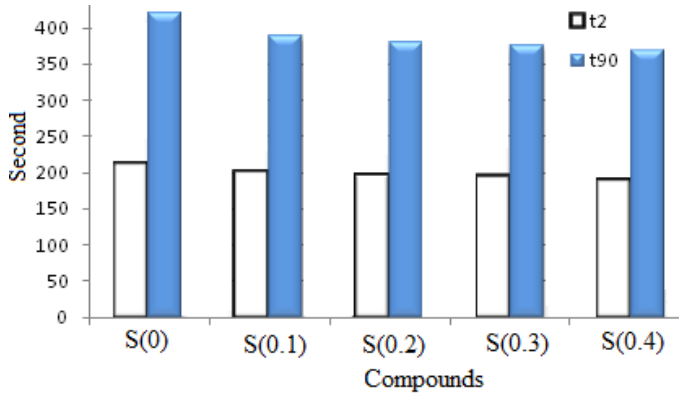

Figure2: The effect of silane amount on the scorch and cure times ofnanocomposites

Dispersion of organoclay

High-acting shear stress on the layers of organoclay during the mixing process and also the presence of polar curing agents in the compound favor the intercalation of the polymer chains into the galleries of organoclay and facilitates the dispersion of the layered silicates in polymeric matrix. In this work due to extremely high viscosities of rubbers (NR and BR), high shear stresses act on the clay layers during melt mixing and results in peeling off of the layers. Also, curatives used in the compounds including zinc oxide, accelerator, stearic acid, and sulfur, due their polar nature affect the intercalation process.

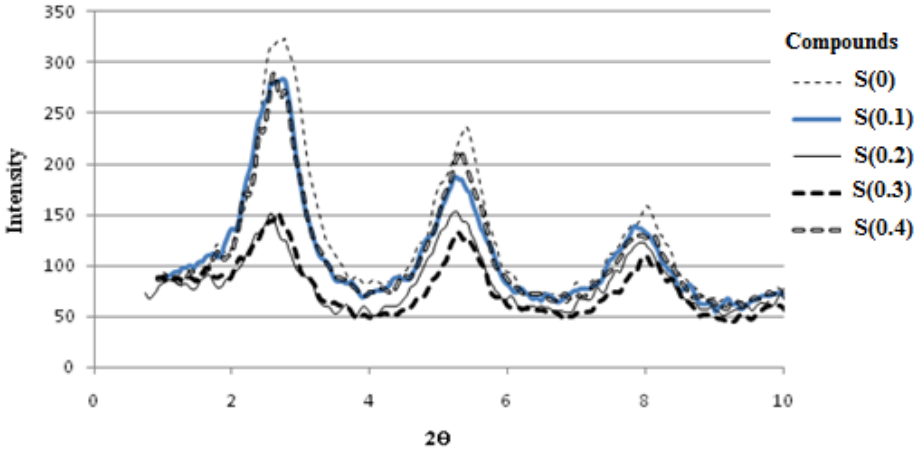

Figure3: X-Ray diffraction patterns of NR/BR/organoclaynanocompositescontaining different amounts of silane

Figure 3 shows the XRD patterns of NR/ BR/organoclay nanocomposites with different amounts of silane. The lowest diffraction peaks of the patterns represent the 001 plane reflections of the silicate layer. This peak for the nanocomposites containing 0, 0.1, 0.2, 0.3, and 0.4%, silane can be observed at 2θ angle equal to 2.77, 2.66, 2.62, 2.64, and 2.64 degrees corresponding to basal spacing of 3.791, 3.84, 3.891, 3.88 and 3.87nm respectively. In fact, intergallery distances in all of compatiblized nanocomposites containing silane are larger than that of incompatiblized one. It indicates that in presence of silane, more rubber molecules have been intercalated into the organoclay interlayer. Also 002 and 003 diffraction peaks are slightly shifted to lower angles in the XRD patterns of the NR/ BR/organoclay nanocomposites containing silane. Accordingly, the incorporation of compatibilizer in nanocomposite facilitates the penetration of polymer molecules in between the silicate layers. However, this does not result in complete disruption of the silicate tactoids or stacks. As a consequence the organoclay is intercalated by the rubber and not exfoliated. Finally, it is found that the best clay dispersion is achieved by adding silane in the amount of 0.2%. The results can be explained by mechanism of compatiblization which is shown in Figure 4.

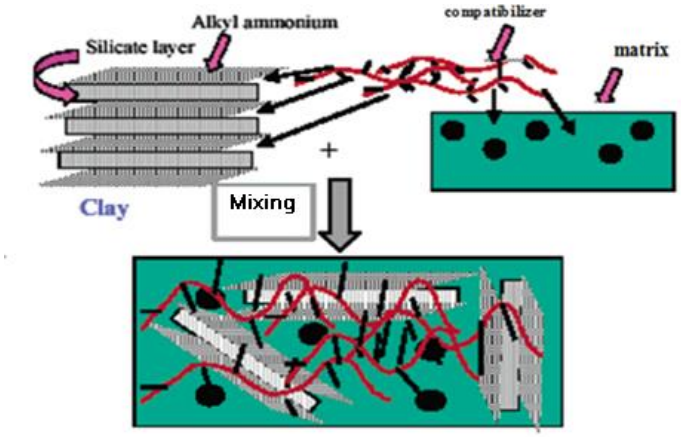

Figure 4: Mechanism of interaction of compatibilizer with the organoclay and rubber chain [4].

Mechanical properties

Figure 4 shows that the tensile strength and module of nanocomposites are increased by using up to 0.2% of silane due to more intercalation of the polymer molecules in to the interlayer distance of organoclay, confirmed by XRD results, and increasing of the interaction and surface area between organoclay and rubber molecules. However the use of a greater amount of silane results in the decreasing of tensile and module of nanocomposite. The same results are observed for the effect of silane on elongation at break (Figure 6).

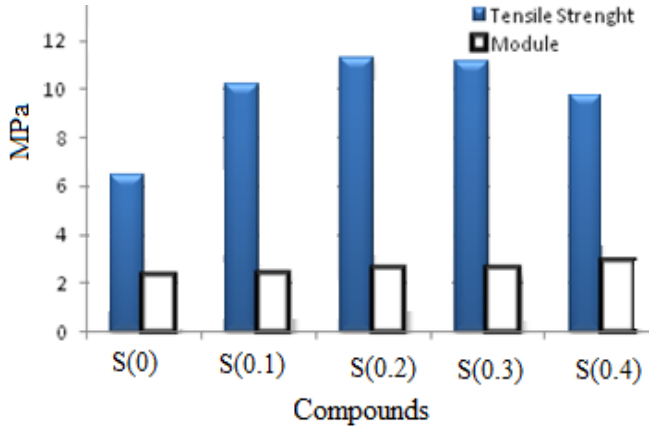

Figure 5: Tensile properties of NR/BR/organoclaynanocompositescontaining different amounts of silane

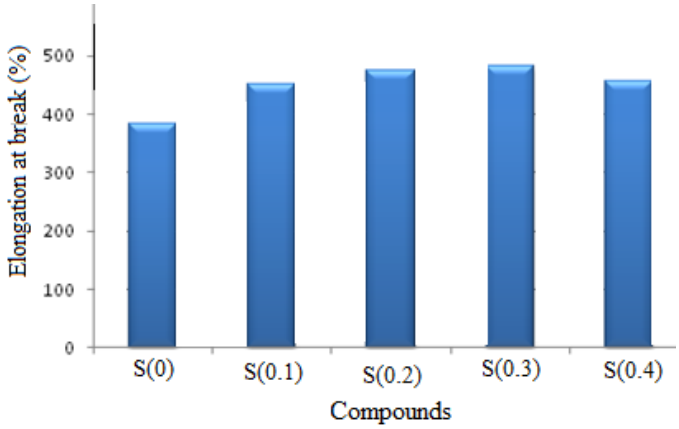

Figure 6: Elongation at break of NR/BR/organoclay nanocomposites containing different amounts of silane

Conclusion

The obtained results in this work show that the use of silane in NR/BR/organoclaynanocomposite causes a decrease in both scorch and cure times as well as an increase in the difference between maximum and minimum torque of rheometry which can be attributed to presence of sulfur atoms in the structure of silane and also the increase in the surface area between organoclay and polymer chains. The Xray diffraction patterns of nanocomposite confirmed a greater intercalation of polymer molecules in the presence of silane. Meanwhile incorporation of silane up to 0.2%, improved the tensile properties of nanocomposite.

References

[1] Gu, Z., Gao, L., Song, G., Liu, W., Li, P., & Shan, C. 2010. Octadecylammoniummontmorillonite/natural rubber/cis-1,4-polybutadiene nanocomposites. *Applied Clay Science* 50:143–147.

[2] Reichert, P.,Nitz, H., Klinke, S., Brandsch, R., Thomann, R., & Mulhaupt, R. 2000. Poly(propylene)/organoclaynanocomposite formation: Influence of compatibilizer functionality and organoclay modification. *Macromolecular Materials Engineering* 275:8-17.

[3] Li, J., Wu, J., &Chan,C. 2000.Thermoplastic nanocomposites. *Polymer* 41: 6935-6937.

[4] Halimatudahliana, Ismail, H., & Nasir, M. 2002. The effect of various compatibilizers on mechanical properties of polystyrene/polypropylene blend. *Polymer Testing* 21: 163-170.

[5] Park, H.M., Liang, X., Mohanty, A.K., Misra, M., &Drzal, L.T.2004. Effect of compatibilizer on nanostructure of the biodegradable cellulose acetate/organoclay nanocomposites *Macromolecules,* 37(24): 9076-9082.

[6] Alkadasi, N., Hundiwale, D.G., &Kapadi, U.R. 2004. Studies on the effect of silane coupling agent (2.0 percent) on the mechanical properties of fly ash filled polybutadiene rubber. *Journal of Scientific & Industrial Research* 63:603-609.

[7] *Pongdhorn*, S., *Sirisinha*, C., *Thepsuwan, U., &Hatthapanit, K.* 2006. Roles of silane coupling agents on propertiesof silica-filled polychloroprene. *European Polymer Journal* 42(3):479-486.

[8] Nakason, C., Nuansomsri, K.,Kaesaman, A., & Kiatkamjornwong, S. 2006. Dynamic vulcanization of natural rubber/high-density polyethylene blends: Effect of compatibilization, blend ratio and curing system. *Polymer Testing* 25(6): 782-796.

[9] Pasbakhsh, P., Ismail, H., Fauzi,m.n.a., & Bakar; A.A. 2009. Influence of maleic anhydride grafted ethylene propylene diene monomer (MAH-g-EPDM) on the properties of EPDM nanocomposites reinforced by halloysite nanotubes. *Polymer Testing* 28(5): 548-559.

[10] Zhang, H.,Datta, R.N.,Talma, A.G., & Noordermeer, J.W.M. 2010. *European Polymer Journal* 4(4): 754-766.

PROPERTIES OF HDPE/NR BLEND-LAYERED SILICATE NANOCOMPOSITES PREPARED BY MELT BLENDING

Engku Zaharah Engku Zawawi[1,a], Sahrim Hj Ahmad[2,b], Rozaidi Rasid[2,c]
Shamsul Bahri Ab Razak[3,d]
[1]Faculty of Applied Sciences, UniversitiTeknologi MARA, Shah Alam, Selangor, Malaysia.
[2]School of Applied Physics, Faculty of Science and Technology,
Universiti Kebangsaan Malaysia, Bangi, Selangor, Malaysia.
[3,d]Universiti Malaysia Terengganu, Malaysia

Abstract

Polymer nanocomposites of high density polyethylene (HDPE) and natural rubber (NR) blend were prepared using an organoclay (I.44P) via melt compounding in an internal mixer. The phase morphology of nanocomposites were characterizes by using X-ray diffraction, scanning electron microscope (SEM) and transmission electron microscope (TEM). The physical properties were examined with dynamic mechanical analysis and tensile tester. Test specimens were fabricated by compress moulding after the blending process. The X-ray diffraction results indicated intercalation of blend into the silicate interlayer of nano-filler and partially exfoliated of silicate layer in the blend. The organoclay was well dispersed in the matrix from the observation of transmission electron microscope. The tensile test showed that the stiffness and tensile strength of HDPE/NR blend was enhanced by the addition of low loading of organically modified montmorillonite. The incorporation of organoclay also increased the storage modulus of the nanocomposites.

Keywords: *Intercalation, melt blending, nanocomposites, organoclay, thermoplastic natural rubber*

Introduction

Thermoplastic natural rubber (TPNR) is known as a blend of natural rubber and polyolefin andits properties are between that of rubber and thermoplastic. The use of natural rubber (NR) is an advantage since it can be processed using conventional thermoplastic machinery. However, blending of rubber and plastic produces a thermoplastic elastomer (TPE) with inferior in their technical properties because of the presence of a weak rubbery phase and interface dispersed in a continuous plastic matrix [10]. This limitation can be overcome by modify their technical properties with the addition of fillers.

Currently, nanostructured fillers have become the main focus of attraction in the technology of polymer industries. Many researchers had studied the influence of silicate nano-fillers on the properties of polymer systems [5,13].This interest derives from the fact that the addition of small amount of nanofillers can significantly change a properties of polymer such as enhancement of tensile strength, modulus of elasticity, gas-barrier property, electrical conductivity, magnetic susceptibility and thermal stability properties[1,2]. The unique properties of polymer nanocomposites are achieved by dispersing nanometer scaled layered silicates having large surface area and aspect ratio in polymer matrices [6]. Naderi [8]reported that the dimensions of the interface and strength of the interaction significantly influence the tensile strength properties of nanocomposites. Therefore it is believed that the physical, mechanical and thermal properties of this polymer can be improved by adding the nanoclay into the TPNR even at low nanoclay composition. The morphology and mechanical behaviour of TPE reinforced with silicate clays have been studied by many research groups [3,4,5,15].

Polyethylene (PE) is the most widely used polyolefin polymer, due to many useful properties, light weight, low cost and good processability. One of the effective ways to fabricate PE/clay nanocomposites is by melt intercalation. In the melt intercalation process, the clay layers are directly dispersed in the molten polymers using the melt processing techniques. Normally good intercalation increased the modulus and strength but decreased the toughness of the nanocomposites[9,11,17].Therefore the presence of rubber phase in the PE/clay nanocomposites will improve the toughness of these nanocomposites. The aim of this study is to investigate the effect of organoclay (I.44P) content in the blend of HDPE/NR (TPNR) on the mechanical properties and correlation with their morphological properties of a composites prepared by melt blending process.

Material and methods

The HDPE material was provided by Polyethylene Malaysia Sdn. Bhd. The organoclay (nanomer I.44P) obtained from Nanocor was used as the reinforcement filler. This nanoclay was chosen according to its known suitability for polyolefin matrices. Natural rubber (NR), Standard Malaysia Rubber, SMR L was purchased from Guthrie (M) Bhd.

Nanocomposites containing 0, 1, 3 and 5 wt% of organoclay was prepared by melt-mixing in a Haake Rheomix (Model 600) with roller rotor and a mixing head with volumetric capacity of 69 cm^3. Mixing was performed for 14 min at a temperature of at 160^oC and speed of 80 rpm. HDPE pallet and NR were blended first for 4 minutes and was then mixed with organoclay. Prior to melt-mixing the organoclay was dried in the oven at 80 ^oC for 16 hours. The samples were then prepared by press moulded using hydraulic hot press, at a temperature of 160 ^oC and pressure of 100 bar, for a time period of 5 min followed by 5 min cooling under the same pressure.

Mechanical properties (tensile strength and tensile modulus) were measured using the Testometric tester at a crosshead speed of 50 mm/min, in accordance with ASTM D638. At least five specimens of each composition were tested for the tensile measurements, and the average values were reported. The dynamic mechanical properties of the nanocomposites were measure with a TA Instruments (Universal V3.IE). The three point bending method was used at a frequency of 1 Hz, in the temperature range of -100 to 120 ^oC. The heating rate was 5 $^oC \cdot min^{-1}$. The test was performed using rectangular bars with dimensions approximately 60 mm × 10 mm × 3 mm. The storage modulus and loss tangent (tan δ) values were measured for all samples under same conditions.

X-Ray Diffraction **(**XRD) measurements were performed to examine the basal spacing (d_{001}) of pure organoclay and nanocomposites using Bruker D8 Advance diffractometer. The samples were scanned over a 2θ range of 2-10^o.Transmission electron microscope (TEM) analysis was performed on ultra-thin film sample of nanocomposites, prepared by ultracryo-microtome with a diamond knife at -100^{o}C. The structure was observed using a Philips TEM model CM12 microscope. Scanning Electron Microscope study on the fracture surfaces of the gold-coated tensile test specimens were examined with a LEO 1450VP scanning electron microscope (SEM) at an acceleration voltage of 5 kV to evaluate the possible differences in fracture behaviour and to analyse clay dispersion.

Results and discussion

The XRD patterns of the composites of HDPE/NR with organoclay are presented in Figure 1. The d-spacing of organoclay calculated from Bragg's law was found to be 26 Å. The results clearly showed that the plane peak of the organoclay shift to angles smaller than that of organoclay, indicating that HDPE/NR has intercalated into the silicate layers of the clay. Thus has expended the basal spacing of the organoclay to 38 Å. The second peaks (d_{002}) shows there are some of intercalated of the blend matrices in between the Org-MMT platelets during

melt processing of the nanocomposites or might due to stacked clays. Modesti et al. 2006 reported this may due to the degradation of some alkyl chains during processing.

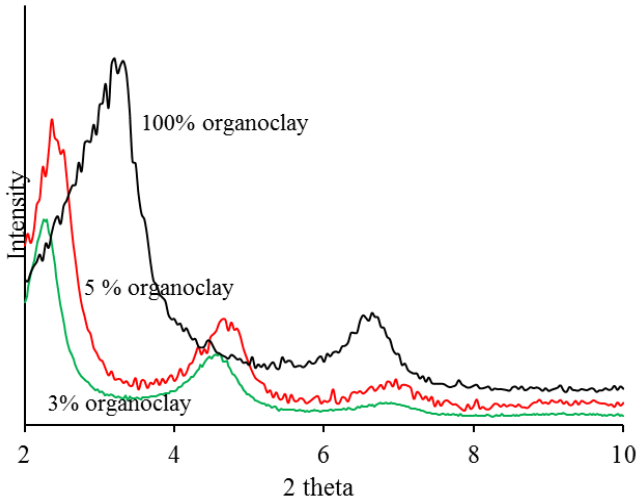

Figure1: XRD patterns of as received 20A clay and HDPE/NR-organoclay composites prepared by melt-compounding

TEM was used to determine the degree and level of dispersion of the nanoclays in the polymer matrix. TEM of HDPE/NR-organoclay composites in Figure 2(a) and (b) showing uniform distribution of organoclay with some small tactoids of staked clay layers are present in the matrix. The dark images represent clay tactoids [16,6] and the gray base represents the matrix and for the HDPE/NR nanocomposites with higher clay content (Figure 2(b)), larger tactoids are seen as compared to Figure 2 (a). Their corresponding high magnification views in Figure 2(c) and (d) shows existing of exfoliated nanoclay layers.

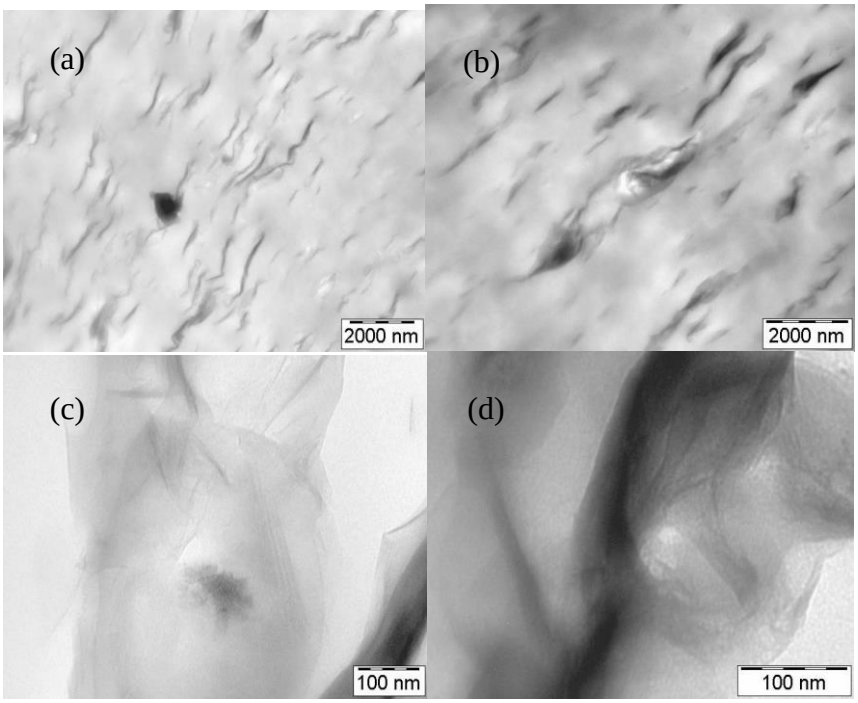

Figure2: TEM micrograph of HDPE/NR-organoclay composites of (a) 3 and (b) 5 wt% of organoclay and high-magnification of TEM of nanocomposites (c) 3 and (d) 5 wt%

Figure 3 shows scanning electron micrographs of the HDPE/NR blend and nanocomposites of 3 and 5 wt% organoclay after tensile test. Wavy shear banding was observed on the fracture surface for HDPE/NR blend and nanocomposites. This indicates that HDPE/NR blend matrix under-went a plastic deformation during tensile test, resulting in extensive fibrillation of the matrix (Figure 3a). Incorporation of 5% organoclay into matrix does not suppress shear yielding or fibrillation of the matrix (Figure 3c). All the HDPE/NR-organoclay nanocomposites still fracture in a ductile mode during the tensile test.

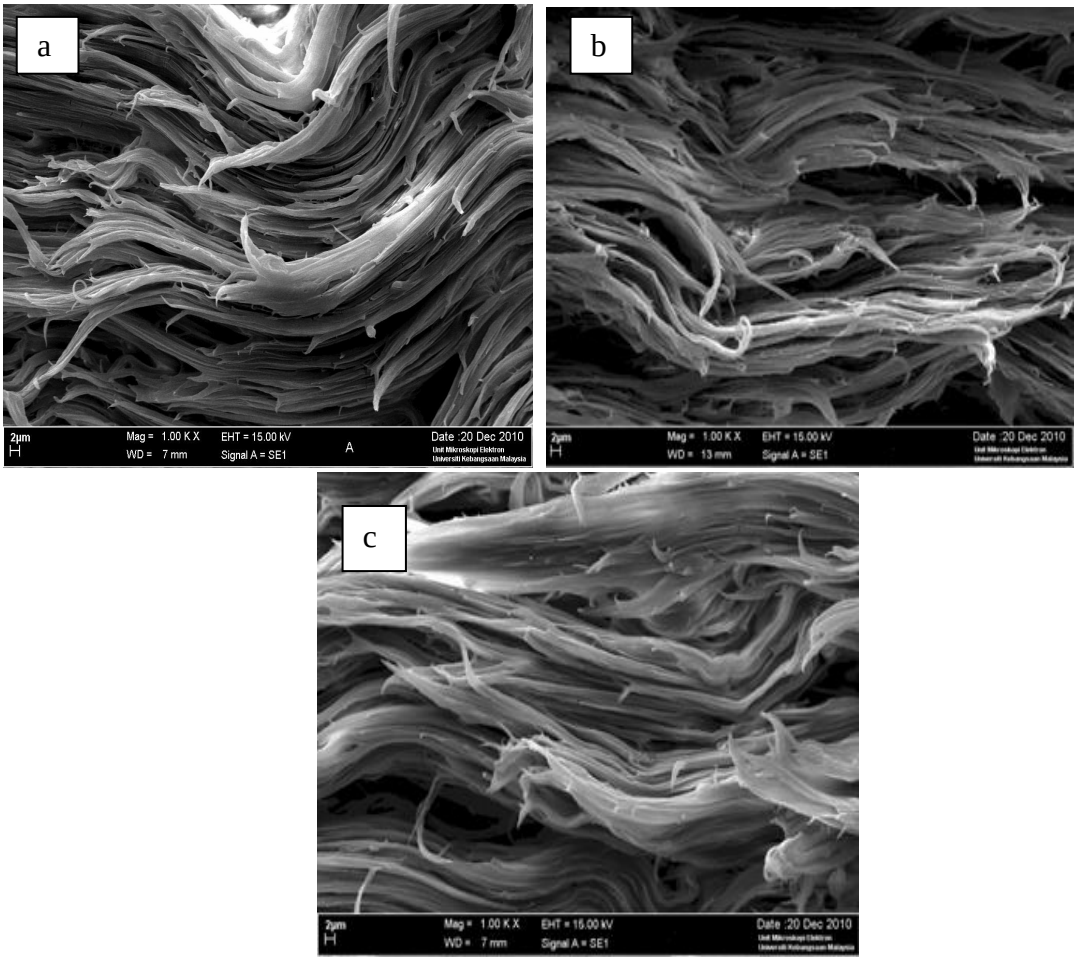

Figure3:SEM micrographs of the (a) HDPE/NR blend, (b) nanocomposites of 3 wt% clay and (c) nanocomposites 5 wt% clay after tensile test

The tensile modulus and tensile strength of HDPE/NR blend and their nanocomposites are shown plotted versus organoclay content in Figure 4(a) and (b) respectively. The results in Figure 4(a) shows the addition of 5 wt% organoclay had increased the tensile modulus up to 50%, indicating the stiffening effect of organoclay on HDPE/NR blend due to the high modulus of organoclay and also attributed to the reinforcing characteristics of nanoclay with high aspect ratio [6]. Addition of 5wt% organoclay showed an increment in tensile strength (Figure 4b) up to 37 % as compare to the neat blend. The increased in the tensile strength with the increasing of clay loading is possibly due to the increased in the interfacial interaction and also attributed to the effect of organoclay uniformly dispersion as nanolayers in the polymer matrix. The mechanical properties of nanocomposites are directly related to the homogeneous clay

dispersion and exfoliation or intercalation in the polymer matrix. According to Tjong [14] it is known that a homogeneous dispersion of clay nanolayers in a polymer matrix will provide maximum reinforcement via load transfer and deflection of cracks resulting from an applied load.

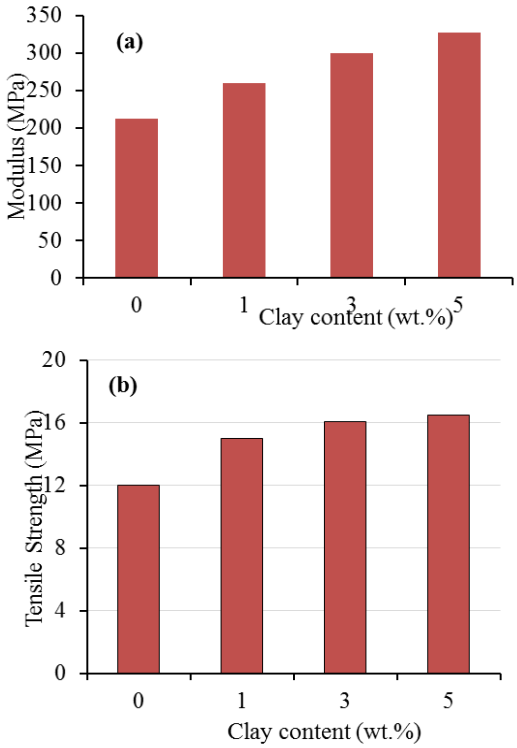

Figure4:Effect of the organoclay content on the (a) tensile modulus and (b) tensile strength of HDPE/NR/organoclay composites

Figure 5 depicts the results of storage modulus (E') of the materials over a range of temperature for the prepared samples. At the temperature below -60^{o}C the nanocomposites have a higher storage modulus (E') as compared to that of HDPE/NR blend. In general the three materials showed a similar trend in the storage modulus of the nanocomposites with the increasing in clay content. This results probably due to the increased in the stiffness of the matrix with the reinforcing effect imparted by the organoclay [12]. As the temperature approaches 20^{o}C, the modulus of the nanocomposites drops to match that of the HDPE/NR blend. The increasing in segmental polymer chain movement with temperature was lead to this behaviour. Figure 6 shows the loss tangent (tanδ) versus temperature for the samples. Tan δ are used to indicate the mechanical absorption or internal friction of the viscoelastic system. A high tan δ value signifies a material that will demonstrate a highly an inelastic deformation behaviour. The results show incorporation of organoclay up to 5 wt% does not alter the peak temperature (i.e. glass transition temperature) but slightly increased the peak height.

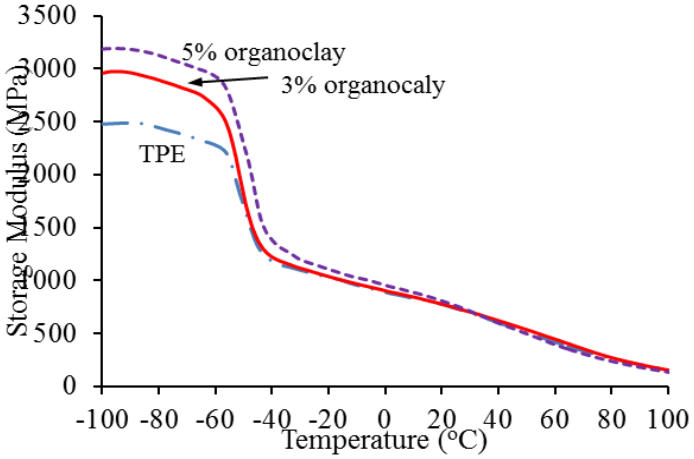

Figure 5: Storage modulus (E') of HDPE/NR blend (TPE) and HDPE/NR-organoclay nanocomposites containing 3 wt.% and 5 wt.%organoclay.

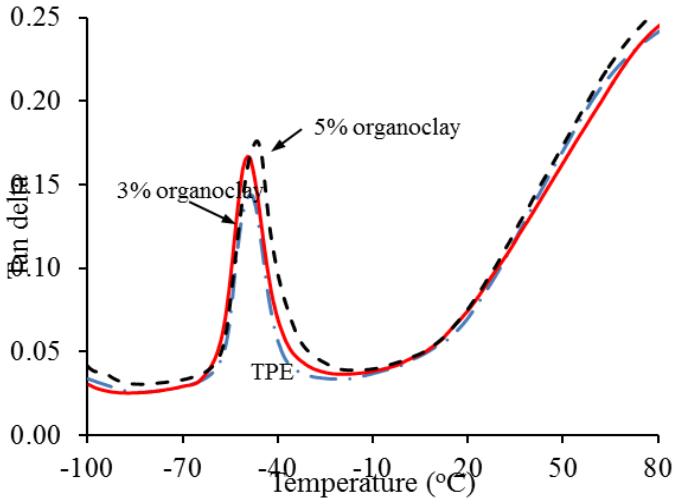

Figure 6: Tan δ of HDPE/NR (TPE) blend and HDPE/NR-organoclay nanocomposites containing 3 wt% and 5 wt% organoclay

Conclusion

TPNR/clay nanocomposites reinforced with 1 to 5 wt% organoclay were prepared by melt mixing followed by compression moulding. The mechanical and morphological of the HDPE/NR-layer silicate nanocomposites were investigate. The presence of organoclay causes an increase of stiffness and tensile strength of the HDPE/NR blend. The tensile fracture surface of neat TPNR and the nanocomposites exhibit a fibrillation.XRD measurements revealed the basal diffraction peak of organoclay in the TPNR nanocomposites shifted to lower angles, which implied the formation of an intercalated structure. TEM observation showed the formation of an intercalated structure in the nanocomposites.

Acknowledgements

Authors would like to express their sincere thanks to Rubber Research Institute of Malaysia for TEM sample preparation and Polyethylene Malaysia Sdn. Bhd. for kindly supplied the HDPE materials.

References

[1] Chiu, F-C., Lai, S. M., Chen, J. W. And Chu, P. H. 2004.*Journal of Polymer Science Part B Polymer Physics*. 42, 4139-4150.

[2] Gopakumar, T. G., Lee, J. A., Kontopodo, M. and Prent, J.S.2002. *Polymer*. 43, 5483-5491.

[3] Kim, D. H., Fasulo, P. D., Rodgers, W. R. and Paul, D. R. 2007. *Polymer*. 48, 5960-5978.

[4] Lu, Y-L., Li, Z., Yu, Z-Z., Tian, M., Zhang, L-Q. and Mai, Y-W. 2007. *Composites Science and Technology*. 67, 2903-2913.

[5] Maiti, M., Bandyyopadhyay, A. and Bhowmick, A. K. 2005. *J Appl Pol Sci*. 99, 1645-1656.

[6] Martins, C. G., Larocca, N. M., Paul, D. R. and Pessan , L. A. 2009. *Polymer*. 50, 1743-1754.

[7] Modesti, M., Lorenzetti, A. Bon, D. and Besco, S. 2006.*Polymer Degradation and Stability.* 91, 672-680.

[8] Naderi, G. Lafleur, P.G. and Dubois, C. 2007. *Polymer Engineering and Science*. 47, 207-217.

[9] Nikkhah, S. J., Ramazani, A., Baniasadi, H. and Tavakolzadeh, F. 2009. *Material and Design*. 30, 2309-2315.

[10] Pechurai, W., Nakason, C., and Sahakaro, K. 2008. *Polymer Testing*. 27, 621-631.

[11] Rong, M.Z., Zeng, M.Q., Zheng, X.Y., Walter, R. and Friedrich, K. 2001.*Polymer*. 42, 167-183.

[12] Sebastien, L., Jannick, D-R, Thi, N. P. And Jean-Francois, G. 2011. *J of Coll and Interface Sci*. 354, 555-562.

[13] Shou, Z., Buxton, G. and Balazs, A.C. 2003. *Composites Interfaces*. 10, 343-363.

[14] Tjong, S.C. 2006. *Material Science and Engineering*. 53, 73-197.

[15] Tjong, S. C. and Ruan, Y. H. 2008. *J ApplPolym Sci*. 110, 864-871.

[16] Xu Y, Ren X, and Hanna, M.A. 2006. *J ApplPolym Sci*. 79, 2146-2155.

[17] Zheng, H., Zhang, Y., Peng, Z. and Zhang, Y. 2004. *Polymer testing*. 23, 217-223.

RHEOLOGICAL STUDY FOR PREDICTING MOLECULAR CHARACTERISTICS OF POLYETHYLENE MELTS

Yodpradthana Samana[1], Pongdhorn Saeoui[2], Chakrit Sirisinha [1,3]

[1] Department of Chemistry and Center of Excellence for Innovation in Chemistry, Faculty of Science, Mahidol University, Bangkok 10400

[2] National Metals and Materials Technology Center, 114 Thailand Science Park Paholyothin Rd., Pathumthani, 12120, Thailand

[3] Research and Development Centre for Thai Rubber Industry, Faculty of Science, Mahidol University, Salaya Campus, Nakhon Pathom Thailand

Abstract

Three commercial grades of high density polyethylene (HDPE) with similar melt flow index (MFI) value as claimed by the manufacturer (IRPC Co., Ltd, Thailand) were investigated for their molecular characteristics including: molecular weight (MW), molecular weight distribution (MWD) and molecular branching by rheological techniques under shear and elongational flows. The present work aimed to find the optimal test conditions for classifying the molecular characteristics of given HDPE resins. Rheological properties of 3 grades of HDPE were measured using a parallel plate rheometer and a haul-off device with various test conditions. Results obtained reveal that the molecular characteristics could be determined effectively under oscillatory shear flow in low frequency region. Noticeably, the magnitude of branching could be monitored efficiently by a stress relaxation test. The longer the relaxation times, the higher the branching degree. Moreover, results of elongational flow as measured from the haul-off device are in good agreement with those of oscillatory shear flow.

Keywords: *Branching, molecular characteristics, rheology, polyethylene*

Introduction

Rheology is known to be useful for predicting processability of polymer melts. Typically, rheological behavior depends strongly on molecular characteristics and composition in polymer compounds [2]. Thus, the rheological properties are useful for solving problems mainly on polymer processing, and for investigating the molecular architecture of polymers including molecular weight (MW), molecular weight distribution (MWD) and degree of branching [9]. In rheological tests, the deformation could be divided mainly into 2 types, namely, shear and elongational deformations. In practice, the former gains more interests from rheologists due partly to the commercial availability of rheometers. The rheological test under shear deformation could be performed under oscillatory or steady flow. Since polymers are viscoelastic materials composing of two elements as spring (elastic part) and dashpot (viscous part), their responses depends strongly on time-scale of deformation. Polymers with different molecular characteristics would respond to such time in different manners [3,4,7,8,10,11].

In other words, the rheological results could be used to predict molecular characteristics of polymers with less complexity than the conventional techniques including a gel permeation chromatography (GPC) or a nuclear magnetic resonance spectroscopy (NMR) [6]. In the case of elongational flow, it is generally accepted to be important in many processing techniques including film blowing, fiber spinning, blow molding and sheet casting [5]. Unfortunately, there are only a limited number of rheometers available in the market. Among those rheometer, the haul-off device is widely used particularly for determining melt strength and drawablility of polymer melts, and for predicting the viscoelastic properties of polymer melts under elongational deformation [1, 12]. The present work aims to differentiate the molecular

characteristics of HDPEs having similar melt flow index (MFI) value under shear and elongation deformation.

Materials and method

Three commercial grades of HDPE, namely, GM2860, GM2865 and G2855, with similar MFI were kindly supplied by IRPC Co., Ltd., Thailand. Molecular characteristics of all HDPE as determined from GPC are shown in Table 1.

Table 1: Molecular characteristics of 3 commercial grades HDPE samples

Sample ID	MFI (g/10min)	Density (g/cm^3)	M_w	M_z	PI
GM2860	0.35	0.960	163,688	1,089,489	18.51
GM2865	0.35	0.964	166,330	948,967	16.37
G2855	0.35	0.955	198,064	1,518,927	15.9

Rheological test under oscillatory shear flow was conducted with the parallel plate rheometer (Physica model MCR500, Germany) equipped with a 25mm rotor. Test specimens were compression molded using a hydraulic hot-press. The frequency sweep test was performed at frequency range of 0.1-100 rad/s under the strain within a linear viscoelastic (LVE) region. A relaxation test was performed for predicting a long chain branching (LCB) degree by monitoring the relaxation modulus (G_t) as a function of time with the pre-shear deformation at 2 s^{-1}. All tests were carried out at test temperature of 190°C. The Goettfert Rheograph 2.5 equipped with the haul-off unit (see Figure 1) was utilized for monitoring the elongational deformation of HDPE melts. The extrudate strand was extruded from the capillary die with L/D ratio of 20/1 and entry angle of 180° at the extrusion rate of 0.2 $mm \cdot s^{-1}$. A measuring wheel equipped with force transducer was controlled in the range of 0-1 Nm. The strand was elongated at 46.5 $mm \cdot s^{-1}$ of starting pull-off speed (v_s) with linear accelerating velocity of 6 $mm \cdot s^{-2}$.

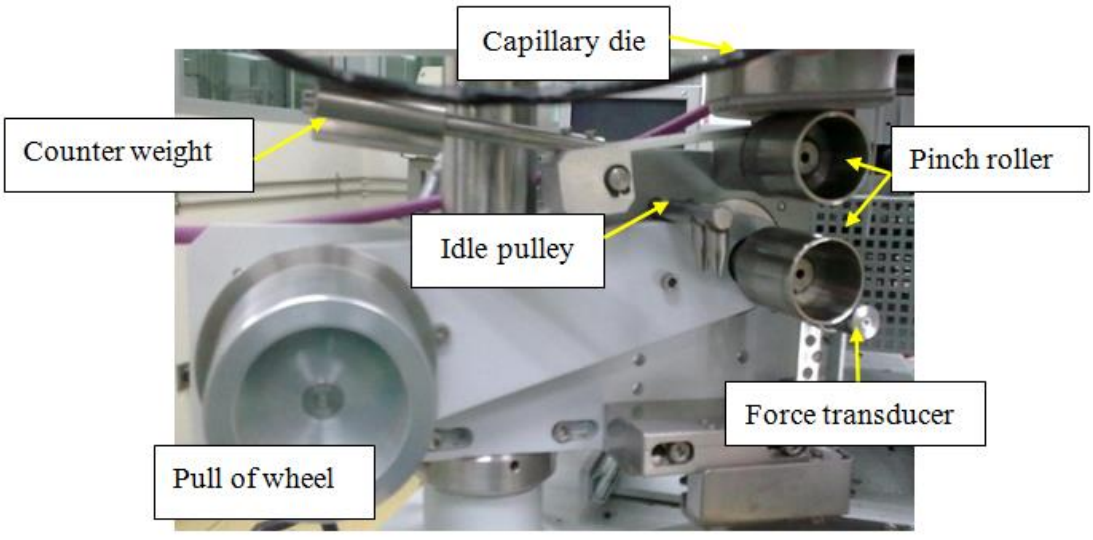

Figure 1: Schematic of Haul-off instrument

Results and discussion

Oscillatory shear flow measurement

Figure 2 shows molecular weight distribution of 3 HDPE samples as measured from GPC results at the test temperature of 145 °C. The average molecular weight of HDPE samples was reported as follows: G2855>GM2865>GM2860. Figure 3 reveals results of complex viscosity (η^*) as a function of angular frequency. With an increase in angular frequency, the η^* decreases, implying the pseudo-plastic or shear-thinning behavior of HDPE melts. The η^* results agree very well with MW results as determined from GPC technique, i.e., the η^* is highest and lowest in G2855 and GM2860, respectively. Referred to Table 1, all 3 HDPE possess similar MFI value, and therefore the discrepancy in viscoelastic behavior via storage modulus (G') as illustrated in Figure 4 suggests the advantageous capability of oscillatory over the capillary rheometers (or the melt flow indexer) for characterizing the molecular characteristics. The G2855 yields the highest G' with lowest frequency dependency in the frequency range of 0.1-1 s^{-1}. This implies the greatest elastic contribution of G2855. Apart from MW, the branching degree is anticipated to be responsible for such high elastic contribution. Nevertheless, the G' of all HDPE appears to superimpose at high frequency which is caused by the insufficient time for molecular motions.

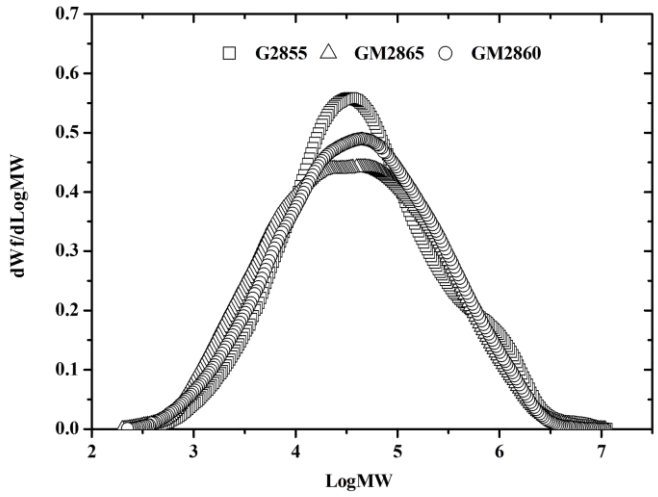

Figure 2: Comparison of MWD of 3 HDPE with similar MFI values

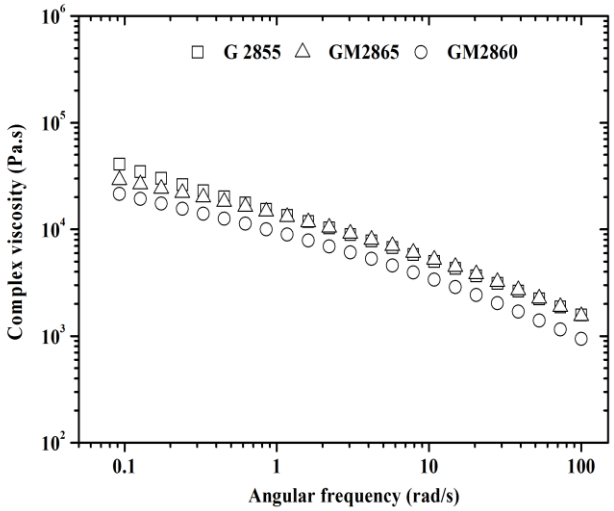

Figure 3: Complex viscosity as a function of frequency of HDPE with different molecular characteristics performed at 190°C

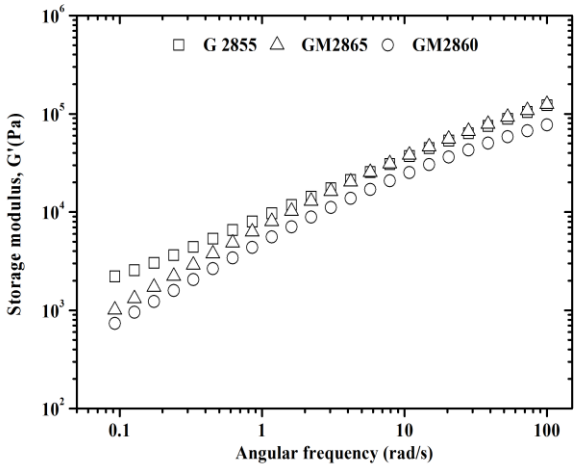

Figure 4: Storage modulus (G') against angular frequency for HDPE samples measured at 190°C

Steady shear flow measurement

Stress relaxation test under steady shear flow is known to provide some information on molecular characteristics, particularly, branching degree in polymers. This is because the presence of branching could act as entanglement points restricting the molecular relaxation process to some extent [11]. Figure 5 demonstrates the relaxation modulus (G_t) as a function of time of 3 HDPEs. Evidently, the slowest relaxation process is observed in G2855, which is in good accordance with its highest G' as discussed previously in Figure 4.

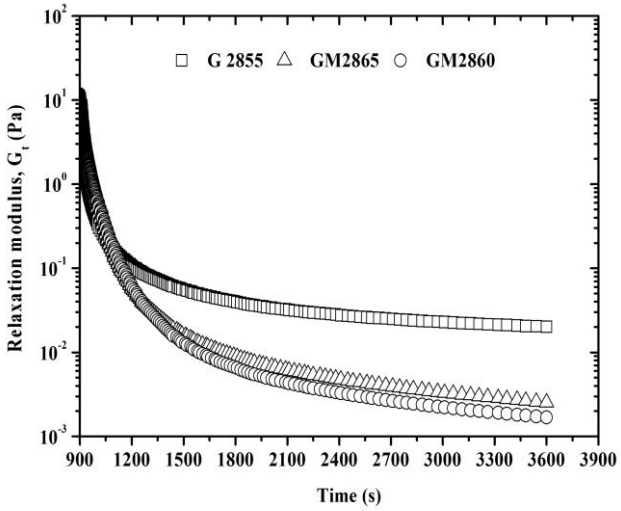

Figure 5: Relaxation modulus versus time at 190°C for HDPE samples

Elongational flow measurement

The effect of branching of all HDPE is emphasized by the utilization of melt spinning technique [12]. Figure 6 exhibits the results of measured force as a function of drawdown velocity. Clearly, the measured force of G2855 is highest suggesting the greatest melt strength. It is possible to state that the magnitude of discrepancy in branching degree could be detected by the elongational flow measurement.

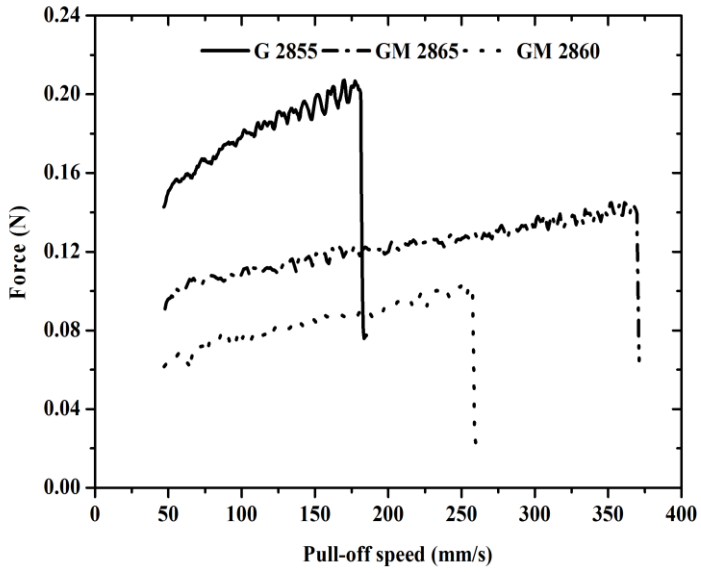

Figure 6: Melt spinning curves at extrusion rate of 0.2 mm·s^{-1}

Conclusion

Molecular characteristics of 3 HDPE with similar MFI value were monitored using rheological properties under shear and elongational flows. A discrepancy in molecular characteristics, especially, branching degree is detectable by the use of rheological behavior in the long time-

scale region (i.e., low frequency). The G2855 reveals relatively high elastic modulus in conjunction with relatively slow stress relaxation process implicating relatively high magnitude of long chain branching (LCB). Moreover, the prediction of LCB degree could probably be conducted via elongational flow by the use of melt-spinning technique. The G2855 yields the highest melt strength which is in line with the shear-flow results.

Acknowledgements

The authors would like to thank IRPC Co., Ltd., Thailand for supplying HDPE resins in conjunction with GPC test, and Center for Innovation in Chemistry: Postgraduate Education and Research Program in Chemistry (PERCH-CIC), Mahidol University for the financial support.

References

[1] Baldi, F., Franceschini, A. & Riccò, T. 2007. Determination of the elongational viscosity of polymer melts by melt spinning experiments: a comparison with different experimental technique. *Rheol. Acta.* 46 (7): 965-978.

[2] Dealy, J.M. & Larson, R.G. 2006. Structure and rheology of molten polymers: from structure to flow behavior and back again, 1-4. Munich: Hanser Gardner Publications, Inc.

[3] Kazatchkov, I.B., Bohnet, N., Goyal, S.K. & Hatzikiriakos, S.G. 1999. Influence of molecular structure on the rheological and processing behavior of polyethylene resins. *Polym. Eng. Sci.* 39 (4): 804-815.

[4] Lin, G-G., Shin, H-H., Chai, P-C. & Hsu, S-J. 2002. Influence of side-chain structures in the viscoelasticity and elongation viscosity of polyethylene melts. *Polym. Eng. Sci.* 42 (11): 2213-2221.

[5] Muke, S., Ivanov, I., Kao, N. & Bhattacharya, S.N. 2001. Extensional rheology of polypropylene melts from the Rheotens test. *J Non-Newtonian Fluid Mech.* 101 (1-3): 77-93.

[6] Nakajima, N. 1999 . Academic rheology and industrial rheology: a personal reflection (to the years 1960-1970). *Appl. Rheol*. 9: 116-125.

[7] Su, F-H. & Huang, H-X. 2010. Influence of polyfunctional monomer on melt strength and rheology of long-chain branched polypropylene by reactive extrusion. *J Appl. Polym. Sci.*116 (5): 2557-2565.

[8] Tian, J., Yu, W. & Zhou, C. 2006. The preparation and rheology characterization of long chain branching polypropylene. *Polymer.* 47 (23): 7962-7969.

[9] Wagner Jr, J. 2010. First (ed.). Multilayer flexible packaging: technology and applications for the food, personal care and over-the-counter pharmaceutical industries, 13-57. USA: Elsevier Inc.

[10] Wei, X., Collier, J.R. & Petrovan, S. 2007. Shear and elongational rheology of polyethylenes with different molecular characteristics. I. shear rheology. *J Appl. Polym. Sci.* 105 (2): 309-316.

[11] Yan, D., Wang, W-J. & Zhu, S. 1999. Effect of long chain branching on rheological properties of metallocence polyethylene. *Polymer.* 40 (7): 1737-1744.

[12] Zhao, J. & Zhong, L. 2010. Elongation properties of low density polyethylene using melt spinning technique. *Polym. Test*. 29 (8): 972-976.

THE INFLUENCE OF MIXING TEMPERATURE ON SILICA REINFORCED NATURAL RUBBER

Siti Salina Sarkawi[2], W. K. Dierkes [1] & J.W.M. Noordermeer[1]
[1]University of Twente, Elastomer Technology and Engineering,
P.O. Box 217, 7500 AE Enschede, the Netherlands
[2]Malaysian Rubber Board, RRIM Research Station Sg. Buloh,
4700 Selangor, Malaysia

Abstract

Silica-rubber technology encompasses four important elements; the rubber polymer, silica, coupling agent and mixing technology. Since silica is highly polar and hydrophilic, it is not compatible with a-polar rubbers such as natural rubber. A bi-functional silane coupling agent is needed to enhance interaction on nano-scale by the creation of chemical links between the silica particles and the rubber molecules. Processing silica compounds is complicated because several chemical reactions need to take place: between the silica and silane or silanization, silane-rubber coupling and crosslinking between the rubber chains. The present investigation on the influence of mixing temperature on the properties of silica-filled natural rubber compounds using a silane coupling agent, demonstrates that the temperature development during the first mixing stage is of paramount importance as it affects the final properties. The rheological properties, Payne effect and rubber to filler interaction as well as physical properties of silica reinforced natural rubber at varying dump temperatures are discussed.

Keywords: *Natural rubber, silica, silane, reinforcement, tire*

Introduction

Mixing silica compounds involves many difficulties due to the large polarity difference between silica and rubber. In enhancing the compatibility of a-polar rubbers and silica, a bifunctional organosilane such as bis(triethoxysilylpropyl) tetrasulfide (TESPT) is commonly used as coupling agent. The formation of a hydrophobic shell around the silica particle by the silica-silane reaction prevents the formation of filler-filler networks by reducing the silica specific surface energy [1]. During vulcanization, coupling of TESPT with the rubber takes place forming silica-TESPT-rubber bonds. The chemical linkage between silica and rubber is thus the key for its reinforcement in the rubber compound.

The dump temperature is of paramount importance while mixing silica and rubber in presence of TESPT as coupling agent. Wolff has found that temperature has a more dominant effect than time in the silica-TESPT reaction [4]. In order to achieve a sufficient degree of silanization, the temperature during mixing should be above 130ºC. However, above 160ºC either the coupling agent starts to prematurely react with the rubber matrix or the TESPT starts to donate sulfur; both result in pre-scorch of the compound. Reuvekamp et al. demonstrated that a mixing time of at least 10 minutes at 150ºC is necessary to ensure complete coupling of the silica and the silane, and that the reaction between the silica and the silane takes place primarily during the first mixing step [2]. In the present study, the effect of mixing dump temperature on the properties of TESPT-modified silica-reinforced natural rubber is investigated. The rheological properties, Payne effect and rubber to filler interaction as well as physical properties of silica-filled natural rubber at varying dump temperatures of the first mixing stage are discussed.

Materials and methods

Standard Malaysian Natural Rubber (SMR 20) was provided by the Malaysian Rubber Board. Silica Ultrasil 7005 and bis-(triethoxysilylpropyl) tetrasulphide (TESPT) were supplied by

Evonik/Degussa GmbH. The compound recipe was based on a truck tire tread composition: SMR20 (100 phr), Ultrasil 7005 (55 phr), TESPT (5 phr), TDAE oil (8 phr), zinc oxide (2.5 phr), stearic acid (1 phr), antioxidant TMQ (2 phr), sulphur (1.4 phr), N-cyclohexyl-2-benzothiazyl sulphenamide or CBS (1.7 phr) and Diphenyl guanidine or DPG (2 phr).

The compounds were mixed in two stages. The first step mixing was done using a laboratory internal mixer Brabender Plasticoder 350S lab station with 70% fill factor, 60 rpm rotor speed and 14 minutes mixing time. The starting temperature of the mixing chamber and rotor was varied from 70 to 120ºC in order to obtain variable dump temperatures. Second step mixing was carried out after 24 hours rest, wherein the curatives were added on a two-roll mill.

The cure characteristics at 150ºC were measured using a RPA 2000 rheometer from Alpha Technologies, under the conditions of 0.833 Hz and 2.79% strain. Filler-filler interactions or Payne effect were determined from RPA strain sweep measurements at 100ºC and 0.5 Hz. The Payne effect was calculated as the difference between storage modulus, G' at 0.56% and G' at 100.04% strain. The Wolff filler-structure parameter, α_f was determined from the ratio between the increase in rheometer torque of the filled compound and that of the unreinforced gum: [3].

$$\frac{D_{\max} - D_{\min}}{D^{o}_{\max} - D^{o}_{\min}} - 1 = \alpha_f \frac{m_f}{m_p} \qquad (1)$$

where $D_{max}–D_{min}$ is the change in torque for filled compound, $D^{o}_{max}–D^{o}_{min}$ is the change in torque for gum compound, m_f /m_p is the weight ratio of filler to polymer, and α_f is a filler specific constant which is independent of the cure system and closely related to the morphology of the filler.

Bound rubber content (BRC) measurements were performed on masterbatches with toluene at room temperature for seven days. Tensile properties of the vulcanizates cured for their respective t_{95} at 150ºC, were measured using a Zwick Z020 tensile tester according to ISO-37. Scanning electron microscopy (SEM) of the fracture surface of vulcanizates was carried out using a JSM-5000 Neoscope Benchtop SEM.

Results and discussion

Cure Characteristics

The effect of dump temperature after the first mixing step can be clearly observed in the cure characteristics of the NR-silica compounds (Figure 1). The compounds with low dump temperature below 150ºC exhibit a two step cure curve with high torque as well as long scorch and cure times. The initial torque rise at the beginning of the vulcanization is associated with flocculation of silica in the compound indicating no or little silanization has occurred in the compound. Compounds with dump temperatures above 150ºC show no appearance of flocculation and provide progressively lower torque and shorter scorch times. Around 150ºC the in situ modification reaction of silica with TESPT occurs sufficiently fast to result in more silica surface covered with TESPT: increased hydrophobation of silica results in better dispersion in the NR. This prevents re-agglomeration of the silica. The compounds with the highest dump temperatures display the lowest maximum torques, no flocculation, the shortest cure time but also reversion of cure. The temperature during mixing will normally rise somewhat higher even than the final dump temperature. At temperature >160ºC, TESPT tends to disproportionate into the corresponding disulfide. The released sulfur reacts with reactive double bonds of NR to form crosslinks. Hence, at high mixing temperature TESPT acts as sulfur donor to NR during mixing, which will cause scorch or prevulcanization in the compound.

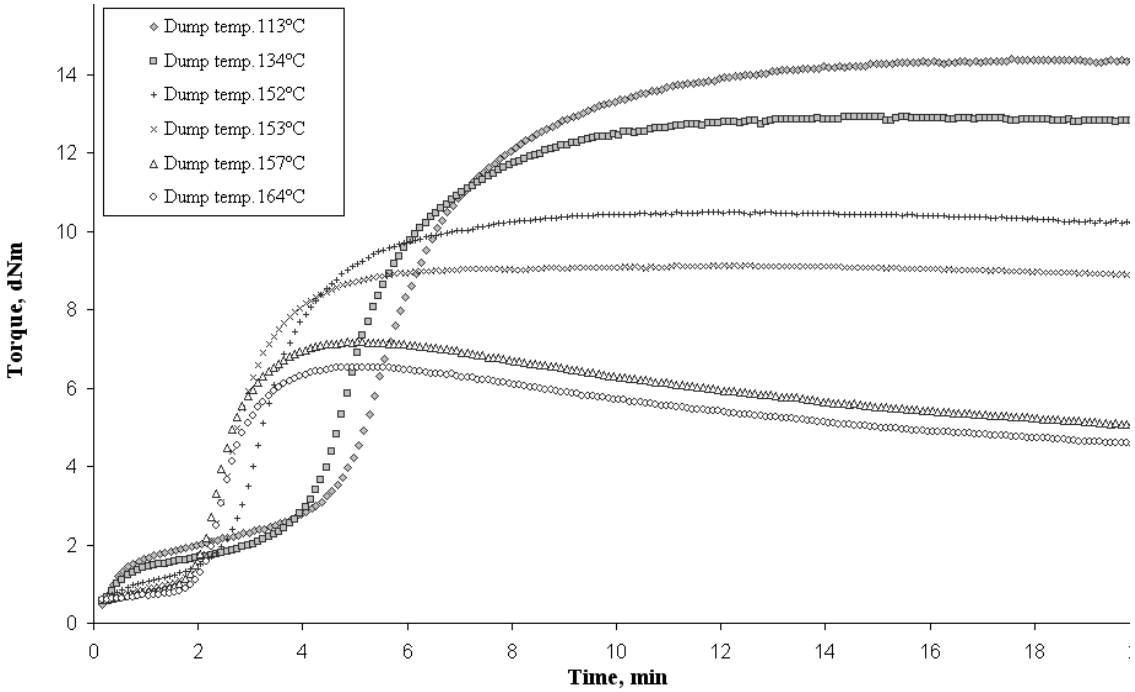

Figure 1: The cure characteristics at 150ºC of NR compounds mixed till different dump temperatures in the first mixing stage

Payne effect and rubber-filler interaction

The Payne effect for the compounds before and after vulcanization is illustrated in Figure 2. With increasing dump temperature, the silica-silica interaction reduces as seen in the drop of the Payne effect. The effect can be seen even more clearly after the compound is vulcanized. The conditions during the initial mixing stage are very important, as they persist into the final properties of the compounds. It also indicates that the reaction between silica and coupling agent may not be complete after the first stage of mixing. The silanization reactions may still continue in the subsequent mixing steps. At higher dump temperature more silanization reactions occur and the silica surface is hydrophobized.

Rubber to filler interaction is improved at higher dump temperature as seen in the bound rubber content of NR-silica compound in Figure 3. Ammonia treatment on the bound rubber of the NR-silica masterbatches separates the physically and chemically bound rubber. The chemically bound rubber content increases with dump temperatures up to 150ºC, but above 150ºC it stabilizes. The rise in chemically bound rubber and decreasing physically bound rubber up to 150ºC can be explained by the higher rate of silanization. At 150ºC, there is saturation in the amount of TESPT which has reacted and the surface of silica covered. Additional interactions above 150ºC between the non-hydrophobized silica surfaces are physical of nature.

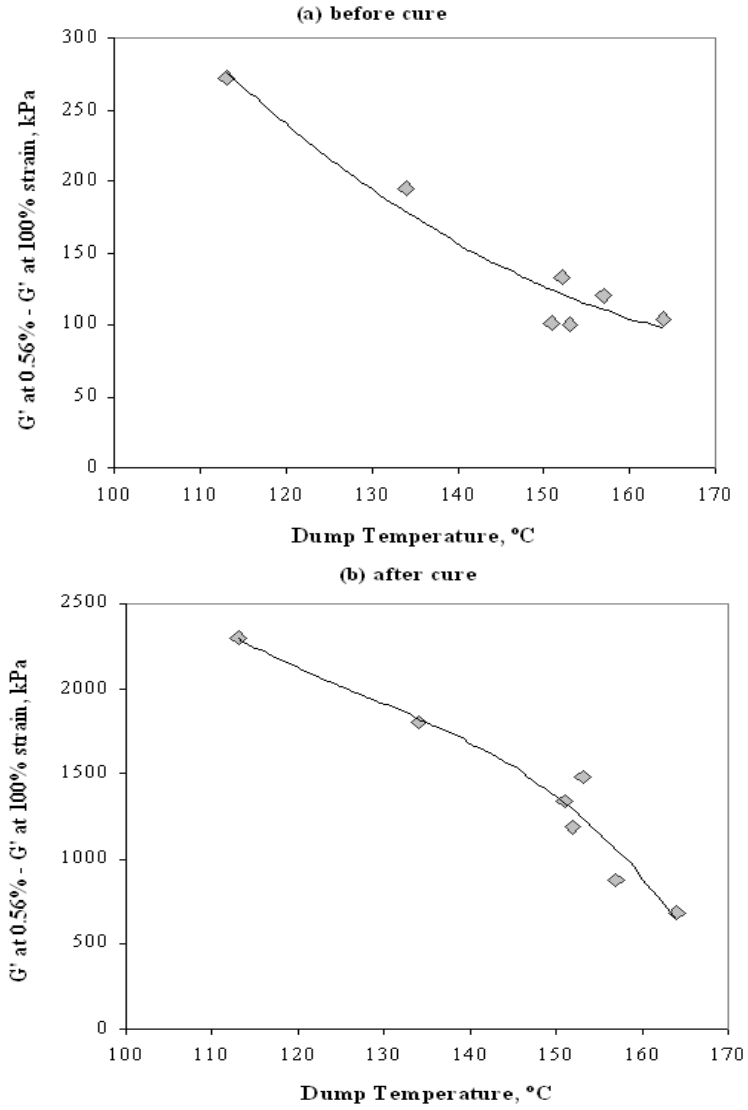

Figure 2: Payne effect of NR-silica compounds versus dump temperature (a) before cure (b) after cure

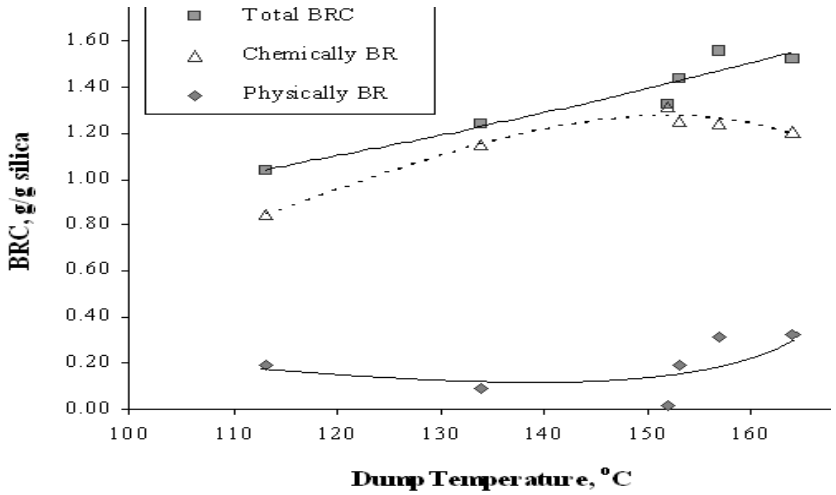

Figure 3: Bound rubber contents (BRC) of silica-filled NR at varying dump temperatures

The Mooney viscosities of the NR-silica compounds at varying dump temperature are depicted in Figure 4 (a). The Mooney viscosity increases with increasing dump temperature up to 150ºC. At dump temperature higher than 150ºC, the Mooney viscosity tends to become constant. It demonstrates that above 150ºC the optimal amount of TESPT is used to cover the surface of silica and this gives maximum silica-TESPT coupling.

The Wolff filler structure, α_f is plotted vs. dump temperature in Figure 4(b). α_f was defined as the structure of the filler as it exists in the vulcanizate after possible breakdown during mixing and vulcanization. With increasing dump temperature, α_f of NR-silica is greatly reduced. The values of α_f at dump temperatures above 150ºC are similar to those reported by Wolff for the TESPT-modified silica-filled NR and for reinforcing carbon black [4]. At higher dump temperatures, the hydrophobation of the silica surface led to reduced silica inter-aggregate interaction. It also indicates more filler to-rubber interaction to occur at higher dump temperature.

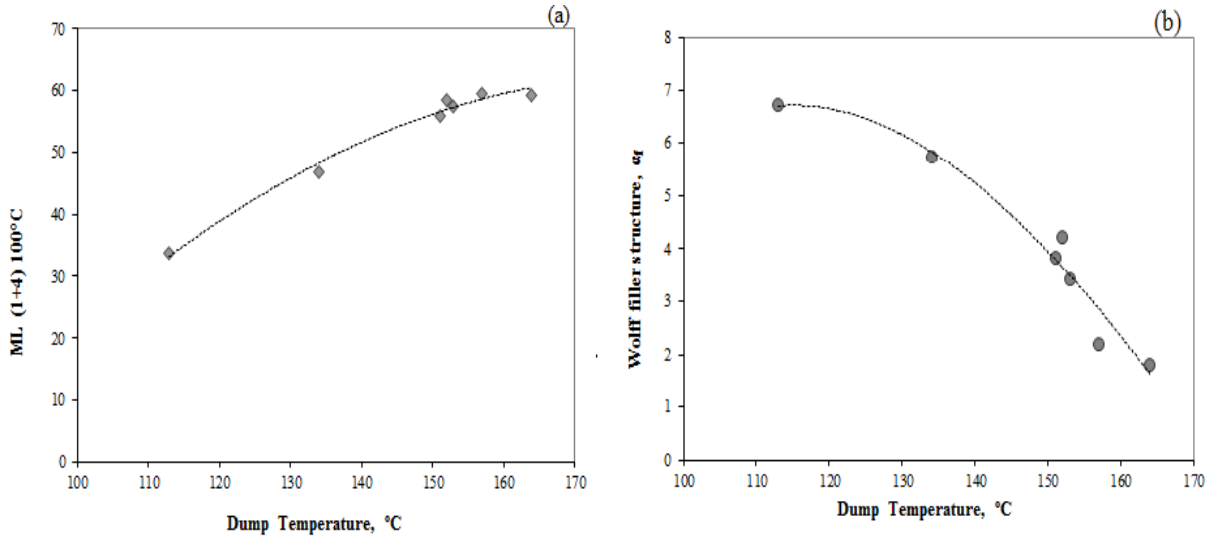

Figure 4: (a) Mooney viscosity and (b) Wolff filler structure parameter, α_f of silica-filled NR as a function of dump temperature

Physical Properties

Tensile properties of silica compounds at varying dump temperature are illustrated in Figure 5. They have an optimum at 150ºC dump temperature. The tensile strength and elongation at break drop at dump temperatures higher than 150ºC. Both moduli at 100% and 300% elongation are also reduced at dump temperatures above 150ºC.

Scanning Electron Microscopy (SEM) surface morphology

The surface morphology of fractured NR-silica vulcanizates is depicted in Figure 6. The macro dispersion (remaining agglomerates $\geq$ 1 μm) of silica in the NR vulcanizates can be seen in these pictures. Significantly less silica agglomerates are observed in the vulcanizate mixed at high dump temperature, due to the increased breakage of silica-silica interactions with higher efficiency of silanization.

Conclusions

The temperature conditions during the initial mixing stage of silica-NR compounds are of paramount importance as they seriously affect the final properties of the compounds. If insufficient temperature is reached during the initial stage, the silanization reaction between silica and coupling agent still continues in subsequent mixing or vulcanization steps. With increasing dump temperature, filler-filler interaction in a NR-silica compound decreases and silica-rubber interaction improves as evidenced by a drop in the Payne effect and increment in bound rubber content. The optimum temperature for silanization of silica with TESPT in NR is 150ºC and this gives a pronounced effect on the physical properties.

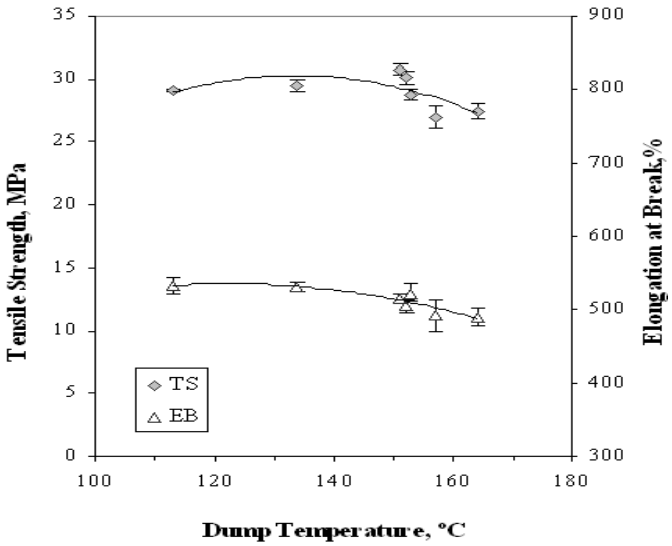

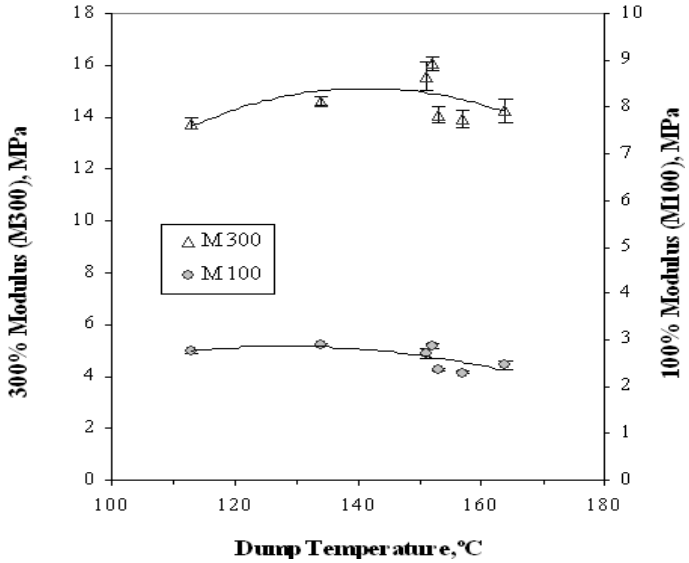

Figure 5: Tensile properties of NR-silica compounds at varying dump temperatures

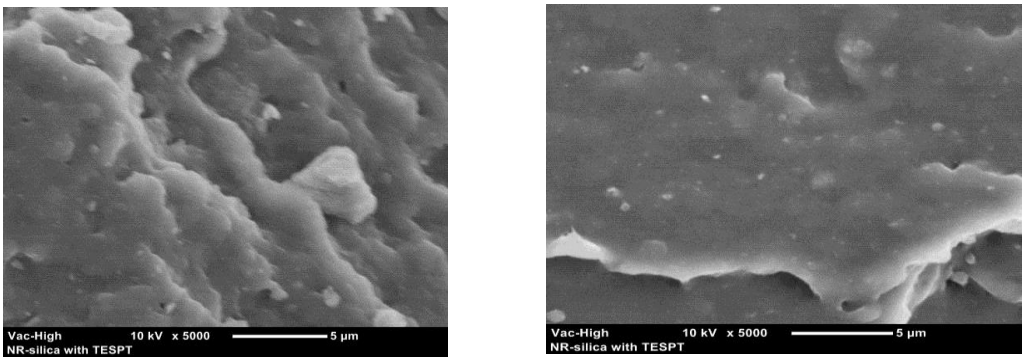

(a) (b)

Figure 6: SEM micrographs of NR-silica vulcanizates at low (a) and high (b) dump temperature

Acknowledgement

The authors would like to express gratitude for financial support from the Malaysian Rubber Board, Malaysia for this project.

References

[1] Noordermeer, J.W.M. and Dierkes, W.K., 2008 In White, J., De, S.K. and Naskar, K. (ed.) *Rubber Technologist's Handbook, Vol.2,* Smithers Rapra.

[2] Reuvekamp, L.A.E.M, ten Brinke, J.W., van Swaaij, P.J. and Noordermeer, J.W.M., 2002, *Rubber Chem. Technol.,75, 187- 198.*

[3] Wolff, S., 1970, *Kautsch. Gummi Kunstst., 23, 7-14;1981, 34, 280-284.*

[4] Wolff, S., 1982, *Rubber Chem. Technol*., *55, 967 – 989;* 1996, *69, 325 – 346.*

INTERFACIAL REACTION BETWEEN PETROLEUM COKE AND POLYPROPYLENE

SharifahShahnaz Syed Bakar[1,2], Rita Khanna[2], KamarudinHussin[1], VeenaSahajwalla[2]
[1]School of Materials Science, Universiti Malaysia Perlis,
Kompleks Taman Muhibbah, 02600 Jejawi, Perlis Malaysia
[2]Centre for Sustainable Materials Research & Technology, School of Materials Science & Engineering, University of New South Wales, Sydney 2052, NSW Australia

Abstract

In-depth wettability investigation was carried out to study interactions between polypropylene and petroleum coke (PC). The effect of two main parameters, temperature and time on the polymer properties and the effect of petroleum coke presence on the degradation process of PP have been determined. The wettability behaviour of PP has been carried out by soaking treatment at temperatures ranging from 200°C to 350°C and heat treatment up to 600°C on the soaked samples. The soaking treatment resulted in a negligible loss of polymer, indicating that PC was able to contain the PP degradation residues in its porous structures from escaping and devolatilized. The effect of heat treatment cycles on the blend of 10% to 90% of PP has also been investigated. No change was detected after Cycle 1 (up to 150°C); traces of polymer residue has been observed after Cycle 2 (up to 600°C); and polymer was completely lost after Cycle 3 (up to 1000°C).

Keywords: *interfacial reaction, petroleum coke, polypropylene, wettability*

Introduction

Plastics production and usage have grown significantly in the last 30 years and continued future growth is expected. Due to the relatively short life spans of plastic goods, there has been a tremendous growth in the generation of plastic wastes. Post-consumer plastic wastes are projected to increase to 30 million tonnes per year in the USA alone with the worldwide waste generation levels being much higher [3]. About 60% of wastes plastics are either incinerated or disposed off in landfills. There are serious environmental concerns regarding the use of these methods and this had led to an increased urgency to develop novel, cost-effective and environmentally sustainable recycling techniques. Although the waste plastic component in municipal solid waste (MSW) amounts to only ~10wt%, plastics have a high volume to weight ratio and are generally not biodegradable [4,5].

There is a scope to develop novel uses for polymeric wastes as a carbon source in industry. The commercial production of aluminium via the Hall-Heroult electrolytic process is an energy intensive process; the production of one tonne of aluminium requires ~13-16 MWhr of direct electric current, up to half a tonne of carbon, and two tonnes of alumina. Alumina is dissolved in a molten cryolite bath, and an electric current is passed through the solution, thereby separating alumina into aluminium and oxygen. The oxygen immediately reacts with the carbon anodes to produce carbon dioxide as an off-gas. The process consumes large amounts of sacrificial carbon from the anodes which are lowered to maintain a constant distance between the anode and the surface of metal pool (part of the cathode); therefore prebaked anodes must be replaced regularly. Carbon anode oxidation is responsible for almost 90% of the on-site CO_2 emissions from aluminium production (1.6 metric tonnes of CO_2 per metric tonne of primary aluminium). There is an increasing need for developing lower cost, robust anodes with performance superior to that of current anodes, with extended life, decreased CO_2 emissions and improved sustainability.

The aim of this research is to develop consumable carbon anodes for the aluminium industry using waste plastics. This study, for the first time, investigates high temperature interactions of polypropylene with petroleum coke. Carbon anodes are manufactured by baking blends of some varieties of coke with hydrocarbon binder, which is generally a coal-tar pitch [2]. Since waste polypropylene is rich in carbon and has low impurity levels, it has potential to be used as a cheap, readily available, auxiliary source of carbon.

Materials and method

Polypropylene used in this study was series PPR 2042 of type clear to opaque, white to off-white solid pellets form of samples purchased from Qenos Pty Ltd. It was a medium flow grade of polypropylene copolymer which has 4.0g/10 min melt-flow index (230°C/2.16 kg) (based on ASTM D1238) and 0.902 g/cm^{3}specific gravity. Petroleum coke clumps was supplied by Rio Tinto Australia. Samples were then sieved to segregates for particular particle size for further analysis and then ground by ring mill into fine powder.

The wettability analysis was prepared by mixing the PC powder with 5wt% phenol folmaldehyde binder and put onto roller milling machine for 24 hours to ensure homogeneous blend. Approximately 1.5 grams of petroleum coke and binder mixture were needed to make a 20 mm diameter x 5 mm thickness substrate discs, using mould and die pressed by 8kNx10 Enerpac 10 Tonne Model PEMA1321 Hydraulic Press machine. These discs were baked at 180°C for 24 hours to carbonize the binder and harden the substrates.

About 0.20-0.30 g of ground polymer was put on the petroleum coke substrate and the assembly was charged into horizontal tube furnace model HTF 6035 equipped with program control panel of Eurotherm 2116, using quartz tube under 1L/min argon flow. The assembly was placed onto graphite rod sample holder which was firstly filled and flattened by alumina powder and were heated at 150°C, 250°C and 350°C for 15 min, 30 min and 60 min (Figure 1). Heat treated assemblies were observed and recorded by digital camera. Assemblies were then mounted in epoxy resin. Mounted samples were then sectioned in the middle and polished for optical and SEM investigations.

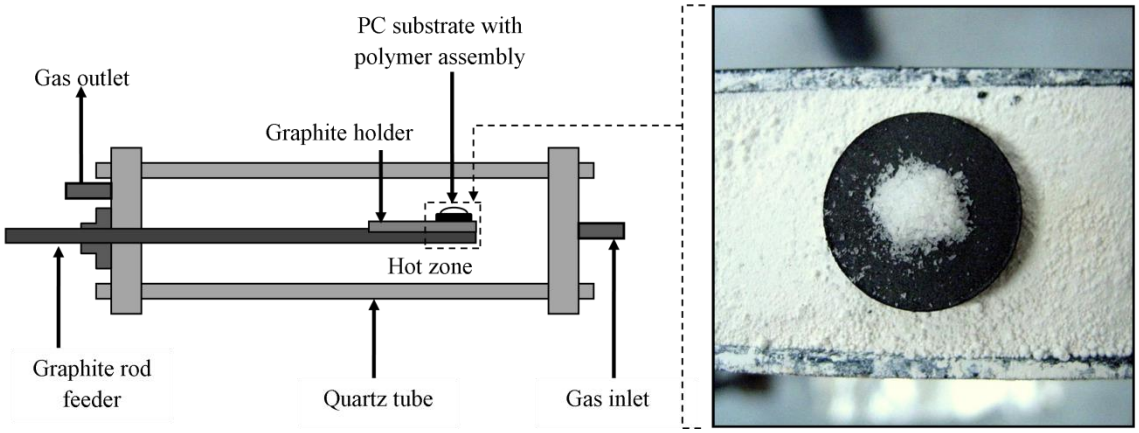

Figure 1: PP powder on PC substrate assembly on alumina powder based graphite holder in horizontal tube furnace

Samples were polished and coated with gold sputter for SEM investigations. Measurements of contact angle and depth of penetration of the molten polymer were carried out with the help of Photoshop CS5 software on SEM micrograph images. The techniques used for the measurement of contact angle and depth of penetration of the polymer melt on the petroleum

coke are shown in Figure 2. Depth of penetration was determined by measuring the distance up to which the polymer melt had gone through the petroleum coke particles.

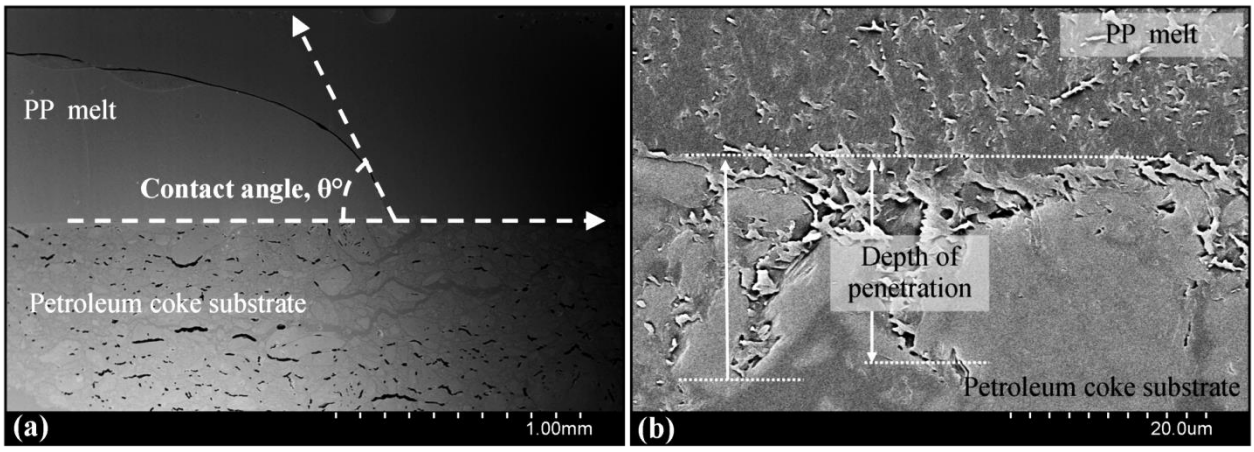

Figure 2: (a) Contact angle measurement and (b) depth of penetration measurement of polymer melt into petroleum coke substrate

The heat treatment of mixtures between PP and PC was carried out to investigate the possible physical or chemical reactions involved. PP has been mixed in full range from 10% to 90% (10% wt step increment) wt ratios, petroleum coke clumps were crushed into smaller aggregates with mortar and pestle and segregated by Retsch Seiving Machine type AS 200 Basic using 2–5 mm screen. Polymers were grounded using Fritsch knife grinder. The mixed samples of polymer and petroleum coke were placed on roller milling machine for 24 hours to obtain homogeneous mixtures. The mixture was put into an alumina crucible, and placed onto graphite rod feeder and held in the cold zone for 10 min to allow 1L/min argon gas to purge the horizontal tube furnace before pushing it into the hot zone. The heating cycles and experimental conditions used for various heat treatments are detailed in Table 1.

Table 1: Heat treatment method of polymer and petroleum coke mixtures

Heating Cycle	Baking method (1 L/min argon flow)
Cycle 1	Ambient temperature – heated to 150°C and dwell for 30 min – cooled to room temperature.
Cycle 2	Ambient temperature – heated to 150°C and dwell for 30 min – heated up to 600°C and dwell for 30 min – cooled to room temperature.
Cycle 3	Ambient temperature – heated to 150°C and dwell for 30 min – heated up to 600°C and dwell for 30 min – heated up to 1000°C – cooled to room temperature.

The treated samples were analyzed to determine the carbon content using LECO CS 444, a carbon and sulphur analyser of non-dispersive, infrared and digitally controlled instrument which is designated to measure the carbon and sulphur content in variety of samples. Sample weights were around 0.5 grams in the crucible and placed into instrument which had been preheated to 1250°C. The decarbonisation occurs at 1250°C and was held at that temperature until the estimation of carbon and sulphur content of the sample charged is complete.The PP sample was subjected to thermogravimetric Analysis (TGA) to determine the decomposition

mechanism. Thermogravimetric study was carried out using Perkin Elmer Thermogravimetric Analyzer – Pyris 1 TGA and analysed by its individual Pyris 1 TGA software.

Results and Discussion

Wettability investigations were carried out at 150°C, 250°C and 350°C focussed on the wettability and interfacial phenomena between PP and PC. Understanding interactions of these materials is important for assessing the compatibility of PP waste polymers with petroleum coke at elevated temperatures. The contact angle and the depth of penetration are reported as a measure of wettability and interfacial phenomena(Figure2). The images of the cross-sectional region of the reacted sample were captured by a digital camera, and these were used in the computation of contact angles. SEM micrographs of the interface were used to calculate the depth of penetration of the polymer into the coke. The interfacial behaviour of waste polymers will depend on the material properties as well as the temperature and the time of contact.

a) Wetting behaviour at 150°C

Figure 3 shows the images of the polymer on the coke substrate after different time intervals at 150°C. The experiment was carried out for time ranging between 15 to 60 min. No change was observed since the polymer did not melt even after 60 min.

i) 15 min ii) 30 min iii) 60 min

Figure 3: PP on petroleum coke substrate after exposure to 150°C for i) 15 min ii) 30 min and iii) 60 min

b) Wetting behaviour at 250°C

Figure 4 shows the variation in the wetting behaviour with time at 250°C. After 15 min, the melt was opaque, exhibiting raw PP properties (Figure 4a). PP melt was uneven in shape and had holes of various sizes in the polymer region. The fracture of the coke surface underneath the interfacial region of melted PP was also observed in this sample. When the sample was reacted for 30 min, some small voids were visible within the PP melt (Figure 4b). These bubbles may be caused by the devolatilization of PP during the heat treatment. The colour of the PP melt was lighter than that seen for the corresponding sample exposed for 15 min. Only one big void was observed in this sample, together with a few smaller cavities on the PP region. The cracking of the substrate was also detected in this sample. Figure 4c shows the wetting behaviour of the polymer after 60 min at 250°C. The PP melt had become yellowish with even lower transparency. Bubble formation was less compared to the sample after 30 min of heating. This indicates the reduced intensity of PP devolatilization after 60 min in the hot zone.

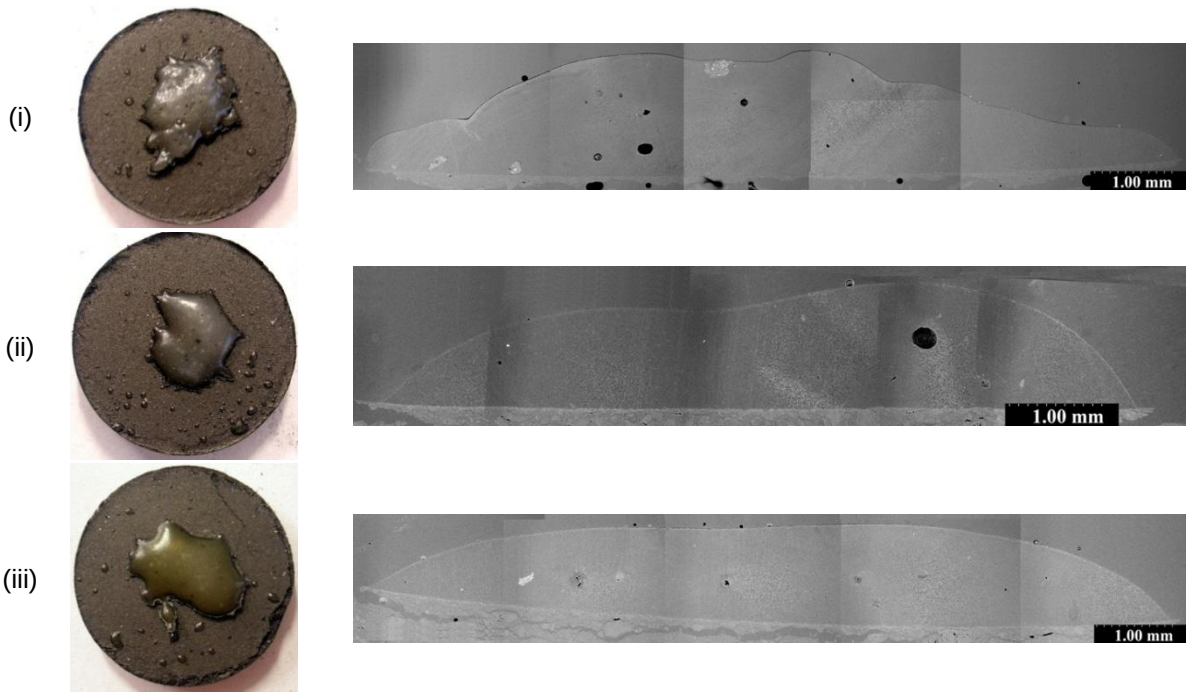

Figure 4: PP on petroleum coke substrate after (i) 15 min, (ii) 30 min and (iii) 60 min of exposure at 250°C

c) Wetting behaviour at 350°C

Figure 5a shows the image of sample after heating at 350°C for 15 min. A large number of small bubbles could be seen and in addition, one large cavity was seen in PP phase, showing the unmelted part of PP, indicating that 15 min is insufficient for PP to melt completely. Figure 5b shows the wetting of the polymer after 30 min of heating at 350°C. As viewed from the top of the PP melt, the sizes of bubbles were noticeably larger and these were present all over the droplet. A large void was also noted along with few cavities from the cross-sectional view. When exposure time was further extended up to 60 min (Figure 5c), the PP was fully melted and complete wetting of the petroleum coke substrate. PP formed a thin layer with a low contact angle on the coke substrate. The solidification of PP upon cooling resulted in the lifting up of the petroleum coke substrate surface.

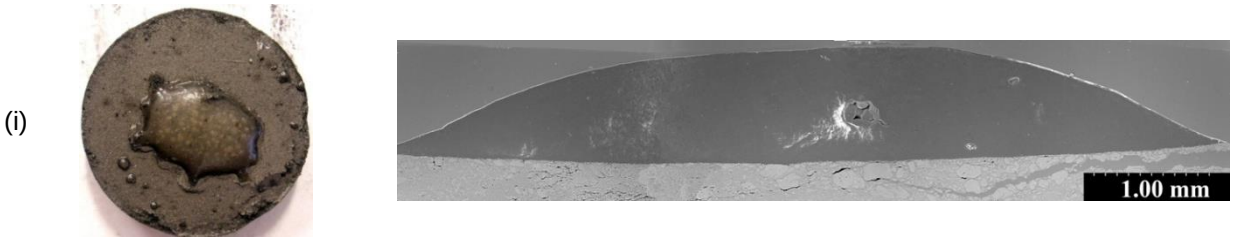

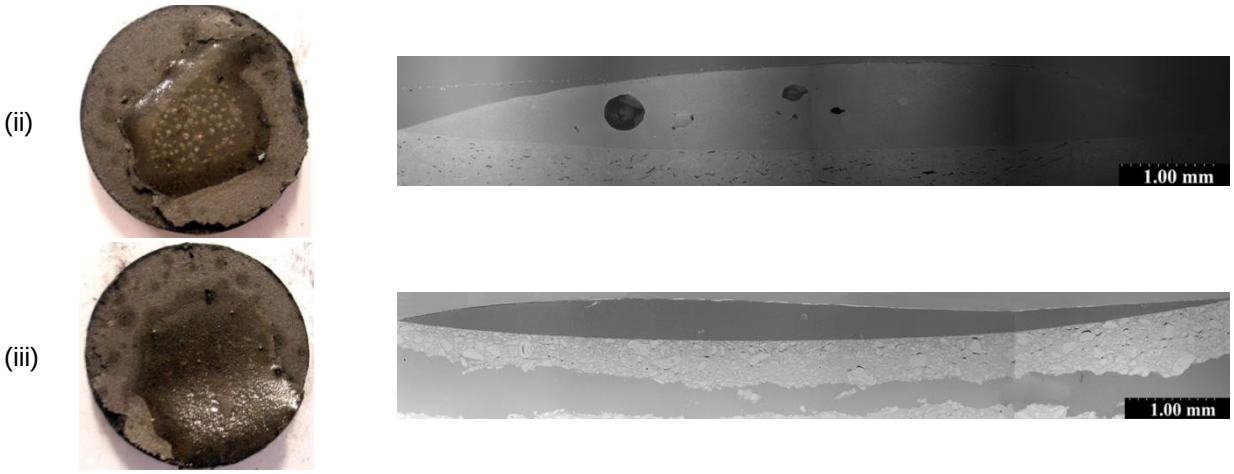

Figure 5:PP on petroleum coke substrate after (i) 15 min, (ii) 30 min and (iii) 60 min of reaction at 350°C

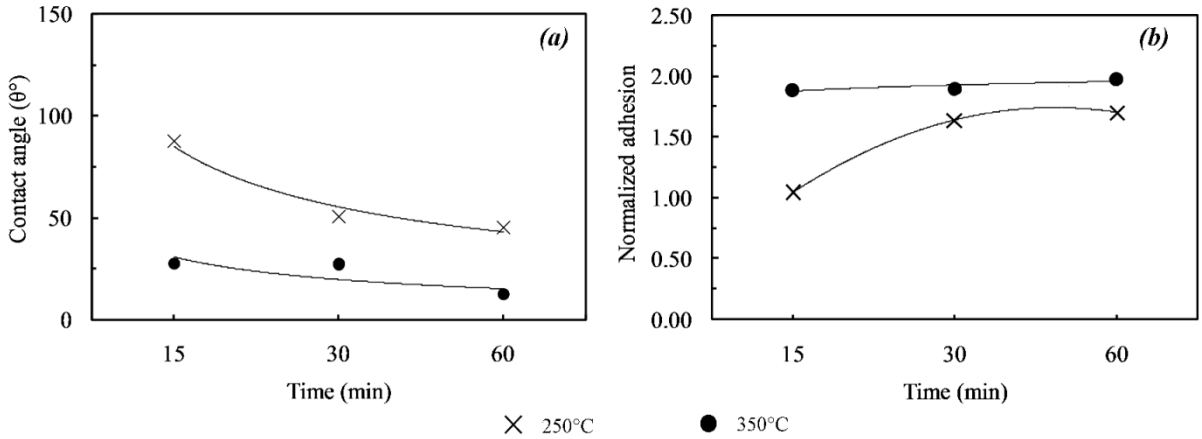

Figure 6: Effect of time and temperature on (a) contact angle and (b) adhesion of PP on PC substrate

When PP is heated, it first contracts and then swells to a much larger volume than its original size. This phenomenon can be seen at initial stage of heating (low reaction temperature and time, e.g. at 250°C after 15 min) where high contact angle was measured. The heating of polymer melt increased the devolatilization rate, which precede the transition from liquid to gas phase. Devolatilization occurs due to bubble transport of gases to the surface and when part of the gas escapes, the viscosity of the melt reduced significantly, allowing some of the melt flow through petroleum coke particles. Continuous bubbling and blistering play important roles in pyrolysis process as they serve as mechanism and products yield of pyrolysis reaction [1].The reduction of melt viscosities due to bubbling and blistering subsequently condensed the molten PP and reduced its contact angle. The eruption of devolitilized gas forms voids and crusty blisters, which tend to contract due to interfacial surface tension upon cooling. After rapid devolatilization, the reduction of the interfacial tension reduced the contraction during the melt solidification and consequently decreased its contact angle. As can be seen in Figure 6, the adhesion increased as the contact angle decreased. The reduction in contact angle shows that the melt of PP has bonded with petroleum coke particles. The increase of temperature has also decreased the melt viscosity and allowed PP to flow through and get trapped in between petroleum coke particles, thus forming the bond inside the substrate.

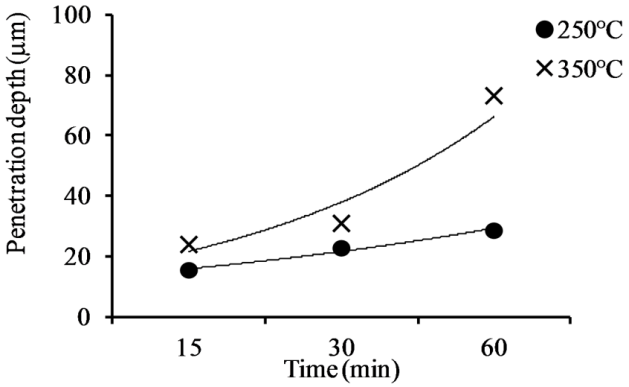

Figure 7: Variation of the penetration depth of PP melt into petroleum coke substrates as a function of heating temperature and time

Figure 7 shows that increasing time and temperature of the experiment generally increasethe penetration depth of the PP melts into PC substrate. The increasing heat treatment time also accelerated the degradation of PP, resulting in the rapid production of gaseous and liquid products. The degradation process produced gases, as indicated by bubble formation. Similar effect was observed with increase in temperature. The degradation of the polymer decreased its viscosity allowing it to penetrate deeper into the petroleum coke substrate.

Blends of PP and PC were prepared with the concentration of polymer in the blend ranging from 10% to 90%. The baking treatment of sample was carried out to investigate the effect of slow baking (2°C/min heating rates) in inert conditions (pyrolysis) on the polymer and petroleum coke. The experiments were carried out in three temporal cycles, and the maximum temperature of each cycles were raised from 150°C (Cycle 1) to 600°C (Cycle 2) and 1000°C (Cycle 3). The heating rate of 2°C/min was maintained under 1L/min argon flow. The experiment was conducted under isothermal conditions to allow slow softening and melting. This also enabled the polymer to stay in the liquid phase to wet petroleum coke particles.

The percent of residue from the mixtures collected after the baking cycles have been plotted in Figure 8. The baking of cycle 1, where the mixture was heated from ambient to 150°C and allowed to dwell for 30 min, showed negligible weight loss. The normalized weight loss of about 0.21 to 0.72% in each sample indicates primarily the evaporation of moisture.

In Cycle 2, the baking of mixtures (heating up to 600°C and dwell time of 30 min) has showed mass loss, which was seen to be proportional to the percentage of PP in the mixtures. The data shows that after heating and dwelling at 600°C, there were some traces of PP still remaining in the samples, except for the 10% PP sample mixtures where there was 10 percent loss of PP after the heating of Cycle 2.

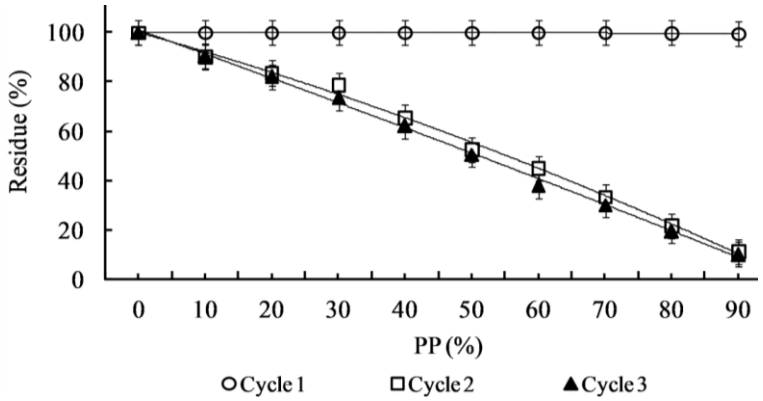

Figure 8: Residue (%) of PP and PC mixtures after heat treatment

However, after Cycle 3, the weight loss increased proportional to the increase in the percentage of PP in the mixtures. The mixtures of 20-50% PP has showed some traces of PP portion left in the residues. However, the sample with 60-90% of PP had completely decomposed, leaving no residues of the polymer. The mixtures with 90% PP has the highest rate of loss as it has the highest PP percentage, which has been totally decomposed in the high temperature heating cycle.

The percentage of carbon content of the raw PP and PC and their mixtures were measured by LECO and presented in Figure9. The carbon percentage of raw PP, PC and their mixtures are in the range of 97.6% (raw PC) to 89.1% (90:10 mixtures after Cycle 1). Both petroleum coke and polypropylene had a high carbon percentage. The mixtures of both components were therefore expected to have high carbon percentages. The carbon in mixture sample of 50:50 at the third cycle of heat treatment has the highest percentage, followed by samples treated in Cycle 2 and Cycle 1. The third cycle has generated more carbon since high temperature treatment has decomposed PP and resulted in more carbon residue, while the volatiles have been released. As compared to Cycle 1 and 2, where volatiles due to incomplete pyrolysis still exist, the weight percentage of carbon had increased in the case of Cycle 3.

The lowering trend of carbon content (%) by the increasing of raw PP ratio indicates that the increase of PP has simultaneously decreased the total carbon available in the mixtures. This is due to the fact that the more PP ratio, the more volatiles in the mixtures. These volatiles were released in the heat treatment. Higher heating as conducted in Cycle 3 released more volatiles, thus increasing the carbon content in the blend as compared with Cycle 2 (incomplete devolatilazation) and Cycle 1 (no reaction due to low temperature).

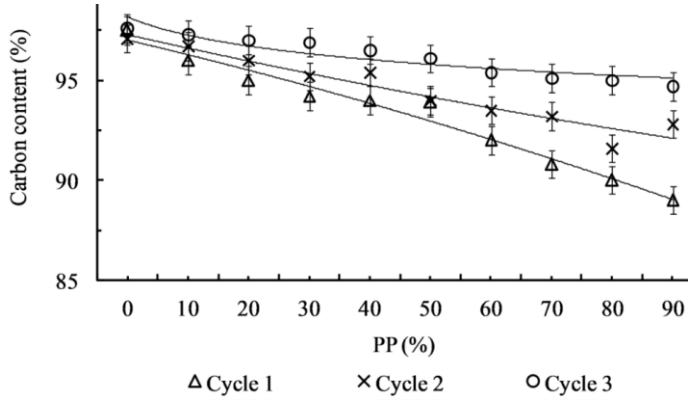

Figure 9: Carbon content (%) of PP and PC mixtures

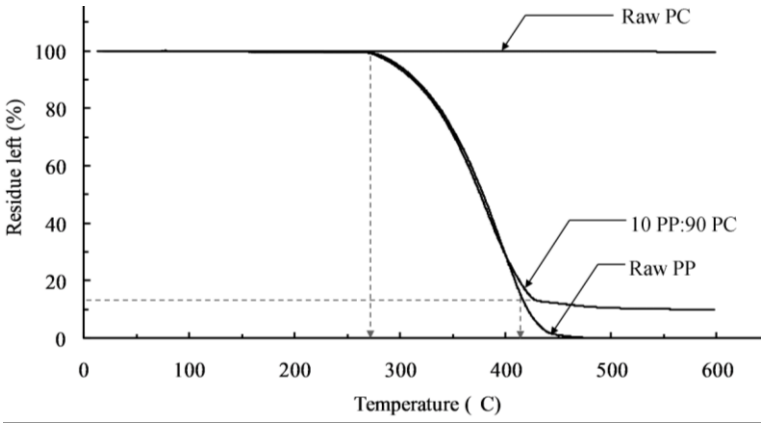

Figure 10: TGA profiles of raw PP, raw PC and mixtures their mixture of 10:90

Figure 10 shows the TGA profiles of raw PC, raw PP and their mixtures with 10% PP (90% PC). The graph shows that no residue of PP was left after 500°C while PC shows no changes throughout the heating. As for the mixture sample, the weight started to reduce around 280°C and the reduction continued until 430°C where the graph became almost a plateau around 12 to 9% weight residues.

Conclusion

An in depth investigation on PP and its blends with PC has been presented in this paper. The primary analysis was carried out by investigating the wettability and interfacial phenomena of PP and PC, where the increasing time and temperature (250°C to 350°C) resulted in an improved wettability and penetration of PP melt into PC substrate. The highest penetration depth was obtained at 350°C after 60 min of heat treatment with a penetration depth of 73 µm. The formation of gaseous bubbles and blisters indicate devolatizatilization of PP at these low temperatures. The flow of melt into PC particles had limited the heat transfer and decomposition of PP.

The influence of PC on the pyrolysis yield from PP was investigated in three heating cycles. PP was mixed with PC in the concentration range of 10 to 90% (w/w) in 10% steps. During Cycle 1 (up to 150°C), no reaction was observed probably due to low temperatures, as PP begins to melt only around 160-170°C. Reaction started to take place during Cycle 2 (up to 600°C), where the extent of solid residue was in proportion to the PC% content in the blends; some traces of PP were observed in most of the sample blends. The data from the heat treatment of Cycle 3 (up to 1000°C) shows that some traces of PP were still remaining in composition up to 50%. No PP was observed in higher PP mixtures. The TGA profile on 90% PC: 10% PP mixture indicates that PP started to decompose around 280°C till 430°C, and the weight loss became a plateau around 9-12% of weight residue.

References

[1] Attar, A. 1978. *Bubble Nucleation In Viscous Material Due To Gas Formation By A Chemical Reaction: Application To Coal Pyrolysis.* AIChE Journal 24(1) pp. 106-115

[2] Couderc, P., Hyvernat, P. & Lemarchand, J. L. 1986. *Correlations between ability of pitch to penetrate coke and the physical characteristics of prebaked anodes for the aluminium industry.* Fuel 65(2) pp. 281-287

[3] Curlee, R. T.1986. *Plastics recycling: Economic and institutional issues.* Conservation & Recycling 9(4) pp. 335-350

[4] Lee, K.H. &. Shin, D.H. 2007. *Characteristics of liquid product from the pyrolysis of waste plastic mixture at low and high temperatures: Influence of lapse time of reaction.* Waste Management 27(2) pp. 168-176

[5] Panda, A. K., Singh, R. K. & Mishra, D. K. 2010. *Thermolysis of waste plastics to liquid fuel: A suitable method for plastic waste management and manufacture of value added products--A world prospective.*Renewable and Sustainable Energy Reviews 14(1) pp. 233-248

EFFECT OF ORGANOCLAY ON MECHANICAL PROPERTIES OF PALM OIL BASED POLYURETHANE NANOCOMPOSITE

Soo Kai Wai, Sahrim Hj. Ahmad & Syazana Ahmad Zubir [1]
School of Applied Physics, Faculty of Science & Techology,
Universiti Kebangsaan Malaysia Malaysia.

Abstract

In this study, phosphonium salt treated montmorillonite (P-MMT) and ammonium salt treated montmorillonite (cloisite 30B) on the palm oil based rigid polyurethane foam was investigated. The polyurethane nanocomposite was produce by adding this organoclay to the palm oil based resin with loading percentage from 0 to 4.5% (w/w). The tests conducted were compression test, hardness test and also SEM observation. The result of compression stress and modulus testing indicated that both RPUF/P-MMT and RPUF/cloisite 30B gave the higher value at 2.5% loading. The hardness for RPUF/P-MMT and RPUF/cloisite 30B respectively gave the higher value at 2.5% and 0.5%. The degree of reinforcement obtained depends on the concentration of the filler, type of the salt treated clay and dispersion of the filler. The SEM micrographs clearly indicated that the effect of such factor in the mechanical properties of the foam. Good dispersion of the P-MMT than cloisite 30B in rigid polyurethane foam will gave the higher mechanical properties of RPUF/P-MMT than RPUF/cloisite 30B.

Keywords: *Compression, harness, organoclay, polyurethane foam*

Introduction

In very recent years polymer nanocomposites have drawn a great deal of interest because these materials possess high potential to achieve great property improvement by adding small amount of nanoparticles in the polymer matrix. Nanocomposites exhibit superior properties when compared with their microcomposites counterparts. An addition of small amount of nanoparticles can significantly improve a variety of properties without sacrificing the lightweight of polymer matrices. It is known that a small amount of well-dispersed nanoparticles in the polymer may serve as nucleation sites to facilitate the bubble nucleation process [1].

The biggest disadvantage of polyurethane (PU) foams when used as structural or semistructural materials is their low mechanical strengths, such as compressive strength and tensile strength, which are key physical properties of materials to stand strain when being used. Recently, clay, or montmorillonite, has been successfully introduced to a polymer system and extensively used in the polymer industry either as a reinforcement to improve the physical, mechanical properties of the final polymer or as a filler to reduce the amount of polymer used in the shaped structures, thereby lowering the high cost of the polymer systems. The special structure of clay plays important roles in improving mechanical, thermal, and diffuse barrier properties of polymer-layered silicate nanocomposites. To date, a great deal of effort has been devoted to the development of nanostructured PU/clay composites. These investigations show that PU/clay composites exhibit an improvement in elongation, insulation, aging, tensile modulus, and strength, but a decrease or no enhancement in compressive strength [2, 3].

PUFs/caly nanocomposites are comparatively new class of composite materials where at least one phase has dimension in the nanosize range. In these composites, clay is reported to act as cell opener where ultrasonic treatment often gave homogeneous cell size and improved dimensional stability. High mechanical and thermal properties compared with conventional composites are also expected by the filler effect of clay. However, it is difficult to

achieve complete exfoliation of the silica layers due to the strong electrostatic interactions between silicate layers and intragallery cations [4].

Since the development of nylon 6/montmorillonite (MMT) nanocomposites in early 1990's, organically modified MMT (organoclay) has been widely used in many polymers such as polyethylene, polypropylene, polystyrene, poly(methyl methacrylate), polyimide, polyvinylidenefluoride, ethylene propylene diene monomer rubber, bismaleimide, poly(acrylonitrile-butadienestyrene), epoxy resin, polyurethane (PU and so on. The organoclay may act as a reinforcement agent to improve the mechanical properties of the polymers, or as a flame retardant additive to improve the thermal stability and flame retardancy of the polymers.Since pristine MMT are intrinsically hydrophilic while most polymers are hydrophobic, to disperse MMTs in the polymer matrics, it is necessary to replace the hydrophilic inorganic cations (Na^+, Ca^+, or K^+) residing in the gallery space of MMTs with more organophillic cations [5]. This paper reported the study of phosphonium salt treated montmorillonite (P-MMT) and ammonium salt treated montmorillonite (cloisite 30B) on the mechanical properties of palm oil based rigid polyurethane foam was investigated.

Materials and method

Materials

Palm kernel Oil polyol and 2,4-diphenyl diisocyanate (MDI) were obtained from Maskini Polyol Sdn. Bhd, Malaysia. Tegoamin N, N, N´, N´´, N´´-Pentamethyldiethyltriamine (PMDETA) and dibutyltin dilaurate (DBTDL) as a catalyst were obtain from Degussa/Goldschmidt Chemical Corporation, Singapore and Aldrich, USA respectively. Polyurethane additive such as silicone surfactant (Tegostab B 8443) was obtained from Degussa/Goldschmidt Chemical Corporation, Singapore. Tetraoctyl phosphonium bromide that use for modifying organoclays were obtained from Merck. Na-montmorillonite (Na-MMT) and cloisite 30B were obtained from Southern Clay Products.

Methods

The unmodified MMT clay, Na-MMT and ammonium salt treated montmorillonite (cloisite 30B) were purchased from Southern Clay Products Inc. (USA). Phosphonium salt treated montmorillonite (P-MMT) was prepared by using method of ion exchange of Na-MMT (Delite HPS) in water solution. In order to prepare nanocomposites were the organonanoclays were firstly mixed with mixture of the polyol resin . Three hundres g mixture of the polyol resin (100 parts by weight, pbw palm kernel Oil polyol, 0.5 pbw Tegostab B 8407, 0.1 pbw PMDETA, 0.25 pbw DBTDL and 0.5 pbw water) was agitated vigorously with a speed of 500 rpm for 60 s. The organonanoclays were added based on weight percentage of the overall weight of the system. The organoclays was added varied at 0.5, 2.5 and 4.5% (w/w). The blend was then mixed with MDI at ratio of 100:110. The mixture was then poured into mould had dimensions of (19 × 25 × 7.5) cm^3 and was coated with a mold release agent (wax). The composites were conditioned at room temperature for 16 h before further characterizations.

Characterization of the PU composite

Compression Test

The compression test was conducted according to standard ASTM 1621. Samples were cut into dimension of (30 × 30 × 30) mm^3. The test was carried out using Instron Universal Test Machine *model Testometri M350-10ct* at cross-head speed of 30 mm/min until the thickness was reduced to 90% of its original thickness. The compressive stress and modulus were recorded an average of five specimens.

Hardness

A Portable shore D hardness tester was used with measurement being conducted according to ASTM D2240 standard to determine the hardness of the sample. The specimens were laid flat on a hard surface and a portable hardness tester *Shore A model Affri* was pressed on them. The values of the shore D hardness index obtained represent the mean of five reading.

SEM analysis

The SEM analysis was used to study the distribution of organoclay in composites. The analysis was carried out using *SEM chamber model VPSEM*. Before that, the samples were coated with gold using *gold sputter coater model SC500*.

Results and Discussions

Figure 1 showed the trend in compression strength of PU composites with 0, 0.5, 2.5 and 4.5% (w/w) of cloisite 30B and P-MMT respectively. When addition of cloisite 30B or P-MMT nanocomposite showed the higher value than pure PU is due to the increased internal strength of the PU matrix due to the higher degree of hydrogen bonding among the urethane groups and the finer cell structure of the nanocomposites. With a finer and more uniform cell structure, rigid PU foam/organoclay nanocomposites can withstand more strain in applications [2], Compressive strength of both systems showed a higher value with the addition of 2.5% of organoclay. The P-MMT filled composite give a slightly higher value than cloisite 30B is due to the more improvement in interface interactions between PU matrices and P-MMT [5]. The reduction of the compression strength with addition of 4.5% organoclay is due to the disruption in PU system which can create the disorder to the cellular structure [6].

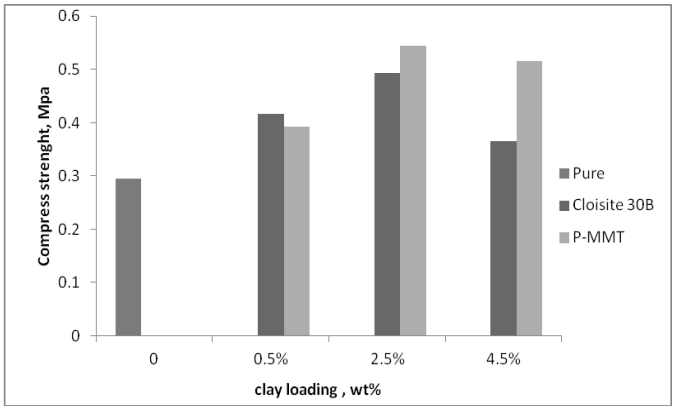

Figure 1: Compression strength of BTPU composite

Figure 2 shows the compression modulus of PU composites with 0, 0.5, 2.5 and 4.5% (w/w) of cloisite 30B and P-MMT respectively. At 2.5% cloisite 30B and P-MMT nanoclay loading, the compressive modulus reached the maximum which were 10.2 MPa and 10.4 MPa respectively. The increase in the compressive modulus of 2.5% nanoclay polyurethane foams was due to the higher density and smaller cell size of foam composites. The nanoclay was much easier to be uniformly dispersed into polyol resin at a low loading, resulting in more uniform and smaller cell size. At 4.5% nanoclay loading, the compression strength reduced probably due to uniformly dispersed in the resin mixture[7]. This would cause less uniform and some larger cell size due to the excessive coalescence of the nucleating sites. Besides that, at higher filler loading the filler has the tendency to tear the wall of the cellular structure. These walls, which tend to support the whole system becoming weakened and upon higher loading,

the PU system would lose its strength. This is clearly shown in the decrease in modulus which indicates the poor rigidity of the PU foam [8].

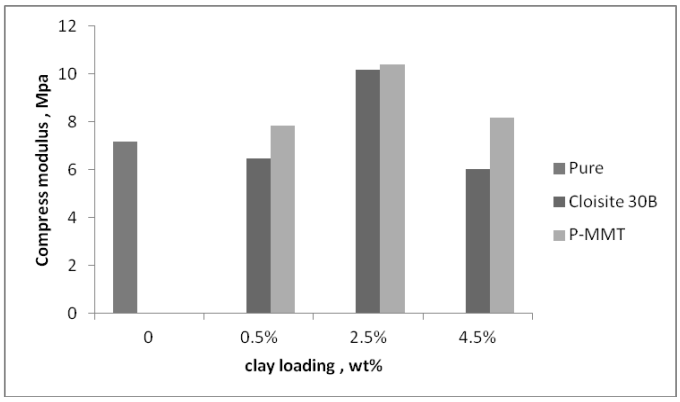

Figure 2: Compression modulus of BTPU composite

Figure 3 shows hardness of PU composites with 0, 0.5, 2.5 and 4.5% (w/w) of cloisite 30B and P-MMT respectively. The hardness of PU composite that obtain will be difference by addition of cloisite 30 B and P-MMT. At 2.5% P-MMT nanoclay loading, the hardness was reached the maximum. The increase in the hardness of the foam is due mainly to the random dispersion of the fillers into the polyurethane matrix [9]. Addition too much of cloisite 30B have worked negatively to destroy the foams hardness properties significantly. The hardness properties of 4.5% cloisite 30B showed the lower value than the pure PU.

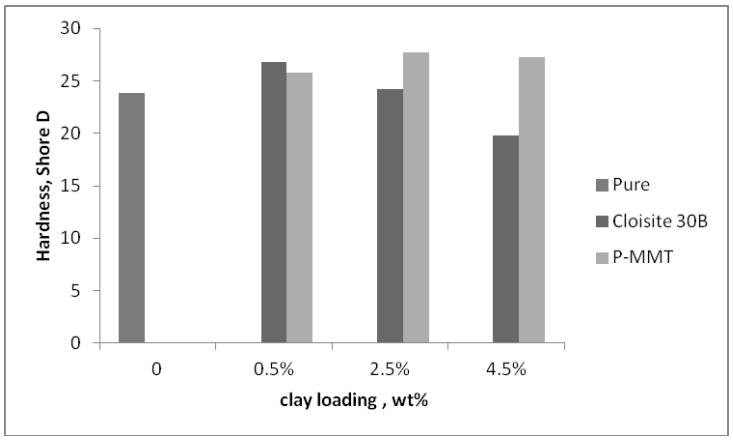

Figure 3: Hardness of BTPU composite

Figure 4 shows the SEM micrographs of the PU control and PU composites with 0.5, 2.5 and 4.5% (w/w) of cloisite 30B and P-MMT respectively. Figure 4(a) shows the smooth structure of the PU control. Figure 4(b) and Figure 4(c) show that the 2.5% (w/w) of nanoclays were nicely embedded in the matrix. It was clear that the interfacial region between it is [8]. The Figure 4(d) and Figure 4(e) show that when 4.5% (w/w) cloisite 30B and P-MMT added to the system respectively, the cell structure ruptured could be seen more obvious. It made the stress cannot be transferred from the matrix to the nanoclay continuously. The addition of 4.5% (w/w) nanoclay also causes the agglomeration at the cell wall. Agglomeration causing the cell structure become supersaturation and ruptured due to the higher loading of the nanoclay. Figure 4(d) shows the most obvious agglomeration, thus the reduction in the mechanical proproties of cloisite 30B filler is much higher than P-MMT [10].

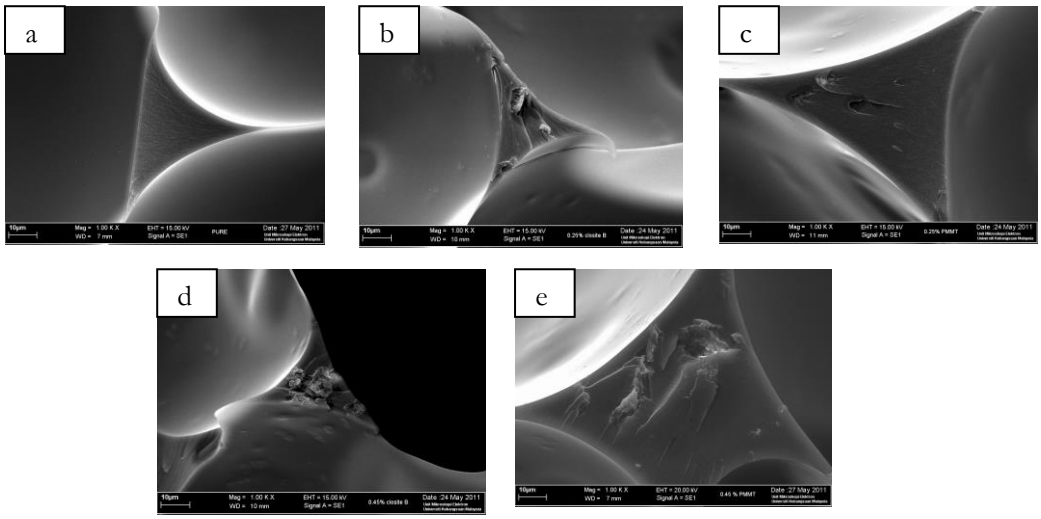

Figure 4: SEM micrograph of BTPU composite filled with a difference percentage loading of filler (a) Control (b) with 2.5% (w/w) cloisite 30B (c) with 2.5% (w/w) P-MMT (d) with 4.5% (w/w) cloisite 30B and (e) with 4.5% (w/w) P-MMT

Conclusion

Phosphonium salt treated montmorillonite (P-MMT) and ammonium salt treated montmorillonite (cloisite 30B) which used as the filler in the PU foam had showed the improment in the compression strength and compression modulus at 2.5% (w/w). The good dispersion and interfacial strength of phosphonium salt treated montmorillonite (P-MMT) in the PU matrix bring to the more better mechanical properties than ammonium salt treated montmorillonite (cloisite 30B). The improvement in the hardness for the P-MMT filled PU foam was much better than cloisite 30B. The SEM microghrphs was used to support the finding in the analysis of mechanical properties.

Acknowledgement

The author would like to thank Universiti Kebangsaan Malaysia for providing the facilities.

References

[1] Modesti, M., Lorenzentti, A. & Besco, S. 2007. *Polymer engineering and science*:1352-1358

[2] Xu, Z., Tang, X., Gu, A. & Fang, Z. 2007a. *Journal of Applied Polymer Science* 106:439-447.

[3] Xu, Z., Tang, X., Gu, A., Fang, Z. & Tong, L. 2007b. *Journal of Applied Polymer Science* 105:2988–2995.

[4] Kim, S.H., Lee, M.C., Kim, H.D., Park, H.C., Jeong, H.M., Yoon, K.S. & Kim, B.K. 2010. *Journal of Applied Polymer Science* 117:1992–1997.

[5] Xu, Z., Kong, W., Zhou, M. & Peng, M. 2010. *Chinese Journal of Polymer Science* 28(4):615−624

[6] Norzali, N.R.A., Badri, K.H. & Nuawi, M.Z. 2009. *Malaysia Polymer International Conference (MPIC 2009)*: 34-43.

[7] Liang, K. & Shi, S.Q. 2011. *Journal of Applied Polymer Science* 119:1857–1863.

[8] Badri, H. K., Othman, B. Z. & Razadi, M. I. 2005. *Iranian PolymerJournal* 14(5):441-448.

[9] Latinwo, G.K., Aribike, D.S., Susu, A.A. & Kareem, S.A. 2010. *Nature and science* 8(6):23-26.

[10] Badri, K.H. & Redwan, A.M. 2010. *Sains Malaysiana* 39(5):769–774.

SHAPE MEMORY BEHAVIOR OF PALM OIL POLYOL AND POLYCAPROLACTONEDIOL BASED THERMOPLASTIC POLYURETHANE

Syazana Ahmad Zubir[1], Sahrim Ahmad[1], Norazwani Muhammad Zain[1], Soo Kai Wai[1]& Ernie Suzana Ali[2]

[1]School of Applied Physics, Faculty of Science and Technology, Universiti Kebangsaan Malaysia (UKM), Selangor, Malaysia

[2]Department of Applied Physics, Faculty of Science and Technology, Universiti Sains Islam Malaysia (USIM), Negeri Sembilan, Malaysia

Abstract

Palm oil based polyurethanes with variations in percentage of palm oil polyol were successfully synthesized via two-step polymerization process with polycaprolactonediol (PCL) as soft segments. Palm oil polyol was introduced with the purpose of providing hyperbranched structure to assist more interactions between the precursors due to the presence of huge amount of functional groups. The thermal, mechanical and shape memory properties of the resulting polymers were investigated accordingly. The produced thermoplastic polyurethanes (TPU) were proven to be harmless to human health due to complete reactions that took place in the system. X-ray diffraction curves showed presence of crystalline soft segment phase which is important in triggering the shape memory effect. TPU with 20% palm oil polyol content showed exceptional mechanical and shape memory properties in which suggesting that it is the optimum value for the intended feed molar ratio used in the present work.

Keywords: *Palm oil polyol, polyurethane, shape memory, thermoplastic*

Introduction

Shape memory polymers are classified as smart materials in which they posses special ability of changing their shape through the application of external stimulus such as thermal, electrical or environmental change. Polyurethane particularly had captured great attention among researchers due to its easier processing, broader switching temperature and wider range of applications [1]. The shape memory effect exhibited due to the thermal incompatibility of soft and hard segment domains in polyurethane in which they will segregate to form two separate phases [2]. The hard segments form physical crosslinks through hydrogen bonding, dipole-dipole interactions or crystallization that enable the formation of permanent shape while the other phase acts as molecular switch that allows for the fixation of temporary shape [3].

There are two types of polyol that can be utilized to form soft segments in polyurethane; polyester and polyether polyols. In this work, a polyester polyol; polycaprolactonediol (PCL) was used as soft segments owing to its melting temperature ranging between 50 to 60°C that allow the possibility to fix the temporary shape for the intended applications in biomedical field. In addition, the exceptional features of PCL such as good solubility, excellent blend-compatibility, biocompatible and biodegradable make it the best choice for the current research [4]. Besides PCL, another polyester polyol with hyperbranched structure, palm oil polyol was consumed in order to help in crosslinking process and further improved its mechanical properties. The hyperbranched structure is believed to be helpful in mixing process due to the presence of large number of functional groups [5]. The addition of vegetable oil in the system helps in reducing one's reliance on petroleum based products and varying its employment to wider applications possible. On top of that, vegetable oils are more attractive by being economical and environmental friendly.

In the present study, polyurethanes based on palm oil polyol and polycaprolactonediol were prepared through prepolymer method. The produced thermoplastic polyurethane were

characterized using Fourier-transform infra-red (FTIR), x-ray diffraction (XRD), differential scanning calorimetric (DSC), mechanical and shape memory tests.

Materials and method

Materials

Palm oil polyol (M_W = 900 g·mol^{-1}, hydroxyl number = 120 mg KOH·g^{-1}) used in this study was supplied by Rovski Industries Sdn. Bhd., Subang Jaya and Polycaprolactonediol (PCL) (M_W = 4000 g·mol^{-1}, hydroxyl number = 28 mg KOH·g^{-1}, melting point = 55 to 60°C) was purchased from Perstop Polyols, UK. Meanwhile, 4,4'- diphenylmethane diisocyanate (MDI) (M_W = 250.25 g·mol^{-1}, melting point = 39°C), chain extender 1,4- butanediol (BD) and catalyst dibutyltindilaurate (DBTDL) were purchased from Sigma Aldrich (M) Sdn. Bhd., Petaling Jaya.

Method

Both polyols used in this work were first dried at 45°C overnight in order to remove any possible moisture present while MDI was used as received. Table 1 shows the formulation of TPU at different compositions. There were two stages involved for the synthesis; prepolymer and polyurethane preparations. The prepolymer was prepared according to the modified procedure of [6] with feed molar ratio of 1:6:5 referring to polyol: MDI: BD. In the first stage, MDI and PCL were reacted at 80°C in 500 ml round bottom flask equipped with a thermometer, flow of dry nitrogen gas and mechanical stirrer. The reaction took place for half an hour before certain percentage of palm oil polyol was added and reacted for another 2.5 h with stirring speed of 500 rpm.

In the second stage, the prepolymer, BD and catalyst were melt-blended in Brabender internal mixer at 90°C with rotor speed of 50 rpm. The mixing was continued for approximately 20 min until the torque reached plateau. The produced polyurethane was then further compressed using hydraulic hot press at the temperature of 150°C using 0.5 mm thick rectangular stainless steel mold.

Table 1: Compounding formulations of TPU polymer

Sample Name	Percentage of Palm Oil Polyol in Molar Ratio (%)	Hard Segment Content (%)
10R(165)	10	36.4
20R(165)	20	40.2
30R(165)	30	44.5
40R(165)	40	49.4

Characterization

The chemical bonding exist in the samples were analyzed with Fourier transform infrared spectroscopy using Perkin Elmer FT-IR model Spectrum GX. The scans were conducted on a thin film samples and all spectra were collected using 16 scans at 4 cm^{-1} resolution. The frequency covered was from 4000 to 400 cm^{-1}.

X-ray diffraction curves of TPU were recorded using X-ray diffractogram model *Siements D 500*. The range of 2θ was from 10 to 40° at room temperature. The sampling interval taken was 0.025° at a scan rate of 1°·min^{-1}.

Thermal properties of the samples were assessed using differential scanning calorimetric model *Mettler Toledo model 822E* purged with liquid nitrogen. Two thermal scans were involved during measurements. The samples were heated from 20 to 250°C at scanning rate of 10°C·min^{-1} in the first thermal scan. Then, they were quenched from 250 to -100°C at cooling rate of 20°C·min^{-1}. In the second thermal scan, the samples were heated again from -

100 to 250°C at a rate of 10°C·min^{-1}. In this work, the second thermal scan was examined for analysis.

Mechanical test was carried out at room temperature using *tensile tester machine Instron 5567*. The specimens were prepared according to ASTM D638-type V. The load cell used was 1kN with gauge length and strain rate of 25 mm and 50 mm·min^{-1} respectively. Minimum of five measurements were taken for consideration.

Shape memory behavior of the TPU was investigated according to [5] where the samples were first heated to 60°C and molded into ring-like form. Then, they were immersed into ice-water bath without removing the constraint. After 10 min, the mold was removed and constraint removal angle (θ_{cr}) was recorded. The value for final angle, θ_f was taken after the samples were heated back to 60°C. Figure 1 illustrates the sequence of the shape memory test. Under this condition, shape fixity and shape recovery are defined as follow:

$$\text{Shape fixity (\%)} = \theta_{cr} / 90° \times 100. \quad (1)$$

$$\text{Shape recovery (\%)} = (90° - \theta_f) / 90° \times 100. \quad (2)$$

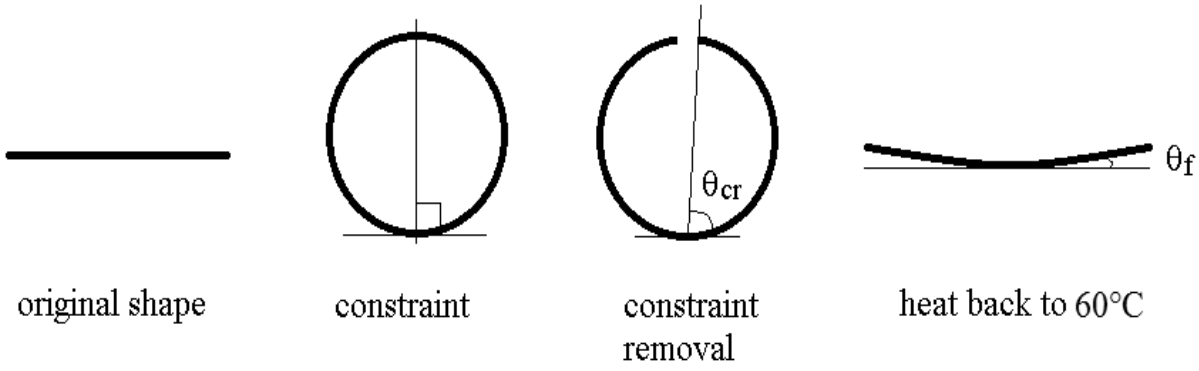

Figure 1: Schematic diagram of the shape memory effect behavior

Results and Discussion

According to FTIR spectrum, the existence of MDI can be traced from NCO peak at 2260 to 2280 cm^{-1}. The FTIR spectrum for palm oil based polyurethane containing the highest amount of MDI in Figure 2 shows that there is no trace of NCO group at the respective wavenumber suggesting that complete reaction had taken place in the system and that the TPU produced was harmless to human health.

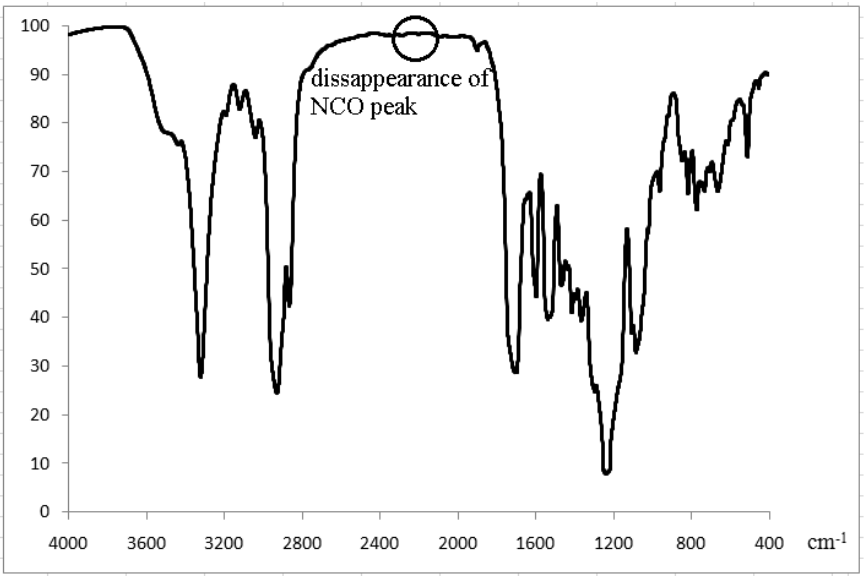

Figure 2: FTIR spectra of polyurethane with 40% palm oil polyol content

In thermoplastic polyurethane, the crystallization of soft segment domains is one of the main contributions for the shape memory effect to take place in which it is responsible for the fixation of the temporary phase [7]. In the current work, the hyperbranched polymers showed the existence of crystalline phase. This is due to the presence of two prominent peaks in XRD diffractogram at 21.3° and 23.6° (Figure 3) which attributed to (100) and (200) planes of PCL crystals [8].

Polyurethane with 20% palm oil polyol content showed highest crystallinity compared to the others. The crystallinity intensity decreased with increasing palm oil polyol concentration due to the interference of hard segment domains that impede the crystallization of PCL crystals. Consequently, TPU loading with 40% palm oil polyol had developed into almost amorphous phase.

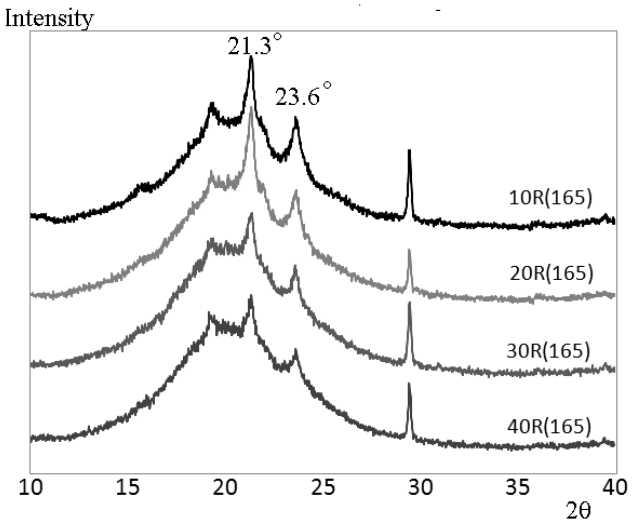

Figure 3: XRD diffractograms of palm oil based polyurethane with various palm oil polyol contents

Table 2 summarizes the DSC results of palm oil based polyurethane with different palm oil polyol content. The values for melting transition temperature, T_m were less pronounced for each composition in which they differ by only 1°C. As one can see, the heat of fusion for TPU with 20% palm oil polyol content is greater than the rest. This phenomenon is in accordance with the result obtained by XRD as discussed earlier. The heat of fusion decreased with increasing concentration of palm oil polyol, as a consequence of chain mobility restrictions induced by hard segment domains. Moreover, the chain packing of polymer structures are more ordered in samples with lower hard segments content may cause the decreasing pattern in melting enthalpy.

Table 2: Thermal properties of palm oil based polyurethane

Sample Name	Transition Temperature (°C)		Enthalpy
	T_g [a)]	T_m [a)]	ΔH_m (J/g) [a)]
10R(165)	-45.57	42.8	17.86
20R(165)	-41.83	42.6	17.9
30R(165)	-42.65	42.3	17.6
40R(165)	-44.49	41.8	17.4

[a)] Measured on heating in the second thermal scan

A typical plot of stress vs. strain curve of palm oil based PU with various palm oil polyol contents was shown in Figure 4 and the detailed results were summarized in Table 3. The graph suggests that all samples show ductile behavior. As the percentage of palm oil polyol is increased, the strength and strain at failure increase remarkably especially at 20% and 30% palm oil polyol content. The modulus decreases with increasing hard segments content indicate that the samples are less rigid as more palm oil polyol is introduced.

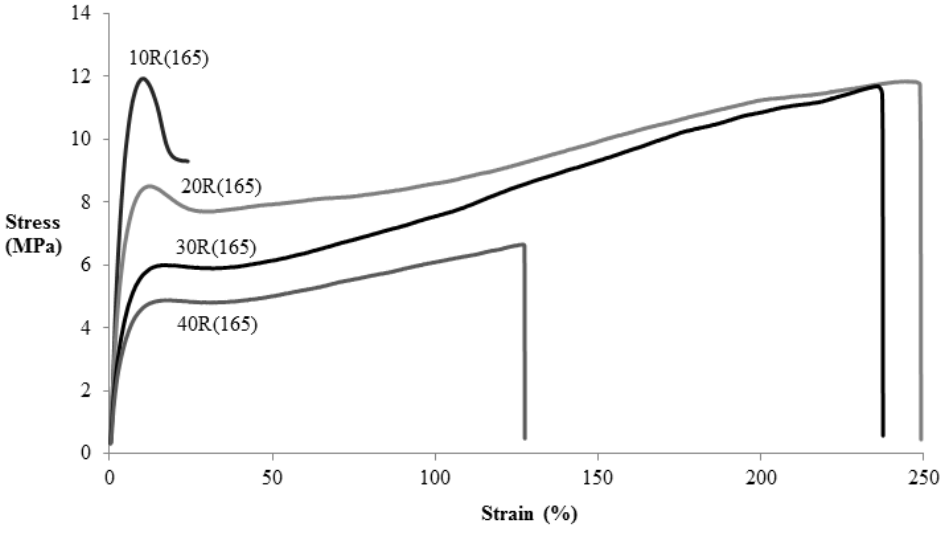

Figure 4: Stress strain curve of palm oil based polyurethane with various palm oil polyol content

Table 3: Mechanical properties of palm oil based polyurethane

Sample name	Modulus (MPa)	Stress at Break (MPa)	Strain at Break (%)
10R(165)	279.2	8.2	25.8
20R(165)	197.9	10.7	241.3
30R(165)	147.5	11.3	238.7
40R(165)	129.4	6.4	129.5

Figure 5 shows the temporary shape of the TPU upon the removal of constraint and the permanent shape after constraint removal. The shape memory properties of thermoplastic polyurethane were excellent in the system with 20% palm oil polyol as can be seen in Table 4. This shows good agreement with the previous result suggesting that it is the optimum loading of palm oil polyol for the particular feed molar ratio. The shape fixity decreases with increasing hard segments content. This could be due to partial crystallization of soft segments that is not sufficient to sustain the deformed ring shape and an instantaneous shrinkage occurred once the constraint was removed. The lacking of enough restrictions induced by hard segment domains over chain slippage upon deformation could also contribute to the reduction in shape fixity [9]. However, the shape recovery remains outstanding in samples up to 30% palm oil polyol content. This may be due to the formation of stable hard segment domains at the temperature above melting point of soft segments crystals and the presence of adequate phase separation taking place in the system.

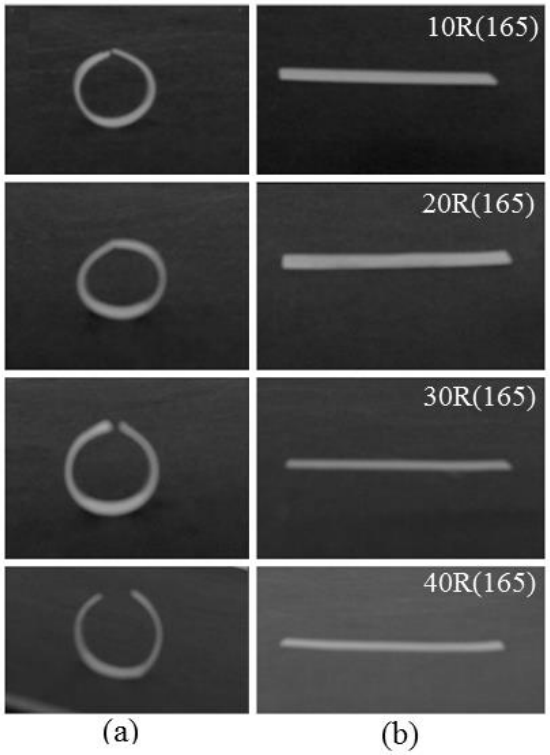

Figure 5: Shape memory behavior of thermoplastic polyurethane at 60°C; (a) temporary shape upon removal of constraint and (b) permanent shape upon reheating at 60°C.

Table 4: Shape memory properties of palm oil based polyurethane

Sample Name	Shape Fixity (%)	Shape Recovery (%)
10R(165)	97.2	100
20R(165)	100	100
30R(165)	94.4	100
40R(165)	88.3	96.7

Conclusion

Thermoplastic palm oil based polyurethanes showed improved thermal, mechanical and shape memory properties especially in PU system with 20 and 30% palm oil polyol content. This is due to the presence of sufficient amount of palm oil polyol that appropriately assist in crosslinking process in consequence of its huge number of functional groups. The produced polyurethanes exhibit sufficient crystallization behavior in which prominent for triggering shape memory effect.

Acknowledgement

The authors would like to express their ultimate gratitude to Universiti Sains Islam Malaysia, Universiti Sains Malaysia and Ministry of Higher Education for supporting the work financially.

References

[1] Hu, J. 2007. *Shape memory polymers and textiles*, 9. England: Woodhead Publishing Limited.

[2] Meng, Q., Hu, J & Zhu, Y. 2008. *J. Biomater. Sci. Polymer Edn*. 19(11):1437-1454.

[3] Paik, H.I., Goo, N.S., Jung, Y.C. & Cho, J.W. 2006. *Smart Mater. Struct*. 15:1476-1482.

[4] Woodruff, M.A. & Hutmacher, D.W. 2010. *Prog. Polym. Sci*. 35:1217-1256.

[5] Rana, S., Karak, N., Cho, J.W. & Kim, Y. H. 2008. *Nanotechnology*. 19:495707.

[6] Jana, S. C., Gunes, I. S. & Cao, F. 2008. *Polymer* .48:2223-2234.

[7] Liu, C., Qin, H. & Mather, P.T. 2007. *J. Mater. Chem*. 17:1543-1558.

[8] Sahoo, N.G., Jung, Y.C., Yoo, H.J. & Cho, J.W. 2006. *Macromol. Chem. Phys*. 207:1773-1780.

[9] Cao, F. 2008. *Shape memory polyurethane nanocomposites*. Ph.D Dissertation, University of Akron, Akron. 94-103.

CASSAVA STARCH-FILLED NATURAL RUBBER COMPOSITES: EFFECTS OF FILLER LOADING

N. Q. Duy[1,2], A. R. Azura[1], H. Ismail[1]

[1]School of Materials and Mineral Resources Engineering, Universiti Sains Malaysia, 14300 Nibong Tebal, Penang, Malaysia

[2]Rubber Research Institute of Vietnam, 236 Nam Ky Khoi Nghia Street ward 6, District 3, Ho Chi Minh City, Vietnam

Abstract

Cassava starch-filled natural rubber (NR) composites are prepared using a laboratory two-roll mill. The effect of cassava starch content on the cure characteristics, morphology, tensile and tear properties of cassava starch/NR composites are investigated using cassava starch loadings up to 25 phr. The SEM results showed that the cassava starch granules can be observed in the composite. The maximum torque of the composites increased with increasing cassava starch loading while the scorch time and cure time slightly decreased. The tensile strength and elongation at break are decreased at 10 phr and higher loadings of cassava starch. Moduli (M100 and M300) increased slightly with higher filler loading. However, tear strength decreased with an increased of cassava starch loading.

Keywords: *Cassava starch, composites, natural rubber*

Introduction

Natural rubber (NR) is an unsaturated elastomer with some good properties, such as high strength, outstanding resilience, and high elongation at break. However, NR will gradually degraded at high temperature or when exposed to oxygen, ozone or ultraviolet [1]. To overcome these limitations of NR and expand its application, the modifications of NR are crucial. Various methods can be employed to modify NR. One of the ways is chemical modification, in which other groups or atoms are introduced onto the NR molecular chains, and thus derives epoxidized NR [2], chloridized NR [3], grafted NR [4]. Another simple and economical way is to blend intensifiers or fillers including carbon black, silicate, zinc and aluminum with NR [5-8]. With the gradual exhaustibility of petroleum and the higher demand of environmental protection, starch stays as natural, cheap, abundant and biodegradable resource, which has been identified to modify NR. The mechanical properties of NR filled with starch are dominated by many factors, such as the dispersing ability, the interfacial combination and the type of starch. Many studies have contributed to the improvement of the mechanical properties of starch/NR composites [9-15].

In this work, the effect of cassava starch loading on properties of cassava starch-filled natural rubber composites was studied. The study focused on processing torque, morphology and tensile properties of cassava –starch filled natural rubber composites.

Materials and method

Materials

Natural rubber (STR 5L) was purchased from Yala latex industry co., Ltd Thailand. Zinc oxide, stearic acid, sulfur, toluene, Dibenzothiazonle Disulfide (MBTS), Diphenyl guanidine (PDG), 2-Mercapto benzimidazole (MB) are obtained from Bayer Sdn. Bhd Malaysia and Cassava starch is obtained from Thye Huat Chan Sdn Bhd Malaysia.

Preparation of the rubber compounds and vulcanizates

A conventional vulcanization system is used for compounding. The formulation is shown in Table 1. The rubber mixes are prepared on a laboratory two-roll mill *(Model XK-160)* maintained at 70±5°C according to ASTM D3184.

The cure characteristics of the rubber compounds were studied using a Monsanto Moving Die Rheometer (MDR 2000) according to ASTM 2240-93 at 150°C. The respective cure t_{90}; scorch times t_{s2}; and Maximum torque M_H were determined from the rheograph. The compounds were subjected to compression molded at 150°C using the respective cure times, t_{90}.

Tensile properties

Dumbbell-shaped samples were prepared from molded sheets according to ASTM D412. Tensile tests were performed under room temperature with an Instron model 3366 machine with a speed of extension of 500 $mm \cdot min^{-1}$. The results were calculated from average of five samples.

Tear properties

The tear test was performed according to ASTM D 624. Type T (Trouser tear strength) was used to measure the tear properties. The tests were performed at 25±3°C using a crosshead speed of 50 $mm \cdot min^{-1}$. The results were calculated from average of five samples.

Table 1: Formulation of cassava starch filled natural rubber composites

Ingredients	Content (phr)
Natural rubber (STR 5L)	100.0
Zinc oxide	5.0
Stearic acid	2.0
MB	0.5
MBTS	0.5
PDG	0.5
Sulfur	2.0
Cassava starch	0, 5, 10 ,15, 20, and 25

Scanning electron microscopy (SEM) analysis

The fracture surface morphology of the cassava starch/NR composites is investigated with scanning electron microscopy (SEM), model 50 VP (Germany). Fractured surfaces of the specimens are coated with a thin gold layer of about 20 nm thickness to avoid electrostatic charging during examination.

Results and Discussion

Cure characteristics

The effect of cassava starch loading on the scorch time t_{s2} and cure time t_{90} of cassava starch/NR composites is shown in Table 2. It can be observed that both values slightly decreased with increasing cassava starch loading. The results indicated the influenced of cassava starch on the vulcanization process of natural rubber. The effect can be ascribed as the influence of hydroxyl groups in the cassava molecule on accelerating the time to incipient cure [15]. As a result, the level of hydroxyl groups also played a significant role on accelerating the cross-linking reaction. The effect of hydroxyl groups on vulcanization is also presented from the cure rate index results.

Cure rate index is a measure for the rate of vulcanization based on the difference between optimum vulcanization and incipient scorch time. The cure rate index is calculated as follows [16].

$$Cure\ rate\ index = \frac{100}{(t_{90}-t_{s2})} \quad (1)$$

The maximum torque (M_H) increased with increasing cassava starch loading is shown in Table 2. This may be attributed to the modulus of cassava starch, thus the incorporation of cassava starch increased the stiffness of the cassava starch/NR composites. The levels of hydroxyl groups in the cassava starch molecules and the presence of unsaturated molecules played a significant role on the stiffness of unvulcanized and vulcanized rubber sample [15].

Table 2: Curing characteristics of cassava starch/NR composites

Curing characteristics	Cassava starch powder loading (phr)					
	0	5	10	15	20	25
Maximum torque (dN.m) (M_H)	6.61	7.27	7.60	8.31	8.46	8.92
Scorch time (min) t_{s2}	3.34	3.16	2.87	2.92	2.91	2.94
Cure time (min), t_{90}	7.19	6.94	6.65	6.62	6.58	6.43
Cure rate index (%)	25.97	26.45	26.45	27.02	27.24	28.49

Morphology of cassava starch/NR composites

Figure 1 shows SEM images of cassava starch and the tensile-fractured surface of cassava starch/NR composite. Figure 1a shows the size of the cassava starch granules is around 5-15 µm, and the shape of the circular or polygonal. In Figure 1b, Figure 1c and Figure 1d can be observed that the cassava starch granules exist in in the composite. The particle size of cassava starch in the composites remains almost the same as that of the original cassava starch. The surface of the composite is coarse, and some apparent craters of cassava starch particle on the fracture surface of composite, which suggest that the interfacial adhesion between cassava starch and natural rubber is relatively weak. The fracture surface of the composite becomes coarser with increasing cassava starch loading.

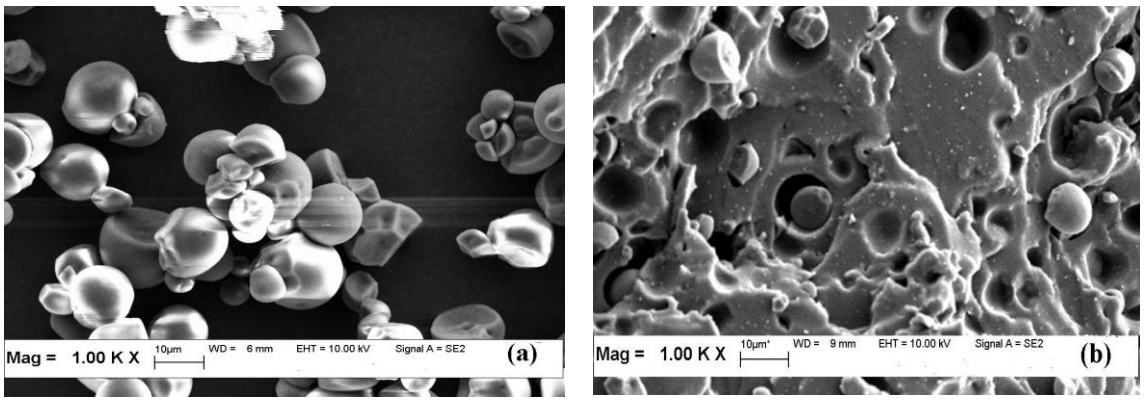

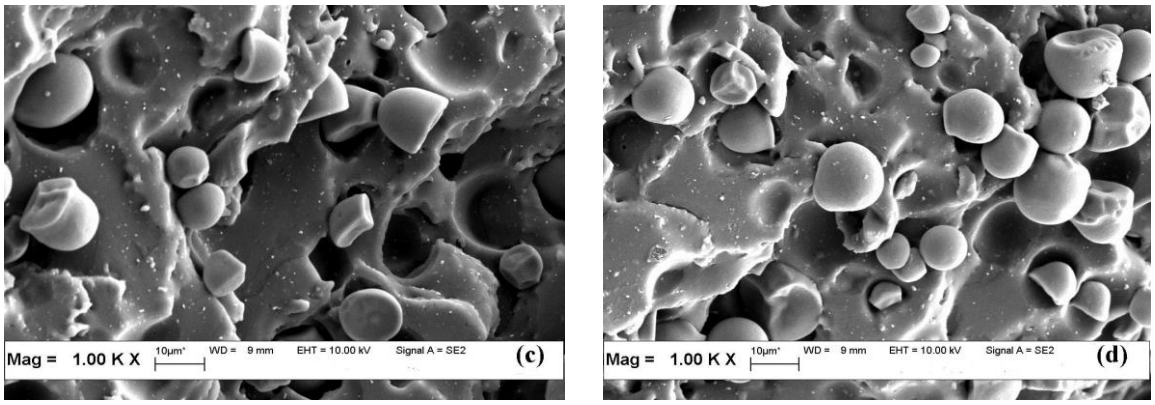

Figure 1: SEM micrographs of cassava starch particles and composites: (a) pure cassava starch; (b) cassava starch (10 phr)/NR composite; (c) cassava starch (20 phr)/NR composite; (d) cassava starch (25 phr)/NR composite

Tensile properties

The effect of cassava starch loading on the tensile strength of cassava/NR composites is shown in Figure 2. The tensile strength almost maintained up to 10 phr of cassava loading, then decreased considerably with higher loadings of cassava filler. It might be explained that this reduction of tensile strength may be due to the morphology and the concentration of cassava starch particles in the composites [17]. In addition, the interface between cassava and rubber is relatively weak resulted from the hydroxyl group in cassava and un-polarized rubber. Therefore, the increasing of cassava loading will lead to the rise of interface that caused the decreased in tensile properties.

The strength of the compounds decreases due to the inability of the cassava starch particles to support stress transfer from the elastomeric phase. The results obtained are in agreement with the elongation at break in Figure 3.

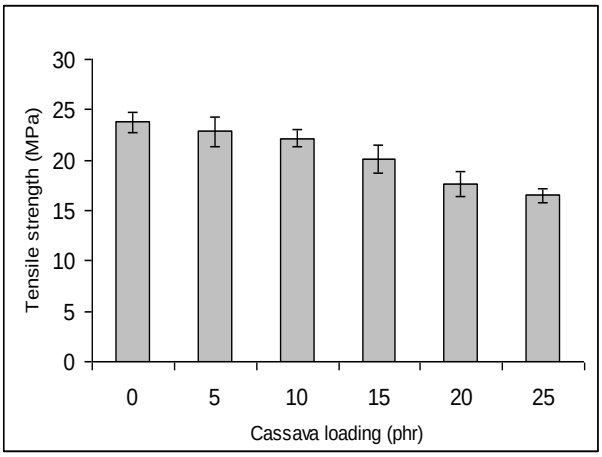

Figure 2: The effect of cassava starch loading on the tensile strength of cassava/NR composites

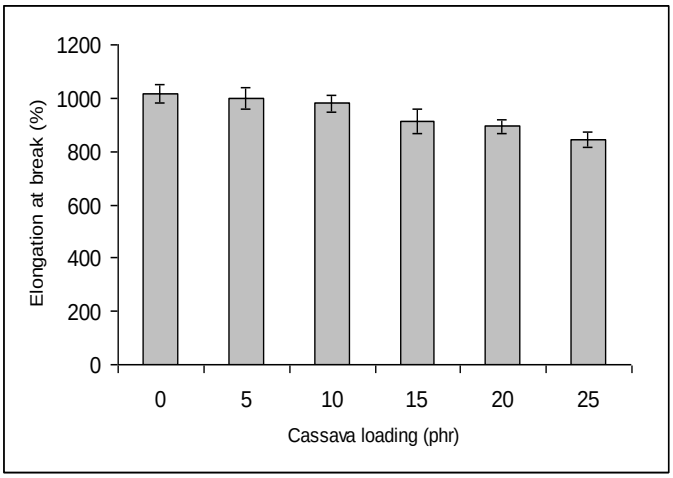

Figure 3: The effect of cassava starch loading on the Elongation at break of cassava/NR composites

Figure 4 and Figure 5 shows the tensile Modulus, M100 (modulus at 100%) and M300 (modulus at 300%) which measured the stiffness of rubber composites. Similar to normal fillers, cassava starch also can improve tensile modulus with increasing its loading in the composition of the formulations [5, 6, 7, 8]. In the present study, a small influenced of cassava starch loading on both M100 and M300 are observed. This observation was in agreement with the change of M_H represented in Table 2.

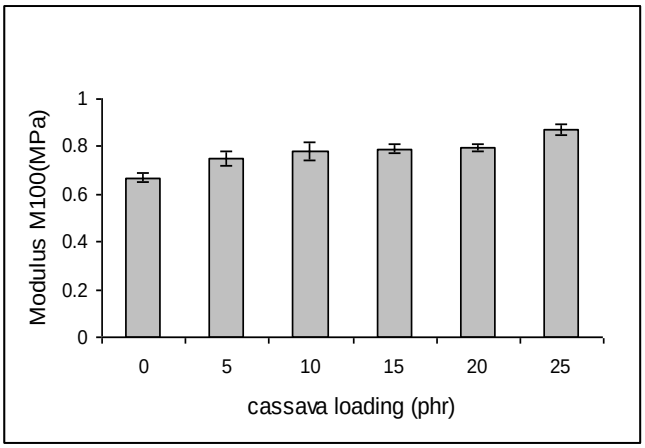

Figure 4: The effect of cassava starch loading on the Modulus M100 of cassava/NR composites

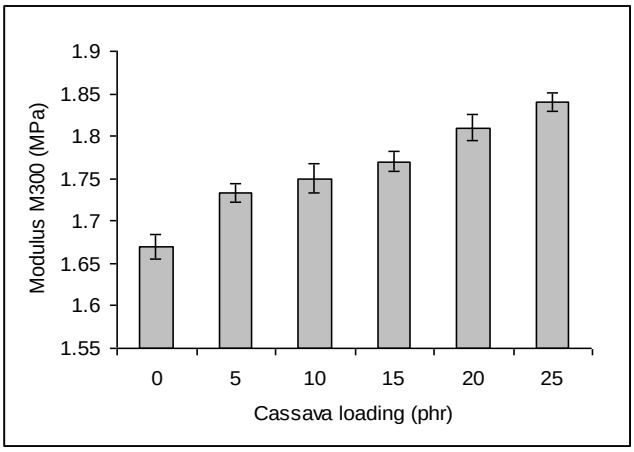

Figure 5: The effect of cassava starch loading on the Modulus M300 of cassava/NR composites

Tear properties

Figure 6 shows the tear strength of cassava/NR composites at different cassava starch loadings. It can be observed that tear strength decreased gradually with an increased in cassava starch. However at the loadings higher than 5 phr, tear strength decreased slightly. Tear strength of composites may increase or decrease with increasing filler loading which strongly contributed from filler type, shape and properties. The decreased in tear strength may attributed to the nature of the cassava starch filler, which is irregular-shaped, and its capability to support stress transmitted from polymer matrix is rather poor, and also probably because of the rigid interface between the cassava molecules and rubber phase [17, 18].

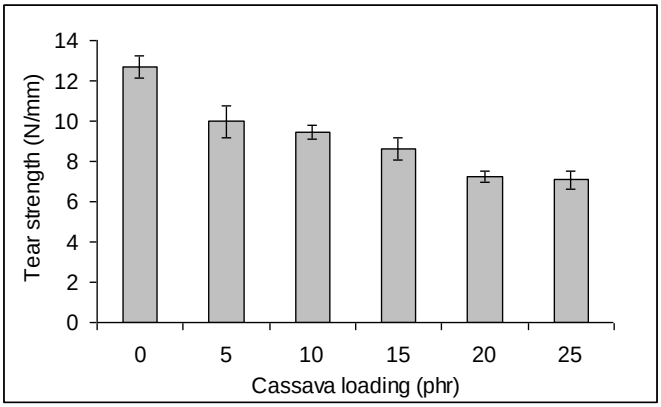

Figure 6: The effect of cassava starch loading on the tear strength of cassava/NR composites

Conclusion

For cassava starch-filled natural rubber (NR) composites with cassava starch loading up to 25 phr, the effect of the cassava starch loading on the mechanical properties of the composites are as follows:

1. The scorch time and cure time decreased with increasing of cassava starch loading.

2. The increasing of cassava starch loading caused the decreasing trends of tensile, elongation at break and tear strength due to poor compatibility between cassava starch and natural rubber.

Acknowledgement
This work is supported by the Short term Grant (Grant No. 304 / PBAHAN / 60312019) and Rubber Research Institute of Vietnam (RRIV). The authors gratefully acknowledge the support and research facilities provided by Universiti Sains Malaysia.

References

[1] Mei-Hua Zhou et al. 2001. *Applied Polymer Science*. 79:2464-2470.
[2] Chantanan thevy Ratnam et al. 2001. *European Polymer.* 37:1667-76.
[3] He-ping Yu et al. 2004. *Thermochimica Acta.* 410:119-123
[4] Si-Dong Li et al. 2003. *Applied Polymer Science.* 90:1227–1232.
[5] V. Tangpasuthadol et al. 2008. *Applied Polymer Science.* 109:424-433.
[6] Ismail, H et al. 2004. *Polymer Plastic Technology and Engineering.* 43:1323 1344.
[7] J. Anuar et al. 2007. *Polymer Plastic Technology and Engineering.* 46:667-674.
[8] Anoop Anand K et al. 2010. *Polymeric materials.* 59:33-44.
[9] R. A. Buchanan et al.1971. *Starch/Stärke.* 23:350.
[10] R. A. Buchanan et al. 1974. *Starch/Stärke.* 26: 165
[11] A.J.F. Carvalho et al. 2003. *Carbonhydrate Polymers.* 53: 95-99.
[12] You-Ping Wu et al. 2004. *Macromolecular Rapid communications*. 54:565-570.
[13] You-Ping Wu et al. 2006. *Carbonhydrate Polymers.* 65: 109-113.
[14] Antoine Rouilly et al. 2004. *Polymer.* 45:7813-7820.
[15] C. Nakason et al. 2006. *Materials Letters.* 59:4020-4025.
[16] Annual Book of ASTM Standards, vol. 09 01, Rubber, Natural and Synthetic—General Test Methods, Carbon Black, designation D 2084 ASTM. Philadelphia; ASTM, 2000.
[17] M.J Zaini et al. 1996. *Polymer International.* 40:51-55.
[18] Ismail, H et al. 2003. *Polymer-Plastics Technology and Engineering*. 42:81-103.

Impact Property Changes and Chemical Resistance Analysis of Polypropylene/ Poly (Acrylonitrile-Butadiene-Styrene) Blends

Mohamad Al Hafiz Ibrahim, Azman Hassan, Mat Uzir Wahit, Munirah Mokhtar
Department of Polymer Engineering, Faculty of Chemical Engineering, Universiti Teknologi Malaysia, 81310 UTM Skudai, Johor, Malaysia.

Abstract

This study aims at investigating the effect of blend ratio of polypropylene/poly(acrylonitrile-butadiene-styrene) (PP/ABS) on chemical resistance and impact properties. Blends of PP/ABS ranging from 80/20 to 50/50 wt% were extruded by twin screw extruder and were molded using injection molding in order to evaluate the chemical resistance towards acetone and gasoline and also to investigate the changes occurred in impact strength. The results showed that the chemical resistance of PP/ABS blends towards acetone and gasoline decreased with increasing ABS content. Immersion in gasoline produced significant effect in impact strength of PP/ABS blends. The impact strength was increased after the immersion in gasoline whereby acetone did not affected the impact strength of PP/ABS blends.

Keywords: *Chemical resistance**,** impact properties, polymer blends*

Introduction

Polymer blending has been considered as an effective method for the development of new polymeric materials. The properties of polymer blends are influenced by the properties of each components and degree of dispersion of the minor component [1]. Polymer blends are produced primarily to enhance the toughness of the composition. Many plastics are widely used because of their chemical resistance, low weight and mechanical strength. Indeed, plastics find widespread use in chemical plants, in distribution systems for natural gas and water, and in effluent and sewage disposal network [2].

This present study focuses on the blending of PP with ABS. As a non-polar, high molecular weight paraffinic hydrocarbon, PP has outstanding chemical resistance, the best of all thermoplastics to organic chemicals. Indeed, there is no solvent for PP that can dissolve PP completely, although it may swell in some cases. One of the advantages of ABS relative to reinforced polyolefins is its chemical resistance. The polar nitrile groups make ABS quite resistant to a variety of solvents and uptake of water is relatively low. This chemical resistant has allowed ABS entry into a wide variety of home appliances and automotive area [3].

Recently Singha and Thakur [4] reported that polymer composite with different dimension of show different chemical resistance behavior. They observed that resistance towards chemicals decreases with the increase in fiber dimension. Another study on chemical resistance evaluation was done by Shamsudin *et al.,* [5] which reported the effect of SEBS on PS/PP blends in term of chemical resistance. Their results showed that the chemical resistance of PS/PP blends increased with increasing SEBS content at relatively lower PP content but decreased with increasing SEBS content at higher PP content. Since the studies on chemical resistance of polymer blends including PP/ABS blends have received very little attention among researchers, therefore in this study, investigation on PP/ABS blends in term of chemical resistance and mechanical properties was carried out using two different reagents which are acetone and gasoline.

Materials and Methods

Materials

The material used in this study was obtained from commercial sources. The selected type of polypropylene used in this study was PP homopolymer (TITANPRO 6331) supplied by Titan Petchem (M) Sdn. Bhd. The ABS was provided Toray Plastics Malaysia Sdn. Bhd, graded as TOYOLAC 100 322. Both of these resins are originally in the form of pellet. The characteristics of the PP and ABS are summarized in Table 1.

Table 1: Characteristics of polymers used in this study

Properties	TITANPRO 6331	TOYOLAC 100 322
Melt flow rate (g/10 min)	14 (at 230°C)	15 (at 220°C)
Tensile strength at yield	360 $kg \cdot cm^{-2}$	48 MPa
Flexural modulus	17500 $kg \cdot cm^{-2}$	2280 MPa
Notched Izod impact strength at 23°C	2.6 $kg.cm \cdot ck^{-1}$	226 $J \cdot m^{-1}$
Water absorption after 24 h	0.02%	0.3%

Blend Preparation

Blends of PP and ABS were prepared using 25 mm diameter twin screw extruder *(Brabender Plasticoder PL2000)* with a screw ratio of 30:1 length to diameter. ABS with the weight fractions ranged from 0.2 to 0.5 with the increment of 0.1 was mixed with the PP using extruder. The temperatures of the extruder were set at 210 to 220°C in feeding and barrel zones respectively. The screw speed of the extruder was set at 50 rpm. Samples were injection molded on *JSW 100 Ton Injection Molding* to produce the test sample in the form of Izod impact bar (ASTM D256-10). The temperature for injection molding were set at 180°C, 220°C, 230°C and 240°C. All the samples were dried in an oven for 80°C for 24 h and then were cooled in desiccator.

Chemical Resistance Analysis

For the chemical resistance test, the dried samples were immersed in two different chemical reagents which were acetone and gasoline. The chemical resistance towards acetone and gasoline were analyzed through two swelling effect and weight loss. This testing method was carried out in accordance to ASTM D543-06 with the specified time of 24 and 168 h of immersion. Changes in mass were reported for swelling effect for time duration of 24 and 168 h which indicates short and long period of time. Percentage of swelling can be obtained by using the following equation [2]:

$$\text{Percentage of swelling} = \frac{(m_2) - (m_1)}{m_1} \times 100 \quad (1)$$

Where m_1 = Swollen weight of the sample after immersion

m_2 = Initial weight of the sample before immersion

Weight loss was determined after 168 hours of immersion. Before that, the samples were dried in an oven to get the consistent weight and then were cooled in desiccator before weighed.

Izod Impact Strength

The impact strength of PP/ABS blends before and after immersion was measured by notched Izod impact tester *(Toyoseiki Tokyo)* to determine the mpact strength before and after immersion in chemical reagents. The impact test was performed in accordance to ASTM D256-10. Five samples were tested for each blend.

Results and Discussion

Chemical resistance towards acetone

Chemical attack normally occurred before total dissolution of polymeric material takes place. Swelling effect is a type of chemical attack which represented by the percentage of weight increase after the immersion. PP has a good chemical resistance towards acetone since the weight increased in PP is minimal and less than 2% and with that, it indicates that the structure of PP is hard to be broken when attacked by the group of ketone from acetone. However, the effect of acetone on pure ABS, especially on its dimension and weight changes was clearly observed. ABS was completely dissolved within 24 h after the immersion in acetone which indicates that ABS has a weak chemical resistance and severe effect towards acetone.

As a non-polar and high molecular weight paraffinic hydrocarbon, PP has an outstanding chemical resistance, the best of all thermoplastics to organic chemicals. Since PP contains only hydrogen and carbon and does not contain polar atoms, the resistance towards chemical reagents including acetone has increase due to strong hydrogen bonding inside the PP structure. The degree of crystallinity could also affect the chemical resistance of the material. The higher the degree of crystallinity of the material, the greater its chemical resistance will be. e.g. homopolymer PP have more chemical resistance than the random copolymer PP [6]. ABS is resistant to chemical attack from acidic and alkaline solutions, but is severely degraded by most polar solvents [3]. Most of the structure of ABS is amorphous; it is generally more prone to chemical attack. The weakness of ABS towards chemical attack of acetone is probably due to the presence of styrene which contains benzene ring in the polymer structure causing it to have relatively more open structure. In particular, there is a much stronger tendency towards chemical dissolution than in the case with semi-crystalline polymers such as PP.

One of the methods to determine the chemical resistance is by swelling effect. Figure 1 shows the swelling effect of PP/ABS blends after the immersion in acetone for 24 and 168 h. The chemical resistance of PP/ABS blends was decreased with the increasing ABS content. The significant increase in swelling was observed at the blend containing 40% (w/w) of ABS which probably occurred because of more void space available in the blend and it is relatively open structure causing the structure of the blend easier to be penetrated by the solvent molecules. As the time of immersion increase, the swelling effect increased and the difference between swelling effect for 24 and 168 h can be clearly seen that these materials cannot withstand the chemical attack from acetone for long period of immersion. As for pure ABS, total dissolution takes place within 24 h and the result indicates that ABS has severe effect towards acetone and its chemical resistance is weak.

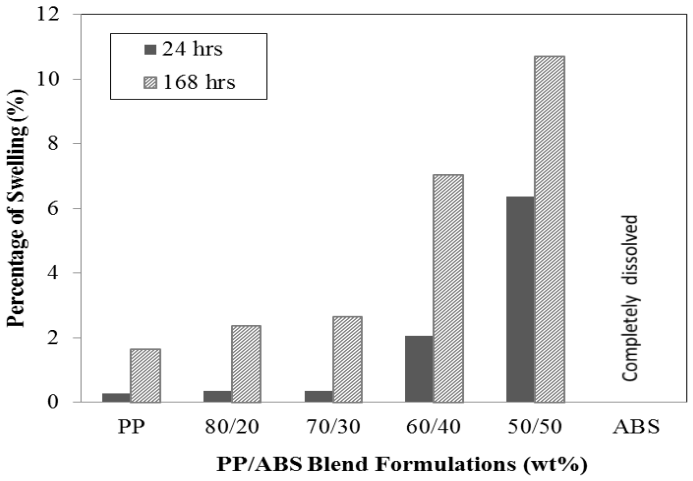

Figure 1: Swelling effect on various PP/ABS blends after immersion in acetone for 24 and 168 hours.

Chemical resistance behavior of PP/ABS blends were also evaluated by studying the weight loss of the samples after 168 h of immersion. The determination of polymer dissolution was done after the sample achieves consistent weight after. The amount of polymer dissolved can be shown by the weight losses. For weight loss, the samples were dried in an oven until it reached constant weight and then cooled in desiccator to prevent moisture uptake. Figure 2 illustrates the weight loss of various PP/ABS blends after 168 h of immersion in acetone.

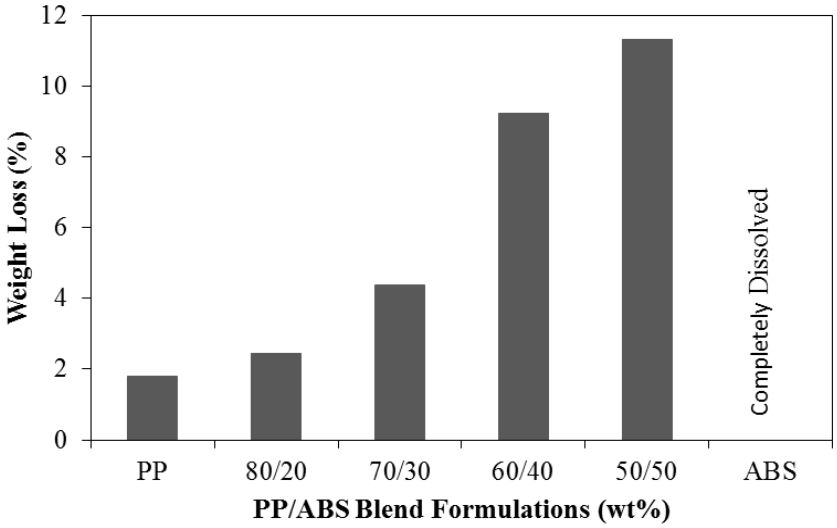

Figure 2: Weight loss of PP/ABS blends after 168 hours of immersion in acetone.

The results of the weight loss were consistent with the results of swelling effect from the previous discussion in which PP still shows the better chemical resistance compared to pure ABS, which has the weakest chemical resistance and completely dissolved in acetone after 168 hours of immersion. From Figure 1 and Figure 2, both findings show the reduction in chemical resistance, especially at 60/40% (w/w) of PP/ABS blend. It was probably due to the increase in ABS content which contains aromatic ring that makes the blend vulnerable to the

chemical attack. The higher the percentage of the weight loss the weaker the chemical resistance of the blends can be towards the chemical reagent.

Chemical resistance towards gasoline

The blends were also immersed in gasoline in order to study the effect of swelling and the weight changes of PP/ABS blends towards different chemical reagent, for 24 and 168 h. As mentioned previously, the swelling effect and the weight changes are types of chemical attack which occurs when the polymer materials are being exposed to other chemical reagents. Using the same technique as immersion in acetone, the percentage of swelling was calculated and the result was displayed as in Figure 3.

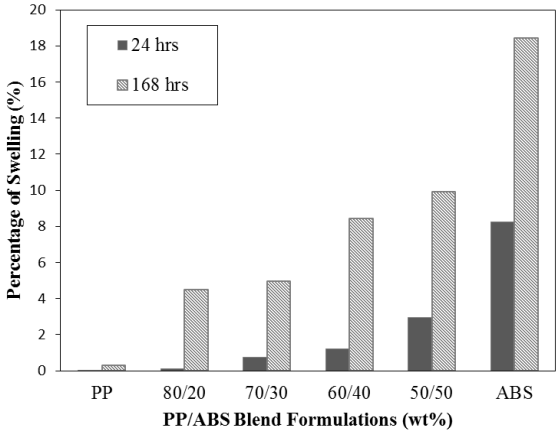

Figure 3: Swelling effect on various PP/ABS blends after immersion in gasoline for 24 and 168 hours.

Since PP and ABS are widely used in automotive industry, these materials have potentially to be exposed to the chemical reagents especially to gasoline. By comparing the percentage of swelling of PP/ABS blends towards gasoline and acetone, it was observed that the chemical resistance of PP/ABS blends towards gasoline is better than acetone. Pure PP only swells about 0.2% after 7 days (168 h) of immersion in gasoline compared to about 1.7% of swelling of PP in acetone. Since a typical molecular structure of gasoline is isooctane (C_8H_{18}), the chemical attack is difficult to occur. The chemical reaction could not occur between PP and gasoline since PP is a non-polar material, which makes PP impossible to be reacted chemically with other non-polar solvents.

However, by incorporation of polar group in PP. i.e. ABS, the chemical reaction could occur between gasoline and PP/ABS blends. The presence of aromatic ring inside ABS structure makes the blends potentially expose to the chemical attacks that can affect the chemical resistance of PP/ABS blends. The higher the content of ABS, the weaker the chemical resistance of the blends could be. Pure ABS does not dissolved in this solvent for specified time unlikely in acetone because of hydrocarbon chains in gasoline that makes its chemical attack not strong enough to penetrate ABS structure completely, but there is possibility for pure ABS to dissolve completely if the immersion occurs in long period of immersion.

Figure 4 illustrates the effect of PP/ABS blend composition on chemical resistance towards gasoline. The weight loss increase with increasing ABS content as expected. The weight loss of PP is minimal and can be neglected unlikely ABS which has weight loss of about 13% within 168 h of immersion and it signified the weakest chemical resistance. There were significant changes in term of weight loss and swelling effect for 80/20% (w/w) of

PP/ABS, probably occurred because of the effect of aromatic ring as discussed previously. An increase from 20 to 50 % (w/w) of ABS increased the weight loss of about 2 to 6%, respectively, which is relatively quite low compared to immersion in acetone. Overall results revealed that gasoline had a weaker effect on PP/ABS blends compared to acetone.

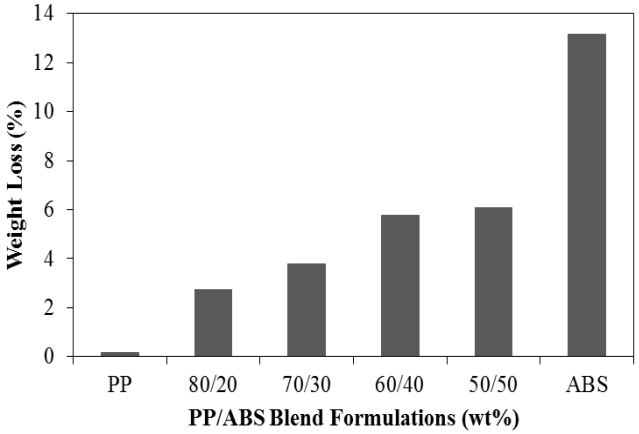

Figure 4: Weight loss of PP/ABS blends after 168 hours of immersion in gasoline.

Impact strength

Figure 5 shows the effect of acetone and gasoline on the impact strength of PP/ABS blends. The impact strength of neat PP and ABS before immersion is 27 and 226 $J \cdot m^{-1}$, respectively. The impact strength of non-immersed PP/ABS blends gradually increased as ABS content increases. This finding was consistent and in agreement with Hyung *et al*., [1] and Chong *et al*., [7], which also found that the impact strength of PP/ABS blends increased with increasing content of ABS. No significant changes was observed in the impact strength of immersed and non-immersed PP/ABS blends, which indicates that acetone does not contribute any significant effect on the impact strength of PP/ABS blends. It was probably due to the ketone group in acetone cannot penetrate deeper in PP chains but can only attack the chain at the surface. However, the impact strength of blends increased significantly after immersed in gasoline. This is possibly due to the strong hydrogen bonding that lies inside PP/ABS blends. After immersion in gasoline, hydrogen bonding of isooctane in gasoline contributed the strength to the chain of PP/ABS blend that makes the hydrogen bonding even stronger than before immersion. Meanwhile, the impact strength of pure ABS after immersion is lower than before immersion is due to the lack of hydrogen bonding of PP and due to the open structure caused by aromatic ring structure that weakened its impact strength. Overall the results revealed that gasoline had a stronger effect on PP/ABS blends on the impact strength compared to acetone.

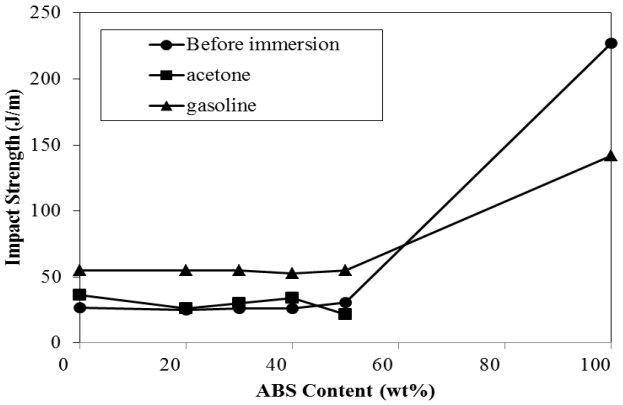

Figure 5: Impact strength of PP/ABS blends before immersion and after immersion in acetone and gasoline.

Conclusion(s)

The study has investigated the effect of acetone and gasoline on the chemical resistance of pure PP and ABS and also on the PP/ABS blends. ABS was completely dissolved in acetone solvent due to the presence of aromatic ring. The chemical resistance of PP/ABS blends towards acetone decreased with increasing ABS content. However, the chemical resistance of PP/ABS blends towards gasoline was found to be better than acetone and ABS was not completely dissolved in gasoline. On the other hand, immersion in gasoline had caused the impact strength of PP/ABS blends increased significantly compared to the impact strength of non-immersed blends. Meanwhile, immersion in acetone did not give any changes on PP/ABS blends in term of the impact strength.

Acknowledgements

This research was supported by a grant (Vot. No. 4F060) from the Ministry of Science, Technology & Innovation, Malaysia. The authors would like to thanks to Research Management Centre (RMC), UTM, MMRA Research Alliance, Idemitsu Petrochemicals (M) Sdn. Bhd and staffs from Polymer Department, Faculty of Chemical Engineering, Universiti Teknologi Malaysia.

References

[1] Hyung, G.L., Yu, T. S., Yun, K. L. and Woo, N. Y. 2009. *Macromolecular Research*. 17(6):417-423.

[2] Samsudin, S. A., Hassan, A., Mokhtar, M. and Syed Jamaluddin, S. M. 2006. *Malaysian Polymer Journal*. 1(1):11-24.

[3] Adams, M.E., Buckley, D.J., Colborn, R.E., England, W.P. & Schissel, D.N. 1993. *Acrylonitrile-butadiene-styrene polymers*. United Kingdom: Rapra Tech Ltd.

[4] Singha, A. S. and Thakur, V. K. 2009. *Polymer-Plastics Technology and Engineering*. 48:736-744.

[5] Shamsudin, S.A. 2002. *Mechanical Properties and Chemical Resistance of Polystyrene/Polypropylene Blends: Effect of SEBS as a Compatibilizer*. Master. Universiti Teknologi Malaysia, Skudai

[6] Tripathi, D. 2002. *Practical guide to polypropylene*, 59-61. United Kingdom: Rapra Tech Ltd.

[7] Chong, K. K., Yu, T. S., Yong, S. K., Hyung, G. L. and Woo, N. K. 2007. *Macromolecular Research*. 15(4):308-314.

INFLUENCE OF ORGANOCLAY LOADING ON THE IRRADIATION INDUCED CROSSLINKING AND DEGRADATION OF EVA/SMR L BLEND

Y. Munusamy[1], H. Ismail[2], C.T. Ratnam[3]

1 Petrochemical Engineering Department, Faculty of Engineering & Green Technology, Universiti Tunku Abdul Rahman, Jalan Universiti, Bandar Barat, 31900 Kampar, Perak, Malaysia.

2 Polymer Division, School of Materials & Mineral Resources Engineering, Universiti Sains Malaysia, 14300 Nibong Tebal, Penang, Malaysia.

3 Radiation Processing Technology Div., Malaysian Nuclear Agency, Bangi, 43000 Kajang, Selangor DE, Malaysia

Abstract

Ethylene vinyl acetate (EVA)/Standard Malaysian Natural Rubber (SMR L)/organoclay nanocomposites were prepared by melt blending technique. The EVA: SMR L ratio was fixed at 50:50 and organoclay loading was varied from 0 to 10 phr. All the samples were irradiated using a 3.0 MeV electron beam machine with doses ranging from 50 to 200 kGy. The effect of organoclay loading on the crosslinking and degradation nanocomposites was studied. At lower irradiation dose (50, 100 and 150 kGy), the organoclay reduced the crosslinking yield significantly. However, at 200 kGy the crosslinking yield was not much affected by the organoclay loading as evidenced from the gel fraction results. Different level of irradiation dose was also found to form different phase morphology on the nanocomposites as shown in the scanning electron micrographs. Decrement of crosslink network formation with incorporation of organoclay increased tan $delta_{max}$ values for the nanocomposites compared to neat EVA/SMR L at irradiation dosage 100 kGy. In contrast at 200 kGy irradiation dose, tan $delta_{max}$ decreased with the incorporation of organoclay. Analysis on FT-IR spectrums proved that the nanoscale dispersion and barrier effect of organoclay influenced the crosslinking degradation of the nanocomposites.

Keywords: *Crosslinking, electron beam irradiation, nanocomposite, organoclay*

Introduction

Electron beam (EB) irradiation is an effective method to crosslink polymer matrix at low temperatures and after the product is formed, thus, inhibits pre-crosslinking problems [1, 2]. Previously the effect of irradiation crosslinking was studied in polyvinyl chloride (PVC)/epoxidized natural rubber (ENR 50) blend [3] nylon 1010 and high impact polystyrene blend [4] and low density polyethylene (LDPE)/ EVA blend [5].

When polymers are subjected to EB irradiation, other than crosslinking, degradation might also occur. At the microscopic level polymer degradation is characterized by macromolecular chain splitting, development of low mass fragments, production of free radicals and oxidation. These affect the macroscopic properties such as mechanical strength, color, electrical conductivity and etc. [6]. Extensive studies had been carried out to determine the influence of polymer chain orientation and structure on the crosslinking and degradation of EB irradiated polymer matrix [7, 8]. However studies on the effect of nanofiller on the crosslinking and degradation of EB irradiated nanocomposites are scarce.

Therefore in this work, the effect of organoclay loading on the crosslinking and degradation of EB irradiated ethylene vinyl acetate (EVA)/Standard Malaysian Natural Rubber (SMR L)/organoclay nanocomposites was studied. This blend has a large potential as a zero halogen material to substitute plasticized PVC in various applications [9, 10]. Incorporation of organoclay improves the mechanical properties, thermal stability, flame retardancy and

resistance to water absorption of the blend as been proven in our earlier research work [11]. The improvement of these properties is largely contributed by the nanoscale dispersion and the unique barrier properties of organoclay. Both of these criterions of organoclay are also expected to influence the crosslinking and degradation of polymer matrix significantly.

Materials and method

Materials

EVA with 15% vinyl acetate content was supplied by The Polyolefin Company (Singapore) Pte. Ltd. (Cosmothene EVA H2020). The natural rubber used was Standard Malaysian Rubber (SMR L) purchased from Kumpulan Guthrie Sdn. Bhd, Seremban, Malaysia. Organoclay was supplied by Nanocor, Inc, USA (Nanomer 1.30T). Nanomer 1.30T was surface modified montmorillonite with 15 to 30% (w/w) octadecylamine. The organoclay is in powder form with 18 to 23 μm mean dry particle size.

Method

Prior to blending organoclay was vacuum dried at 80°C for 24 h [12]. The EVA/ SMR L nanocomposites were prepared by melt mixing in a Haake Rheomix Polydrive R 600/610 at 120°C and rotor speed of 50 rpm. The blend ratio of SMR L and EVA was fixed at 50:50 and the organoclay loading was varied from 0 to 10 phr. The nanocomposites were compression molded in an electrically heated hydraulic press, KAO compression molding machine to produce sheet with 1 mm thickness.The molded sheets were irradiated using a 3 MeV *electron beam accelerator NHV EPS-3000* at a dose range of 0 to 200 kGy. The acceleration energy, beam current, and dose rate were 2 MeV, 2 mA, and 50 kGy per pass, respectively.

Extend of crosslinking was determined by gel fraction method. The blends were solvent extracted with xylene for 48 h at 140°C and the extracted samples were dried at constant weight. The gel fraction was calculated according to Equation 1:

$$Gel\ fraction = (W/Wo) \times 100 \quad (1)$$

where W and W_0 are the weight of the dried sample after extraction and the weight of the sample before extraction, respectively.

The phase morphology of selected compositions was studied using Field emission scanning electron microscopy, *FESEM SUPRA36VP-24-58*. The selected samples were cryogenically fractured and the rubber phase was selectively extracted. The extraction was done to make clear contrast between the dispersed and continuous phases of the blends.

Dynamic mechanical analysis was performed in three point bending mode using *Metler Toledo DMA861^e* at temperature intervals from -110 to 70°C for all the samples with heating rate 5°C/min and using a frequency of 1 Hz. The samples with the dimension of 60 x 12 x 3 mm (*l* x *w* x *t*), were used.

FT-IR test was done *using Perkin Elmer System 2000* with 32 scans at 4 cm^{-1} resolution and within the wave number range of 400-4000 cm^{-1} for all neat EVA/SMR L and its nanocomposites. FT-IR testing on neat EVA/SMR L and its nanocomposites were done directly on the sample surface through Attenuated Total Reflectance (ATR) technique. The carbonyl index (CI) was determined using Equation 2:

$$CI = \frac{A_{1738}}{A_{2850}} \quad (2)$$

where A_{1738} is the absorbance of the ketonic carbonyl stretching vibration at 1738 cm^{-1} and A_{2850} is the absorbance of the methylene C-H symmetric stretching vibration at 2850 cm^{-1}; the latter absorption is an internal standard that compensates for differences in film thickness.

Results and Discussion

Crosslink Evaluation and Phase Morphology of Irradiated Nanocomposites

The gel fraction yield increased with increment in irradiation dosage, as shown in Figure 1. The enhancement of gel fraction yield was more significant when the irradiation dosage was more than 100 kGy. At irradiation dosages of 50, 100, and 150 kGy, the gel fraction yield was significantly reduced with the increase in organoclay loading.

The energy from EB radiation will knock out one hydrogen atom from polymer chain, thus produce EVA and SMR L macro molecular radicals [13]. These radicals can be scavenged by organoclay, thus the radical-radical interaction hindered and the crosslink network formation will be reduced [14]. Natural montmorillonite (MMT) consists of negatively charged layered silicates [15]. It is noteworthy that organoclay used in this research is modified with 15 to 30% (w/w) octadecylamine and therefore some percentages of the organoclay surface still remain negatively charged. The negatively charged surfaces can terminate macromolecular polymer cations [16]. In addition organoclay nanoparticles also block the sites for crosslinking in the polymeric matrix due to the nano level dispersion of organoclay [17]. However, at 200 kGy, the gel fraction yield was not much affected by organoclay loading. At this irradiation dosage large amount of free radicals will be formed and it can overcome the scavenging and blocking effect of organoclay, thus, form more crosslink networks.

Effect of different level of irradiation dosage on the phase morphology of EVA/SMR L blend and its nanocomposites was studied using SEM micrographs. Non-irradiated neat EVA/SMR L exhibit co-continuous phase morphology is as shown in Figure 2(a). At irradiation dosage 100 kGy, the SMR L phase becomes dispersed in the continuous EVA phase. However most of the dispersed domains are large in size and due to low electron beam energy at 100 kGy some of the lightly crosslinked SMR L phase domains are in elongated shapes (see Figure 2(b) and Figure 2(c)). As the irradiation dosage was increased up to 200 kGy, the SMR L phase exits as spherical dispersed domains with smaller domain size (see Figure 2(d) and Figure 2(e)).

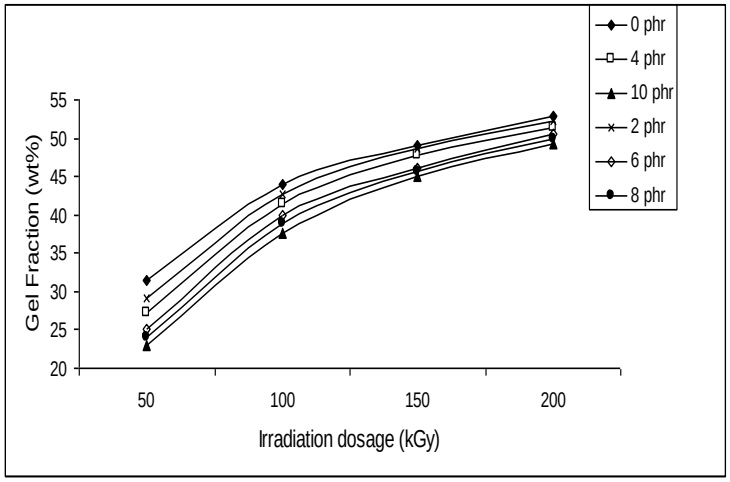

Figure 1: Effect of irradiation dosage and organoclay loading on the gel fraction yield of EVA/SMR L blend and the nanocomposites.

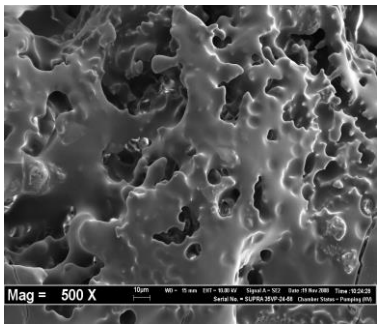

a. 0 kGy/EVA/SMR L/0 phr

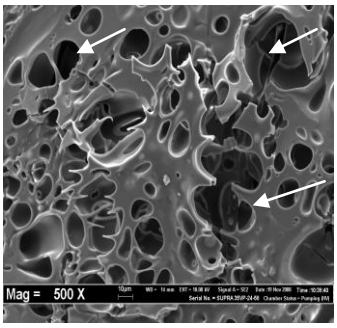

b. 100 kGy/EVA/SMR L/2 phr

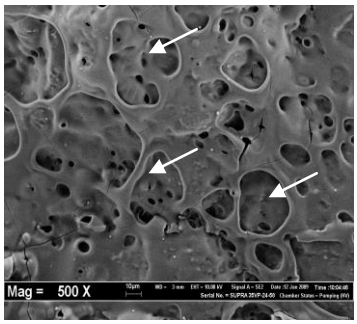

c. 100 kGy/EVA/SMR L/8 phr

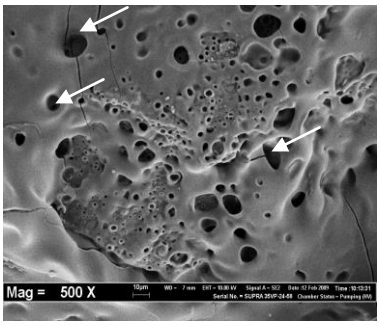

d. 200 kGy/EVA/SMR L/2 phr

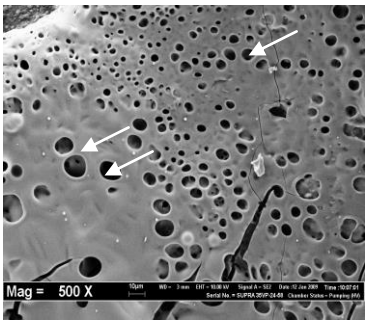

e. 200 kGy/EVA/SMR L/8 phr

Figure 2: SEM micrographs of etched cryogenically fractured surfaces for non irradiated neat EVA/SMR L and irradiated EVA/SMR L nanocomposites at magnification 500X (white arrows indicates the SMR L phase).

FT-IR Analysis

Exposure of EVA/SMR L matrix to electron beam irradiation will lead to formation of free radical species. These radicals can undergo crosslinking to form three dimensional networks. However crosslinking is not the only reaction that occurs when the nanocomposites were exposed to electron beam irradiation. Chain scission and oxidation of the polymeric chain might also occur. The FTIR spectra for neat EVA/SMR L and its nanocomposites are shown in Figure 3.

FT-IR spectra can be used to evaluate extends of crosslinking, oxidation and chain scission of the polymeric matrix upon exposure to different irradiation dosage. The area under selected peaks on FTIR spectra and carbonyl index were calculated in order to have a better insight on the reactions that occur during irradiation.

Figure 4 shows the variation of area under absorbance at 1462 cm^{-1} as a result of C-H bending of >–CH_2 [18]. It is clear that the absorption increases at 100 kGy and then decrease at 200 kGy for the neat EVA/SMR L and its nanocomposites. Large amount of free radicals are formed at 100 kGy due to chain scission, thus increase >–CH_2, whereas at 200 kGy this radicals can recombine and form crosslinking. At 100 kGy, increment in organoclay loading increases the absorption tremendously. As mentioned earlier, organoclay blocks the sites for crosslinking, thus the polymer macromolecular radicals' exits as free radicals which will not be able to form crosslinks. This finding is in conjunction with the gel fraction results.

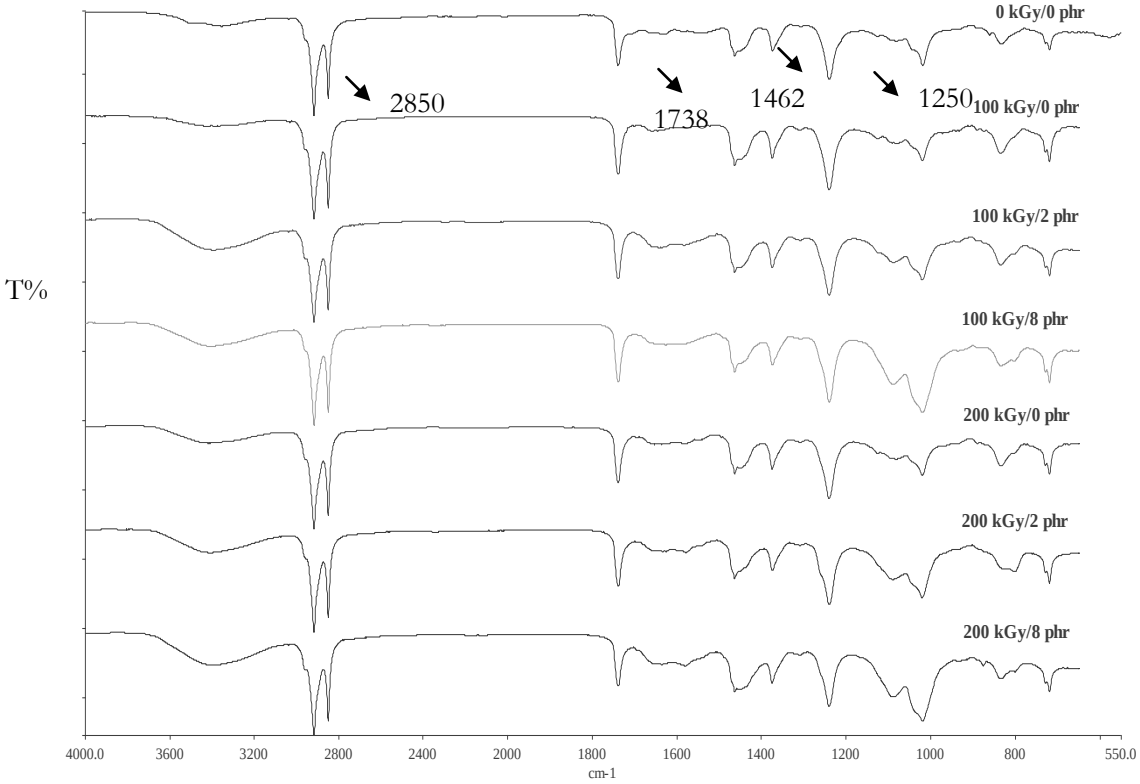

Figure 3: FTIR spectra for non irradiated neat EVA/SMR L and irradiated EVA/SMR L nanocomposites.

The variation of absorbance at 1250 cm^{-1} is plotted against irradiation dosage in Figure 5. This peak corresponds to C-O stretching. At 0 and 8 phr organoclay loading, the area increased up to 100 kGy and then decreased at 200 kGy. At 100 kGy irradiation dosage degradation due to oxidation is dominant. At 2 phr organoclay loading the area under the peak remain almost constant due to the barrier effect of organoclay which will inhibit oxidation. The effect of organoclay in retarding oxidation is further confirmed by carbonyl index analysis.

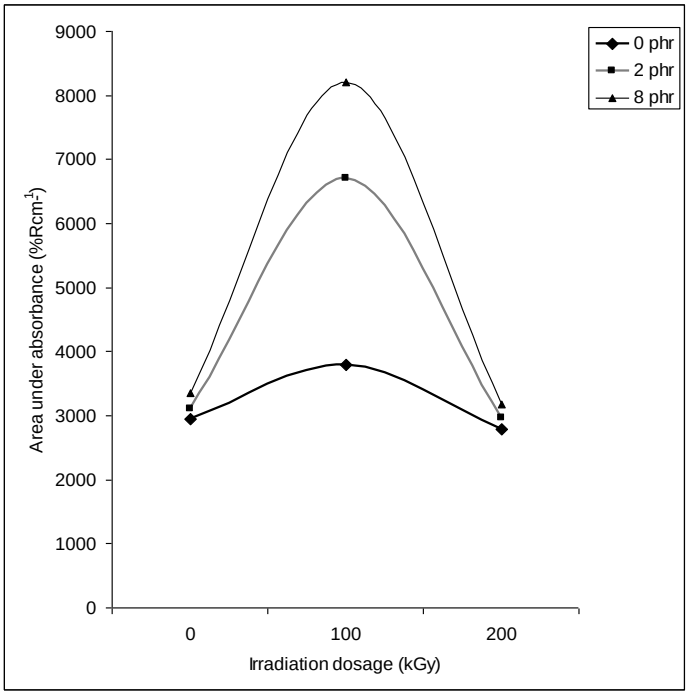

Figure 4: Change in concentration of 1462 cm^{-1} due to C-H bending of $–CH_2$ in non - irradiated and irradiated neat EVA/SMR L and its nanocomposites.

The carbonyl indexes for all the non irradiated samples are almost constant as shown in Figure 6. This is attributed by the carbonyl group in EVA. Incorporation of organoclay does not play any significant role in influencing the content of carbonyl group in the non irradiated samples. When the samples were exposed to irradiation, increment in carbonyl index indicates oxidation degradation. Oxidation degradation is more prominent at 100 kGy. Incorporation of organoclay reduces oxidation degradation due to the barrier effect especially at 2 phr loading.

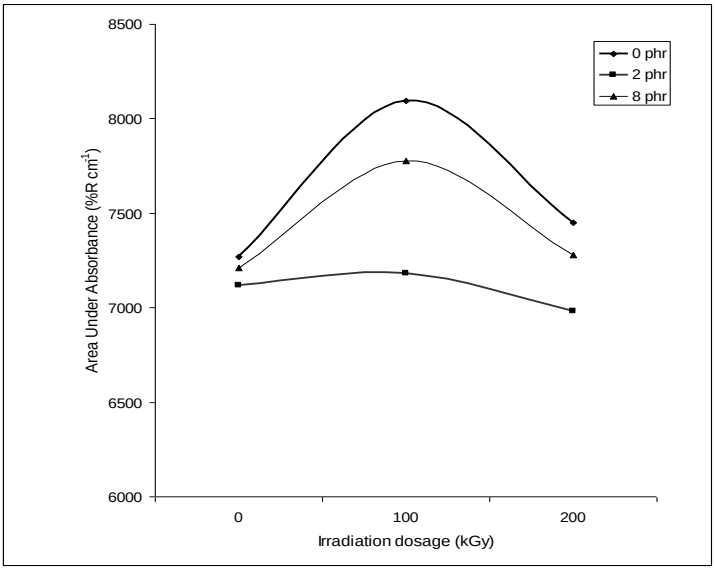

Figure 5: Change in concentration of 1250 cm^{-1} due to C-O stretching in non and irradiated neat EVA/SMR L and its nanocomposites.

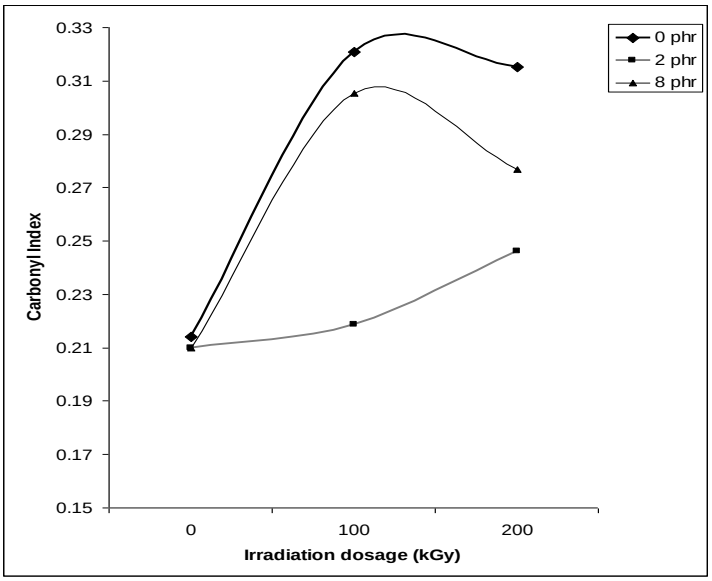

Figure 6: The carbonyl index values for non irradiated and irradiated neat EVA/SMR L and its nanocomposites.

Dynamic Mechanical Analysis

Generally for immiscible blend, the tan δ curves show the presence of two damping peaks corresponding to the glass transition temperature (T_g) of the individual polymers [21]. It is apparent from Figure 7 and Figure 8 that the tan δ_{max} for all the irradiated neat EVA/SMR L and its nanocomposites were lower compared to the non irradiated neat EVA/SMR L. The decrement in tan δ_{max} is caused by any restriction in the main chain mobility of the polymer at the T_g. The tan δ_{max} results imply that irradiation reduces the mobility of the molecules. Three dimensional networks resulting from radiation induced crosslinking will restrict the chain motion therefore the material was not able to flow even at higher temperature.

At irradiation dosage 100 kGy, low crosslink network formation caused the 2 and 8 phr organoclay filled nanocomposites to exhibit high tan $delta_{max}$ values compared to irradiated neat EVA/SMR L, as shown in Figure 14. Organoclay platelets blocks the recombination reaction of polymer macro radicals effectively at irradiation dosage 100 kGy as evidenced from large increment of area under the peak for >-CH_2 bending at 1462 cm^{-1} from FT-IR results. These free macro radicals will facilitate the easy movement of EVA and SMR L chains. Moreover when the free radicals were scavenged by organoclay, the surface chemistry of organoclay will be altered and this might reduce the interaction between the organoclay and polymer matrix, thus, reduces the demobilizing effect of polymer chains by the organoclay. However to conform this, further studies have to be conducted. In contrast at 200 kGy irradiation dosage increment of organoclay loading caused decrement in tan $delta_{max}$ values, as shown in Figure 15. Such trend of results is attributed to the filler effect of the organoclay in a highly crosslinked EVA/SMR L blend network. In other words, the increase in organoclay loading merely decreases the flow ability the blend network formed at 200 kGy, thus resulting in a decline in tan delta $_{max}$ values.

The extracted T_g values from the tan delta peaks of Figure 7 and Figure 8 are summarized in Table 1. The T_g values for all the irradiated samples are higher compared to the non irradiated neat EVA/SMR L. It was expected that both T_{g1} and T_{g2} for irradiated samples will decrease with incorporation of organoclay due to the lower crosslink network formation. However T_{g2} values for the irradiated nanocomposites are higher compared to the irradiated neat EVA/SMR L except for nanocomposites with 2 phr organoclay loading irradiated at 100 kGy. The T_{g2} values are contributed by EVA phase of the blend. EVA is a polar polymer which can form good interfacial interaction with octadecylamine on the surface of organoclay compared to SMR L phase which is non-polar in [19]. Thus, the increment in T_{g2} value with incorporation of organoclay might be due to the dominant demobilizing effect of organoclay on the polymer-organoclay interface. However at 100 kGy irradiation dosages the nanocomposite with 2 phr organoclay loading exhibit T_{g2} value lower compared to the irradiated neat EVA/SMR L. Formation of large amount of macro radicals which does not recombine to form crosslinks for this sample and low organoclay loading which gives low demobilizing effect, increases the mobility of polymeric chain. T_{g1} which is contributed by the SMR L phase was not influenced by demobilizing effect of organoclay.

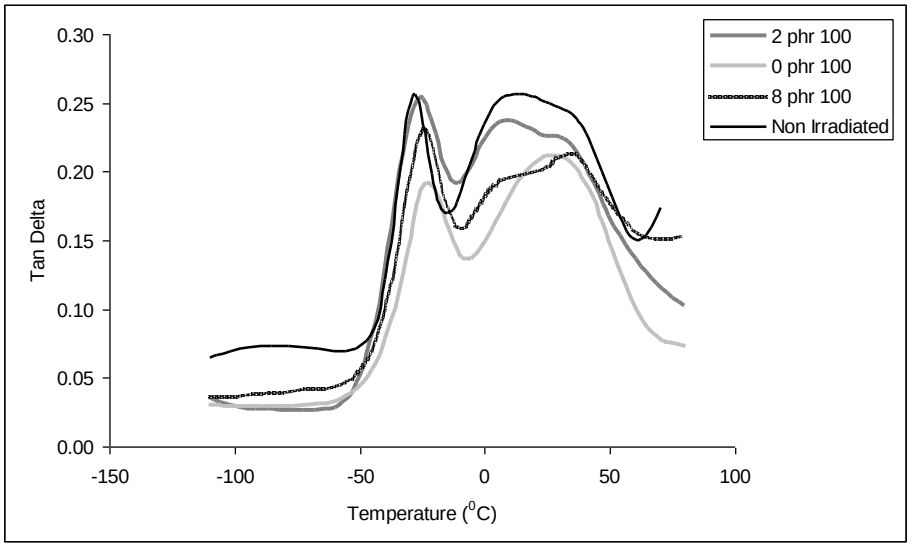

Figure 7: Tan delta as a function of temperature for non irradiated neat EVA/SMR L and 100 kGy irradiated EVA/SMR L nanocomposites.

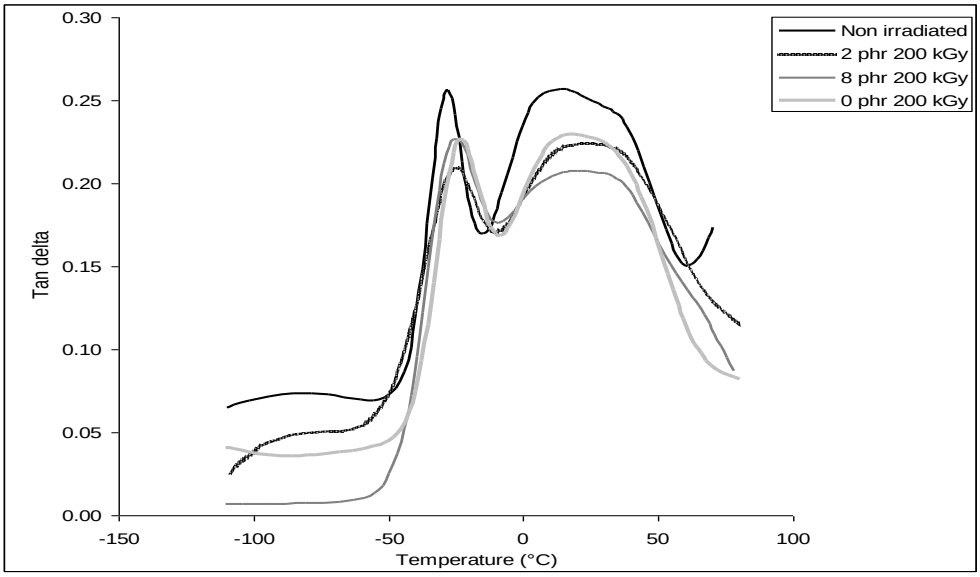

Figure 8: Tan delta as a function of temperature for non irradiated neat EVA/SMR L and 200 kGy irradiated EVA/SMR L nanocomposites.

Table 1: Glass transition temperatures (T_g) for non irradiated and irradiated neat EVA/SMR L and its nanocomposites.

Irradiation Dosage (kGy)	Organoclay Loading (phr)	T_{g1}	T_{g2}
0	0	-35.54	10.87
	0	-23.20	19.64
100	2	-24.63	14.58
	8	-23.91	21.26
	0	-23.39	20.92
200	2	-23.87	23.61
	8	-23.74	26.07

Conclusion

Incorporation of organoclay reduces the crosslink network formation at lower irradiation dose. As the irradiation dose increased, formation of large amount of macro radicals increases the formation of crosslink network even at high organoclay loading. This was also supported by FT-IR analysis. It was evident from Carbonyl Index values that organoclay can reduce oxidation degradation during exposure to irradiation. The extent of crosslink network formation upon irradiation influences the tan $delta_{max}$ values of the nanocomposites. It contrasts, T_g values are found to be dominated by the demobilizing effect of the organoclay in EVA phase as compared to the irradiation-induced crosslink network formation.

References

[1] Ratnam, C.T., Nasir, M., Baharin, A. and Zaman, K. 2001. *J. Appl. Polym. Sci.* 81:1914.

[2] Bhattacharya, A.2000. *Prog. Polym. Sci.* 25:371.

[3] Ratnam, C.T. and Zaman, K. 1999. *Nucl. Instrum. Methods. Phys. Res. Sect B.,* 152:335.

[4] Dong, W., Chen, G. and Zhang, W. 2001. *Radiat. Phys. Chem.* 60:629.

[5] Sharif, J., Aziz, S.H.S.A., and Hashim, K. 2000. *Radiat. Phys. Chem.* 58:191.

[6] Sangappa, Demappa, T., Mahadevaiah, Ganesha, S., Divakara, S., Pattabi, M. and Somashekar,
R. 2008*. Nucl. Instrum. Methods. Phys. Res., Sect B.* 266:3975.

[7] Miličević, D., Trifunović, S., Popović, M., Milić, W.T. and Suljovrujić, E. 2007. *Nucl. Instrum.*
Methods. Phys. Res., Sect. B, 260:603.

[8] Mishra, J.K., Chang, Y.W., Lee, B.C. and Ryu, R.H. 2008. *Radiat. Phys. Chem.* 77:675.

[9] Yong, M.K., Ismail, H. and. Ariff, Z.M. 2007. *Polym. Plast. Technol. Eng.* 46**:**361.

[10] Munusamy, Y., Ismail, H., Mariatti, M., and Ratnam, C.T. 2008. J*. Reinf. Plast. Compos.* 27:1925.

[11] Ismail, H., Munusamy, Y., Mariatti, M. and Ratnam, C.T. 2008. *Polym. Plast. Technol. Eng.* 47:752.

[12] Yang, I. and Tsai, P. 2006. *Polymer,* 47:5131.

[13] Ghazali, Z. Johnson, A.F. and Dahlan, K.Z. 1999. *Radiat. Phys. Chem.* 55:73.

[14] Chattopadhyay, S., Chaki, T.K. and Bhowmick, A.K. 2001a. *J. Appl. Polym. Sci.,* 79:1877.

[15] Zulfiqar, S., Kausar, A., Rizwan, M. and Sarwar, M.I. 2008. *Appl. Surf. Sci.* 255:2080.

[16] Lu, H., Hu, Y., Kong, Q., Chen, Z. and Fan, W. 2005. *Polym. Adv. Technol.* 16:688.

[17] Munusamy, Y., Ismail, H., Mariatti, M. and Ratnam, C.T. 2009. *J. Vinyl. Addit. Techn.*15:39*.*

[18] Chattopadhyay, S., Chaki, T.K. and Bhowmick, A.K. 2001b. *J. Appl. Polym. Sci.* 81:1936.

[19] Munusamy, Y., Ismail, H., Mariatti, M., and Ratnam, C.T. 2008. J*. Reinf. Plast. Compos.* 27:1925.

INVESTIGATION ON IMPROVEMENT OF MECHANICAL PROPERTIES OF KENAF/E-GLASS FIBER COMPOSITES BY MERCERIZATION AND ACETYLIZATION PROCESS

A.M Ya'acob[1], Azhar Abu Bakar[2], Hanafi Ismail[2], Khairul Zaman Dahlan[3]

[1]Aerospace Department; University Kuala Lumpur-MIAT, Malaysia

[2]Material and Mineral Resources Engineering Dept, Universiti Sains Malaysia

[3]Malaysia Nuclear Agency, Malaysia

Abstract

Kenaf/E-glass fiber composite samples were fabricated using untreated bast kenaf fiber, NaOH treated bast kenaf fiber and acetyl treated bast kenaf fiber. Samples were fabricated to compare the mechanical properties at different fiber loadings hence also to justify the significant effects between treated and untreated kenaf fiber. A further comparison was made with corresponding properties of 100% (w/w) E-glass fiber composites and 100% (w/w) epoxy sample. All samples were prepared using typical hand layup preparation techniques. Result showed NaOH treated samples exhibited the highest tensile strength. However, the highest flexural strength result was shown by the untreated sample. Studies also showed high impact values were observed for all 10% (w/w), 20% (w/w) and 30% (w/w) kenaf/ E- glass fiber composites samples.

Keywords: *E - glass fiber (E - GF), fiber reinforce composites, kenaf fiber, weight ratio*

Introduction

This report presents the comparison results between untreated and treated bast kenaf / E - glass fiber hybrid reinforced composites with various ratio of fiber reinforcement. According to Khalil et al. [1], chemical treatment increases the wettability of the fiber-matrices. In addition, NaOH treated natural fibers resulted in an increase in wettability, higher distribution of fiber inside matrix and minimum isolation of fiber-matrix hence higher mechanical properties. NaOH treatment removes the tilosis and cuticle from the fiber surfaces hence produces a rough fiber surfaces. A study done by Rong et al. [2] showed all chemical treatments resulted in greater extensibility and lower modulus thus related to the structural variation in the ultimate cells, swelling and partial removal of lignin and hemicellulose. According to Rong et al. [2], pretreatment of the natural fiber resulted in chemical and structural changes not only for the fiber surface but also in the distinct cells hence in turn influences the properties of the fibers and composites. Rong et al. [2] also stated that chemical methods bring about an active surface by introducing reactive groups and provided the fibers with higher extensibility through partial removal of lignin and hemicellulose.

Materials and method

Materials

Kenaf fiber in bast form was obtained from Malaysian Agricultural Research and Development Institute (MARDI), Malaysia thru Malaysian Nuclear Agency. Glass fiber use was fabric type non-prepreg glass fiber (120-38 STD E-glass). In this work the resins used was Alpha Epoxy resins (Part A and B)

Method

Fiber treatment – alkali

The kenaf fibers was soak in 6.0% alkali solution for 4 h at room temperature, washed with distilled water and dried at room temperature for 48 h and oven dry at less than 50°C for 6 h.

Acetyl Fiber treatment

The kenaf fiber was subjected to 18% NaOH solution for 5 min at ambient temperature followed by washing with distilled water. The fiber then was treated with 2.5% H_2SO_4 as neutralizing agent, washed and dried. The next step was to soak the kenaf fiber in a 50% acetic acid aqueous solution for 5 min where the fiber was then washed and air dried.

Preparation of untreated fiber
Raw kenaf fiber was washed with distilled water and dried at room temperature for 48 h.

Fabrication of composites
Hybrid samples of kenaf and E-glass fiber produced for this study utilized the bidirectional orientation concept where one fiber layer runs in the weft direction and the second fiber layer runs in the warp direction. Kenaf fiber was chosen randomly, clean and cut base on the length of the mold of 30 cm x 30 cm. The matrix ratio used in this study was 2:1, where epoxy resin and hardener were mixed well to achieve a proper mixing by using air pressure mixing tool. Wet layup method was used to fabricate the samples by laying down each fiber in sequence and with kenaf core. In order to provide compression pressure to the composites preparations, an air pressure vacuum fixed at approximately 21 ± 3 Hg pressure was used by means of vacuum bagging method.

Characterization
Tensile testing was accordance with ASTM D 3039 and D 5083. Tensile tests were carried out using Llyold 30 kN machine. A gauge length of 50 mm with cross head speed of 0.02 $inch.min^{-1}$ was employed. The average width and the specimen length were 25.4 mm and 172 mm respectively. The determination of flexural properties was accordance with ASTM D 790-98 and 92 for standard test methods for flexural properties of un-reinforced and reinforced plastics and electrical insulating materials using Instron 3–point bending system. The flexural test uses support span-to-depth ratio of 16:1 and the length of span of 100.0 mm with regards to an average of 6.0 mm sample thickness. The specimen's end prior to testing is 20 mm. Test specimen used was measured at 12.7 mm x 127 mm for width and length respectively. The crosshead speed was fixed at 2.6 $mm.min^{-1}$. Impact properties were determined accordance with ASTM D 256 under specific conditions of humidity of 50 % at temperature of 73°F. The width of all specimens was fixed at 12.7 mm and the length were standardize at 127.0 mm. The breaking energy for all specimens was estimated using 11.0 Joule pendulum. The fibers were then examined in an SEM microscope type FEI Quanta 400 and observation was done at room temperature using high vacuum.

Results and discussion
Tensile strength
Tensile strength results in Figure 1 shows NaOH treated samples provide the highest tensile strength and almost similar to a 100% (w/w) E-glass fiber composites samples. The untreated samples however show fluctuation pattern. Based on given result, it shows that the lowest tensile strength was given by the acetyl treated composites samples with only slight increase in overall tensile strength. With regards to the tensile modulus, results showing both NaOH treated and untreated samples provide consistency in the modulus. However, acetyl treated composites samples provide inconsistent pattern whereby 10% (w/w) and 30% (w/w) acetyl treated samples provides high modulus with comparison to a 20% (w/w) acetyl and 100% (w/w) E- glass fiber composites samples.

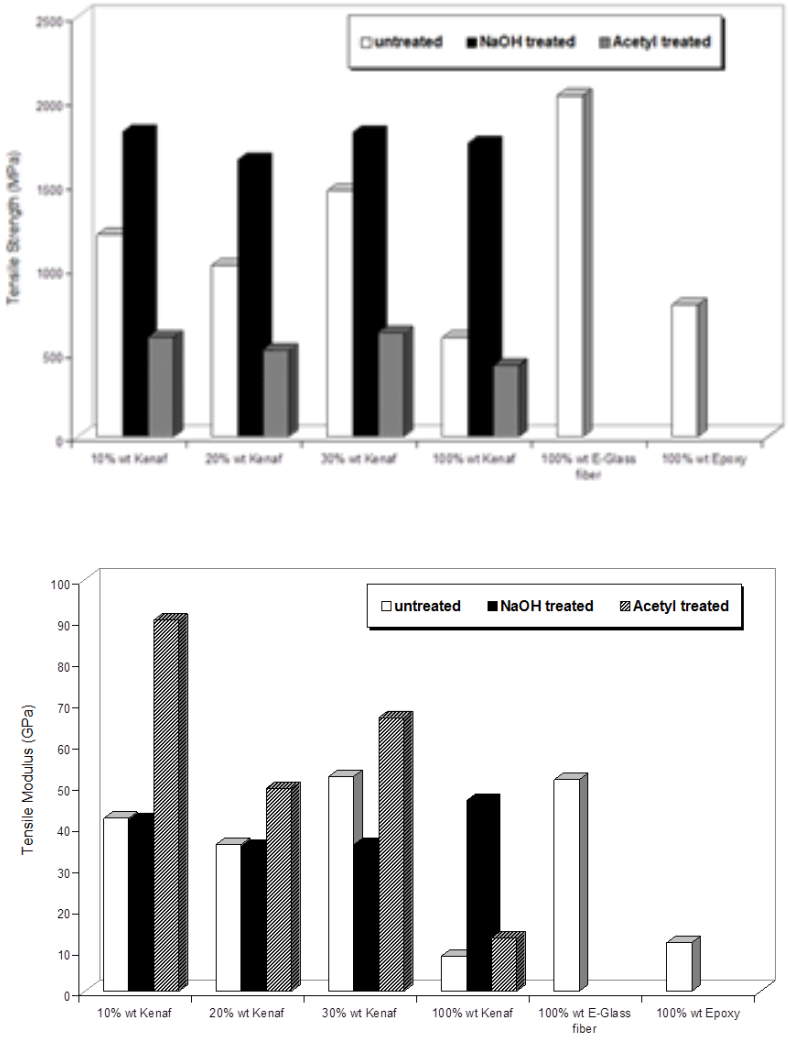

Figure 1: Overall tensile strength and modulus results comparison

Flexural strength

Figure 2 shows overall flexural strength for both treated and untreated samples. Highest flexural strength result was shown by the untreated sample except for the 100% (w/w) kenaf. Overall untreated flexural strength was similar to a 100% (w/w) E-glass fiber composites samples. Only slight increase was observed for NaOH treated samples with regards to the flexural strength. However, results also shows that acetyl samples provide inconsistent pattern. Flexural modulus results for both untreated and NaOH treated composites samples show similar results except for 100% (w/w) kenaf. Consistency was observed for both NaOH and acetyl treated composites samples with acetyl showing the lowest flexural modulus result.

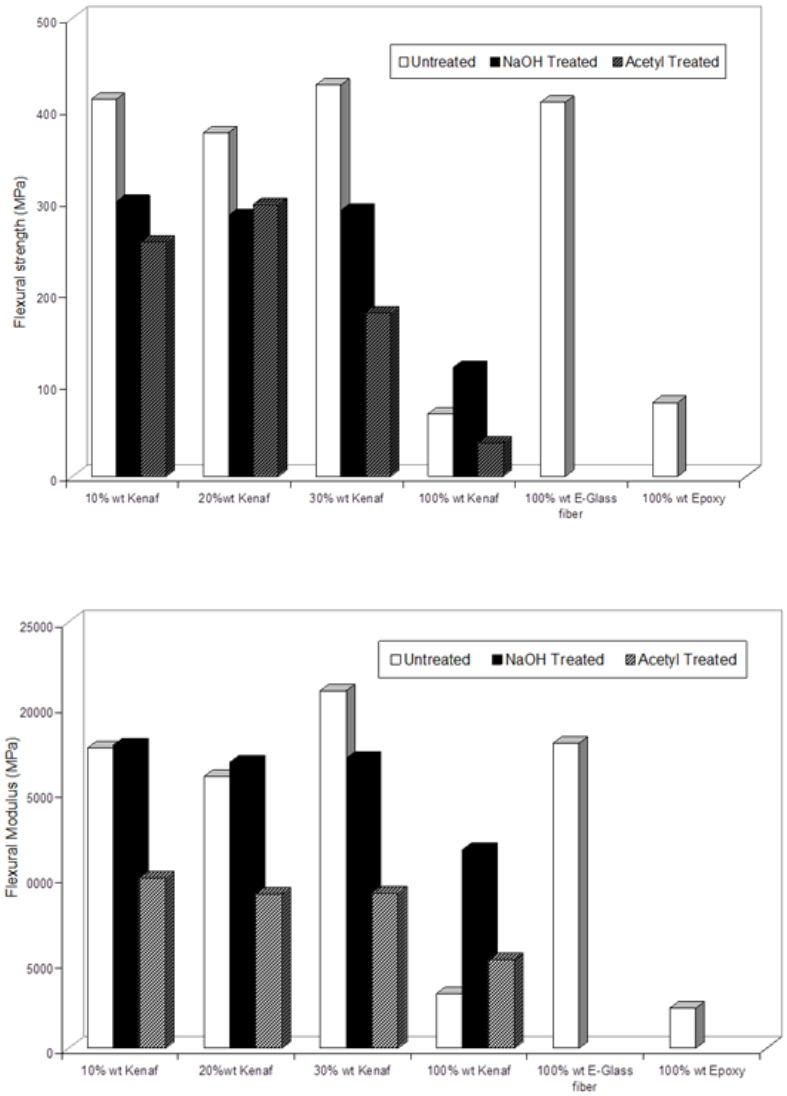

Figure 2: Overall flexural strength and modulus results comparison

Impact strength

Observation on the resilience value is shown in Figure 3. Overall impact result shows a high impact value for 10% (w/w), 20% (w/w) and 30% (w/w) kenaf/ E- glass fiber composites samples with comparison to the 100% (w/w) E-glass fiber composites. A consistent impact value was observed for 10% (w/w) hybrid samples. However, only slight difference was observed for all samples with regards to the impact value. Overall 100% (w/w) kenaf composites samples showed the lowest impact value.

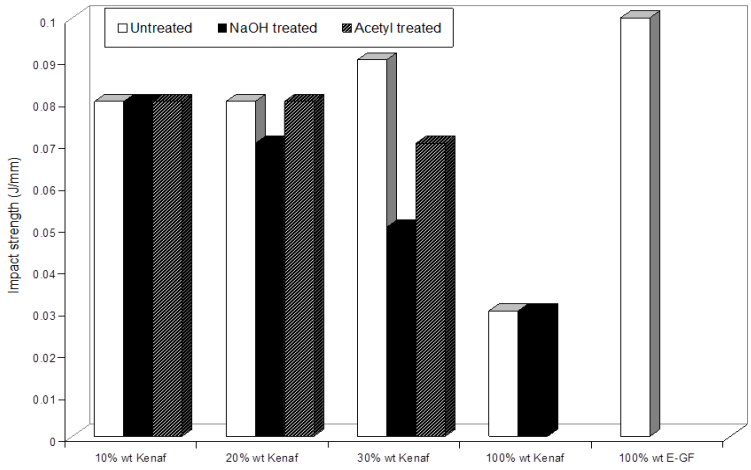

Figure 3: Overall impact comparison comparison between untreated, NaOH treated and acetyl treated samples

Fiber-matrix interaction

The results for SEM micrograph observations are shown in Figure 4 for both treated and untreated samples. Observation on 10%(w/w) untreated composites samples showing high porosity, the presence of fiber aggregation and surface impurities, cellulose porous structure (lumen) due to non-treated fibers and high voids areas resulted in low fiber-matrix adhesion. The 10% (w/w) treated NaOH kenaf composites show flat resin surfaces and fiber bundles fiber breakage. Micrograph for acetyl treated kenaf at 10% (w/w) showing high surface impurities, and visible kenaf porous lumen.

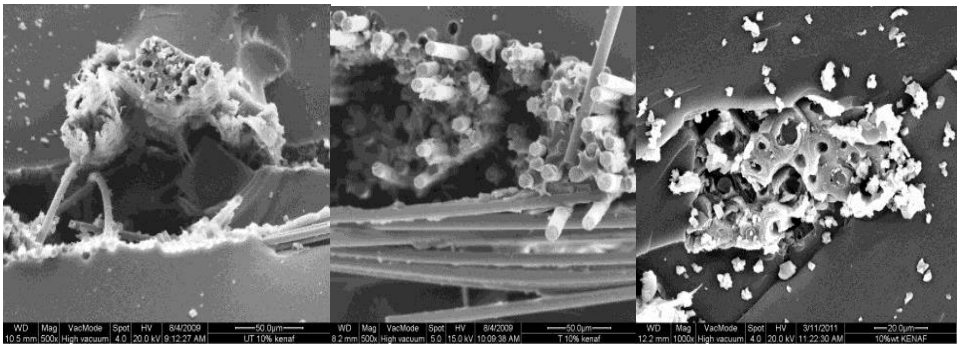

(a) (b) (c)

Figure 4: Fractured surface for (a) 10% (w/w) kenaf composite untreated at 500x magnification (b) 10% (w/w)kenaf composite treated NaOH at 500x magnification and (c) 10% (w/w) kenaf composite acetylization at 1000x magnification

Figure 5 for 20% (w/w) untreated shows visible cellulose porous structure (lumen) as prove of non treated fibers, high surface impurities, poor interfacial bonding and kenaf fiber aggregation. The 20% (w/w) treated NaOH kenaf composites show the presence of cavities or voids, surface porosity and river pattern (resin rich region). Micrograph for acetyl treated kenaf at 20% (w/w) shows high surface impurities, visible kenaf porous lumen and void areas.

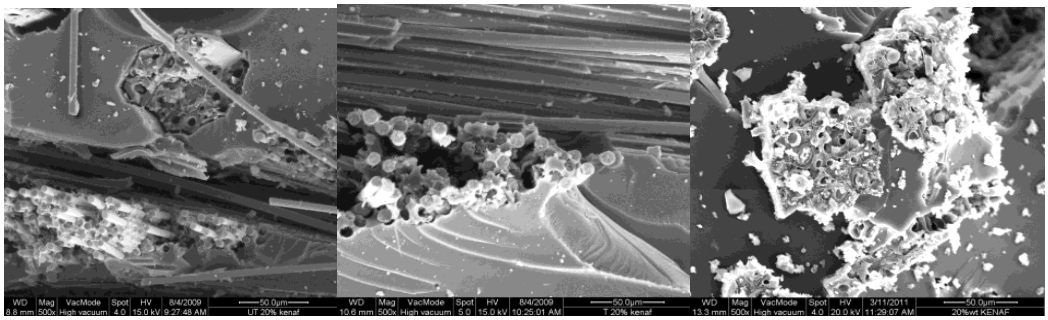

(a) (b) (c)

Figure 5: Fractured surface for (a) 20%(w/w) kenaf c o m p o s i t e untreated at 500x magnification (b) 20% (w/w) kenaf c o m p o s i t e treated NaOH at 500x magnification and (c) 20% (w/w) kenaf composite acetylization at 500x magnification

Figure 6 for 30% (w/w) untreated samples showing phase separation between the E-glass fiber and kenaf fiber thus showing an indication of poor fiber-matrix adhesion, high porosity and inhomogenity at fractured surface areas. However, the 30% (w/w) treated NaOH kenaf composites shows even matrix surface that most probably resulted from proper curing stages. The 30% (w/w) treated NaoH hybrid samples also showing fiber bundles, good resin encapsulation thus showing good resin-fiber adhesion and well entrapped kenaf fibers. Micrograph for acetyl treated Kenaf at 30% (w/w) showing high porosity, high surface impurities, visible kenaf porous lumen, high void areas and fractured formation due to fiber pull out.

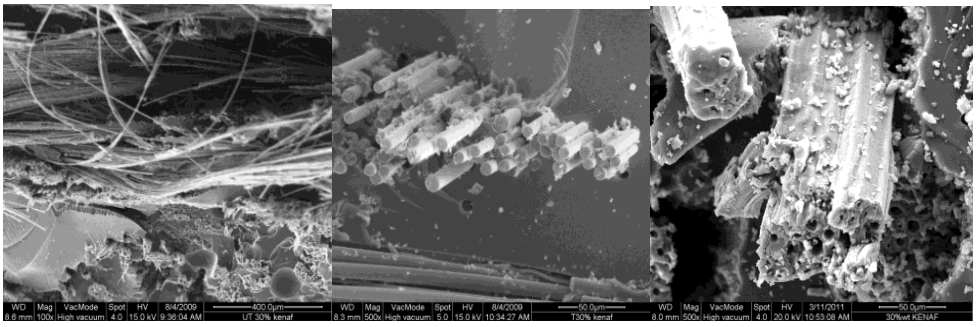

(a) (b) (c)

Figure 6: Fractured surface for (a) 30%(w/w) kenaf composite untreated at 100x magnification (b) 30%(w/w) kenaf composite treated NaOH at 500x magnification and (c) 30%(w/w) kenaf composite acetylization at 500x magnification

Theoretical Prediction

Prediction of tensile modulus using Halphin-Tsai model for kenaf/ E-glass fiber composites is given in Figure 7. I was observed that when the volume fraction of the fibers increased, the tensile modulus was also increased. The inconsistency for the tensile modulus results for untreated, NaOH treated and acetyl treated samples with comparison to the theoretical model can be justified due to possibilities of inconsistency in the fiber distribution and fiber breakage during processing as well as surface impurities.

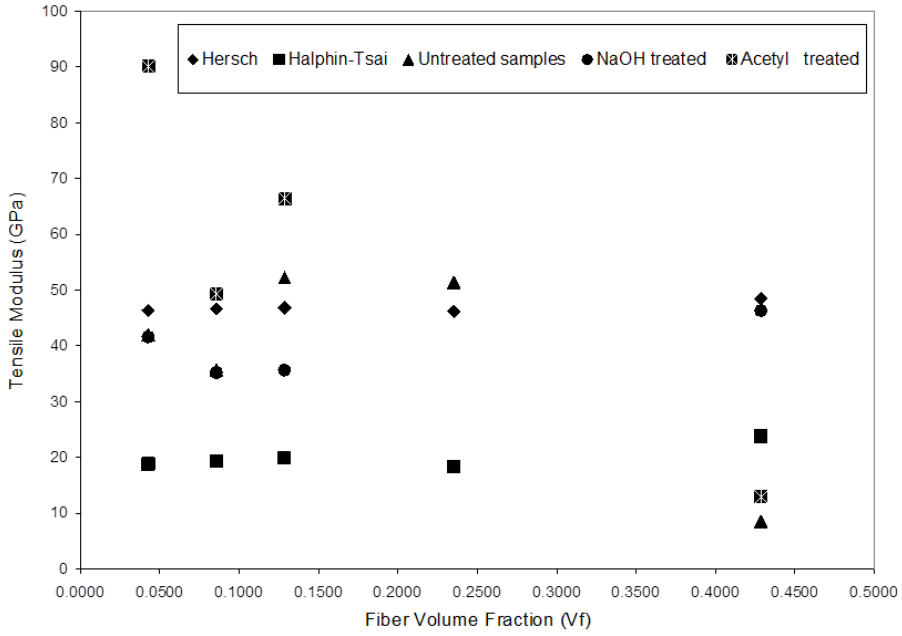

Figure 7: Prediction of tensile modulus using Halphin-Tsai model

Conclusion

Several conclusions were made base on this investigation as below;

a) NaOH treated samples provided the highest tensile strength and the lowest tensile strength was given by acetyl treated composites samples. Both NaOH treated and untreated samples showing consistency in the modulus.

b) Highest flexural strength result was shown by the untreated sample. Flexural modulus results for both untreated and NaOH treated composites samples showing similar results.

c) Overall impact result showing high impact value for 10% (w/w), 20%(w/w) and 30%(w/w) kenaf/ E-glass fiber composites samples with comparison to the 100% (w/w) E-glass fiber composites.

d) Overall micrograph for fractured surfaces showing non homogeneous surfaces hence resulted in poor fiber-matrix adhesion.

Acknowledgements

The author would like to thank Universiti Kuala Lumpur for initial financial support in the form of short term research grant. (Vote number: STR06040). The author is also thankful to Dr. Khairul Zaman Hj Dahlan, Director Radiation Processing Technology Division, Nuclear Agency Malaysia, Bangi for providing bast kenaf fiber and giving permission in using Instron, DSC and SEM for this experiment.

References

[1] Abdul Khalil Shawkataly; Rozman Hj Din. (2004); Gentian dan komposit lignoselulosik; Penerbit Universiti Sains Malaysia

[2] Min Zhi Rong; Ming Qiu Zhang; Yuan Liu; Gui Cheng Yang; Han Min Zeng. (2001); The effect of fiber treatment on the mechanical properties of unidirectional sisal-

reinforced epoxy composites; Composites Science and Technology; 61; pp 1437 – 1447
[3] ASTM D 3039 Standard test method for tensile properties of fiber-resin composites
[4] ASTM D 5083 Standard test method for tensile properties of reinforced thermosetting plastics using straight sided specimens
[5] ASTM D 790-98 and 92 for standard test methods for flexural properties of un-reinforced and reinforced plastics and electrical insulating materials
[6] ASTM D 256 Standard Test Method for impact

COMPARISON OF ACIDIC AND ALKALINE TREATMENTS IN EXTRACTION OF CELLULOSE FROM PINEAPPLE LEAVES

Mohd Razali Shamsuddin, Siti Norfatihah Fauzee, Muhammad Ismail Idris, Rosilah Azmi & Rizafizah Othaman

School of Chemical Sciences and Food Technology
Faculty of Science and Technology
Universiti Kebangsaan Malaysia 43600 Bangi, Selangor, Malaysia

Abstract

Pineapplesare vastly cultivated in Malaysia for their fruits. The other parts of the plants especially the leaves are usually turned into wastes. This research is aimed to exploit the wastes by extracting the cellulose from the pineapple leaves. Acidic and alkaline treatments were employed to compare the characteristics and the yield of the cellulose from these treatments. Firstly, the dried pineapple leaves were cut, ground and sieved.Then, the sample was pretreated with toluene-ethanol solution in Soxhlet extractor. In acidic treatment, the pretreated sample was hydrolyzed with 10% and 17% NaOH, rinsed, dried and then heated by using a mixture of $NaClO_3$ and CH_3COOH. Alkaline treatment was a reverse process of acidic treatment where the pretreated sample was heated, rinsed, dried and then hydrolyzed. The samples were characterized and the yield was calculated from the mass. FTIR spectrums showed that the alkaline treatment was more effective to obtain pure cellulose than that of acidic treatment. The SEM micrographs showed that the surface of the cellulose from acid and acidic treatment was smooth but the XRD diffractograms showed that the crystallinity of the cellulose was lower than those from alkaline treatment. Both acid and alkaline treatment gave about 40% yield of insoluble cellulose. Cellulose from alkaline treatment was higher in purity and crystallinity.

Keywords*: acidic treatment, alkaline treatment, extraction of cellulose, pineapple leaves, soxhlet extractor*

Introduction

The pineapple (Ananas *comosus*) is a perennial plant with a rosette of long (50–180 cm), narrow,sharp tip, fibrous and spiny leaves [1]. The leaves may be green or variegated in color [2]. In present, Malaysia is one of the world major producers of pineapple other than Thailand, Philippines, Indonesia, Hawaii, Ivory Coast and others [3]. The fruit can be consumed fresh, juiced or canned and can be used for many processed food industries such as in jem-making industries [4]. The remaining outer peel (skin) and core from the canning are called the pineapple bran, which becomes food for ruminants.

Pineapple leaf fibre is an important natural fibre with high strength and stiffness. These fibres are hygroscopic, relatively inexpensive and abundantly available with superior mechanical properties. Thus, the leaves are sometimes turn into coarse textiles and threads in some Southeast Asian countries [1]. Table 1 shows the chemical composition of pineapple leaves fibre studied by Jayanuddin et al.[5]. Main components of the fibreare cellulose (70% - 80%), lignin (5% -12%) and ash (1.1%).

Table 1: Chemical composition of pineapple leaves fibre

Chemical composition	Percentage composition (%)
Cellulose	69.5-71.5
Pentose	17.0-17.8
Lignin	4.40-4.70
Pectin	1.00-1.20
Fat and wax	3.00-3.30
Ash	0.71-0.87
Other component	4.50-5.30

Sources: Jayanuddin et al. [5]

Cellulose, a main content of the plant fibre is an organic compound with structural formula $(C_6H_{10}O_5)_n$. Cellulose was a long chain natural polymer of anhydroglucose that bind on first and fourth carbon atoms with β-glycosidic bonds [6]. There are few methods to extract cellulose such as liquid extraction and bleaching method [7; 8; 9], Jayme-Wise and diglikolmetileter-HCl [10] and steam explosion [11].

In this study, we extracted the cellulose from pineapple leaves by acid and alkaline treatments. The characteristics of the cellulose were studied and compared to determine which method is suitable to extract the cellulose from pineapple leaves fibre. The comparison was made in term of yield, chemical and physical properties of the cellulose.

Materials and method

Material

The pineapple leaves were collected from Bera, Pahang, Malaysia. The fresh pineapple leaves were cleaned and cut into pieces of 1 cm × 1 cm. Next, the cut leaves were soaked for 24 hours and dried under sunlight for a few days. The dried pineapple leaves were then ground by a grinder BH Chopper For Cutting Machine FFC-23 with speed of 5800 rpm and 3 kW power. After that, the sample was dried in Universal Memmert Oven (model UFB400) at the temperature of 105ºC until the water content in the sample was vaporized. The dried sample was kept in air thight container. All chemicals used in this study were reagent grade chemicals obtained from Sigma Aldrich Company.

Method

Pre-Treatment byToluene-Ethanol Solution

5 g of the pineapple leaves sample was pre-treated in a soxhlet extractor of Branstead Electrothermal EME6 02050. The sample was filled in a thimble and the mixture of toluene-ethanol solution in the ratio of 2:1 v/v was poured into a 250 ml round bottom flask of the soxhlet extractor. The set-up was heated for 24 hours. After that, the sample was boiled in boiling deionized water for another 3 hours. The sample was then filtered and dried at 105°C.

Cellulose Extraction by Acid and Alkaline Treatment

The cellulose extraction process was carried out with two different methods of acid and alkaline treatments.

Acid Treatment

In acid treatment, the pre-treated sample was treated with 10% followed by 17% of sodium hydroxide solution (NaOH). Both experiments were carried out in sonicator water bath (Branson 2200) for 45 minutes at 25°C and 70°C, respectively. After that, the sample was rinsed with 20 ml of 1% hydrochloric acid until pH 7, rinsed with deionized water and dried.

Next, the sample was placed in a thimble and immersed in a beaker with 14 g.L^{-1} sodium chlorite and 1.7 mL acetic acid solution, heated and sonicated in a sonicator water bath at 70°C for 3 hours. The sample was then rinsed and dried.

Alkaline Treatment

The alkaline treatment was a reversed steps of acid treatment. Alkaline treatment started by the treatment with sodium chlorite and acetic acid solution and followed by the treatment with10% and 17% NaOH solution. Other conditions are the same with acid treatment as mentioned above.

Characterizations

Extraction yields

The overall percentage of yield of the extracted cellulose can be determined by calculating the mass of the cellulose obtained divide by the initial mass of the pineapple leaves sample used.

$$\%\,Y = \frac{m_f}{m_i} \times 100\,\% \quad (1)$$

Where $\%Y$ is the overall percentage of yield of the extracted cellulose, m_f is the mass of the cellulose obtained from the extraction process and m_i is initial mass of the pineapple leaves sample used.

Chemical properties

Functional groups on the surface of the cellulose sample were determined by using Fourier Transform Infrared Spectroscope (FTIR, Perkin Elmer Spectrum 400 FTIR/FT-NIR with Spotlight 400 Imaging System) at wavelength number from 400-4000 cm^{-1}. In this study, ATR-FTIR was used where the Attenuated Total Reflectance (ATR) helps to amplify the vibration of the functional group to be detected by the detector. Table 2 identifies some of the typical functional groups correspond to cellulose, hemicellulose and lignin [12; 13].

Table 2: Typical functional group represent of cellulose, hemicellulose and lignin

Fibre component	wave number (cm^{-1})	wave number (exp.) (cm^{-1})		Functional group	Compounds
		Acid	Alkaline		
Cellulose	400-2995	3337	3331	OH	Acid, methanol
	2890	2890	2893	H-C-H	Alkyl, aliphatic
	1640	1637	1638	Fibre-OH	Adsobed water
	1270-1232	-	-	C-O-C	Aryl-alkyl ether
	1170-1082	1027	1023	C-O-C	Pyranose ring skeletal
	1108	1157	1156	OH	C-OH
Hemicellulose	4000-2995	3337	3331	OH	Acid, methanol
	2890	2890	2893	H-C-H	Alkyl, aliphatic
	1765-1715	-	-	C=C	Ketone and carbonyl
	1108	117	1156	OH	C-OH
Lignin	4000-2995	3337	3331	OH	Acid, methanol
	2890	2890	2898	H-C-H	Alkyl, aliphatic
	1730-1700	-	-		Aromatic
	1632	1637	1638	C=C	Benzene streching

				ring
1613,1450	-	-	C=C	Aromatic skeletal mode
1430	1425	1424	O-CH_3	Methoxyl-O-CH_3
1270-1232	-	-	C-O-C	Aryl-alkyl-ether
1215	-	-	C-O	Phenol
1108	1156	1156	OH	C-OH
700-900	894	894	CH	Aromatic hydrogen

The thermochemical properties were analyzed by Thermal Gravimetry Analysis (TGA) and Differential Thermal Gravimetry Analysis (DTGA) (Mettler Toledo, TGA/SDTA 85f). In this method, the samples were thermally treated at various temperatures at the rate of 10 °C.min^{-1} to determine the degradation of the composition in each sample.

Physical properties

The physical property of the cellulose from pineapple leaves in terms of the % crystallinity of the cellulose and the purity of the sample was determined using a Bruker D8 advanced X-ray diffractometers (XRD). The % crystallinity of the fibres was obtained by integrating the area under the crystalline peak after subtracting the background and air scatter [9]. The crystalinity index (I_c) was given by following equation [14];

$$I_c = \frac{I_{(002)} - I_{(am)}}{I_{(002)}} \times 100\% \quad (2)$$

where $I_{(002)}$ is the counter reading at peak intensity at 2θ angle close to 26° representing crystalline material and I_{am} is the counter reading at peak intensity at 2θ angle close to 18° representing amorphous material in cellullosic fibres.

Morphological studies

A Leo 1450 VP model variable pressures Scanning Electron Microscope (SEM) from United Kingdome with a signal power of 15 kV were used to determine the longitudinal features of the pineapple leaves powder and the cellulose obtained. The samples were mounted on conductive adhesive tape on sample holder, sputter coated with gold and observed under the SEM. The surface morphology of every sample and the width of a single fibre were measured from the SEM micrographs.

Results and Discussion

Extraction Yields

Table 3 shows the results of yields of cellulose extracted from acidic and alkaline treatment. The results showed that about 46.4% and 46.0% of the cellulose were extracted from acidic and alkaline treatment, respectively. The overall yields was higher than those obtained by Idris [15] and Azmi [16], which used the same chemicals but using the different approaches. The higher yields proved that the extraction methods employed in this study were more suitable to extract cellulose from pineapple leaves. However, there are no difference in yield can be seen from acid and alkaline treatments.

Table 3:Yield of cellulose

Item	Acid treated		Alkaline treated	
		Idris [15]		Azmi [16]
Yield of pre-treatment (%)	93.0	93.5	93.4	93.6
Yield of extraction (%)	49.9	18.2	49.3	40.0
Overall yield (%)	46.4	17.0	46.0	37.4

Chemical properties

Figure 1 displays the FTIR spectra of the cellulose from acid and alkaline treateds and the pre-treated pineapple leaves. There were two kind of absorbent regions. The first region located at low wavelength on the range of approximately 650-1800 cm^{-1} and the another one located on higher wavelength in the approximate range of 2700-3500 cm^{-1}.The peaks at wavelength number of 3337-3331 cm^{-1} and 2918-2890 cm^{-1} , whichexisted in all spectra referred to the free-OH and stretch C-H group on the sample, respectively.

It was found that the extracted cellulose from each treatment was pure without the content of lignin (the wavelength number in the range of 1500-1600 cm^{-1}) and hemicellulose (wavelength number in the range of 1765-1715 cm^{-1}) as can be seen from the peak at the wavelength number of 1515 cm^{-1} and 1730 cm^{-1} from the pre-treated pineapple leaves spectrum.

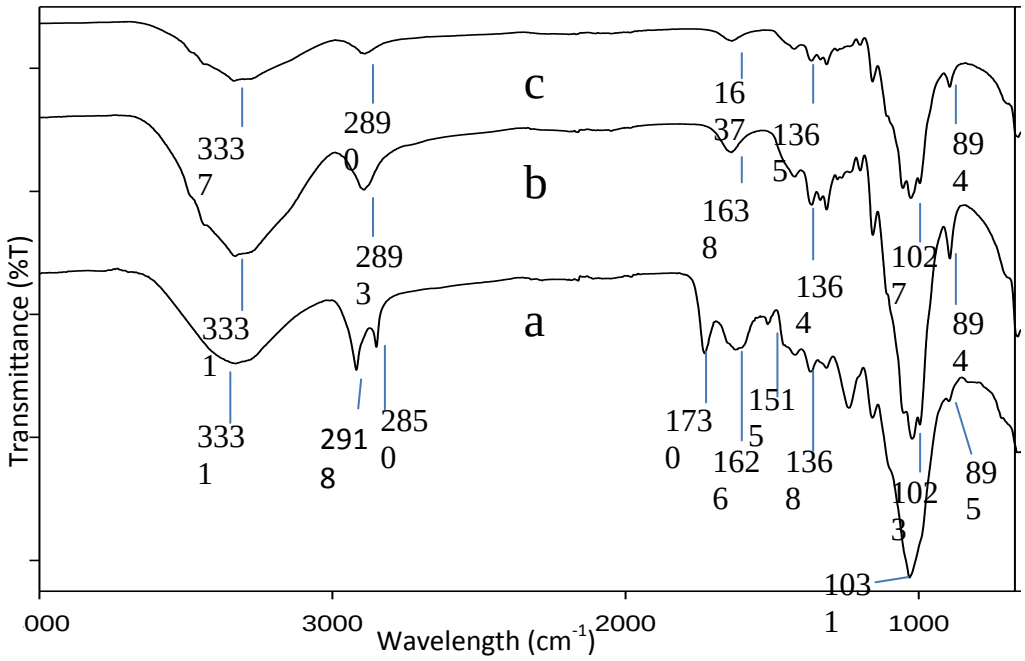

Figure 1: FTIR spectra of; (a) untreated pineapple leaves, (b) alkali treated cellulose, (c) acid treated cellulose

Thermal properties

Figure 2 and 3 are the Thermal Gravimetric Analyzer (TGA) and Differential Thermal Gravimetric Analyzer (DTGA) results, respectively. In Figure 2, the first slope at around 100°C was from the vaporization of water in the sample. The second slope was the decomposition of cellulose which started from 315°C until 380°C for the cellulose sample obtained from both acid and alkaline treatments. The results are consistent with the finding of Yang et al. [17] stated that the decomposition of cellulose started at 315°C until 400°C. Moreover the mass

loss shown in Figure 3 from 300°C until 400°C was solely from cellulose. On the other hand, the decomposition of the pineapple leaves started at lower temperature of 200°C and ended at approximately 300°C but showed higher residual mass compared to cellulose. This is because the pineapple leaves composed of a certain ratio of cellulose, hemicelluloses, lignin and volatiles which contributed to the decomposition behaviour. The decomposition of hemicellulose starts at 200°C and continues up to 315°C, and lignin from 280 to 500°C while cellulose start degrades at 290°C to 360°C [18; 19; 20; 21).

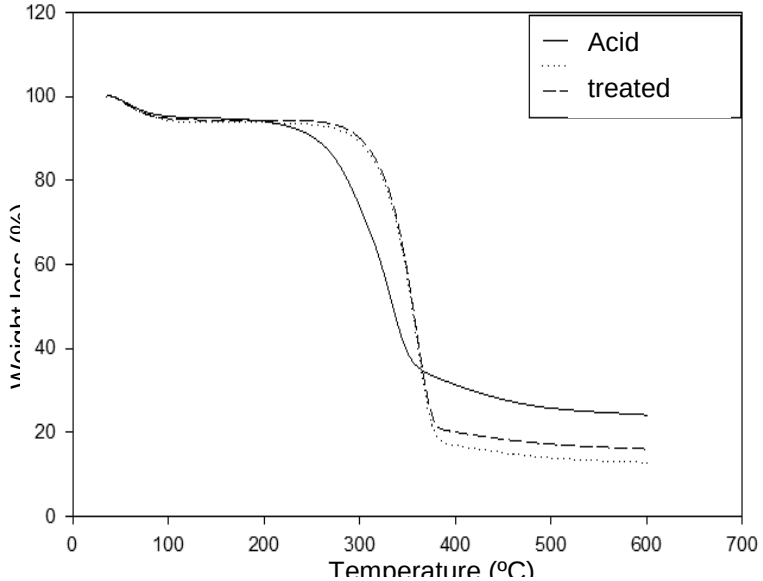

Figure 2: Thermogravimetric Analysis (TGA) of untreated fibers, acid and alkali treatment of cellulose from pineapple leaves

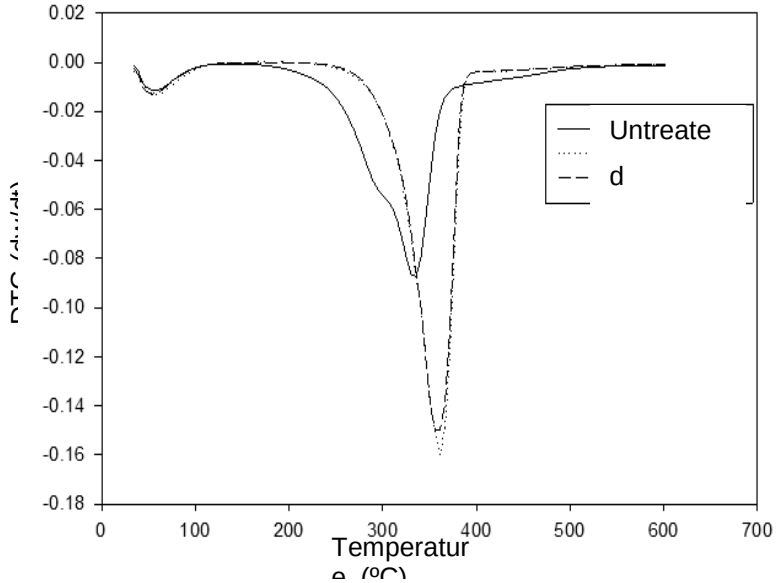

Figure 3: Differential Thermal Gravimetric (DTG) of untreated fibers, acid and alkali treatment of cellulose from pineapple leaves

Physical properties

According to Park et al.[22], there are five crystalline peaks in cellulose XRD diffractograms. Therefore, the XRD analysis is used to determine the crystallinity of the fibres as shown in Figure. 4. Usually, cellulose peak at 002 plane or 2θ angle close to 22° is used for the determination of crystallinity degree by researchers [9]. The 002 peak is obvious and sharper compared to other peaks and we can prove that at 2θ =22°, the peaks become sharper starting from untreated fiber to acid treated fiber. The sharper peaks indicate that the crystallinity of the cellulose had improved after the treatments. The removal of amorphous substances such as hemicellulose and lignin from the alkali and acid fiber led to more crystal part of the cellulose were exposed.

The crystalininty of the cellulose was calculated using equation (2). Table 4 shows the crystalinity index for these three sample. It was found that the cellulose obtained from alkali treatment has the highest crystallinity index of 63.53% followed by the acid treated cellulose (57.74%) and the untreated sample (41.63%) indicates that alkaline treatment was the more suitable extraction method of cellulose from pineapple leaves compared to acid treatment.

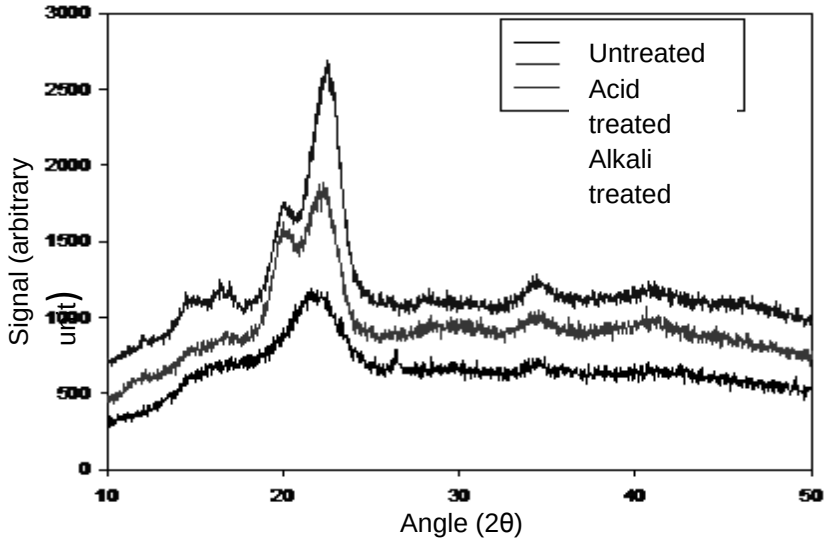

Figure 4: X-ray Diffraction Diffractogram of of untreated fiber, acid and alkali treatment of cellulose from pineapple leaves

Table 4: Crystalinity index of the sample

Fiber types	Crystallinity Index (%)
Untreated fiber	41.63
Acid treated fiber	57.74
Alkaline treated fiber	63.53

Morphological studies

Figure 5 shows the SEM micrographs of the untreated pineapple leaves fibre under different magnifications. The fibres are bulky and in a form of several macrofibrilsin bundle. The macrofibrils compose of the cellulose and hemicelluloses bound by lignin [23]. The surface was rough and the diameter of the fibre was around 50 μm.

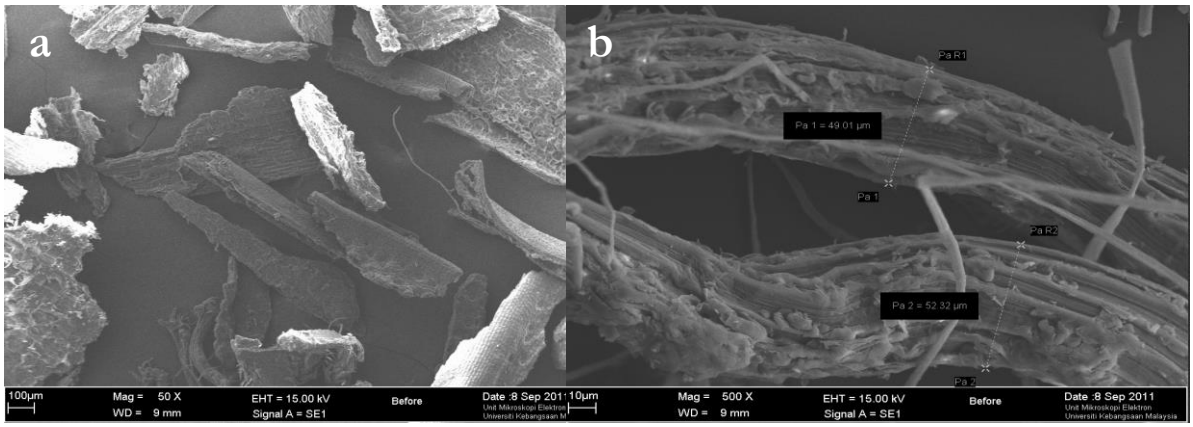

Figure 5: SEM Micrographs of (a) untreated fiber at 50× magnification; (b) untreated fiber at 500× magnification

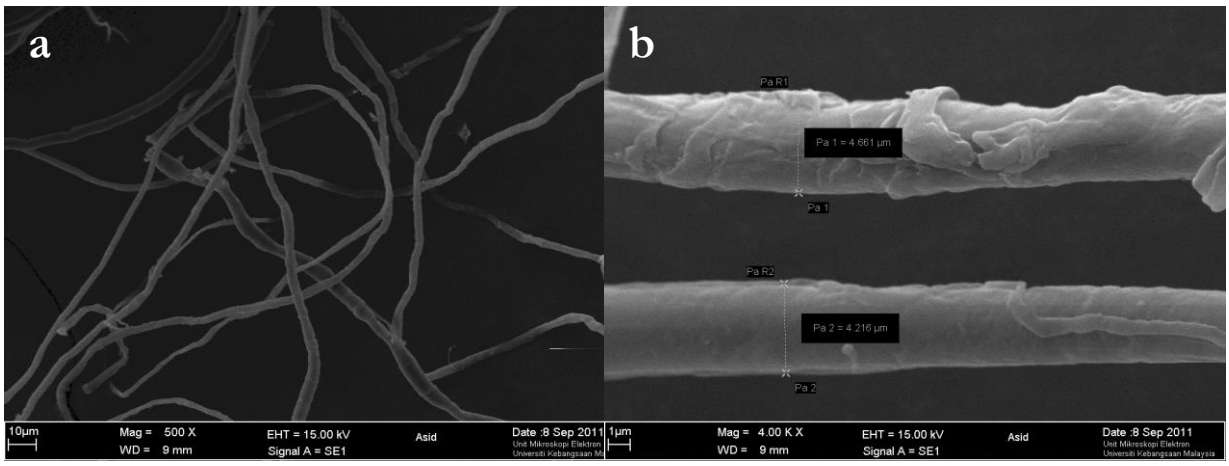

Figure 6: SEM micrographs of cellulose extracted from pineapple leaves; (a) acid treated with 200× magnification (b) acid treated with 4000× magnification

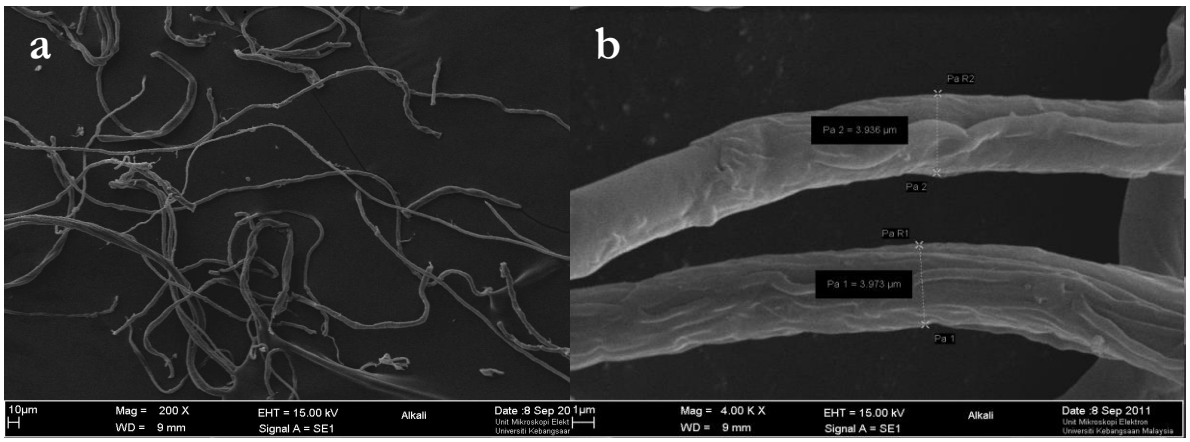

Figure 7: SEM micrographs of cellulose extracted from pineapple leaves; (a) alkaline treated with 200× magnification, (b) alkaline treated with 4000× magnification

Figure 6 and 7 are SEM micrographs for cellulose from acid and alkaline treated, respectively. Compared to Figure 5, the diameter of the material was reduced showing that the fibre was successfully broken into cellulose microfibrils. Table 4 displays the diameter comparison of all

the samples. It can be seen that the diameter of the cellulose from alkaline treatment was similar to those from acid treated. Apparently, the surfaces of the cellulose from both treatments were smooth showing that lignin and hemicelluloses were removed from the samples.

Table 4: Average diameter of pineapple leaves fibres and celluloses

Fibre Types	Average diameter (μm)
Untreated	50.7
Acid Treated	4.4
Alkaline Treated	3.9

Conclusions

In this study, cellulose was extracted from pineapple leaves by using two different methods of acid and alkaline treatments. The cellulose was characterized by FTIR, TGA & DTGA, XRD and SEM and comparison of the properties of the cellulose were discussed. FTIR spectra showed that pure cellulose was obtained from the treatments and no presence of hemicellulose and lignin were detected. The SEM micrographs showed that the surface of the cellulose from acid treatment was smooth but the XRD diffractograms showed that the crystallinity of the cellulose was lower than those from alkaline treatment. Both acid and alkaline treatment gave about 46% yield of insoluble cellulose. Cellulose from alkaline treatment was higher in purity and crystallinity.

Acknowledgements

This work was financially supported in part by UKM-HEJIM-INDUSTRI-13-2010, UKM-ST-02-FRGS0150-2010 and Polymer Research Center (PORCE), National University of Malaysia.

References

[1] Ai Van Tran. 2006. Chemical analysis and pulping study of pineapple crown leaves. *Industrial Crops and Products* 24 :66–74.

[2] Rosie, L. 2000. http://www.hort.purdue.edu/ext/senior/fruits/pineapple3.htm [5th September 2011]

[3] Reddy, N., Yang, Y. Natural cellulose fibers from soybean straw. *Bioresource Technology* 100: 3593–3598

[4] Malaysian Pineapple Industry Board. 2011. Usul Nanas. http://www.mpib.gov.my/web/guest/asal_usul_nanas [5th September 2011]

[5] Jayanuddin , Hartono, R. & Jamil , N.H. 2010. Pengaruh konsentrasi dan waktu pemutihan serat daun nanas menggunakan hidrogen peroksida. Seminar Rekayasa Kimia dan Proses ISSN: 1411-4216

[6] Sun, J.X., Sun, X.F., Zhao, H., & Sun, R.C. 2004. Isolation and characterization of cellulose from sugarcane bagasse. *Polimer Degradation and Stability* 84: 331-339

[7] Carreher C.E.jr. 2007. Polymer Chemistry. Edisi ke-7. Boca Raton: CRC Press

[8] Zhou, Y., Williams, H.S., Farquhar, G.D. & Hocart, C.H. 2010. The use of natural abundance stable isotropic ratios due to indicate the presence of oxygen containing chemical linkages between cellulose and lignin in plant cell walls. *Phytochemistry*. 71: 982-993

[9] Moran, J.I., Alvarez, V.A., Cyras, V.P. & Vazquez, A. 2008. Extraction of cellulose and prepatation of nano cellulose from sisal fibres. *Cellulose* 155: 149-159

[10] Cullen, L.E. & MacFarlene, C. 2005. Comparison of cellulose extraction methods for analysis stable isotope ratios of carbon and oxygen in planet material. *Tree-Physiology* 25:563-569

[11] Cherian, B.M., Leao, A.L., Souza, S.F., Thomas, S., Pothan, L.A. & Kottaisamy, M. 2010. Isolation of nanocellulose from pineapple leaves fibres by steam explosion. *Carbohydrate polymer* 81: 720-725

[12] Oh, S. Y., Yoo, D.I. & Seo, G. 2005. FTIR analysis cellulose treated with sodium hydroxide and carbon dioxide. *Carbohyd Res* 340: 417-428

[13] Nelson, M.L. & O'Connor R.T. 1946. Reaction of certain infrared bands to cellulose crystalinity and crystal lattice type. Part II: a new infrared ratio for estimation of crystalinity in cellulose I and II. Journal of Applied Polymer Science 8(3): 1328-1341

[14] Mwaikambo L.Y. & Ansell M.P. 2002 Chemical modification of hemp, sisal, jute and kapok fibers by alkalization. *Journal of Applied Polymer Science*. 84:2222-2234

[15] Idris, I. 2011. Pengestrakan dan pencirian selulosa daripada daun nanas menggunakan rawatan asid. Latihan Ilmiah. Universiti Kebangsaan Malaysia

[16] Azmi, R. 2011. Pengestrakan dan pencirian selulosa daripada daun nanas menggunakan rawatan alkali. Latihan Ilmiah. Universiti Kebangsaan Malaysia.

[17] Yang, H., Yann, R., Chen, H., Dong Ho, L. & Zheng, C. 2007 Charecteristics of hemicellulose,cellulose and lignin pyrolysis. *Fue*l, (in press)

[18] Mansaray, K.G. & Ghaly, A.E. Biomass and Bioenergy. Vol. 17 (1999), pp. 19-31

[19] Tomczac, F., Satyanarayana, K.G. & Sydenstricker, T.H.D. Applied Science and Manufacturing. Vol. 38, A (2007), pp. 1710–1721.

[20] Kim, H. -J. & Eom, Y.G. Mokchae Konghak. Vol. 29, No. 3 (2001), pp. 59–67.

[21] Rosa, M. F., Chiou, B., Medeiros, E.S., Wood D.F., Williams, T.G., Mattoso, L.H.C., Orts W.J. & Imam, S.H. Bioresource Technology. Vol. 100 (2009), pp. 5196–5202.

[22] Park, S., Baker, J.O., Himmel, M.E., Parrila, P.A. & Johnson, D.K. 2010. Cellullose crystallinity index: measurement techniques and their impact on interpreting cellulose performance. *Biotechnology for biofuels*. 3:10

[23] Ophart, C.E. 2003. . Carbohydrate-Cellulose.

CONVERTING PALM STEARIN ALKYD INTO CURABLE RESINS

Desmond Teck Chye Ang & Seng Neon Gan
Chemistry Department, University of Malaya,
50603 Kuala Lumpur, Malaysia

Abstract

UV curable coating is a type of environment friendly coatings as it emits minimal, if any volatile organic compounds (VOC) during curing. This aims of this work is to synthesise UV curable resins from palm stearin alkyd, and to investigate the effect of introducing different types of unsaturated diacids into the alkyd chains. A total of six maleinised alkyds were prepared, where three of them used different amounts of maleic acid (AlkMA), while the other three used maleic anhydride (AlkMAH). Spectroscopic characterisations were performed on the alkyds to verify the incorporation of -OOC-CH=CH-COO- into the alkyd resins. The film properties of the UV-cured coatings were investigated using methods adopted from ASTM, and the results show that despite of having similar repeating units, AlkMA coatings exhibited better film properties compared to AlkMAH coatings. The differences between the two series were presumably due to different distribution of -CH=CH- in the main chains.

Keywords: Alkyd, -CH=CH- distribution, Palm stearin, UV curable coating

Introduction

Alkyds are tough resins produced from the reaction of polyacids with polyols, in the presence of fatty acids as part of its composition [1]. It is an example of synthetic resin which has strong and established market segments, with annual production of approximately 200,000 tonnes [2; 3]. The high demand for alkyd is due to its flexibility to be physically and chemically modified to suit many applications. For example, alkyd can be modified with epoxy resin to improve resistance to bases and corrosion; with silicones for better heat resistance and weathering; and with isocyanates to improve the hardness and chemical resistance of the coatings [4].

Alkyds are usually produced from drying oils, or directly formulated with unsaturated fatty acids, as high level of unsaturation in the resin is crucial to promote good drying ability. Many researchers have reported the superiority of drying oil alkyd for surface coating applications over those formulated from non-drying oil. For examples, rubber seed oil alkyd, tobacco seed oil alkyd and soya oil alkyd were found to have better film properties with shorter drying time compared to non-drying oil alkyd [5; 6; 7]. In fact, most of the commercial alkyd resins for surface coating applications were synthesised from drying oil, such as soya oil or linseed oil. In the current work, non-drying oil, palm stearin is chosen as the source of fatty acids in alkyd synthesis due to its economical advantages. Palm stearin is the solid fraction of palm oil and can be viewed as a by-product from palm olein production. It has relatively low level of unsaturation, and is always traded at a discounted price [8]. It is an easily accessible raw material in Malaysia, the second largest producer of palm oil in the world [7].

The unmodified palm stearin alkyd is not able to air-dry by itself [9] as the oil composed of only 35% of unsaturated fatty acids. In this paper, the alkyds were synthesised using a portion of unsaturated diacids. Two sets of alkyds were prepared, with the first set synthesised with maleic acid, and the second set with maleic anhydride. They were then formulated into UV curable resins. Environment friendly coatings are becoming the vogue in the surface coating market owing to the strict regulations on the emission of VOC and hazardous air pollutants (HAP) from the coating industries. In addition to being environment

friendly, radiation curable coating also proven to be superior compared to the conventional solvent-based coatings, in terms of rapid curing time, improved film properties, and economically beneficial [10].

In our previous publications, we have proven that palm stearin alkyd with different level of unsaturation could produce coatings with different UV curing time and different film properties [11; 12;13]. However, the amount of -CH=CH- may not be the only factor that affects the properties of a coating. The performances of the two sets of alkyd coatings (AlkMA and AlkMAH) in this work were compared, and the results showed that despite of having similar amount of unsaturation, the former could produce coatings with better film properties and shorter curing time. Presumably, the difference in the reactivity of maleic anhydride and maleic acid produced alkyds with different -CH=CH- distribution along the alkyd chain that influenced the properties of the UV-cured coatings.

Materials and method

Materials

Glycerol (99.5%), and refined, bleached and deodorised palm stearin (RBD palm stearin) were kind gifts from Emery Oleochemical (M) Sendirian Berhad, and they were used as received. The following chemicals were supplied and used without further treatments: phthalic anhydride (PA) from DC Chemical Korea, $Ca(OH)_2$ from HmbG Chemicals, maleic acid (MA), maleic anhydride (MAH) and benzophenone 99% from Sigma Aldrich. Methyl methacrylate 99% (MMA) from Sigma Aldrich was treated with 1.5% w/v NaOH to remove inhibitor and subsequently dried over activated molecular sieves.

Synthesis

Mixture of palm stearin and glycerol was heated at 230^{o}C for approximately 2 hrs, with $Ca(OH)_2$ as the catalyst for the alcoholysis process. Solubility test (in ethanol) was conducted on the product to confirm the completion of the alcoholysis process. The reaction mixture was allowed to cool down to <150°C before adding mixture of diacids into the reaction mixture. Subsequently, the temperature was gradually increased to 220^{o}C and held constant until the acid number of the mixture has dropped to below 10% of the initial value. Table 1 list the compositions of the alkyds. AlkPA was cooked without unsaturated diacids to serve as control.

Table 1: Compositions of alkyds

Alkyd codenames	Amount / mol				
	Palm stearin	Glycerol	PA	MA	MAH
AlkPA	1.09	1.81	1.73	-	-
AlkMA1	1.09	1.81	1.38	0.35	-
AlkMA2	1.09	1.81	1.21	0.52	-
AlkMA3	1.09	1.81	1.04	0.69	-
AlkMAH1	1.09	1.81	1.39	-	0.35
AlkMAH2	1.09	1.81	1.21	-	0.52
AlkMAH3	1.09	1.81	1.04	-	0.69

Characterisations of alkyds

FTIR scan was conducted on alkyd coated on KBr cells from 400 - 4000 cm^{-1} at a resolution of 4 cm^{-1}, using Perkin Elmer FTIR spectrometer (RX1*)*. ^{1}HNMR and ^{13}CNMR characterisation was carried out on the alkyds dissolved in deuterated chloroform and analysed using JEOL JNM-GSX 270 NMR spectrometer. As for the viscosities of the alkyds, they were measured

using Ubbelohde viscometer with glycerol solutions as the standards, and the tests was carried out in water bath at 30^{o}C.

Coating preparations

Coating mixtures were prepared by mixing 3 parts of alkyds with 2 parts of MMA (reactive diluents), followed by the addition of 9 parts per hundred parts of resin (phr) of benzophenone to serve as UV photoinitiator. The mixtures were stirred to homogeneity at room condition before being applied on mild steel panels and irradiated with 225 mW.cm^{-2} of UV light (λ 365 nm). Film thickness of the coatings was set at 25 µm.

Film properties

Film hardness of the cured coating was determined via pencil hardness test (PHT) as described in ASTM D3363. The hardest pencil grade which fails to scratch the coating was recorded. Film adhesion was measured using crosshatch adhesion tape test based on ASTM D3359. Thermal degradations of the alkyd coatings were studied using thermal gravimetric analyser (*TGA 6, Perkin Elmer*), from 50 to 900^{o}C at 15^{o}C.min^{-1} in N_2 atmosphere. DSC analyses were carried out as well using Mettler Toledo DSC-822e at a heating rate of 20^{o}C.min^{-1} from -60^{o}C to 65^{o}C in N_2 atmosphere to determine the T_g of the films.

As for the water and alkali resistance test, the coating mixtures were applied on glass panels and cured under UV light. The coatings were conditioned at room condition for 24 hrs prior to the test. The water resistance test was carried out by immersing the coated panels in distilled water for 18 hrs. The results were reported in terms of presence of any whitening observed upon removing the panels from the immersion and also the time needed for the whitening to disappear after it was removed and left to dry under room conditions. Another set of coatings were prepared to measure the % weight increase of the coatings during their immersion in water. For alkali resistance test, the coated panels were immersed in aqueous NaOH solution (30g.L^{-1}) and the duration of alkali immersion needed for film defects to become apparent was recorded. The water and alkali test methods were adopted from ASTM D1647.

Results and Discussion

FTIR and ^{1}HNMR Characterisations

FTIR spectra of AlkMA3 and AlkMAH3 in Figure 1 are similar to each other, suggesting they have similar structures. Peak at 1660 cm^{-1} is present in the spectra of maleinised alkyds (Figure 1a and 1b) due to the stretching of -C=C- of the incorporated diacids, but absent in the spectrum of the control alkyd, AlkPA. ^{1}H-NMR spectra of the two maleinised alkyds in Figure 2 have also confirmed that there is no significant structural difference between them.

The amount of -OOC-CH=CH-COO- incorporated into the alkyds was calculated by integrating the peak at 6.9 ppm in the ^{1}H-NMR spectra, and the results were tabulated in Table 2. In both series of alkyds, the amount of -OOC-CH=CH-COO- incorporated is lower than the amount introduced in the formulation. Presumably small amount of cross-linking could have taken place during the cook. The increasing viscosities of the alkyds in each series agree with the occurrence of crosslinking during the synthesis.

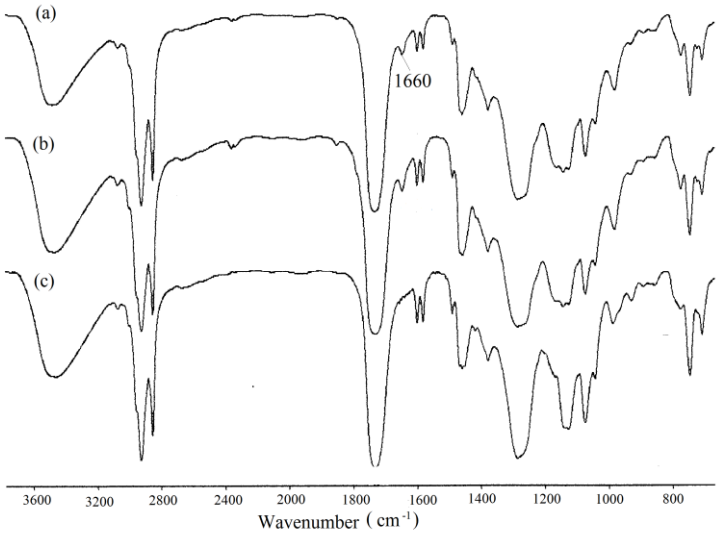

Figure 1: FTIR transmittance spectra of (a) AlkMA3, (b) AlkMAH3, and (c) AlkPA

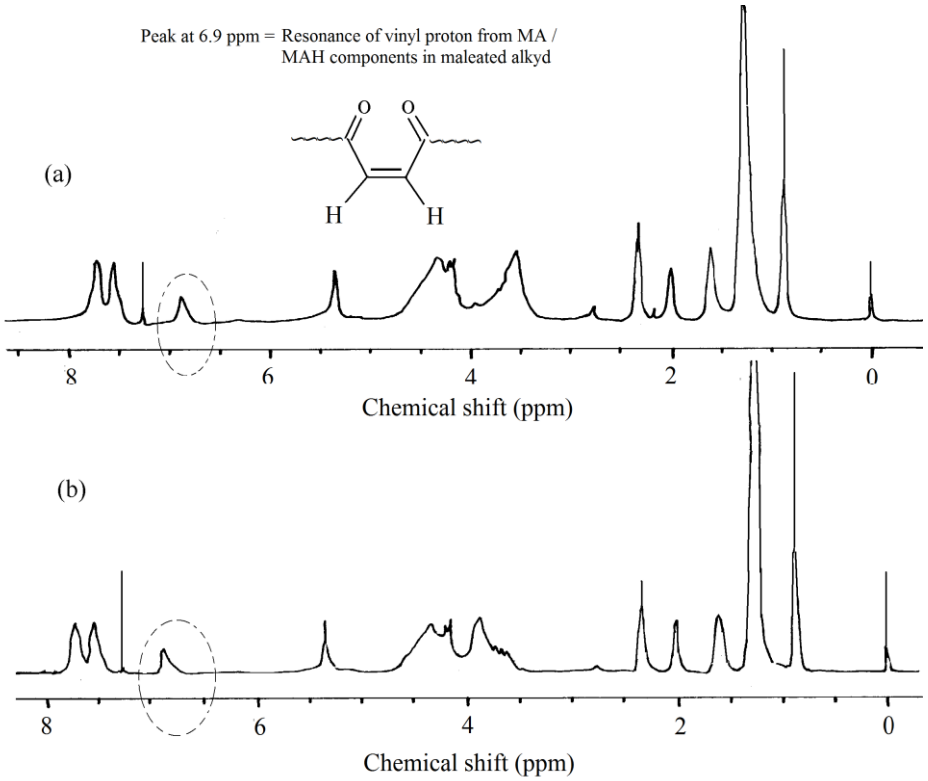

Figure 2: ^{1}H-NMR spectra of (a) AlkMA3, and (b) AlkMAH3

Table 2: Amount of -OOC-CH=CH-COO- introduced in alkyds

Parameters	AlkMA1	AlkMAH1	AlkMA2	AlkMAH2	AlkMA3	AlkMAH3
Amount of -OOC-CH=CH-COO- from formulation, / (x 10^{-4} mol / g resin)	4.83	4.88	7.31	7.41	9.82	9.99
Amount of -OOC-CH=CH-COO- from HNMR analysis, / (x 10^{-4} mol /g resin)	2.20	1.92	3.53	3.85	4.15	5.43
Viscosity of 35% w/w of alkyd solution in toluene / (mPa.s)	9.20	9.35	12.75	11.7	20.25	13.55

Despite having similar FTIR and ^{1}H-NMR spectra, and comparable amount of unsaturation, the two series of alkyds showed differences in their curing time and film properties as reported in the later part of this paper. The differences shown are attributed to different distribution of incorporated unsaturation in the alkyd chains. AlkMAH series was synthesised using mixtures of PA and MAH as the diacids. MAH was reported to have higher reactivity compared to PA as shown in Table 3 [14] and is expected to react with the primary -OH of the glycerol to form a half ester and a free carboxylic acid group. This would be followed by the reaction of PA with the 1^{o} -OH of the glycerol to form a half ester and a free carboxylic acid group. As all the anhydrides have reacted, the -COOH groups would then react with the remaining -OH groups (presumably mainly 2^{o} -OH) to form the ester linkages which lead to the building up of alkyd chains.

As for the AlkMA series, they were cooked using mixture of PA and MA as the source of diacids. PA is expected to react with the 1^{o} -OH of the glycerol to form a half ester and free carboxylic acid first. Subsequently the MA (which is a dicarboxylic acid) would then compete with the free carboxylic acid of the half ester to react with the remaining -OH groups (a mixture of 1^{o} and 2^{o} -OH). As the -COOH groups are less reactive than the anhydride, the extent and rate of polycondensation would be less than in the AlkMAH series under similar reaction conditions. The system is expected to produce alkyd chains with relatively more random distribution of -CH=CH- along the alkyd main chain.

Table 3: Relative rate of hydrolysis of some anhydrides

Anhydrides	Relative rate of hydrolysis
Acetic	0.99
Succinic	1.00
Methylsuccinic	1.39
Itaconic	1.12
Maleic	9.96
Phthalic	3.99
Citraconic	6.62

^{13}C-NMR Characterisation

^{13}C-NMR analyses were performed to investigate the relative distribution of diacids in the alkyd chains. Focus was given on the peak that corresponds to -COO- of the alkyds, shown in Figure 3. The peaks were assigned after considering the electron withdrawing effect experienced by the carbons and also based on comparisons between the spectra. Peaks at 167.5 ppm are split into 2 regions, with the upper field corresponds to resonance of -COOH of PA, while the lower field is from -COO- of ester linkages of PA components in the alkyd chain. The ratio of the two peaks was calculated and shown in Figure 4. The results indicate that the relative amount of carbon E is consistently higher in AlkMAH series, suggesting there are higher proportion of -COOH from incorporated PA in the series as compared to in AlkMA. Considering the results from ^{13}C-NMR interpretation, together with fact that all the alkyds were cooked to similar acid number, it would be logical to presume that there are higher portion of maleinised components at the chains' terminals or as branches to the alkyd main chains in AlkMA series. Thus, the -C=C- of the diacid would be more exposed and readily available for crosslinking reaction.

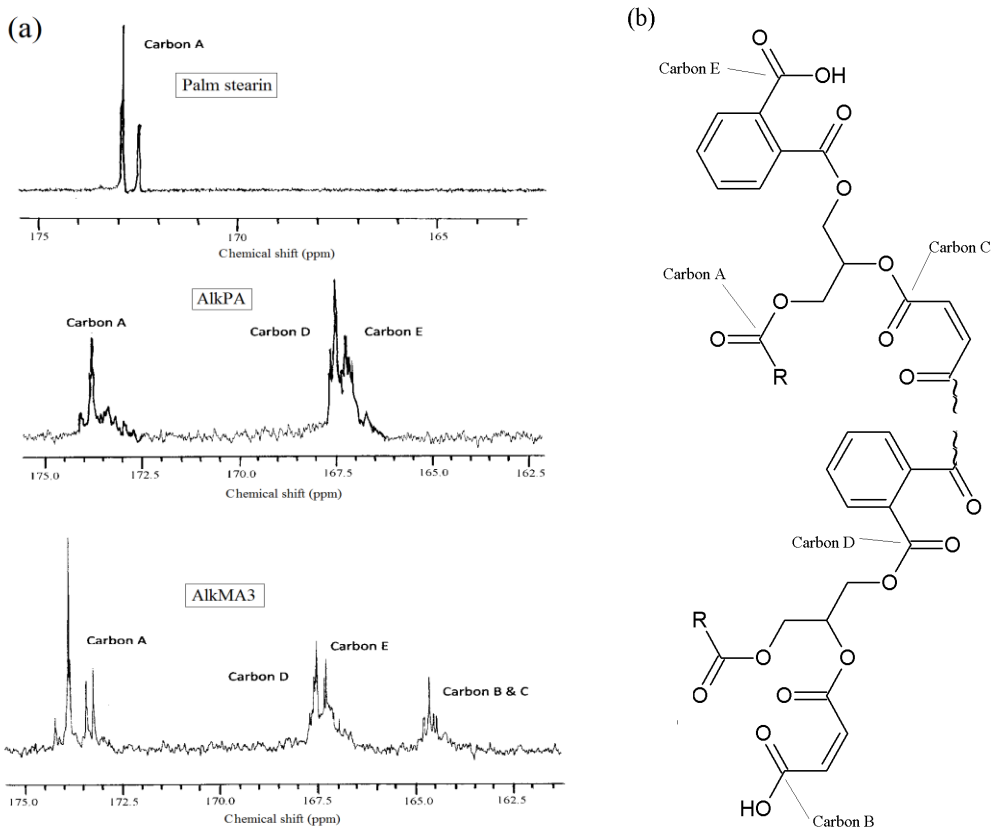

Figure 3: (a) Expanded ^{13}C-NMR spectra of palm stearin, AlkPA and AlkMA3, (b) Plausible structure of maleinised alkyds

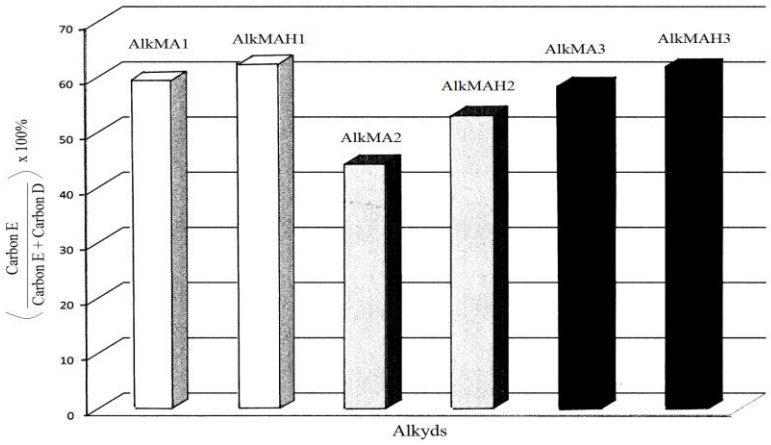

Figure 4: Relative % of Carbon E in AlkMA and AlkMAH series

Tack Free Time and Film Properties

Table 4 summarises some of the properties of the dry-though alkyd coatings. The two series of alkyds produced coatings with different tack-free time and film properties. As shown, coatings from AlkMA series achieved tack-free state faster than those from AlkMAH, and the films of AlkMA coatings were found to be harder as well. Presumably, greater extent of crosslinking was achieved in AlkMA coatings and consequently improved the film hardness and tack-free time of the coatings.

As expected, the water and alkali resistance of AlkMA coatings are better than AlkMAH coating. AlkMAH1 film showed whitening from the immersion due to limited extent of crosslinks in its system. The high crosslink densities in AlkMA coatings are able to improve the impermeability of the coatings, hence increased their resistance towards water and alkali solution. Figure 5 shows the % weight change of the coatings during immersion in water, and as expected, AlkMA coatings experienced lower weight % increase as compared to AlkMAH coatings. Despite of the differences, incorporation of unsaturation into the alkyd chain proved to enhance the water resistance of the coatings. The improvement is rather obvious as the unmodified alkyd (AlkPA) coating experienced as high as 71.8% weight increase, while the modified alkyd coatings experienced <15% weight increase.

Table 4: Physicochemical properties of alkyd coatings

Alkyd coatings	Tack-free time / s	Film hardness	Adhesion	Water resistance [a]	Alkali resistance [b]
AlkMA1	60	4B	5B	I	2.92
AlkMAH1	90	6B	5B	II	3.33
AlkMA2	45	3B	5B	I	13.03
AlkMAH2	60	4B	5B	I	6.66
AlkMA3	45	H	5B	I	15.60
AlkMAH3	60	4B	5B	I	7.00

[a] Coatings' condition after 18 hrs immersed in water (I = not visibly affected, II =Presence of whitening but disappear in 2 hrs of drying at room condition)

[b] Duration of immersion in 30g.L^{-1} aqueous NaOH before apparent film defects (mins)

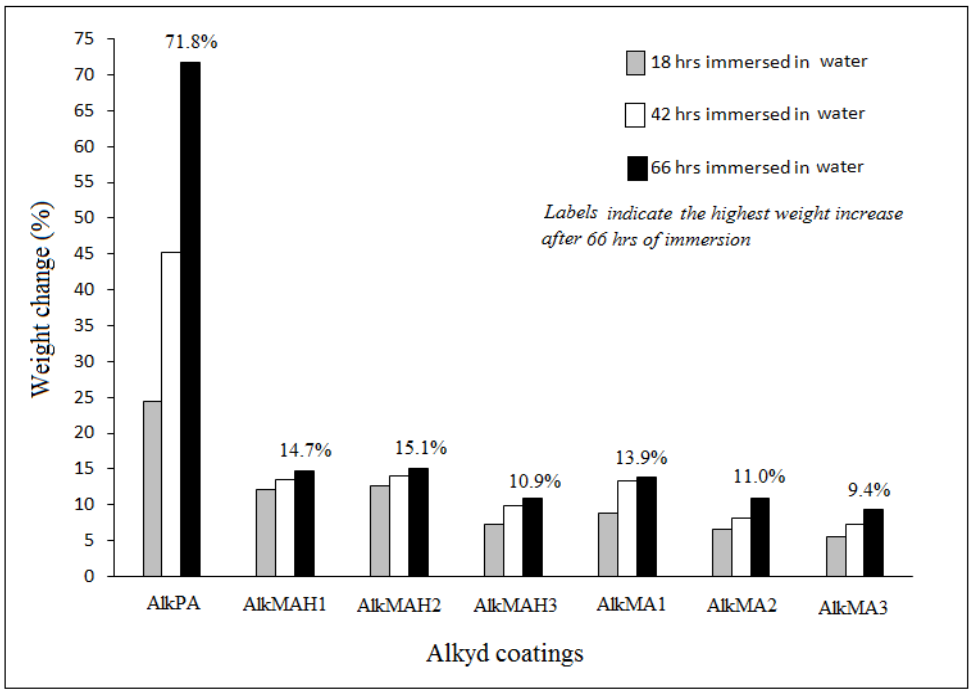

Figure 5: Percentage weight increase of alkyd coatings during water resistance test

TGA thermograms of the two series of alkyd coatings are shown in Figure 6. AlkMA coatings have better thermal stability compared to AlkMAH coatings especially at temperature < 400^{o}C. Presumably, the random and higher amounts of crosslinks in AlkMA coatings have led to stronger reinforced structures that could withstand higher temperature. The onset of degradations of the alkyd coatings are shown in Table 5, along with the T_g of the coatings obtained from DSC analyses. At equivalent level of unsaturated diacid incorporation, AlkMA coatings have higher T_g than those of AlkMAH. Higher crosslinking would restrict the chain movements thus increase the T_g of the system.

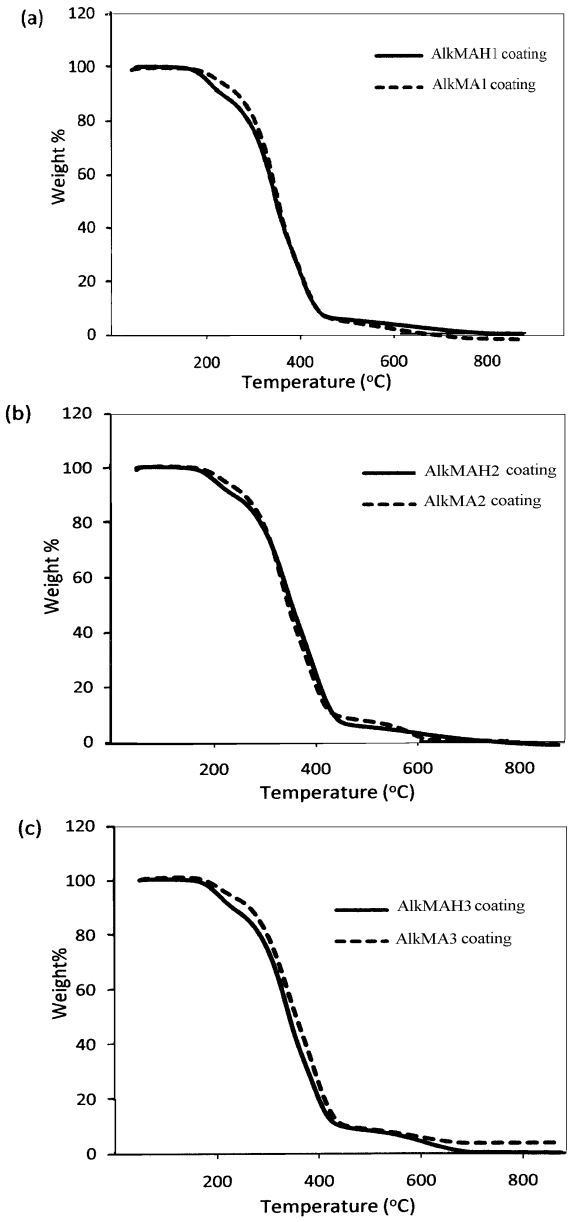

Figure 6: TGA thermograms of (a) AlkMA1 and AlkMAH1 coatings, (b) AlkMA2 and AlkMAH2 coatings, and (c) AlkMA3 and AlkMAH3 coatings

Table 5: T_g and onset of degradations of alkyd coatings

Alkyd coatings	T_g / ^oC	Onset of degradation / ^oC
AlkMA1	0.65	184.1
AlkMAH1	-0.48	170.2
AlkMA2	1.75	187.0
AlkMAH2	-0.54	169.9
AlkMA3	9.87	179.6
AlkMAH3	2.71	172.0

Conclusions

Two series of alkyds were successfully cooked using palm stearin. In order to increase the amount of unsaturation in the system, the alkyds were formulated with significant amount of unsaturated diacids. Two different series of alkyds were synthesised, with one of the series cooked using using maleic acid and the second series using maleic anhydride. Although the amount of -OOC-CH=CH-COO- incorporated in the two series of alkyds were comparable, their coatings exhibited different film properties, attributed to different -CH=CH- distributions in the alkyd chains prior to UV curing. AlkMA series exhibited more random distribution of -CH=CH-. Consequently, it produced coatings with better film hardness, better water and alkali resistance, higher T_g and better thermal stability, as the -CH=CH- groups are able to participate more effectively in cross-linking during the curing process.

References

[1] Patton, T.C. 1962. *Alkyd Resin Technology*. New York: John Wiley and Sons.

[2] Manea, M. 2008. *High Solid Binders*. Hannover: Vincents Network GmbH.

[3] Jones, F. N. 2005. *Ullmann's Encyclopedia of Industrial Chemistry*. Weinheim: Wiley-VCH.

[4] Deligny, P., Tuck, N., & Oldring, P.K.T. 2000. *Resins for Surface Coatings*. Chichester: John Wiley and Sons.

[5] Aydin, S., Akcay, H., Ozkan, E., Guner, F.S., and Erciyes, A.T. 2004. *Prog. Org. Coat. 51, 273-279.*

[6] Ikhuoria, E.U., Maliki, M., Okieiman, F.E., Aigbodion, A., Obaze, E.O., & Bakare, I.O. 2007. *Prog. Org. Coat. 59, 134-137.*

[7] Issam, A.M., and Cheun, C.Y. 2009. *Malaysia Polymer Journal 4, 42 - 49* Oil World 2008.

[8] Abdullah, R. 2010. *Prices of Selected Oils and Fats and Prospects of Palm Oil in 2009*. Malaysia: MPOB.

[9] Teo, K.T. and Gan, S.N. 1997. *Paint and Ink International Oct 1997, p26-30.*

[10] Schwalm, R. 2007. *UV coatings: basics, recent development and new applications*. UK: Elseview.

[11] Ang, D.T.C & Gan, S.N. 2012. *Pigment and resin technology 41, 302-310.*

[12] Ang, D.T.C & Gan, S.N. 2012. *Prog. Org. Coat. 73, 409-414.*

[13] Ang, D.T.C & Gan, S.N. 2012. *J. Appl. Polym. Sci. 125, E306-E313.*

[14] Trivedi, B.C., & Culberston, B. M. 1982. *Maleic Anhydride.* New York: Plenum Press

GAS BARRIER PROPERTIES OF REGENERATED CELLULOSE/MONTMORILLONITE NANOCOMPOSITE FILMS PREPARED VIA IONIC LIQUIDS

Shaya Mahmoudian[1], Mat Uzir Wahit[2*] & A.F. Ismail[3]

[1] Department of Textile Engineering, Kashan Branch, Islamic Azad University, Kashan, Iran
[2]Center for Composites, Universiti Teknologi Malaysia, 81310 UTM, Johor, Malaysia
[3]Advanced Membrane Technology Research Centre (AMTEC),
Universiti Teknologi Malaysia, 81310 UTM, Johor, Malaysia

Abstract

Regenerated cellulose (RC)/Montmorillonite (MMT) nanocomposite films were prepared using solution casting method via a green ionic liquid solvent, 1-butyl-3-methylimidazolium chloride (BMIMCl). The effect of MMT (filler) loading on the gas barrier properties of the nanocomposite films was investigated. The regenerated cellulose and the nanocomposite films were characterized using X-ray diffraction (XRD) and scanning electron microscopy (SEM). Oxygen and carbon dioxide permeability rates of the films were measured using a constant-pressure system. XRD result indicated exfoliation of MMT into single layers which demonstrates preparation of true nanocomposites. SEM images revealed smooth fractured surface with good interaction between cellulose and MMT. RC/MMT nanocomposite films exhibited improved oxygen and carbon dioxide barrier properties compared to RC and permeability values decreased gradually with increasing MMT concentration up to 6% (w/w). The increase in barrier property of the nanocomposites indicated the dominant role of MMT platelets in barrier improvement.

Keywords*:* Gas permeability, ionic liquids, nanocomposite, regenerated cellulose

Introduction

In recent years biopolymers have attracted more interest as alternative for petroleum based polymers due to increasing environmental concerns and decreasing fossil resources [1:2]. Cellulose is the most abundant natural polymer in nature and it is currently one of the most promising polymeric resources, being the component of paper, textiles, membranes, artificial fibers, etc. Cellulose has many attractive properties such as, biodegradability, renewability, biocompatibity, non toxicity, and low cost [3]. However, only about 2% of cellulose renewed annually are used as raw material in manufacture of cellulose material and goods [4; 5]. Cellulose cannot be processed as a conventional thermoplastic polymer, and it has to be regenerated prior to use. However, cellulose regeneration in difficult to achieve, because of its stiff molecules and close chain packaging via strong hydrogen bonding between molecules. Therefore, the research and development of more effective cellulose processing methods is necessary to make full use of cellulose resources [6; 7].

The most important and oldest technique for cellulose regeneration was polluting viscose process and it is still applied for the production of regenerated cellulose (RC) fibers. Despite continues improvement in past decades, more than 2 tone of auxiliaries (e.g. sodium hydroxide, carbon disulphide, sulfuric acid) and significant volume of fresh water are required per ton of RC materials produced [8;9]. Recently, several cellulose solvents such as LiCl/N,N-dimethylacetamide (DMAc) [10], NaOH/urea aqueous solution [11], LiCl/1,3-dimethyl-2-imidazolidinone (DMI) [12] , N-methylmorpholine-N-oxide (NMMO) [13;14] have been developed for cellulose processing. However these solvents have some drawbacks such as toxicity, volatility, side reactions and high cost [8].

Room temperature ionic liquids are group of new solvents which have many attractive properties such as thermal and chemical stability, non flammability, low melting point, low

vapor pressure and ease of recycling [15;16]. Recently, it has been found that room temperature ionic liquids can be used to dissolve cellulose. Rogers and his coworkers [17; 18] reported for the first time that ionic liquid 1-butyl-3-methylimidazolium chloride (BMIMCl) has a good dissolving power for cellulose which opened up a new way of developing a class of cellulose solvent systems.

In recent years, organically modified layered silicate such as montmorillonite (MMT) has been widely used as reinforcement to prepare polymer nanocomposites due to its easy availability, low cost and more importantly environmental friendliness. Polymer/MMT offer tremendous improvement in wide range of physical and engineering properties at low filler (MMT) loadings. MMT with nano-sized layered structure has a large surface area providing sufficient interfacial regions in polymer nanocomposites for enhancement in thermal and tensile properties with low loading into the polymer matrix [19; 20; 2].

This work presents an environmentally friendly preparation of RC/MMT nanocomposite films by incorporation of MMT into microcrystalline cellulose matrix using ionic liquid, BMIMCl as solvent. The structure and gas barrier properties of RC/MMT nanocomposite films are investigated.

Materials and method

Materials

Microcrystalline cellulose a commercial reagent from Sigma with average powder size 50 µm, Avicel type with the degree of polymerization of 350 was used. Ionic liquid, 1-butyl-3-methylimidazolium chloride (BMIMCl) was supplied by Sigma Aldrich. Organo-modified montmorillonite, Nanomer 1.30TC was obtained from Nanocore Inc. (Arlington Heights IL, USA.) Nanomer 1.30TC is organically modified with octadecylamine.

Preparation of nanocomposites

Cellulose/MMT nanocomposite films were prepared according to the following procedure; Cellulose was dissolved in ionic liquid BMIMCl using magnetic stirring for 4 h at 85˚C. Meanwhile MMT nanoclays (2, 4, 6 and 8%(w/w) with respect to cellulose content) were dispersed in BMIMCl using sonicator (Model FB15053, Fisher Scientific Co., Germany) for 30 min and then stirring for 4 h at 85˚C. Two solutions were mixed and stirred for 24 h at 85˚C to get a homogenous cellulose/MMT/ionic liquid solution with cellulose concentration of 8% (w/w). After degassing the solution in vacuum oven, it was casted on a glass plate with thickness of about 0.3 mm and immersed immediately into distilled water bath at room temperature for 24 h. The obtained nanocomposite films were washed with running water and dried in a vacuum oven at 30°C for 3 h.

Characterization

X-ray diffractometry (XRD) was performed on a Siemens (Berlin, Germany) D5000 X-ray diffractometer with Cu-Ka radiation. The X-ray diffraction patterns were recorded with a step size of 0.05˚ and scanning speed of 0.02˚/min from 2□ = 2 to 80˚. The wave length of X-ray beam is 0.15147 nm.

Scanning electron microscopy (SEM) was performed on a Philip XL 40 SEM with acceleration voltage of 20 kV. The RC and RC/MMT nanocomposites films were frozen in liquid nitrogen, cryo-fractured, and vacuum dried. The fracture surface of the films was coated with gold prior to analysis.

Oxygen and carbon dioxide permeability rate were measured using a constant-pressure system and a soap bubble flow meter. The permeation tests were carried out at 25˚C with feed gas pressure of 5 bar gauge. The measurement was repeated three times for each sample. The pure gas permeability was calculated using Eq. (1):

$$P = \frac{l}{A\,\Delta p}\frac{dV}{dt} \qquad (1)$$

where P is the permeability, Δp is the pressure difference across films (Pa), A is the effective surface area (12.5×10^{-4} m^2), l is the thickness of nanocomposites (m), t is the permeation time (s), V is the volume of the gas permeated through the membrane ($m^3_{(STP)}$).

Results and Discussion

X-ray Diffraction Studies

The XRD patterns of MMT, RC and RC/MMT nanocomposite films with 6% (w/w) MMT content are shown in Figure 1. The diffraction pattern of organo-modified MMT exhibited a diffraction peak at 2θ = 4.1°, corresponding to interlayer spacing of (001) plane with distance of 21.2 Å for alkylammonium modified silicate. The high interlayer spacing of MMT is due to the organic modification of MMT. MMT modification leads to an increase in the interlayer spacing, which would favor polymer chains to enter into the interlayer-galleries of MMT [21; 22] . In RC, the peak at 2θ = 12.2° assigned to (1$\bar{1}$0) plane and the broad reflection peak at around 2θ = 20.5° are assigned to the (110)/(020) lattice planes of known cellulose II crystalline structure [23; 24]. The d-spacing peak of MMT 1.30TC in cellulose matrix disappeared indicates as random dispersion and possible exfoliation of MMT plate in cellulose nanocomposite. Lee et al. [25] also showed that the absence of MMT peak in cellulose/MMT nanocomposite material demonstrates a true nanocomposite with exfoliated MMT in cellulose matrix.

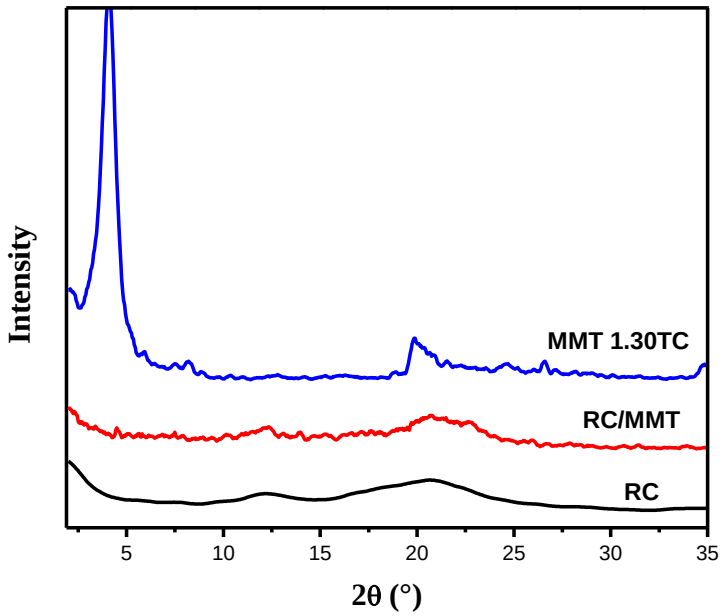

Figure 1: XRD patterns of MMT 1.30TC, RC/MMT nanocomposite film with 6% (w/w) MMT loading and pure RC film.

Scanning Electron Microscopy

Figure 2 shows the cross-sectional SEM image of RC and 6% (w/w) MMT filled RC nanocomposite film. SEM results showed smooth fractured surface with good interaction between cellulose and MMT. It can be seen that MMT layers are wrapped in and covered by cellulose indicating good adhesion between MMT and cellulose. The enhanced cellulose chain

entangling with MMT and its good dispersion may support the improvement in tensile strength as reported in our previous paper [26]. It can be seen that the RC and RC/MMT nanocomposites films regenerated from ionic liquid BMIMCl display a dense and homogenous structure. Formation of a dense structure is due to the appropriate preparation method as well as the high cellulose concentration. Previous studies have shown that the cellulose concentration of lower than 6% (w/w) resulted in a porous structure for RC [27; 28;29]. Moreover the coagulation conditions affect the structure of the RC. Liu and Zhang [30] and Li et al. [31] studied the different coagulation temperatures and reported that the coagulation temperature strongly affect the morphology and structure of the RC. They reported that the best temperature for coagulation bath to get denser structure of RC was between 20-24 °C. The SEM images demonstrated that the preparation method used in this research was suitable to obtain homogenous and dense structure for RC and RC/MMT nanocomposites.

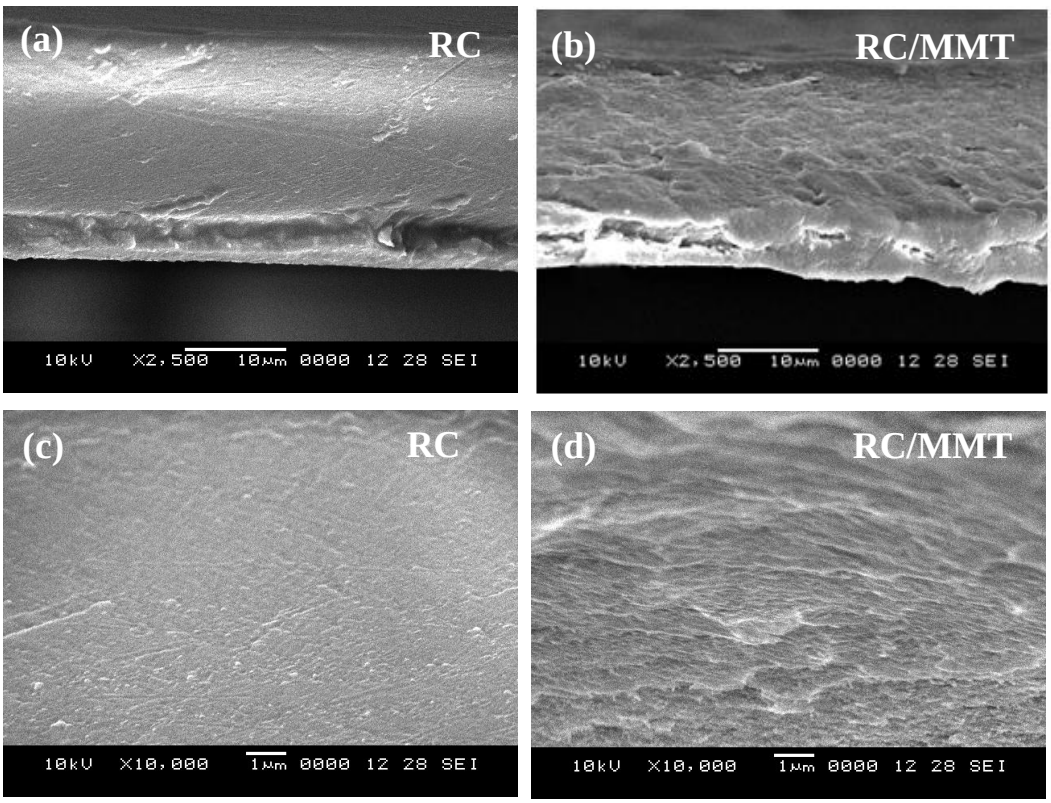

Figure 2: SEM micrographs cross sectional view of (a,c) RC and (b,d) RC/MMT nanocomposite film with 6% (w/w) MMT loading

Gas permeability

Oxygen (O_2) and carbon dioxide (CO_2) permeability of RC and the nanocomposite films are shown in Figure 3. Permeability values decreased gradually with increasing MMT content. O_2 and CO_2 permeability decreased by about 33% and 31%, respectively upon the addition of 6% (w/w) MMT. The reduction in permeability is attributed to the lengthening of diffusion path of the permeating gas molecules by adding MMT due to the increase of the tortuosity, and increasing MMT volume fraction improve these properties [32;33] . Koh et al.[34] also showed that the permeation rate of O_2 and CO_2 through poly (lactic acid) membrane decreased by embedding layered silicate.

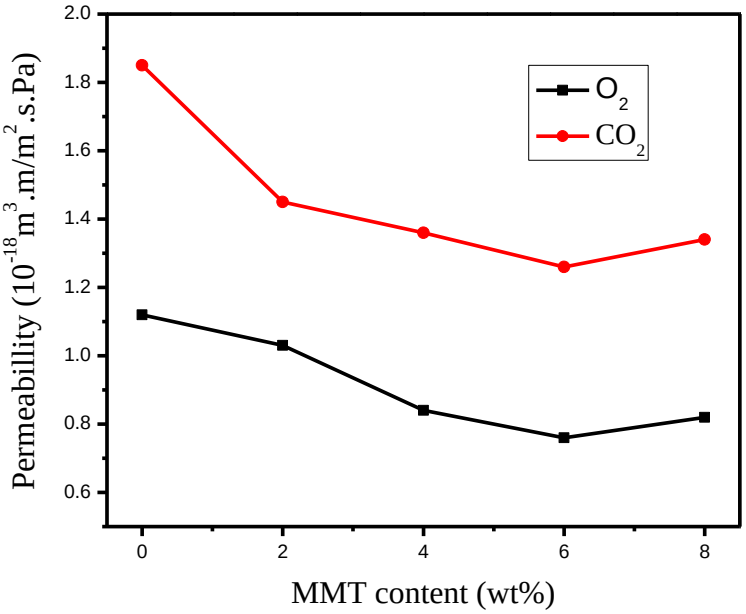

Figure 3: Permeability values of RC and RC/MMT nanocomposite films with O_2 and CO_2

The permeability values increased for the nanocomposite film with 8% (w/w) MMT, maybe due to the aggregation of MMT layers. The tortuosity in nanocomposites is connected directly to the degree of the dispersion of the nanoplatelets. The fully exfoliated nanocomposites present much higher values for the tortuosity factor and aspect ratio in comparison with intercalated nanocomposites. Figure 4 shows the effect of MMT dispersion on the turtuosity and gas permeation through nanocomposites.

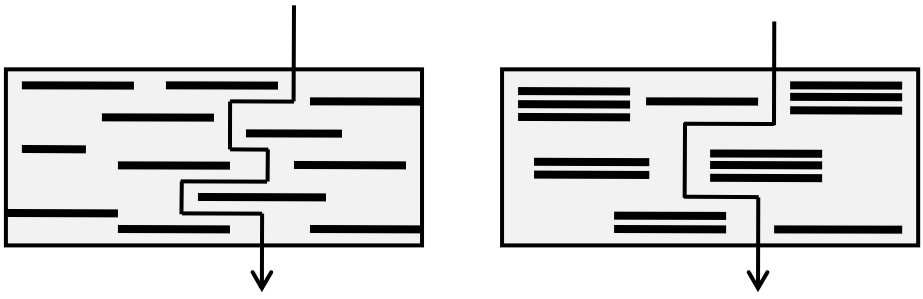

Figure 4: Schematic illustration of the tortuous path in (a) exfoliated and (b) intercalated nanocomposites

As it can be seen in Figure 3, permeability of CO_2 through RC and RC/MMT nanocomposites is higher compared to O_2. The CO_2/O_2 permeability ratio were in the range of 1.40- 1.64. This ratio is within the suitable range for designing films/coating for fruits and vegetables. Higher ratio will allow less accumulation of CO_2 and vice versa. Higher permeability of CO_2 is due to its smaller kinetic diameter (kinetic diameter of O_2: 3.46 Å > CO_2: 3.30 Å) combined with its greater solubility towards cellulose [35;36]. Previous studies also reported CO_2/O_2 permeability ratio of >1 for regenerated cellulose/soy protein [36] and regenerated cellulose/starch/lignin films [5], Wu and Yuan [37] studied gas permeability of dry

and water-swollen RC membrane prepared from NMMO. A higher permeation rate for CO_2 compared to O_2, N_2, CH_2 and H_2 was observed. They also reported that the prepared membrane is useful for separation of CO_2 from other gases, and the gas permeability rate and permselectivity can be controlled by water content of the membrane.

Conclusions

Regenerated cellulose/montmorillonite nanocomposite films has been fabricated and characterized for morphological and gas barrier properties. RC/MMT nanocomposite films were prepared by solution casting method via ionic liquid, BMIMCl as solvent. XRD result indicates exfoliation of MMT into single layers during preparation. SEM results showed smooth fractured surface with good interaction between cellulose and MMT. RC/MMT nanocomposite films exhibited improved barrier properties compared to RC. Permeability values decreased gradually with increasing MMT concentration up to 6% (w/w). This enhancement in barrier properties was attributed to the good adhesion between two phases, the high aspect ratio of MMT particles combined with perfect dispersion of MMT in cellulose matrix.

Acknowledgments

The authors would like to acknowledge the fundamental research grant scheme (FRGS) Vote No: 78690 by Universiti Teknologi Malaysia from Ministry of Science, Technology and Innovation (MOSTI).

References

[1] Scott, G. 2000. *Polymer Degradation and Stability, 68*, 1-7.

[2] Sinha Ray, S., & Bousmina, M. 2005. *Prog. Mater. Sci., 50*(8), 962-1079

[3] Klemm, D., Heublein, B., Fink, H. P., & Bohn, A. 2005. *Angew. Chem., Int. Ed. Engl., 44*(22), 3358-3393.

[4] Hermanutz, F., Meister, F., & Uerdingen, E. 2006. *Chemical Fibers International, 56*(6), 342-344.

[5] Wu, R. L., Wang, X. L., Li, F., Li, H. Z., & Wang, Y. Z. 2008. *Bioresour. Technol., 100*(9), 2569-2574.

[6] Bredereck, K., & Hermanutz, F. 2005. *Review of Progress in Coloration and Related Topics, 35*(1), 59-75.

[7] Zhu, S., Wu, Y., Chen, Q., Yu, Z., Wang, C., Jin, S., et al. 2006. *Green Chem., 8*(4), 325-327.

[8] Heinze, T., & Liebert, T. 2001. *Prog. Polym. Sci., 26*(9), 1689-1762.

[9] Woodings, C. 2002. Cellulose Fibers, Regenerated *In: Encyclopedia of Polymer Science and Technology*, 532-569. Warwickshire: John Wiley & Sons, Inc.

[10] Terbojevich, M., Cosani, A., Conio, G., Ciferri, A., & Bianchi, E. 1985. *Macromolecules, 18*(4), 640-646.

[11] Zhang, L., Ruan, D., & Zhou, J. 2001. *Ind. Eng. Chem. Res., 40*(25), 5923-5928.

[12] Tamai, N., Tatsumi, D., & Matsumoto, T. 2004. *Biomacromolecules,* 5(2), 422-432.

[13] Fink, H. P., Weigel, P., Purz, H. J., & Ganster, J. 2001. *Prog. Polym. Sci., 26*(9), 1473-1524.

[14] Rosenau, T., Hofinger, A., Potthast, A., & Kosma, P. 2003. *Polymer, 44*(20), 6153-6158

[15] El Seoud, O. A., Koschella, A., Fidale, L. C., Dorn, S., & Heinze, T. 2007. *Biomacromolecules, 8*(9), 2629-2647

[16] Olivier-Bourbigou, H., Magna, L., & Morvan, D. 2009. *Appl. Catal. A., 373*(1-2), 1-56.

[17] Rogers, R. D., & Seddon, K. R. 2003. *Science, 302*(5646), 792-793

[18] Swatloski, R. P., Spear, S. K., Holbrey, J. D., & Rogers, R. D. 2002. *J. Am. Chem. Soc., 124*(18), 4974-4975
[19] Alexandre, M., & Dubois, P. 2000. *Mater. Sci. Eng., R., 28*(1-2), 1-63.
[20] Chivrac, F., Pollet, E., & Avérous, L. 2009. *Mater. Sci. Eng., R., 67*(1), 1-17.
[21] Cerruti, P., Ambrogi, V., Postiglione, A., Rychly• , J., Matisova-Rychla• , L., & Carfagna, C. 2008. *Biomacromolecules, 9*(11), 3004-3013.
[22] Xu, W.-B., Bao, S.-P., & He, P.-S. 2002. *J. Appl. Polym. Sci., 84*(4), 842-849.
[23] Chen, X., Burger, C., Fang, D., Ruan, D., Zhang, L., Hsiao, B. S., et al. 2006. *Polymer, 47*(8), 2839-2848.
[24] Ruan, D., Zhang, L., Lue, A., Zhou, J., Chen, H., Chen, X., et al. 2006. *Macromol. Rapid Commun., 27*(17), 1495-1500
[25] Lee, J., Sun, Q., & Deng, Y. 2008. *Journal of Biobased Materials and Bioenergy, 2*, 162-168.
[26] Mahmoudian, S., Uzir Wahit, M., A.A., Y., & Nematzadeh, N. 2011. *Key Eng. Mater., 472*, 786-791
[27] Chen,H. Z., Wang, N., & Liu, L.-Y. 2012. J. *Chem. Technol. Biotechnol., 87*(12), 1634-1640.
[28] Dogan, H., & Hilmioglu, N. D. 2008. *Carbohydr. Polym., 75*(1), 90-94
[29] Zhang, L., Ruan, D., & Gao, S. 2002. *J. Polym. Sci. Part B: Polym. Phys., 40*(14), 1521-1529.
[30] Liu, S., & Zhang, L. 2009. *Cellulose, 16*(2), 189-198.
[31] Li, R., Zhang, L., & Xu, M. 2011. *Carbohydr. Polym., 87*(1), 95-100.
[32] Azeredo, H. M. C. d. 2009. *Food Research International, 42*(9), 1240-1253
[33] Choudalakis, G., & Gotsis, A. D. 2009. *Eur. Polym. J., 45*(4), 967-984.
[34] Koh, H. C., Park, J. S., Jeong, M. A., Hwang, H. Y., Hong, Y. T., Ha, S. Y., et al. 2008. *Desalination, 233*(1-3), 201-209.
[35] Robeson, L. M. 1991. *J. Membr. Sci., 62*(2), 165-185
[36] Wu, H., Wang, X. L., Wang, Y. Z., Bian, X. C., & Li, F. 2009. *Ind. Eng. Chem. Res., 48*(15), 7132-7136.
[37] Wu, J., & Yuan, Q. 2002. *J. Membr. Sci., 204*(1-2), 185-194.

THERMAL PROPERTIES OF LOW DENSITY POLYETHYLENE/PALM KERNEL SHELL COMPOSITES: EFFECT OF ECO-DEGRADANT

B. Y. Lim*, H. Salmah & P. L. Teh

School of Materials Engineering, Universiti Malaysia Perlis,
Taman Muhibah, 02600 Jejawi, Perlis

Abstract

The thermal properties of low density polyethylene (LDPE)/palm kernel shell (PKS) composites were studied. The composites with and without eco-degradant were prepared and subjected to thermogravimetric analysis (TGA) with scan temperature of 30ºC to 650ºC. It was found that the higher filler loading tend to reduce the onset temperature as the PKS had lower degradation temperature compared to that of LDPE**.** The addition of eco-degradant into the composites provided better interfacial bonding between the LDPE matrix and PKS filler. The LDPE/PKS composites with eco-degradant showed higher onset temperature and lower total weight loss compared to the composites without eco-degradant. The presence of eco-degradant provided better thermal stability of LDPE/PKS composites.

Keywords*: eco-degradant, low density polyethylene, palm kernel shell, thermal properties*

Introduction

Low density polyethylene (LDPE) is one of the thermoplastic that has been used extensively in packaging and agricultural purpose. Since LDPE is non-degradable, most of the LDPE had ended up in the landfill after they had served their purpose, for example as single use food packaging material. Thus, its increasing usage has resulted in environmental issue. One of the ways to reduce LDPE usage is through incorporation of organic fillers into polymeric composites.

The natural fillers have advantages such as low densities, low cost, nonabrasive nature, low energy consumption, high filling level possible, high specific properties and biodegradability over synthetic fibres [1; 2]. Several studies were carried out to prepare thermoplastic composites using organic filler such as wood fibres and flour, henequen, jute, sisal, and kenaf [3; 4; 5; 6; 7; 8]. Palm kernel shell is hard stony endocarps that surround the kernel of the oil palm. It is agricultural waste products obtained in the processing of palm oil and usually been burnt as waste material [9]. Due to its light density and high availability, it is suitable to be used as natural filler in polymeric composite.

Most of the natural fillers have low degradation temperatures (~200ºC), which make them inadequate for thermoplastics processing that require temperatures higher than 200ºC. The thermal property of the natural filler filled polymeric composites is strongly dependant on the thermal stability of the fillers. The thermal stability of wood pulp/polyethylene bio-composites was found to be significantly higher than pure wood pulp [10]. In a study of jute filled high density polyethylene composites, the decomposition temperature for the maleic anhydride grafted polyethylene (MAPE) treated composites was higher than that of the untreated composites and the percentage of weight loss in degradation processes was also less than the untreated composites, indicating that the presence of MAPE enhanced the thermal stability of the composites [11].

In this study, the thermal properties of LDPE, PKS, LDPE/PKS composites with and without eco-degradant prepared at different filler loading were determined using thermogravimetric analysis (TGA). Fourier transform infrared spectroscopy (FTIR) was used to investigate the functional group in the composites with and without eco-degradant.

Materials and method

Materials

The LDPE was supplied by Titan Chemical, Johor, Malaysia with density of 0.922 g.cm^{-3} and MFI of 0.33g.10 min^{-1}. The palm kernel shell that used as fillers was obtained from Malpom Oil Palm Processing, Penang, Malaysia. The palm kernel shell was dried at 80ºC for 24 hours to evaporate the moisture content. Then the cleaned palm kernel shell was crushed into powder form and sieved. The average particles size of 75 µm was measured by using Malvern particle size analyzer. The eco-degradant was supplied by Behn Meyer Polymers Manufacturing Sdn. Bhd. It was light brown free flowing pellets with density of 0.940 kg.m^{-3}.

Composites Preparation

Composites were prepared by using a Z-Blade mixer at temperature of 180ºC and rotor speed of 50 rpm. The LDPE was loaded into the mixing chamber for 5 minutes. After 5 minutes, filler was added and mixing continued for 10 minutes. The total mixing time of composites was 15 minutes. Finally, the composites were removed from the mixing chamber and pressed into thick round pieces. For the preparation of composites with eco-degradant, LDPE and eco-degradant were charged into the mixing chamber for 5 minutes until they completely melt. Then the filler was added and mixing continued for 10 minutes. Hot press procedures involved preheating at 180ºC for 9 minutes followed by compressing for 6 minutes and subsequent cooling under pressure for 4 minutes. Table 1 refers to formulation of the LDPE/PKS composites with and without eco-degradant.

Table 1: Formulation for LDPE/PKS composites with and without eco-degradant.

Materials	Without eco-degradant	With eco-degradant
LDPE (php)	100	100
PKS (php)	0, 10, 20, 30, 40	10, 20, 30, 40
Eco-degradant (php)*	-	5

* 5 php based on weight of LDPE

Thermogravimetric analysis (TGA)

Thermogravimetric analysis was carried out using Perkin Elmer Pyris Diamond TG-DTA. The samples were weighed about 15-25 mg, and subjected to heating rate of 20ºC.min^{-1} at temperature range of 30ºC to 650ºC under nitrogen flow of 50 ml.min^{-1}.

Fourier transform infrared spectroscopy analysis

Fourier transform infrared (FTIR) spectra of the LDPE/PKS composites were acquired by using Perkin Elmer Spectrum 100 FTIR in ATR (Attenuated Total Reflectance) mode. For each spectrum, 4 consecutive scans with 4.0 cm^{-1} resolution were used. The scan range was 650 - 4000 cm^{-1}.

Results and Discussion

Figure 1 shows the thermogravimetry analysis (TGA) curves of LDPE, PKS, and LDPE/PKS composites at different PKS loading. It can be seen that the weight loss of PKS started at 40ºC. This was due to the evaporation of volatile and moisture content of PKS. The degradation of PKS started to take place rapidly at 204ºC and finished at 379.2ºC. The weight loss of LDPE occurred in a one step degradation process from 400ºC to 500ºC. The LDPE started weight loss at 280.9ºC and continued very slowly before reaching the temperature of

400ºC. Above 400ºC, the degradation process took place rapidly due to the further breakdown of the LDPE into gaseous products at higher temperature.

The derivative thermogravimetry (DTG) thermograph of LDPE/PKS composites at different PKS loading is shown in Figure 2. The curve shows two decomposition peaks for the PKS indicated its two-step degradation. The first and second peak temperatures were 282.3ºC and 344.8ºC, respectively which showed the degradation of cellulose and lignin. According to Nicholas [12]**,** cellulose decomposed at 280ºC and ended at 300ºC to 350ºC and lignin decomposed at 300ºC to 350ºC and ended at 400ºC to 450ºC. The thermal degradation of the LDPE/PKS composites was a combined phenomenon of thermal degradation of PKS and LDPE. The first two steps degradation of weight loss was due to the degradation of PKS, while the following weight loss was caused by the degradation of LDPE.

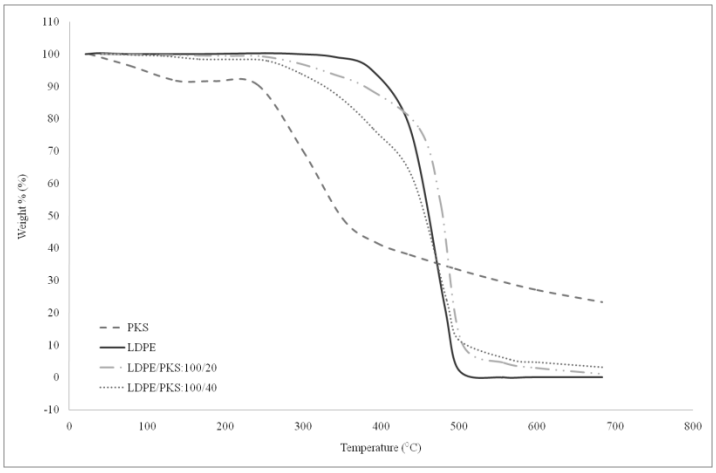

Figure 1: Comparison of thermogravimetric analysis of PKS, LDPE, and LDPE/PKS composites at different filler loading

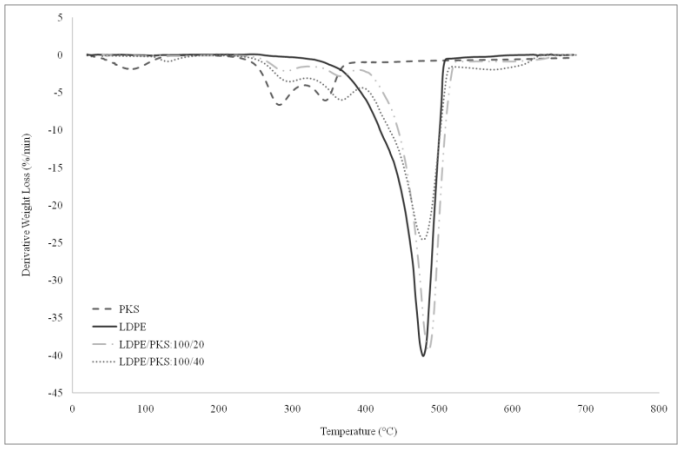

Figure 2: Comparison of derivative thermogravimetry (DTG) curves of PKS, LDPE, and LDPE/PKS composites at different filler loading

Figure 3 and 4 show the TGA and DTG curves of the LDPE, LDPE/PKS with and without eco-degradant at 40 php filler loading. At similar filler loading, the composites with eco-degradant exhibited higher onset temperature at 238.2ºC compared to that of composites without eco-degradant at 235.8ºC. From Figure 4, it shows that the DTG curve of the LDPE/PKS composites with eco-degradant was slightly shifted to the right, which was higher temperature. Besides, the onset temperature, peak temperature and end degradation temperature of the composites with eco-degradant were higher compared to the composites without eco-degradant. The presence of eco-degradant was able to improve the interfacial interaction between the PKS and LDPE.

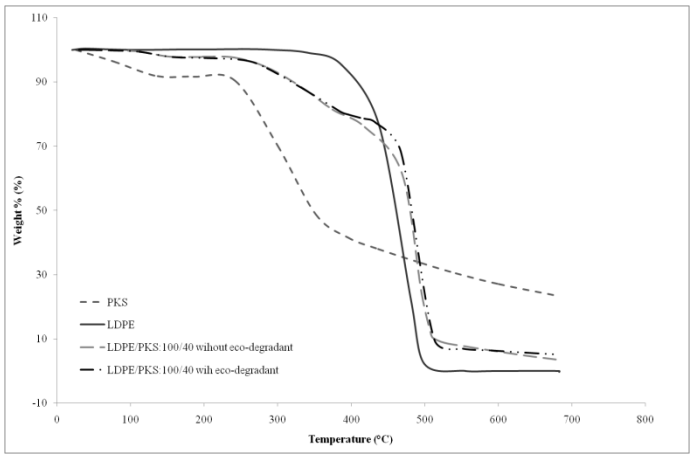

Figure 3: Comparison of thermogravimetric analysis of LDPE and LDPE/PKS composites with and without eco-degradant.

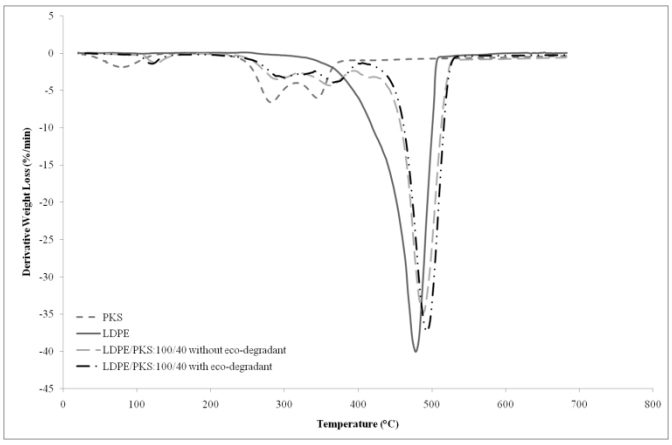

Figure 4: Comparisons of derivative thermogravimetry (DTG) curves of LDPE and LDPE/PKS composites with and without eco-degradant.

Table 2 summarized the derivative data (DTG) for the PKS, LDPE and LDPE/PKS composites with and without eco-degradant. The addition of the PKS into LDPE decreased the onset temperature due to the different thermal properties of PKS compared to LDPE. At higher filler loading, the onset temperature (T_{onset}) and peak temperature of the composites were decreased. This was due to the presence of more lignin and cellulose which have lower decomposition temperature.

Table 2: Themogravimetric data of PKS, LDPE, and LDPE/PKS composites with and without eco-degradant.

Samples	T_{onset} (°C)	Peak Temperature (°C)			$T_{end\ deg}$ (°C)
		1st peak	2nd peak	3rd peak	
PKS	204.3	282.3	344.8	-	379.2
LDPE	280.9	478.0	-	-	508.8
LDPE/PKS : 100/20 without eco-degradant	241.4	291.7	365.5	487.7	525.8
LDPE/PKS : 100/40 without eco-degradant	235.8	288.4	361.2	485.0	526.1
LDPE/PKS : 100/20 with eco-degradant	255.0	307.9	371.9	493.4	531.3
LDPE/PKS : 100/40 with eco-degradant	238.2	298.2	368.6	491.8	532.3

Table 3 shows the total percentage weight loss of PKS, LDPE and LDPE/PKS composites. The PKS had total weight loss of 73% indicated that the char residue of PKS was about 27%; while LDPE underwent 100% total weight loss. The total weight loss of LDPE/PKS composites decreased with increasing PKS loading. At a similar filler loading, the total weight loss of the LDPE/PKS composites with eco-degradant was lower than composites without eco-degradant. Hence, it showed that the eco-degradant had positive effect on the thermal stability of the composites. The better thermal stability of composites with eco-degradant was attributed to the improved interfacial interaction between PKS and LDPE.

Table 3: Percentage weight loss of PKS, LDPE, and LDPE/PKS composites with and without eco-degradant

Temperature	Weight Loss (%)					
	PKS	LDPE	LDPE/PKS : 100/20 without eco-degradant	LDPE/PKS : 100/40 without eco-degradant	LDPE/PKS : 100/20 with eco-degradant	LDPE/PKS : 100/40 with eco-degradant
100	6.77	0.05	0.18	0.39	0.17	0.42
200	1.69	0.04	0.32	1.83	1.04	2.11
300	21.54	0.12	2.89	5.52	1.81	5.22
400	28.87	7.20	8.69	13.84	4.96	12.70
500	7.89	90.20	74.12	60.08	67.78	55.75
600	6.20	2.39	11.97	12.40	21.42	17.06
Total weight loss	72.96	100.00	98.17	94.04	97.18	93.26

Figure 5 shows the FTIR spectra of the LDPE/PKS composites with and without eco-degradant at 20 php of PKS loading. The LDPE showed its characteristic peaks at 2848 cm^{-1} and 2915 cm^{-1} from the asymmetry stretching vibration of CH_3, 1470 cm^{-1} from the CH_2 and CH_3 deformation, and 720-725 cm^{-1} from the CH_2 rocking. The peaks of 1470 cm^{-1} and 670 cm^{-1} were shifted to 1468 cm^{-1} and 660 cm^{-1}, respectively. The infrared transmittance peak of free –OH group of palm kernel shell in LDPE/PKS composites was 3394.97 cm^{-1}. The presence of eco-degrdant in LDPE/PKS composites shifted the peak from 3394.97 cm^{-1} to 3360.04 cm^{-1}. The spectral shifting from higher to lower wave number confirmed that the hydrogen bonds were generated as ester linkage between filler surface and matrix. The LDPE/PKS composites with eco-degradant showed a new peak presence at 1716 cm^{-1} due to carbonyl stretching of the carboxylic acid groups.

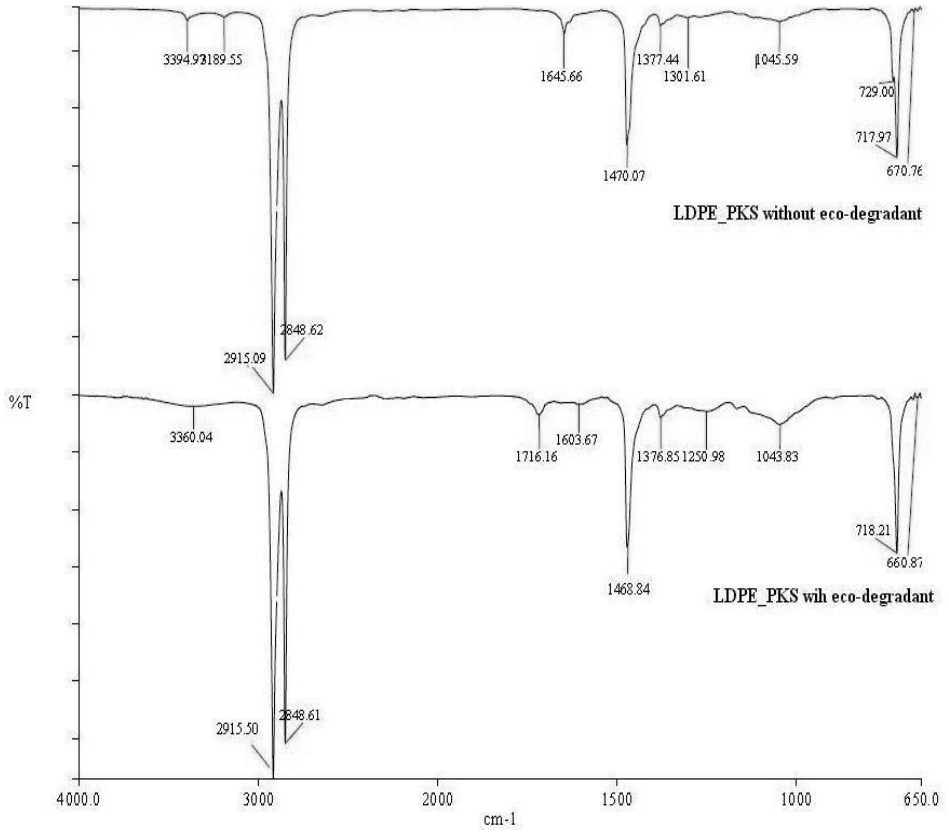

Figure 5: FTIR spectra of LDPE/PKS composites with and without eco-degradant.

Conclusions

The incorporation of the palm kernel shell into the LDPE had changed the thermal properties of the LDPE/PKS composites. The onset temperatures of the LDPE/PKS composites were lower compared to the neat LDPE due to the presence of the PKS with lower degradation temperature. The addition of the eco-degradant had improved the thermal stability of the composites, as lower total weight loss was observed, as compared to the composites without eco-degradant. Through FTIR, it was found out that ester bonding was formed between PKS and LDPE and better interfacial adhesion between filler and matrix was established.

References

[1] Mishra, S., Mohanty, A. K., Drzal, L. T., Misra, M. & Hinrichsen, G. 2004. *Macromol. Mater. Eng.* 289(11): 955-974.

[2] Tserki, V., Matzinos, P., Kokkou, S. & Panayiotou, C. 2005. *Composites, Part A* 36(7): 965-974

[3] Mohanty, S., Verma, S. K., Nayak, S. K. & Tripathy, S. S. 2003. *Int. J. Plast. Technol.* 7(2): 75-87

[4] Herrera-Franco, P. J. & Valadez-Gonzalez, A. 2005. *Composites, Part B* 36(8): 597-608.

[5] Adhikary, K. B., Pang, S. & Staiger, M. P. 2008. *Composites, Part B* 39(5): 807-815

[6] Morreale, M., Scaffaro, R., Maio, A. & La Mantia, F. P. 2008. *Composites, Part A* 39(3): 503-513.

[7] Behjat, T., Russly, A. B., Luqman, C. A., Nor Azowa, I. & Yus, A. Y. 2009. *Eur. J. Sci. Res.* 32(2): 223-230.

[8] Sun, Z.-Y., Han, H.-S. & Dai, G.-C. 2010. *J. Reinf. Plast. Compos.* 29(5): 637-650.

[9] Olanipekun, E. A., Olusola, K. O. & Ata, O. 2006. *Build. Environ.* 41(3): 297-301.
[10] Awal, A., Ghosh, S. B. & Sain, M. 2010. *J. Therm. Anal. Calorim.* 99: 695-701.
[11] Mohanty, S., Verma, S. K. & Nayak, S. K. 2006. *Compos. Sci. Technol.* 66(3-4): 538-547.
[12] Nicholas, D. D. (1982). Degradation and protection of wood. Syracuse University Press.

ISBN 978-967-5878-88-6

POLYMER RESEARCH CENTER (PORCE)
Faculty of Science and Technology
Universiti Kebangsaan Malaysia
43000 UKM Bangi, Selangor D.E., MALAYSIA
Website: www.ukm.my/porce
Email: porce@ukm.my